

REGULATION OF ENERGY ORGANELLE DYNAMICS IN ARABIDOPSIS

By

Ronghui Pan

A DISSERTATION

Submitted to
Michigan State University
in partial fulfillment of the requirements
for the degree of

Biochemistry and Molecular Biology - Doctor of Philosophy

2014

ABSTRACT

REGULATION OF PLANT ENERGY ORGANELLE DYNAMICS IN ARABIDOPSIS

By

Ronghui Pan

Eukaryotic cells are defined by the presence of membrane-delineated organelles, providing the necessary environments for various biochemical reactions. In plants, three organelles – chloroplasts, mitochondria and peroxisomes – are critically involved in many essential aspects of plant physiology, including energy capture, conversion, storage and metabolism. The major protein machineries governing the dynamics of these organelles, including those for protein import and membrane fission, have been identified. However, mechanisms that regulate the major machineries are just beginning to be elucidated in plants and other systems. This dissertation research aims to deepen the understanding of the roles of protein post-translational modifications and membrane lipids in regulating organelle dynamics using the plant model system *Arabidopsis thaliana*. First, I studied the role of cardiolipin (CL), a negatively charged non-bilayer forming phospholipid, in organelle dynamics and plant development. I showed that CL is important for mitochondrial fission in *Arabidopsis* and exerts this function, at least in part, through stabilizing the higher-order protein complex of dynamin-related protein 3 (DRP3), a major division protein for mitochondria and peroxisomes. CL and Cardiolipin Synthase (CLS) both localize specifically to mitochondria. CL deficiency resulted from *CLS* gene disruption or suppression of gene expression leads to mitochondrial elongation and enlargement, abnormal mitochondrial cristae, plant dwarfness and susceptibility to various abiotic stresses. Then I focused on a key form of protein post-

translational modification – ubiquitination, for its role in regulating organelle dynamics. Through a bioinformatic approach, I identified a mitochondrial outer membrane associated deubiquitinase, UBP27, and determined its membrane topology, targeting signal and enzymatic activity. UBP27 is anchored to the mitochondrial outer membrane with the enzymatic domain facing the cytosol. Overexpression of UBP27 reduces mitochondrial length and mitochondrial association of DRP3, suggesting its role in mitochondrial dynamics possibly through affecting the recycle of DRP3 from mitochondrial to the cytosol. Finally, I identified a small family of RING domain-containing proteins, namely SP1, SPL1 and SPL2, among which ubiquitin E3 ligase activity had been shown for SP1. SP1 and SPL1 localize to chloroplasts, mitochondria and peroxisomes, while SPL2 localizes to chloroplasts and mitochondria; such proteins that localize to all three major energy organelles had not been reported. I performed initial characterization of these RING domain proteins, and discovered distinct characteristics among them in targeting signal, membrane association, and loss- and gain-of-function mutant phenotypes. I hypothesize that these three related proteins may coordinately regulate the import, division, and/or distribution of chloroplast, mitochondria and peroxisomes. In summary, my work has revealed multiple regulatory mechanisms in the dynamics of *Arabidopsis* mitochondria, peroxisomes and chloroplasts, key organelles that act in concert in a number of plant metabolic pathways essential for energy metabolism.

ACKNOWLEDGEMENTS

I want to acknowledge my beloved grandmother, father, mother and wife. They give me love, encouragement and comfort, so that I can go through all the ups and downs in my life.

In my 20 years of school life, I have been taught by many teachers in 7 different schools. Most of my teachers are very nice to me. They make me who I am today. In particular, I am very blessed to be accepted by Nanjing University and Michigan State University.

In my 5.5 years of graduate school, I want to acknowledge my mentor Jianping Hu, who brings me to a very exciting plant research area. She is very supportive to me in research and gives me very important advice. She is also a good model of scientist to me in many ways. The current and former members of the Hu lab have given me a lot of help in the lab. When I just joined the lab, senior members, including Bong-Kwan, Mintu, Kyaw and Navneet, offered me many instructions on experiments.

I appreciate the precious time and valuable suggestions from my committee members – Drs. Susanne Hoffmann-Benning, Daniel Jones, John Lapres, Beronda Montgomery. Besides, Dr. Laurie Kaguni gave me two opportunities to attend two mitochondria summer school, which were really helpful.

Many people outside the Hu lab have helped me on research. In addition, I made many friends at MSU. I will not list all their names here in case I forget some of them. I am very blessed to know all these people.

TABLE OF CONTENTS

LIST OF TABLES	ix
LIST OF FIGURES	x
KEY TO ABBREVIATIONS	xiii
CHAPTER 1	1
LITERATURE REVIEW The dynamics of plant energy organelles: protein import and organelle fission.....	1
1.1 Introduction.....	2
1.2 Plant mitochondrial protein import machinery.....	4
1.2.1 Outer membrane proteins.....	5
1.2.2 Proteins in the inter-membrane space	6
1.2.3 Inner membrane proteins.....	7
1.2.4 Matrix proteins.....	8
1.3 Plant peroxisomal protein import machinery.....	8
1.4 Fission machineries of plant mitochondria and peroxisomes.....	10
1.4.1 Shared fission factors between mitochondria and peroxisomes.....	10
1.4.1.1 DRP3A and DRP3B: dynamic membrane scissors.....	10
1.4.1.2 FIS1A and FIS1B: membrane anchors for DRP3.....	11
1.4.1.3 Other fission factors shared by mitochondria and peroxisomes.....	12
1.4.2 Mitochondrial-specific fission factors.....	13
1.4.3 Other peroxisomal fission factors.....	14
1.4.3.1 PEX11: promoter of peroxisome elongation.....	14
1.4.3.2 DRP5B: a fission factor shared by peroxisomes and chloroplasts.....	15
1.5 Lack of identified mitochondrial fusion machinery in plants.....	15
1.6 Regulatory mechanisms of mitochondrial dynamics.....	16
1.6.1 Post-translational regulation of mammalian DRP1.....	17
1.6.1.1 Phosphorylation.....	17
1.6.1.2 Ubiquitination.....	18
1.6.1.3 SUMOylation.....	19
1.6.1.4 S-nitrosylation.....	20
1.6.2 Post-translational regulation of <i>Arabidopsis</i> DRP3.....	21
1.6.3 The role of ER-mitochondria association in regulating mitochondrial fission.....	22
1.6.4 The impact of mitochondrial membrane lipids in mitochondrial dynamics.....	23
1.6.4.1 Cardiolipin.....	23
1.6.4.2 Phosphatidylethanolamine.....	25
1.6.4.3 Phosphatidic acid and diacylglycerol.....	26

1.7 Regulatory mechanisms of peroxisomal dynamics.....	27
1.8 Aims of this dissertation research.....	28
CHAPTER 2.....	35
Cardiolipin-mediated mitochondrial dynamics and stress response in <i>Arabidopsis</i>	35
2.1 Abstract.....	36
2.2 Introduction.....	37
2.3 Results.....	40
2.3.1 Mitochondrial localization of CL and CLS in plant cells.....	40
2.3.2 Membrane association and topology of CLS.....	43
2.3.3 Disruption of CLS leads to defects in mitochondrial structure and fission.....	44
2.3.4 Cardiolipin regulates mitochondrial fission through DRP3 proteins.....	46
2.3.5 Cardiolipin stabilizes the mitochondrial-associated DRP3 protein complex.....	50
2.3.6 Cardiolipin plays a role in plant responses to programmed cell death (PCD)-inducing stresses.....	52
2.4 Discussion.....	53
2.4.1 Novel and plant-specific aspects of CL biology uncovered.....	53
2.4.2 CL-mediated mitochondrial fission and fusion.....	55
2.4.3 Different membrane lipid compositions of mitochondria and peroxisomes may contribute to the distinct modes of DRP3 functions on these organelles.....	57
2.4.4 Cardiolipin may link mitochondrial fission to programmed cell death (PCD).....	58
2.5 Methods.....	108
2.5.1 Plant material and transformation.....	108
2.5.2 Gene cloning, plasmid construction, and RT-PCR.....	108
2.5.3 Protein preparation and immunoblot analysis.....	109
2.5.4 NAO staining and microscopy.....	111
2.5.5 Total lipid extraction.....	112
2.5.6 LC/MS analysis.....	113
2.5.7 Co-immunoprecipitation (Co-IP).....	114
2.5.8 Mitochondrial isolation and determination of protein membrane association and topology.....	114
2.5.9 TUNEL assay.....	115
2.5.10 Statistical analysis.....	115
2.6 Acknowledgements.....	116
CHAPTER 3.....	117
The <i>Arabidopsis</i> mitochondrial membrane-bound ubiquitin protease UBP27 contributes to mitochondrial morphogenesis	117
3.1 Abstract.....	118
3.2 Introduction.....	119
3.3 Results.....	123
3.3.1 <i>Arabidopsis</i> UBP27 is localized to mitochondria.....	123

3.3.2	Analysis of UBP27's mitochondrial targeting sequence and membrane topology.....	125
3.3.3	UBP27 hydrolyses casein and possesses ubiquitin protease activity <i>in vitro</i>	126
3.3.4	UBP27 affects mitochondrial morphogenesis.....	127
3.3.5	UBP27 reduces the mitochondrial association of DRP3.....	129
3.4	Discussion.....	130
3.4.1	Evidence for the presence of a mitochondrial deubiquitinase in plants.....	130
3.4.2	UBP27's role in plant mitochondrial dynamics and morphogenesis.....	131
3.4.3	Is the function of DRP3 directly modulated by UBP27?.....	133
3.5	Methods.....	166
3.5.1	Plant material.....	166
3.5.2	Plant transformation.....	166
3.5.3	Gene cloning, plasmid construction, and RT-PCR.....	166
3.5.4	Plant protein preparation.....	167
3.5.5	Immunoblot analysis.....	167
3.5.6	Microscopy.....	168
3.5.7	Mitochondrial isolation, and determination of protein membrane association and topology.....	168
3.5.8	Determination of mitochondrial size distribution.....	168
3.5.9	Phylogenetic tree construction.....	169
3.5.10	Universal protease activity assay.....	169
3.5.11	<i>In vitro</i> deubiquitinase activity assay.....	170
3.5.12	Statistical analysis.....	170
3.6	Acknowledgements.....	171
CHAPTER 4	172
	Characterization of a small family of RING domain proteins associated with <i>Arabidopsis</i> energy organelles.....	172
4.1	Abstract.....	173
4.2	Introduction.....	174
4.3	Results and discussion.....	180
4.3.1	Subcellular localization of members of a small RING-type E3 protein family in <i>Arabidopsis</i>	180
4.3.2	Protein sequence analysis of SP1/SPL family members.....	182
4.3.3	SP1 is integral to the mitochondrial and peroxisomal membrane.....	183
4.3.4	Analysis of SP1 and SPL1 targeting signals.....	184
4.3.5	SP1 and SPL1 play a different role from MUL1 in regulating mitochondrial dynamics.....	186
4.3.6	SPL2 may function in mitochondrial distribution, movement or division.....	189
4.3.7	Next steps in the elucidation of SP1/SPL functions.....	190
4.4	Methods.....	217
4.4.1	Plant materials.....	217

4.4.2 Plant transformation.....	217
4.4.3 Gene cloning, plasmid construction and RT-PCR.....	218
4.4.4 Immunoblot analysis.....	219
4.4.5 Purification of peroxisomal and mitochondrial proteins.....	219
4.4.6 Microscopy.....	220
4.4.7 Yeast two-hybrid assay.....	220
CHAPTER 5.....	221
CONCLUSION AND PERSPECTIVES.....	221
5.1 Membrane lipids.....	222
5.2 Post-translational modifications.....	225
5.3 Broader impacts of this study.....	227
APPENDIX.....	231
REFERENCES.....	240

LIST OF TABLES

Table 2.1. DNA primers used in Chapter 2.....	105
Table 2.2. Vectors used in Chapter 2.....	107
Table 3.1. DNA primers used in Chapter 3.....	164
Table 3.2. Vectors used in Chapter 3.....	165
Table 4.1. DNA primers used in Chapter 4.....	215
Table 4.2. Vectors used in Chapter 4.....	216

LIST OF FIGURES

Figure 1.1. The mitochondrial protein import apparatus in plants.....	31
Figure 1.2. The <i>Arabidopsis</i> peroxisomal matrix protein import machinery.....	32
Figure 1.3. Proteins responsible for mitochondrial and peroxisomal fission in <i>Arabidopsis</i>	33
Figure 1.4. Post-translational regulation of mammalian Dynamin-Related Protein1 (DRP1).....	34
Figure 2.1. Subcellular localization of cardiolipin and CLS in plant cells.....	61
Figure 2.2. Sequence comparison of CLS proteins from different species.....	63
Figure 2.3. CLS-YFP-HA is processed upon mitochondrial targeting.....	66
Figure 2.4. Analysis of organelle targeting signals on CLS.....	68
Figure 2.5. Analyses of mitochondrial membrane association and topology of CLS.....	71
Figure 2.6. Molecular, phenotypic and biochemical analyses of the <i>cls-1</i> mutant and rescued lines.....	74
Figure 2.7. More characterization of <i>cls-1</i>	77
Figure 2.8. Expression profile of the <i>Arabidopsis</i> CLS gene.....	79
Figure 2.9. Mitochondrial morphology in <i>cls-1</i>	81
Figure 2.10. Transmission electron microscopic (TEM) analysis of mitochondrial structure from four-week-old wild-type and <i>cls-1</i> leaves.	82
Figure 2.11. Partial complementation of the mitochondrial morphological phenotype in <i>cls-1</i> by DRP3 proteins.....	84
Figure 2.12. Alignment of the N terminus (containing the GTPase domain) of mitochondrial/peroxisome division DRP proteins from various species.....	87
Figure 2.13. Functional association of CL and DRP3 in mitochondrial fission.....	89
Figure 2.14. DRP3's function in mitochondrial fission depends on interaction with CL.....	92

Figure 2.15. Analysis of the role of a few conserved residues in mitochondrial and peroxisomal fission.....	94
Figure 2.16. Association of CFP-DRP3 and CFP-DRP3 ^{R->E} proteins with mitochondria.....	96
Figure 2.17. Cardiolipin stabilizes DRP3 protein complexes.....	97
Figure 2.18. Analyses of DRP3 ^{R->E} protein self-interaction in tobacco and DRP3 transcript levels in <i>cls-1</i>	99
Figure 2.19. CLS deficient mutants are more susceptible to heat stress and prolonged darkness.....	100
Figure 2.20. Mitochondrial phenotypes of <i>CLS</i> amiRNA lines and characterization of CL's role in plant response to PCD-inducing stresses.....	103
Figure 3.1. Predicted and experimentally confirmed localization, and TMD prediction for all <i>Arabidopsis</i> UBPs.....	136
Figure 3.2. Analysis of the sub-cellular localization of UBP17, UBP25 and UBP27....	138
Figure 3.3. UBP27 is a putative ortholog of the mitochondrial UBPs ScUBP16 and HsUSP30.....	140
Figure 3.4. Sequence comparison of mitochondrial UBP proteins from different species and topology prediction for UBP27.....	143
Figure 3.5. Analysis of mitochondrial targeting signals on UBP27.....	145
Figure 3.6. Immunoblot analyses of the mitochondrial membrane association and topology of UBP27.....	147
Figure 3.7. GST-UBP27 hydrolyzes casein.....	149
Figure 3.8. UBP27 possesses de-ubiquitinase activity <i>in vitro</i>	151
Figure 3.9. Characterization of the <i>UBP27</i> T-DNA insertion lines.....	152
Figure 3.10. Additional characterization of the <i>UBP27</i> T-DNA insertion lines.....	154
Figure 3.11. UBP27 overexpression leads to mitochondrial morphological changes..	156
Figure 3.12. Mitochondrial phenotypes caused by <i>UBP27</i> overexpression.....	158

Figure 3.13. UBP27 overexpression reduces the association of DRP3 with mitochondria.....	160
Figure 3.14. Mitochondrial association of DRP3 is not changed in <i>ubp27</i> loss-of-function mutant.....	162
Figure 3.15. Immunoblot analysis of endogenous DRP3A and DRP3B proteins in wild-type, <i>UBP27</i> loss-of-function mutants and gain-of-function lines.....	163
Figure 4.1. Chloroplast association of SP1, SPL1 and SPL2 in <i>Arabidopsis</i>	193
Figure 4.2. Mitochondrial association of SP1, SPL1 and SPL2 in <i>Arabidopsis</i>	194
Figure 4.3. Peroxisomal association of SP1 and SPL1 in <i>Arabidopsis</i>	195
Figure 4.4. Protein sequence comparison of <i>Arabidopsis</i> SP1, SPL1 and SPL2.....	196
Figure 4.5. Transmembrane domain (TMD) prediction analysis of <i>Arabidopsis</i> SP1, SPL1 and SPL2.....	198
Figure 4.6. Bioinformatics analysis of <i>Arabidopsis</i> SP1, SPL1 and SPL2.....	199
Figure 4.7. Immunoblot analyses of the mitochondrial and peroxisomal membrane association of SP1.....	201
Figure 4.8. Analysis of organelle targeting signals on SP1.....	203
Figure 4.9. Analysis of organelle targeting signals on SPL1.....	205
Figure 4.10. Mitochondrial morphology is not affected by overexpression of SP1 or SPL1.....	207
Figure 4.11. Subcellular localization and yeast two hybrid (Y2H) analysis of <i>Arabidopsis</i> SUMO proteins.....	208
Figure 4.12. Molecular, phenotypic and mitochondrial morphology analyses of the <i>sp1</i> and <i>sp1</i> single and double mutants.....	210
Figure 4.13. SPL2 plays a role in mitochondrial dynamics.....	213
Figure 5.1. A summary of the efforts described in this dissertation to dissect the regulatory mechanisms of plant energy organelle dynamics.....	229
Figure A.1. Domain structure of Mdv1/Caf4 and their homologs or putative homologs.....	238

KEY TO ABBREVIATIONS

35S	Cauliflower Mosaic Virus 35S Promoter
AA	Amino Acid
ABRC	Arabidopsis Biological Resource Center
AD	Activation Domain
ATP	Adenosine-5'-Triphosphate
BD	DNA Binding Domain
BLAST	Basic Local Alignment Search Tool
C	Celsius
Camk α	Ca ²⁺ /Calmodulin-Dependent Protein Kinase I α
CC	Coiled-Coil Domain
CFP	Cyan Fluorescent Protein
CL	Cardiolipin
CLS	Cardiolipin Synthase
Co-IP	Co-Immunoprecipitation
DRP	Dynamin-Related Protein
ER	Endoplasmic Reticulum
EMS	Ethane Methyl Sulfonate
GDP	Guanosine-5'-Diphosphate
GFP	Green Fluorescent Protein
GST	Glutathione-S-Transferase
GTP	Guanosine-5'-Triphosphate

Gtpase	Guanosine Triphosphatase
MARCH-V	Membrane Associated RING-CH-V
Mid	Mitochondrial Dynamics Protein
MIEF	Mitochondrial Elongation Factor
MITOL	Mitochondrial Ubiquitin Ligase
MAPL	Mitochondrial-Anchored Protein Ligase
MUL1	Mitochondrial E3 Ubiquitin Protein Ligase 1
PEX	Peroxin
PTS1	Peroxisomal Targeting Signal 1
PTS2	Peroxisomal Targeting Signal 2
RALA	the Small Ras-GTPase Protein
RALBP1	Effector Protein of RALA
SD	Synthetic Dropout
SD/-HUT	SD Media Lacking Histidine, Uracil, and Tryptophan
SD/-HUTL	SD Media Lacking Histidine, Uracil, Tryptophan, and Leucine
SEN5	SUMO1/Sentrin-Specific Peptidase 5
TBST	Tris-Buffered Saline with Tween 20
TMD	Transmembrane Domain
Ubc9	SUMO-Conjugating Enzyme
UBP	Ubiquitin-Specific Protease
UBQ	Ubiquitin
YFP	Yellow Fluorescent Protein

CHAPTER 1

LITERATURE REVIEW

The dynamics of plant energy organelles: protein import and organelle fission

1.1 Introduction

Eukaryotic cells are defined by the presence of membrane-enclosed structures, including the nucleus and numerous other organelles. In higher plants, three organelles - peroxisomes, mitochondria and chloroplasts – play essential roles in energy capture, conversion, storage and/or metabolism. Hence, they are often referred as plant energy organelles.

Peroxisomes are small single membrane-bounded entities with a diameter of 0.1-1 μm . They perform various crucial metabolic functions, including lipid mobilization, photorespiration, detoxification, hormone biosynthesis and metabolism, and pathogen defense in plants (Hu et al., 2012). Mitochondria, the descendants of ancient endosymbiotic α -proteobacteria, are delineated by double membranes (Lane and Martin, 2010). They participate in many vital physiological processes, such as energy metabolism, programmed cell death, intracellular calcium homeostasis, primary carbon metabolism, amino acid metabolism and the biosynthesis of lipids and vitamins. Mitochondria supply the biological energy ATP and thus are considered the power house of the cell (Millar et al., 2008). Chloroplasts are chlorophyll-containing plastids, which are descendants of ancient endosymbiotic photosynthetic cyanobacteria (Keeling, 2010). Plastids are surrounded by two membranes, the inner envelope membrane (IEM) and outer envelope membrane (OEM). Chloroplasts carry out photosynthesis, the synthesis of fatty acids and amino acids, the metabolism of nitrogen and sulfur, and numerous other functions (Neuhaus and Emes, 2000). There is also a network of internal membranes in chloroplasts called thylakoids, where photosynthetic pigments and major photosynthetic proteins are embedded (Jarvis and López-Juez, 2013).

Some metabolic pathways, including photorespiration, jasmonic acid biosynthesis, and lipid metabolism, require the coordinated functions of peroxisomes, mitochondria and chloroplasts (Peterhansel et al., 2010; Millar et al., 2008; Hu et al., 2012). For example, photorespiration is initiated in chloroplasts by Rubisco, the same enzyme that is also responsible for photosynthetic CO₂ fixation. Photorespiration recycles phosphoglycolate, a toxic compound produced by oxygen fixation in photosynthesis, back to phosphoglycerate, a Calvin cycle intermediate. The photorespiratory pathway in higher plants consists of individual reactions from all three organelles as well as the cytosol (Bauwe et al., 2010). Hence, one can predict that the optimal performance of photorespiration is dependent on the coordination of the functions and dynamics of these three organelles, as well as inter-organellar metabolite transportation.

If considered quantitatively in terms of mass flow, photosynthesis and photorespiration are the two most important processes in the biogeosphere. Photosynthesis plays a major role in the creation of chemical energy and biomass on earth. Photorespiration, however, causes significant losses of carbon and energy, which potentially amounts to 25% of photosynthetic output in C₃ plants (Cegelski and Schaefer, 2006; Sharkey, 1988). Just from this perspective, it is important to understand the regulation of the functions of peroxisomes, mitochondria and chloroplasts in plant cells to achieve the preferable activity of photosynthesis and photorespiration. Progress in this field can potentially lead to tremendous industrial and agricultural values.

To be responsive to various environmental, developmental and physiological cues, chloroplasts, mitochondria and peroxisomes are all very dynamic organelles. The

dynamics of these organelles include changes in number, morphology, distribution, as well as their protein and lipid compositions. The dynamics of chloroplasts, mitochondria and peroxisomes are important for their functional efficiency. Chloroplasts and mitochondria originated from endosymbiosis events and contain their own genomes. However, almost all the mitochondrial and chloroplast proteins are encoded by nuclear genes and have to be imported from the cytosol. Mitochondria and chloroplasts cannot be generated de novo. Instead, they have to be inherited from the parental cells and can only multiply by bacterial-like binary fission (Jarvis and López-Juez, 2013; Carrie et al., 2013). In contrast, peroxisomes do not contain any genetic information, hence, peroxisomal proteins are all nuclear encoded and imported into the organelles from the cytosol after translation. Peroxisomes can propagate through either de novo formation from the endoplasmic reticulum (ER) or peroxisomal fission (Hu et al., 2012).

This chapter focuses on the dynamics of mitochondria and peroxisomes in *Arabidopsis* with respect to protein import and organelle fission.

1.2 Plant mitochondrial protein import machinery

Due to the endosymbiotic origin, mitochondria contain their own genome that encodes proteins as well as rRNA and tRNA (Millar et al., 2008; Friedman and Nunnari, 2014). However, except about 50 proteins, the proteome of mitochondria is almost all encoded by nuclear genes and imported into mitochondria after translation (Millar et al., 2005; Cánovas et al., 2004). The mitochondrial proteome also varies significantly in different tissue types or developmental stages. For example, within ~12-24 hours of seed germination, mature mitochondria emerge from pro-mitochondria that contain no

cristae, with an concurrent increase of mitochondrial metabolic activities (Law et al., 2014; Naydenov et al., 2008; Khanam et al., 2007; Logan et al., 2001; Ehrenshaft and Brambl, 1990; Howell et al., 2006).

Since most mitochondrial proteins have to be imported, the protein import apparatus is a central part of mitochondrial biogenesis (Wiedemann et al., 2004; Dudek et al., 2013; Gebert et al., 2011; Rassow and Pfanner, 2000). A large portion of this apparatus is well conserved across different species. In plants, however, the existence of chloroplasts introduces additional complexities to protein targeting. Hence, plant cells contain some unique factors to maintain the mitochondrial protein targeting specificity against plastid targeting (Duncan et al., 2013). The mitochondrial protein import apparatus comprises protein components located in different sub-compartments of mitochondria, i.e., outer membrane (MOM), inter-membrane space (IMS), inner membrane (MIM) and matrix (Fig. 1.1).

1.2.1 Outer membrane proteins

Translocation of mitochondrial proteins is initiated with the recognition of precursor proteins by the Translocases of the Outer Membrane (TOM). The *Arabidopsis* TOM machinery consists of the conserved proteins TOM40 and METAXIN, as well as plant specific proteins TOM20, TOM9, and OM64 (Fig. 1.1) (Duncan et al., 2013; Braun and Schmitz, 1999).

TOM40 is a β -barrel protein and it functions as the pore forming channel (Lister et al., 2004). Plant TOM20 proteins are C-terminal anchored membrane proteins and function as protein receptors (Rimmer et al., 2011). In normal growth conditions,

disruption of *Arabidopsis* TOM20 functions only causes a little delay in bolting (Lister et al., 2007). TOM9 proteins are considered the orthologs of yeast TOM22, but they are much shorter and lack the cytosolic domain found in yeast TOM22 (Jansch et al., 1998; Macasev et al., 2000). OM64 shows sequence similarities to the plastid receptor TOC64, which does not have growth defects in the *Arabidopsis* null mutant (Lister et al., 2007). *Arabidopsis* mutants deleted for OM64 and all three functional TOM20 proteins are embryonic lethal (Duncan et al., 2013). Thus, TOM20 and OM64 are probably both plant-specific receptors with overlapping functions.

METAXIN is an outer membrane protein important for protein import. It is conserved from mammals to plants. Deletion of *Arabidopsis* METAXIN results in strong plant developmental abnormalities and reduction of protein import. The cytosolic domain of METAXIN interacts with some mitochondrial precursor proteins (Lister et al., 2007). However, the exact role of METAXIN has not yet been clarified.

1.2.2 Proteins in the inter-membrane space

Several protein import factors that are highly conserved across different species are located in the IMS (Carrie et al., 2010b). These include the so-called “tiny TIM” proteins (TIM8, 9, 10 and 13) and MIA40-ERV1 proteins (Fig. 1.1). In yeast, TIM9 and TIM10 form a hexameric chaperone complex, which is essential for yeast viability and the translocation of mitochondrial precursor proteins to the MIM. Moreover, TIM8 and TIM13 also form a chaperone complex (Davis et al., 2007; Koehler et al., 1998; Senapin et al., 2003). The biochemical activity of these *Arabidopsis* TIMs, particularly, TIM9 and

TIM10, was tested in a reconstitution assay, which showed that these TIMs are important for the import of mitochondrial carrier proteins (Lister et al., 2002).

Besides tiny TIMs, the disulfide relay system mediated by MIA40 and ERV1 facilitates the import of IMS located proteins with twin CX(9)C or CX(3)C motifs (Gabriel et al., 2007). Both MIA40 and ERV1 are essential proteins in yeast (Rissler et al., 2005; Chacinska et al., 2004). However, in *Arabidopsis*, only ERV1 is essential. Interestingly, *Arabidopsis* MIA40 is dual localized to mitochondria and peroxisomes. Consistently, MIA40 substrates superoxide dismutase (CSD1) and copper chaperone for SOD1 (Ccs1) are also dual localized to mitochondria and peroxisomes in *Arabidopsis*. This indicates that MIA40 may be involved in the biogenesis of both mitochondria and peroxisomes in *Arabidopsis* (Xu et al., 2013; Carrie et al., 2010a).

1.2.3 Inner membrane proteins

The import of mitochondrial proteins targeted to the MIM and matrix is dependent on the Translocases of the Inner Membrane (TIM). TIM components show better conservation across different species than the TOM components (Carrie et al., 2010b). The imported mitochondrial preproteins associate with either TIM22 or TIM17:23 complexes, after the translocation mediated either directly by the TOM complexes or chaperoned by the tiny TIMs in the IMS (Chacinska et al., 2010). TIM22, TIM17 and TIM23 are pore-forming channel proteins (Chacinska et al., 2009). Other factors such as TIM50, TIM21, mtHSP70, TIM44 and chaperone proteins PAM16 and PAM18, are also associated with the TIM17:23 complexes (Fig. 1.1) (Chacinska et al., 2010; Wagner et al., 2009). Many of these TIM components are highly expressed during

Arabidopsis seed germination and are essential for the viability of the plant (Narsai et al., 2011).

1.2.4 Matrix proteins

After being imported into the matrix, mitochondrial proteins have to be processed to be mature in function. This is mediated by two kinds of peptidases, the Mitochondrial Processing Peptidases (MPP) and the Presequence Peptidase (PrepP) (Fig. 1.1), each having two isoforms in *Arabidopsis* (Kwasniak et al., 2012). MPP cleaves the targeting signal and PrepP degrades the signal peptide after cleavage. Both MPP and PrepP show plant specific features: the *Arabidopsis* MPP has a second function in mitochondrial electron transfer, while PrepP localizes to both mitochondria and chloroplasts (Glaser et al., 2006; Ståhl et al., 2002; Eriksson et al., 1996; Braun et al., 1992).

1.3 Plant peroxisomal protein import machinery

The current model of peroxisome biogenesis is based on the studies from multiple model organisms, especially from yeasts due to the dispensable nature of peroxisomes in yeasts grown in rich media. Peroxisomes are considered semi-autonomous. They can arise through either de novo biogenesis from special ER membrane domains (at least in yeasts and mammals) or fission of existing peroxisomes. ER provides a source for membrane phospholipids and some peroxisome membrane proteins (PMPs) to generate pre-peroxisomes (Schlüter et al., 2006; Mullen and

Trelease, 2006). Pre-peroxisomes need to mature through the import of matrix proteins (Hu et al., 2012).

The core peroxisomal protein import machinery is largely conserved from yeasts to plants and animals. Peroxisome matrix proteins are all imported from the cytosol, mostly using either a C-terminal localized Peroxisome Targeting Signal type 1 (PTS1) or N-terminal localized PTS2 signals (Brocard and Hartig, 2006; Petriv et al., 2004). Several membrane associated peroxins (proteins involved in peroxisome biogenesis) collectively form the protein import apparatus (Fig. 1.2) (Hu et al., 2012). In *Arabidopsis*, peroxisomal matrix proteins are bound to receptors PEX5 or PEX7 prior to peroxisomal entry. PTS1-containing proteins interact with PEX5, while PTS2-containing proteins interact with PEX7 (Lanyon-Hogg et al., 2010). In addition, PEX5 is also required for PEX7 function (Nito et al., 2002). Then the cargo-receptor complexes dock to the import apparatus formed by two membrane proteins PEX13 and PEX14 (Hayashi et al., 2000; Mano et al., 2006). After the translocation of cargo proteins into the matrix, the receptors are recycled back to the cytosol. In yeast, the recycling of PEX5 employs an ubiquitin system, which comprises an ubiquitin-conjugating enzyme PEX4 and three ubiquitin-protein ligases PEX2, PEX10, and PEX12 (Grou et al., 2009). There is no direct evidence for PEX5 ubiquitination in plants, but this ubiquitin-related apparatus is conserved (Fig. 1.2). In *Arabidopsis*, PEX4 is anchored to the membrane by PEX22 (Zolman et al., 2005). Two AAA ATPases PEX1 and PEX6 mediate the departure of PEX5 back to the cytosol (Nito et al., 2007; Zolman and Bartel, 2004). An integral membrane protein APEM9 interacts directly with PEX6 and tether the PEX1-PEX6 complex to the peroxisome membrane (Goto et al., 2011). The knockout mutants of

Arabidopsis PEX2, PEX10, and PEX12 are embryonic lethal (Schumann et al., 2003; Hu et al., 2002; Fan et al., 2005; Sparkes et al., 2003). The precise roles of each peroxins are still obscure and probably more complex than the current model. For example, a mild *pex13* mutant aggravates the *pex5* and *pex14* mutant defects but ameliorates other mutants defected in the recycling of PEX5 (Ratzel et al., 2011). This indicates that maintaining the balance between the import and export of receptors is critical.

1.4 Fission machineries of plant mitochondria and peroxisomes

1.4.1 Shared fission factors between mitochondria and peroxisomes

Mitochondria and peroxisomes both utilize fission to maintain their abundance in the cell and to pass onto subsequent generations. In normal conditions, both mitochondria and peroxisomes appear as numerous discrete small entities in plant cells, indicating that their fission process is very active. As mentioned in the introduction, mitochondria and peroxisomes are metabolically linked. Mitochondrial and peroxisomal dynamics are also strongly linked by sharing of a major part of their fission machineries. The shared fission factors in *Arabidopsis* include Fission1 (FIS1), Dynamin-Related Protein 3 (DRP3), and Peroxisomal and Mitochondrial Division factor1 (PMD1) (Fig. 1.3).

1.4.1.1 DRP3A and DRP3B: dynamic membrane scissors

The core factors of mitochondrial and peroxisomal fission belong to the dynamin-related protein family and are conserved across different kingdoms, e.g., DRP3A and

DRP3B in *Arabidopsis*, hsDRP1 in human and scDNM1 in *Saccharomyces cerevisiae* (Fujimoto et al., 2009; Mano et al., 2004; Aung and Hu, 2012; Zhang and Hu, 2009; Bleazard et al., 1999; Smirnova et al., 2001). These DRPs are large GTPases located in the cytosol before being recruited to the organelles. The crystal structure of hsDRP1 revealed the protein to be composed of a G domain, a bundle signaling element and a stalk (Fröhlich et al., 2013). These large GTPases can form dimers and higher-order complexes. They dynamically localize at the organelle fission sites, form ring-like structure via higher order assembly, and promote membrane fission through assembly-driven and GTP hydrolysis-driven constrictions (Hoppins et al., 2007; Praefcke and McMahon, 2004; Ingeman et al., 2005; Legesse-Miller et al., 2003; Labrousse et al., 1999).

In *Arabidopsis*, DRP3A and DRP3B localize to the tips and fission sites of mitochondria. They also associate with peroxisomes, but with much less frequency. Loss-of-function mutants of DRP3A and DRP3B show significant increase of mitochondrial and peroxisomal length. Hence, DRP3s are very important for the fission of these organelles. Moreover, the organelle fission defects of *drp3A* mutants are much stronger than those of *drp3B* mutants, suggesting that DRP3A functions as the primary peroxisomal/mitochondrial fission DRP in *Arabidopsis* (Zhang and Hu, 2009; Aung and Hu, 2012; Fujimoto et al., 2009; Mano et al., 2004).

1.4.1.2 FIS1A and FIS1B: membrane anchors for DRP3

In *Arabidopsis*, besides DRP3A and DRP3B, two other homologous proteins in the shared fission machinery of mitochondria and peroxisomes are FIS1A and FIS1B

(Zhang and Hu, 2008b, 2009; Lingard et al., 2008). Similar to DRP3, FIS1 proteins are well conserved across different kingdoms (Yoon and Krueger, 2003; James et al., 2003; Karren et al., 2005). FIS1 anchors to the membrane via its C-terminal transmembrane domain with its N-terminal tetratricopeptide repeat (TPR) domain exposed to the cytosol (Tooley et al., 2011; Zhang and Chan, 2007; Koch et al., 2005). The importance of FIS1 proteins in mitochondrial and peroxisome fission is evidenced by organelle fission defects in various FIS1 deficient mutants across different kingdoms (Koch et al., 2005; Kobayashi et al., 2007; Zhang and Hu, 2008b, 2009; Nagotu et al., 2008). In addition, these studies indicate that FIS1 is involved in the recruitment of DRPs from the cytosol to mitochondrial and peroxisome membranes. Interestingly, the *Arabidopsis* FIS1A is also found to localize to chloroplasts (Ruberti et al., 2014). Whether plant FIS1 is involved in the dynamics of chloroplasts is a very interesting question to be answered.

1.4.1.3 Other fission factors shared by mitochondria and peroxisomes

In *Arabidopsis*, the third dual-localized fission factor on mitochondria and peroxisomes is Peroxisomal and Mitochondrial Division factor 1 (PMD1). PMD1 is a plant-specific fission factor, which acts independently from the FIS1-DRP3 complex. PMD1 is a C-terminal anchored membrane protein with multiple coiled-coil domains. PMD1 deficiency results in peroxisomal enlargement and mitochondrial elongation, while PMD1 overexpression increases mitochondrial and peroxisomal abundance and aggregation. PMD1's homolog, PMD2, localizes specifically to mitochondria. The exact roles of PMD1 and PMD2 in plant organelle fission processes remain to be determined (Aung and Hu, 2011).

In the yeast *Saccharomyces cerevisiae*, two homologous proteins MDV1 and CAF4 function as adaptors between scFIS1 and scDNM1. MDV1 and CAF4 physically interact with scFIS1 and scDNM1, as well as themselves. MDV1 and CAF4 each contain an N-terminal extension (NTE) domain with two α -helices, a middle coiled-coil domain (CC) and a C-terminal WD40 repeat region (Tieu et al., 2002; Karren et al., 2005; Schauss et al., 2006; Motley et al., 2008). However, these adaptors do not have apparent homologs in *Arabidopsis* or human.

In metazoans, a coiled-coil domain-containing membrane protein Mitochondrial fission factor (Mff) is tail anchored to both mitochondria and peroxisomes (Gandre-Babbe and Blik, 2008; Otera et al., 2010). In mammals, Mff physically interacts with DRP1 and is a receptor for DRP1 (Otera et al., 2010). Mff does not have apparent homologs in *Arabidopsis* or yeasts, either.

1.4.2 Mitochondrial-specific fission factors

Besides PMD1, DRP3 and FIS1, *Arabidopsis* mitochondrial fission machinery contains a plant-specific fission factor, Elongated Mitochondria1 (ELM1) (Fig. 1.3). Loss-of-function mutants of ELM1 contain extensively elongated mitochondria. ELM1 physically interacts with DRP3 and is involved in the translocation of DRP3 to mitochondria in a FIS1-independent manner (Arimura et al., 2008).

In metazoans, two homologous membrane proteins MiD49 and MiD51 are anchored in the mitochondrial outer membrane, displaying a localization pattern on mitochondria similar to that of mammalian DRP1. Overexpression of MiD49 or MiD51 results in extensive mitochondrial elongation. However, the loss-of-function mutants

were reported with conflicting morphological changes (mitochondrial elongation vs. fragmentation) in different studies (Losón et al., 2013; Zhao et al., 2011; Schuldt, 2011; Palmer et al., 2011a). MiD49 and MiD51 interact with DRP1 and FIS1, both able to mediate the recruitment of DRP1 to mitochondria in the absence of Mff and FIS1 (Losón et al., 2013; Zhao et al., 2011; Schuldt, 2011; Palmer et al., 2011a; Liu et al., 2013). Thus, several proteins are involved in recruiting DRP1 to mitochondria.

1.4.3 Other peroxisomal fission factors

1.4.3.1 PEX11: promoter of peroxisome elongation

In *Arabidopsis*, peroxisome fission is mainly mediated by three evolutionarily conserved families of proteins. These include PEROXIN11 (PEX11), FIS1 and DRP3. Although FIS1-DRP3 complex is shared between mitochondria and peroxisomes, PEX11 function is limited to peroxisomes (Fig. 1.3). PEX11 proteins are integral to peroxisome membrane and mediate peroxisome elongation prior to the action of the FIS1-DRP3 complex. There are five PEX11 proteins (PEX11a to –e), which are classified into three sub-families based on sequence homology, i.e., PEX11a, PEX11b and PEX11c to e. When overexpressed, each PEX11 isoform can induce peroxisome elongation and subsequent increase of peroxisome number. Silencing of these PEX11 proteins causes a reduction of both peroxisome number and size (Orth et al., 2007; Lingard and Trelease, 2006; Lingard et al., 2008). Although individual PEX11 isoforms are partially redundant in peroxisome fission, each of them may still have distinct functions. For example, only two members of the five *Arabidopsis* PEX11 isoforms (i.e.

PEX11d and PEX11e) can complement the yeast *pex11* mutants and confer the yeast null mutant the ability to grow on oleic acid (Orth et al., 2007).

1.4.3.2 DRP5B: a fission factor shared by peroxisomes and chloroplasts

In addition to DRP3A and DRP3B, a third DRP family protein (DRP5B) also localizes to peroxisomes and participates in the fission process (Fig. 1.3) (Zhang and Hu, 2010). There are 16 DRP proteins in the *Arabidopsis* genome, which are classified into 6 subfamilies based on sequence similarities (Hong et al., 2003). DRP5B is a well-known chloroplast fission factor (Gao et al., 2003) distantly related to DRP3A and DRP3B in sequence and only found in plants and algae (Miyagishima et al., 2008). Hence, the involvement of DRP5B in both peroxisome and chloroplast fission process is probably a unique feature of plant and/or algae.

Moreover, even though DRP5B does not associate with mitochondria, the deficiency of DRP5B does cause defects in mitochondrial fission. DRP5B is not a component of the DRP3 higher-order complex (Aung and Hu, 2012). Why mitochondria are elongated in *drp5B* null mutants is unknown. The exact role of DRP5B in peroxisome fission also needs to be determined.

1.5 Lack of identified mitochondrial fusion machinery in plants

Mitochondria are highly tubular and interconnected in typical animal and yeast cells (Chan, 2012), yet highly fragmented in normal plant cells. This suggests that plant mitochondrial dynamics is fission dominant, as opposed to the fusion dominant mitochondrial dynamics in many other eukaryotes.

The molecular mechanism underlying mitochondrial fusion is well characterized in yeast and mammals (Palmer et al., 2011b). Similar to fission, the core of the fusion machinery is also composed of members of the DRP family. The mammalian mitochondrial fusion DRPs are mitofusin 1 and 2 (MFN1/2) on the outer membrane (Eura et al., 2006; Chen et al., 2003) and optic atrophy1 (OPA1) on the inner membrane (Song et al., 2007; Mishra et al., 2014; Ishihara et al., 2006). The corresponding yeast fusion DRPs are FZO1 (Rapaport et al., 1998) and MGM1 (Meeusen et al., 2006; Sesaki et al., 2003; Wong et al., 2000, 2003). Besides the fusion DRPs, other fusion factors have also been characterized in yeast and mammals (Palmer et al., 2011b; Hoppins et al., 2007). In contrast, no plant mitochondrial fusion protein factors have been discovered through either forward or reverse genetics. However, mitochondrial fusion does occur in plants, as revealed by a fluorescence mixing experiment with onion bulb epidermal cells using a mitochondrion-targeted photoconvertible fluorescent protein name Kaede (Arimura et al., 2004a). Mitochondrial fusion in plants is also supported by the observation of reticular mitochondria during G1 to S phase of the cell cycle in *Arabidopsis* shoot apical meristem cells (Seguí-Simarro et al., 2008). Such extensive fusion of mitochondria was detected in cultured protoplasts prior to cell division as well (Sheahan et al., 2005).

1.6 Regulatory mechanisms of mitochondrial dynamics

Mitochondria are very dynamic, being shaped continuously by antagonistic fission and fusion events. The equilibrium of fission and fusion is tuned not only at different developmental stages, but also in stressful environmental and pathological

conditions. To date, the key machineries responsible for mitochondrial dynamics are characterized through extensive studies in various experimental systems, including mammals, yeasts and plants. Moreover, progress has been made on the regulatory mechanisms of mitochondrial fission and fusion. Three types of regulations that contribute significantly to the dynamic nature of mitochondria are discussed in this subchapter: post-translational modifications (PTMs) of mitochondrial fission DRPs, ER-mitochondria interaction, and mitochondrial membrane lipids (Ha and Frohman, 2014; Huang and Frohman, 2009; Chang and Blackstone, 2010; Marchi et al., 2014).

1.6.1 Post-translational regulation of mammalian DRP1

DRPs are the core factors of the fission apparatus. The fission DRPs function in a very dynamic manner. They translocate from cytoplasm to mitochondrial outer membrane, assemble into higher-order ring structure at the fission site, deform and scissor the membrane in a GTP hydrolysis-dependent manner, and relocate back to the cytosol. PTMs of the fission DRPs may modulate multiple aspects of DRP functions, including DRP's dimerization/oligomerization, GTPase activity, localization to and departure from mitochondria, and protein stability. Among all the components of mitochondrial fission and fusion machineries, the mammalian mitochondrial DRP1 is the best characterized with respect to its PTMs, including phosphorylation, SUMOylation, ubiquitination, and S-Nitrosylation (Fig. 1.4) (Palmer et al., 2011b; Chang and Blackstone, 2010).

1.6.1.1 Phosphorylation

Phosphorylation of mammalian DRP1 occurs at different positions, either enhancing or undermining DRP1's fission activity. First, human DRP1 phosphorylation at a conserved serine residue (Ser616) is mediated by the cdk1/cyclin B kinase complex during mitosis (Fig. 1.4) (Taguchi et al., 2007). This phosphorylation is activated by RALA, a small Ras-GTPase and its effector RALBP1, which acts as a scaffold to bring cdk1/cyclin B kinase close to DRP1 and promote DRP1 phosphorylation (Kashatus et al., 2011). Phosphorylated DRP1 contains enhanced ability in mitochondrial fission, possibly assisting the segregation of mitochondria into daughter cell during mitosis.

DRP1 phosphorylation at Ser637 is mediated by cAMP dependent protein kinase A (PKA) (Fig. 1.4), resulting in the inhibition of DRP1's GTPase activity and therefore impaired mitochondrial fission (Chang and Blackstone, 2007; Cribbs and Strack, 2007). This phosphorylation can be reversed by a eukaryotic Ca²⁺/calmodulin-dependent serine/threonine protein phosphatase Calcineurin (Fig. 1.4), which increases mitochondrial associated DRP1 and DRP1's fission activity (Cereghetti et al., 2008). However, in another study, phosphorylation at the same Ser637 site mediated by Ca²⁺/calmodulin-dependent protein kinase I α (CaMKI α) was found to lead to opposite changes of DRP1, i.e. increases in mitochondrial associated DRP1 and its fission activity (Fig. 1.4) (Han et al., 2008). The opposite consequences caused by the phosphorylation of the same residue may suggest the complexity of the regulation of mitochondrial dynamics in different cellular and tissue environments.

1.6.1.2 Ubiquitination

MARCH5 (or MITOL) is a mitochondrial membrane associated ubiquitin E3 ligase in mammals (Nakamura et al., 2006; Yonashiro et al., 2006). MARCH5 physically interacts with the fusion factor MFN2 and the ubiquitinated form of fission factors DRP1 and FIS1 (Nakamura et al., 2006; Yonashiro et al., 2006). MARCH5-mediated ubiquitination of DRP1 is suggested to enhance mitochondrial fission, because silencing of MARCH5 causes disruption of DRP1 distribution and mobility, and hence mitochondrial elongation (Fig. 1.4) (Karbowski et al., 2007).

DRP1 is also ubiquitinated by another ubiquitin E3 ligase named Parkin, which may cause degradation of DRP1 (Fig. 1.4), as DRP1 protein level is increased in Parkin loss-of-function mutants and decreased when exogenous GFP-Parkin is overexpressed (Wang et al., 2011). Furthermore, Parkin mediates the ubiquitination of multiple mitochondrial outer membrane proteins and thus may play multiple roles instead of just the degradation of DRP1 in mitochondrial fission (Chan et al., 2011; Wang et al., 2011).

1.6.1.3 SUMOylation

In addition to ubiquitination, human DRP1 is also covalently modified by the small ubiquitin-like modifier (SUMO) (Harder et al., 2004; Figueroa-Romero et al., 2009). The SUMO1 protein localizes to the mitochondrial fission site and physically interacts with DRP1 (Harder et al., 2004). UBC9, the corresponding SUMO E2 conjugating enzyme, physically interacts with DRP1 (Figueroa-Romero et al., 2009; Harder et al., 2004). A SUMO E3 ligase called MAPL localizes to mitochondrial outer membrane (Fig. 1.4). Overexpression of MAPL, as well as SUMO1 itself, promotes mitochondrial fission via

stabilization of the DRP1 protein (Harder et al., 2004; Neuspiel et al., 2008; Braschi et al., 2009). These studies suggest that SUMOylation positively regulates DRP1 activity.

Similar to ubiquitination, DRP1 SUMOylation can be reversed. SenP5, a SUMO protease, was identified in a suppressor screen, in which overexpression of SenP5 rescued SUMO1-induced mitochondrial fragmentation (Fig. 1.4). Silencing of SenP5 stabilizes DRP1 SUMOylation and induces mitochondrial fragmentation (Zunino et al., 2007), consistent with a positive role of DRP1 SUMOylation in mitochondrial fission. In another study, SenP5 was reported to localize to mitochondria during mitosis. In this case, de-SUMOylation of DRP1 by SenP5 promotes mitochondrial fission, possibly helping to ensure the distribution of the mitochondria to daughter cells in mitosis (Zunino et al., 2009).

SUMOylation is also involved in the regulation of DRP1 in mammalian apoptotic cell death. The activation of Bcl-2-associated X protein (BAX), a pro-apoptotic member of the Bcl-2 protein family, stimulates DRP1 SUMOylation as well as mitochondrial fission (Wasiak et al., 2007). SenP3, another SUMO protease, also mediates DRP1 de-SUMOylation and promotes cell death process after ischemia (Fig. 1.4). Silencing of SenP3 stabilizes DRP1 SUMOylation, blocks DRP1-mediated cytochrome c release, and suppresses caspase-mediated cell death (Guo et al., 2013). As shown above, DRP1 SUMOylation plays multiple roles in mammalian physiology.

1.6.1.4 S-nitrosylation

Protein S-nitrosylation results from the covalent attachment of nitric oxide to the target protein (Hess et al., 2005). Mitochondrial fission in neuronal cells is increased by

nitric oxide treatment (Cho et al., 2009; Barsoum et al., 2006). This increase was suggested to be caused by DRP1 S-nitrosylation at Cys644, which stimulates DRP1's GTPase activity and dimerization (Cho et al., 2009). Additionally, DRP1 S-nitrosylation was detected after the expression of the β -amyloid protein (A β), the main component of the amyloid plaques found in the brains of Alzheimer patients (Nakamura et al., 2010; Barsoum et al., 2006). This induction of DRP1 S-nitrosylation is probably due to nitrosative stress, which was proposed to be stimulated by A β oligomerization (Fig. 1.4) (Cho et al., 2009).

In summary, these findings of post translational regulations of mammalian DRP1 demonstrate the complexity of the regulation of mitochondrial dynamics. The physiological conditions and developmental stages should be taken into consideration when analyzing the functional consequence of a specific post-translational modification. Furthermore, this complexity probably explains why these regulatory mechanisms of mitochondrial fission are hardly conserved across mammals, yeasts and plants.

1.6.2 Post-translational regulation of *Arabidopsis* DRP3

In contrast to the vast amount of information on mammalian DRP1 PTM, our knowledge of the post-translational regulation of *Arabidopsis* DRP3 is very limited. DRP3 phosphorylation has been identified by multiple genome-wide proteomic experiments (Heazlewood et al., 2008; Sugiyama et al., 2008; Durek et al., 2010; Nakagami et al., 2010; Mayank et al., 2012; Wang et al., 2013). For example, phosphorylation at Ser575 on DRP3A was detected by four and at Ser560 on DRP3B by three independent mass spectrometry (MS) studies (Sugiyama et al., 2008;

Nakagami et al., 2010; Wang et al., 2013; Umezawa et al., 2013). DRP3A phosphorylations at Tyr10, Ser13 and Ser787 were identified from auxin-treated root tissue (Zhang et al., 2013), and at Ser787, Ser789, and Ser791 were detected in a phosphoproteomic study conducted on mature *Arabidopsis* pollen grains (Mayank et al., 2012). The consequences of these phosphorylation events have not been determined yet. In addition, DRP3A and DRP3B were reported to undergo mitotic phosphorylation at unidentified sites, which promotes mitochondrial fission during mitosis (Wang et al., 2012).

1.6.3 The role of ER-mitochondria association in regulating mitochondrial fission

An interesting question about mitochondrial fission is how the fission sites in mitochondrial membrane are determined. This question was possibly addressed in yeast with the finding of mitochondria-ER association, which occurs in advance to DRP recruitment (Marchi et al., 2014). ER tubules were first found to associate with mitochondria with a GFP-based approach (Rizzuto et al., 1998). Further, using electron microscopy and tomography, ER tubules were shown to associate with mitochondria and wrap around the mitochondrial fission sites in yeast (Friedman et al., 2011). When ER tubules circle around the mitochondrial membranes, mitochondrial diameter appears to be reduced (from ~210nm to ~140nm, *Saccharomyces cerevisiae*), which was further confirmed by a two-color STORM super-resolution approach (Shim et al., 2012). As such, ER-mitochondria association might contribute to the initiation of mitochondrial fission.

The ER-mitochondria interaction probably alters mitochondrial membrane lipid composition and/or membrane structure, which may help to recruit fission factors inside and/or outside mitochondria. In support of this idea, it was proposed that in mammalian cells, the ER-localized protein Inverted Formin 2 (INF2) mediates the initial mitochondrial constriction through actin polymerization (Korobova et al., 2013). However, ER-mitochondria association has not been reported in plants yet.

1.6.4 The impact of membrane lipids on mitochondrial dynamics

As described above, the key protein factors that regulate mitochondrial dynamics, especially mitochondrial fission, have been well characterized. Significant progress has been made to investigate the PTMs of key protein factors. The roles of diverse membrane lipids in regulating mitochondrial dynamics are beginning to be discovered, too. Lipids can play structural roles in membrane remodeling process, such as the formation of negative membrane curvature, as shown in the fusion of secretory vesicles to plasma membrane (Donaldson, 2009; Vitale et al., 2001; Vicogne et al., 2006; Huang et al., 2005). When exposed on the surface of membranes, lipids may directly interact with proteins, recruiting proteins to the membranes or affecting protein activities (Guo et al., 2007; Huang et al., 2011; Montessuit et al., 2010).

1.6.4.1 Cardiolipin

Cardiolipin (CL) is a dimeric anionic phospholipid that contains a triple glycerol backbone and four acyl groups. It is considered the signature lipid of mitochondria due to its exclusive presence in mitochondria in mammals and yeasts. CL promotes fusion

of the mitochondrial inner membrane through its interaction with the fusion factor MGM1 (a DRP) in yeast (DeVay et al., 2009; Joshi et al., 2012a). The enzymatic processing of MGM1 to generate short isoform of MGM1 (s-MGM1) is dependent on CL. The dimerization and GTPase activity of s-MGM1 is also stimulated by its interaction with CL (Rujiviphat et al., 2009).

In mammalian cells, CL also plays a role in mitochondrial fission by interacting with α -Synuclein, a Parkinson's disease-related protein that promotes mitochondrial fission, by recruiting α -Synuclein to the mitochondrial membrane (Nakamura et al., 2011). Despite the findings of opposite roles of CL in mitochondrial fission and fusion processes, CL appears to be mostly a pro-fusion factor. This is evidenced by the mitochondrial fragmentation caused by CL deficiency in yeast cells lacking UPS1, a positive regulator of CL level (Joshi et al., 2012a).

Besides its role in mitochondrial dynamics, CL is also important in energy metabolism, mainly by stabilizing individual proteins and protein complexes in the mitochondrial electron transport chain (Paradies et al., 2013; Houtkooper and Vaz, 2008). In addition, CL has crucial roles in mammalian apoptosis. CL binds to cytochrome c on the mitochondrial inner membrane in normal conditions. In apoptosis, CL peroxidation contributes to cytochrome c dissociation from the inner membrane. By recruiting and activating pro-apoptotic Bcl-2 family proteins, CL participates in mitochondrial outer membrane permeabilization (MOMP), which leads to the release of cytochrome c and other apoptogenic factors from mitochondria (Paepe et al., 2014; Gonzalez and Gottlieb, 2007). Therefore it appears that CL has multiple roles in

mitochondrial metabolism in mammal and yeast. The roles of CL in plant energy metabolism and stress response are just beginning to be uncovered (see Chapter 2).

1.6.4.2 Phosphatidylethanolamine

Phosphatidylethanolamine (PE), another major lipid of mitochondrial membranes, is also important for mitochondrial fusion. In yeast, PE deficient cells contain fragmented mitochondria with impaired mitochondrial fusion. In a liposome fusion assay, a reduction in PE caused insufficient lipid mixing. Hence, PE deficiency probably alters the biophysical properties of the mitochondrial membrane and reduces membrane fusion kinetics (Tasseva et al., 2013; Chan and McQuibban, 2012). PE deficiency also reduces the generation of s-MGM1, a protein important for mitochondrial fusion (Chan and McQuibban, 2012), suggesting that PE regulates mitochondrial fusion in two aspects - membrane biophysical properties and MGM1 processing.

Combination of CL and PE deficiency in yeast results in stronger morphological defects of mitochondria, including stronger fragmentation. This means PE and CL may have overlapping functions in promoting mitochondrial fusion (Chan and McQuibban, 2012). Yeast cells lacking either CL or mitochondrial PE are viable, but a combination of the two is lethal, indicating that the overlapped functions of CL and PE are essential (Gohil et al., 2005). Loss-of-function mutants of some proteins involved in CL metabolism, such as UPS1 and UPS2 (two homologous mitochondrial intermembrane space proteins) and TAZ1 (a CL-specific transacylase enzyme) have abnormal levels of both CL and PE (Sesaki et al., 2006; Tamura et al., 2009; Xu et al., 2005), indicating

that both the metabolisms and functions of these two non-bilayer forming lipids are related.

1.6.4.3 Phosphatidic acid and diacylglycerol

Similar to CL, phosphatidic acid (PA) is a negatively charged and cone-shaped phospholipid. PA induces the formation of negative membrane curvature, making it an important structural lipid (Kooijman et al., 2003; Ammar et al., 2013). PA can be generated by Mitochondrial surface Phospholipase D (MitoPLD) through the cleavage of CL (Baba et al., 2014; Huang et al., 2011; Choi et al., 2006). It can also be generated from lyso-PA (LPA) by LPA acetyltransferase (Guo et al., 2007). PA is converted to LPA by the PA-preferring phospholipase A1 (PA-PLA1) and to diacylglycerol (DAG) by the PA phosphatase Lipin 1b (Huang et al., 2011; Baba et al., 2014).

Multiple lines of evidence demonstrate a role of PA in mitochondrial fusion process. Overexpression of MitoPLD in mammalian cells causes aggregated and enlarged mitochondrial, similar to the effect of overexpressing a key fusion factor MFN1 (Choi et al., 2006). Silencing of MitoPLD and overexpression of its dominant negative form both induce mitochondrial fragmentation (Choi et al., 2006; Mulyil et al., 2011). Consistently, Overexpression of PA-PLA1 and Lipin 1b induce mitochondrial fission, while their functional disruption leads to elongation (Huang et al., 2011; Baba et al., 2014). The mechanism of PA in mitochondrial fusion is not clear. One possibility is that PA functions through MFN1/2. This is supported by the fact that MitoPLD overexpression cannot promote mitochondrial aggregation when MFN1 and MFN2 are silenced (Chen et al., 2003).

The product of PA dephosphorylation by Lipin 1b is DAG, which is a pro-fission lipid (Huang et al., 2011). The exact role of DAG in the fission process is not clear. However, the roles of DAG in membrane fission events are dissected for other organelles. DAG is important for the recruitment of VPS1, a yeast mitochondrial and peroxisomal fission DRP, to the peroxisomal membrane, and for protein kinase D (PKD) to golgi membrane (Guo et al., 2007; Bossard et al., 2007). These findings may help understanding how DAG regulates mitochondrial fission.

1.7 Regulatory mechanisms of peroxisomal dynamics

Control of peroxisome dynamics by protein post-translational modifications or membrane lipids is much less known. The mitochondrial and peroxisomal DRP proteins in mammals and plants are both regulated by post-translational modifications, which alter their activity in mitochondrial fission. However, if and how these DRP PTMs impact peroxisomal dynamics are still unknown.

In yeast cells, phosphorylation of PEX11 provides a regulatory mechanism for peroxisome fission. In *Saccharomyces cerevisiae*, scPEX11 is phosphorylated at Ser165 and/or Ser167 to promote peroxisome proliferation. The translocation of scPEX11 from ER to peroxisomes is phosphorylation dependent. A cyclin-dependent kinase Pho85 probably mediates this phosphorylation event, as its overexpression stimulates hyperphosphorylation of scPEX11 and peroxisome proliferation (Knoblach and Rachubinski, 2010). In addition, scPEX11 is an in vitro target of Pho85 (Ptacek et al., 2005). In *Pichia pastoris*, ppPEX11 is phosphorylated at Ser173, a different phosphorylation site from that of scPex11p. This phosphorylation is not required for the

translocation of ppPEX11 from ER to peroxisomes, but instead is required for the interaction between ppPEX11 and ppFIS1 (Joshi et al., 2012b). Taken together, these observations in yeast studies demonstrate that the peroxisome fission machinery is indeed regulated at post-translational level. In human cells, the phosphorylation of PEX11 β was also reported in a phosphoproteomic study (Rikova et al., 2007). These phosphorylated residues of yeast PEX11 proteins are not conserved in plants, and whether PEX11 phosphorylation occurs in plants is unknown.

A study in *Penicillium chrysogenum* indicates the association of pcPEX11's function with membrane lipids. The N-termini of PEX11 orthologs contain a conserved amphipathic helix, and the presence of negatively charged phospholipids in liposomes is necessary for pcPEX11's amphipathic helix to induce membrane tubulation (Opaliński et al., 2011). To date, how membrane lipids affect peroxisomal fission machinery functions is still very obscure. But given the importance of membrane lipids in mitochondrial dynamics and the shared fission machinery between these two organelles, it is not unreasonable to speculate that lipids also play critical roles in peroxisome membrane remodeling processes.

1.8 Aims of this dissertation research

In plants, the major protein factors responsible for the dynamics of chloroplasts, mitochondria and peroxisomes, including their fission and protein import processes, have been identified. However, the regulatory mechanisms of the function of these major factors are just beginning to be elucidated. This dissertation research aims to deepen the understanding of the regulation of the dynamics of these key energy

organelles in the plant model system *Arabidopsis thaliana*, focusing on the roles of protein post-translational modifications and membrane lipids. Post-translational modifications of major protein factors provide a quick and direct way to adjust their activities. Phospholipids play structural roles in organelle dynamics by changing the biophysical properties of the membrane, and directly participate in protein-membrane interactions, thus likely to affect multiple aspects of proteins, such as protein association with the membrane, protein complex formation, enzyme activity and even correct formation of protein's three-dimensional structure.

In chapter 2, I focused on CL, a negatively charged non-bilayer forming phospholipid. CL localizes to poles and fission sites of bacterial membranes, and is related with bacterial fission (Renner and Weibel, 2011; Kawai et al., 2004; Lenarcic et al., 2009; Doan et al., 2013). The distribution pattern of CL on bacterial membranes resembles that of mitochondrial fission DRP on mitochondrial membranes. In eukaryotic cells, CL predominantly localizes to mitochondria (Osman et al., 2011), but was also reported to localize to peroxisomes in *Pichia pastoris* (Wriessnegger et al., 2007). Hence, I speculated that CL may be another dual fission factor for mitochondria and peroxisomes. In this chapter, I analyzed the subcellular distribution of CL and Cardiolipin Synthase (CLS), and the targeting signal, membrane topology and loss-of-functions mutants of CLS. CL's role in plant stress response was also investigated. The studies in chapter 3 and 4 are part of our group's efforts to uncover post-translational modifications involved in the regulation of plant energy organelle dynamics. I focused on ubiquitination, which was recently shown to regulate the dynamics of plant chloroplasts and peroxisomes (Ling et al., 2012; Lingard et al., 2009; Kaur et al., 2013). However, no

ubiquitin-related proteins had been identified in plant mitochondria. I started with a search for components of the mitochondrial associated ubiquitin system, including ubiquitin E3 ligases and ubiquitin-specific proteases. In chapter 3, I identified a mitochondrial outer membrane associated ubiquitin-specific protease, UBP27, and characterized its membrane topology, targeting signal, enzymatic activity, and loss- and gain-of-function mutants. UBP27's possible involvement in DRP3' mitochondrial association was also revealed. In chapter 4, I identified a small family of RING domain-containing proteins, namely SP1, SPL1 and SPL2, analyzed their subcellular localization, and preliminarily characterized the targeting signal, membrane association and loss-of-function and gain-of-function mutant phenotypes of these RING domain proteins. The dual or triple localization of these proteins in peroxisomes, mitochondria and chloroplasts and their distinct mutant phenotypes render the SP1/SPL1 family members potential coordinators of the dynamics of chloroplasts, mitochondria and peroxisomes.

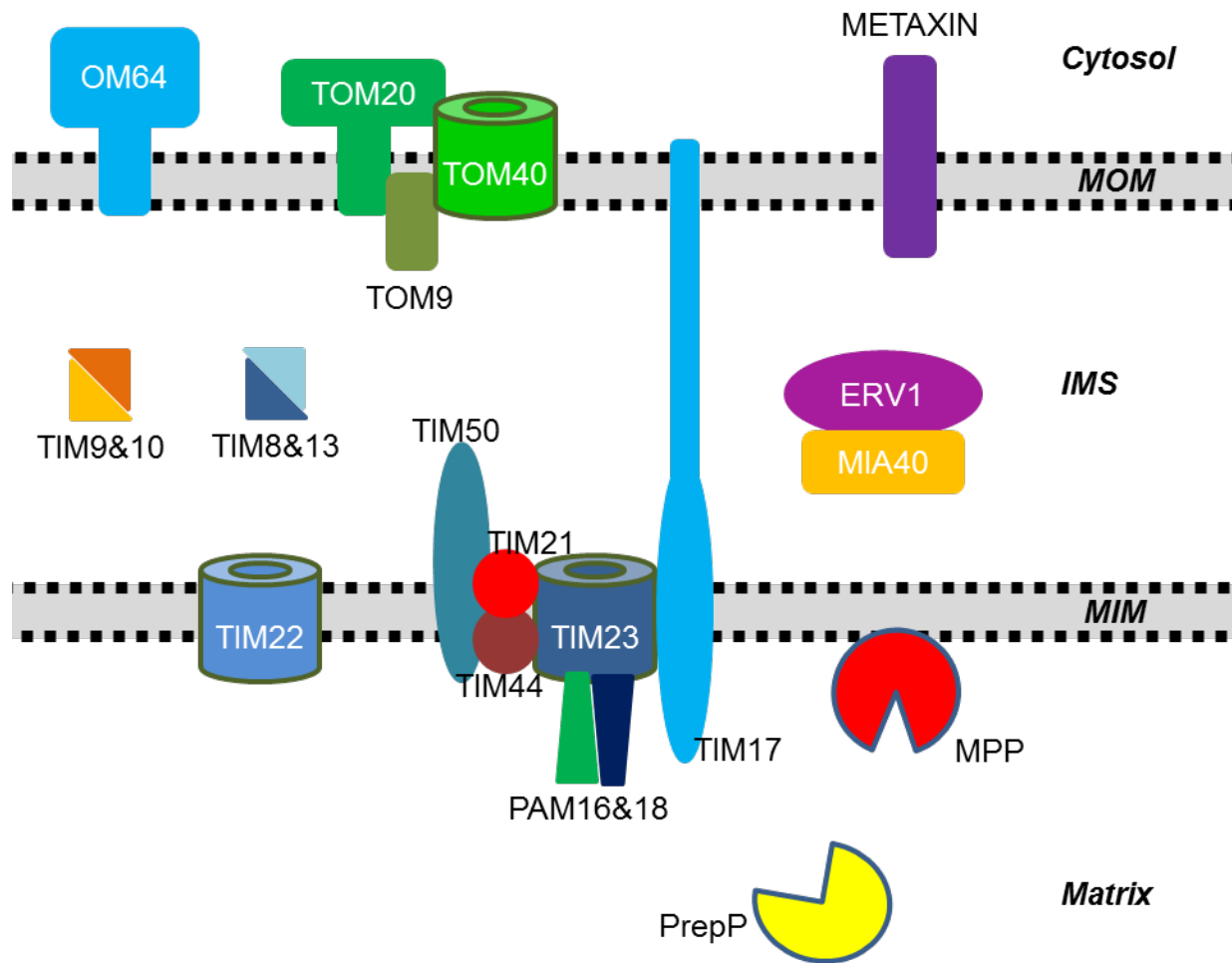


Figure 1.1. The mitochondrial protein import apparatus in plants.

Plant mitochondrial protein import apparatus contains both conserved and plant-specific components. The plant-specific components are TOM20, TOM9, OM64 and TIM17. TOM, translocase of the outer mitochondrial membrane; TIM, translocase of the inner mitochondrial membrane; PAM, presequence translocase associated motor; MOM, mitochondrial outer membrane; IMS, inter-membrane space; MIM, mitochondrial inner membrane; MIA, mitochondrial inter membrane space import and assembly; ERV, essential for respiration and vegetative growth; MPP, mitochondrial processing peptidase; PreP, presequence protease.

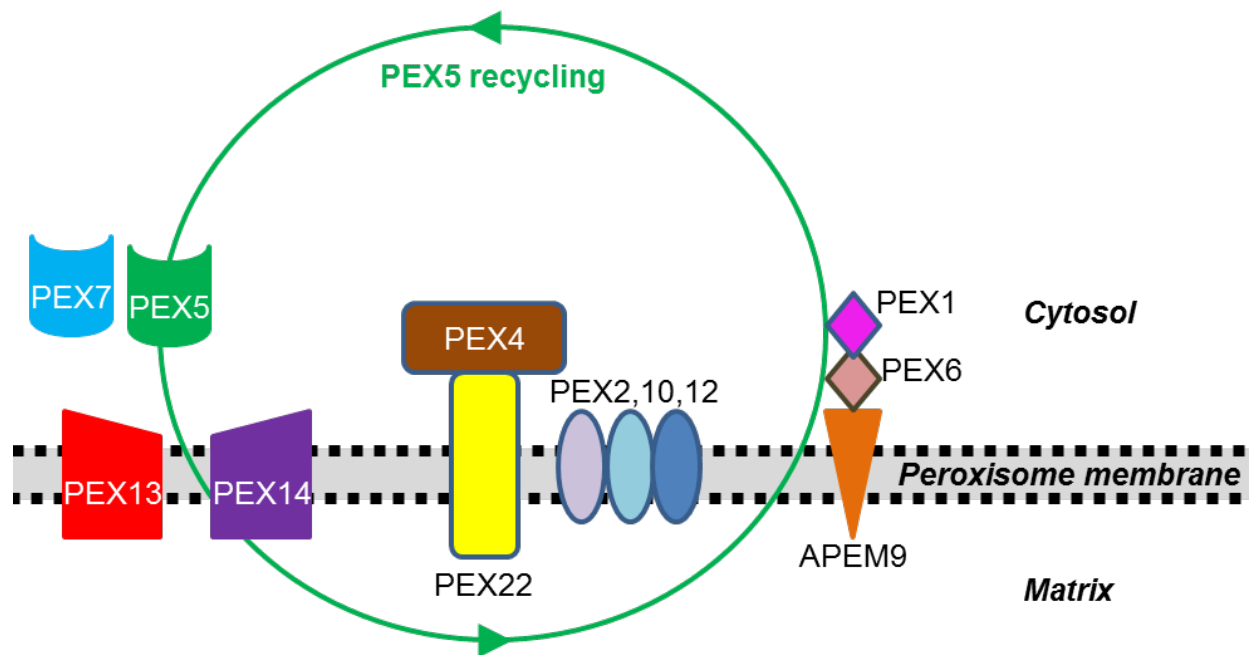


Figure 1.2. The *Arabidopsis* peroxisomal matrix protein import machinery.

Peroxin5 (PEX5) and PEX7 are cytosolic receptors for cargo proteins. The cargo-receptor complexes dock to the import apparatus formed by two membrane proteins PEX13 and PEX14. After cargo release, the receptors can be recycled. In the yeast *Saccharomyces cerevisiae*, PEX5 are recycled via an ubiquitin system, which comprises an ubiquitin-conjugating enzyme PEX4 and three ubiquitin-protein ligases PEX2, PEX10, and PEX12; whether PEX5 is the target of this system has not been shown in plants. PEX4 is anchored to the membrane by PEX22. The departure of ubiquitinated PEX5 back to the cytosol is mediated by the AAA ATPases PEX6 and PEX1, which are tethered by APEM9. The recycling process of PEX7 is still unclear.

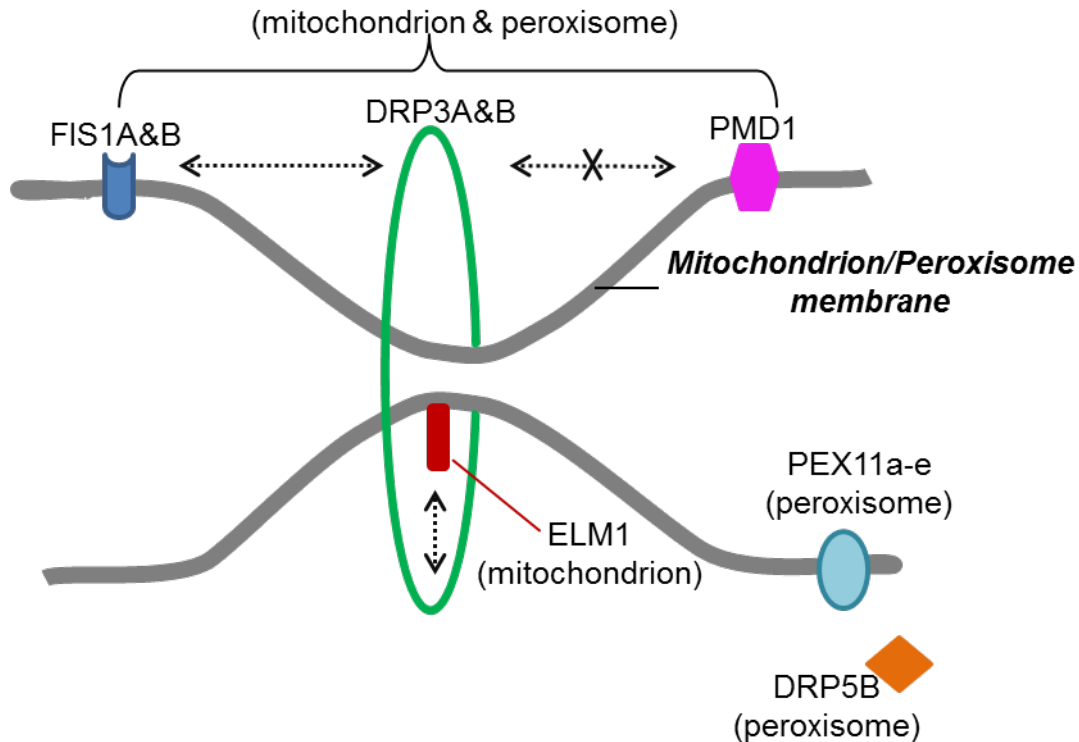


Figure 1.3. Proteins responsible for mitochondrial and peroxisomal fission in *Arabidopsis*.

Dynamamin-related protein 3A (DRP3A) and DRP3B are large GTPases and assemble into ring structures at the organelle fission sites. FISSION1A (FIS1A) and FIS1B are C-terminal anchored membrane proteins possibly responsible for DRP3 recruitment to the organelles. PMD1 functions independently of the FIS1-DRP3 complex. DRP3, FIS1 and PMD1 are shared between mitochondria and peroxisomes. Besides, Elongated Mitochondria 1 (ELM1) is a mitochondrial specific fission factor involved in DRP3 recruitment to mitochondria. PEROXIN11 (PEX11) regulates peroxisome elongation prior to fission. Dashed lines with arrows indicate protein interaction and lines with a cross indicate no protein interaction.

● phosphorylation ● SUMOylation ● ubiquitination ○ S-nitrosylation

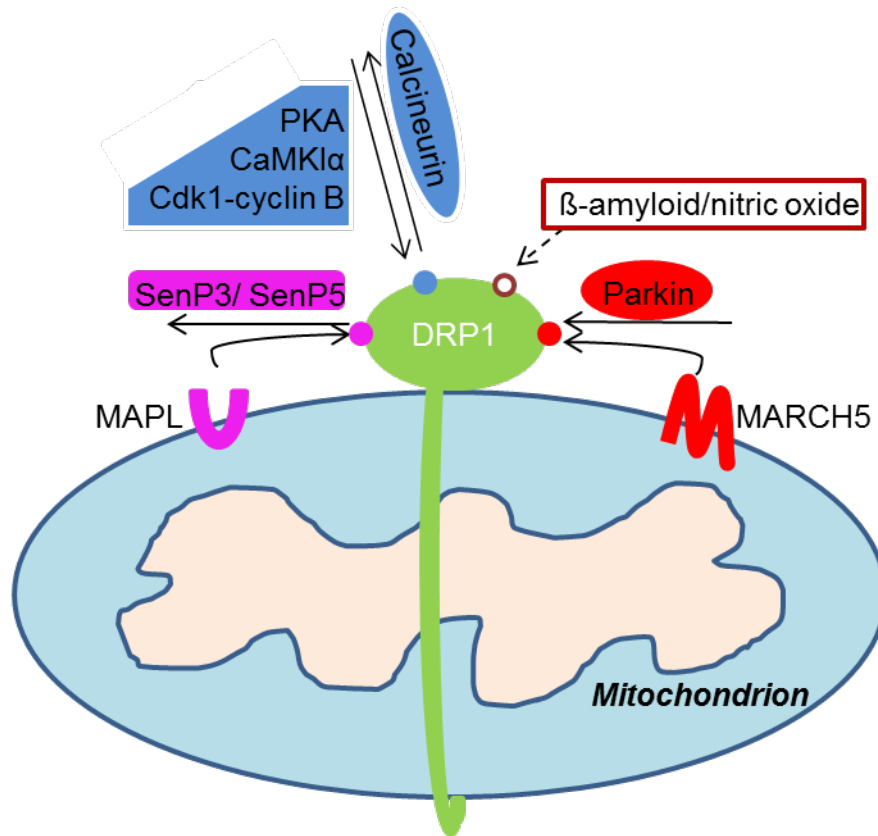


Figure 1.4. Post-translational regulation of mammalian Dynamin-Related Protein1 (DRP1).

Mammlian DRP1 is a target of phosphorylation, ubiquitination, SUMOylation and S-nitrosylation. Phosphorylation is carried out by different enzymes, including cAMP dependent protein kinase A (PKA), Ca^{2+} /calmodulin-dependent protein kinase α (CaMK1 α) and cdk1/cycling B kinase, whereas dephosphorylation is performed by Calcineurin. DRP1 ubiquitination is mediated by ubiquitin E3 ligases Parkin and MARCH5. A SUMO E3 ligase MAPL SUMOylates DRP1. Two SUMO proteases can deSUMOylate DRP1. DRP1 S-nitrosylation occurs during nitric oxide treatment or with the expression of the β -amyloid protein.

CHAPTER 2

Cardiolipin-mediated mitochondrial dynamics and stress response in *Arabidopsis*

The work presented in this chapter has been published:
Ronghui Pan, A. Daniel Jones, and Jianping Hu. (2014)
The Plant Cell 26: 391–409.
doi:10.1105/tpc.113.121095.

2.1 Abstract

Mitochondria are essential and dynamic organelles in eukaryotes. Cardiolipin (CL) is a key phospholipid in mitochondrial membranes, playing important roles in maintaining the functional integrity and dynamics of mitochondria in animals and yeasts. However, CL's role in plants is just beginning to be defined. In this study, we used *Arabidopsis thaliana* to examine the subcellular distribution of CL and cardiolipin synthase (CLS), and to analyze the loss-of-function *cls* mutants for mitochondrial morphogenesis and stress response. We show that CL localizes to mitochondria and is enriched at specific domains, and CLS targets to the inner membrane of mitochondria with its C terminus in the intermembrane space. Further, *cls* mutants exhibit markedly impaired growth, and altered structural integrity and morphogenesis of mitochondria. In contrast to animals and yeasts, in which CL's impact on mitochondrial fusion is more profound, plant CL plays a dominant role in mitochondrial fission and exerts this function, at least in part, through stabilizing the protein complex of the major mitochondrial fission factor, dynamin-related protein 3 (DRP3). CL also participates in plant response to heat and extended darkness - stresses that induce programmed cell death (PCD). Our study has uncovered conserved and plant-specific aspects of CL biology in mitochondrial dynamics and plant response to environmental stresses.

2.2 Introduction

Mitochondria are essential and dynamic organelles that house diverse biochemical pathways in energy production, metabolism, and signaling (Jacoby et al., 2012). To maintain optimal biochemical activities, mitochondria remodel their morphology and function in response to developmental and environmental cues and use continual fission and fusion as an efficient quality control mechanism. Mitochondrial fission and fusion are two topologically opposite but molecularly similar processes that both involve comparable steps of lipid bilayer remodeling, such as local disruption, bending, and bridging (Palmer et al., 2011b). Thus, it is not surprising that Dynamin-like GTPases (DRPs) are at the core of both mitochondrial fusion and fission machines (Chan, 2012). In contrast to typical animal and yeast cells, in which mitochondria are highly tubular and interconnected, normal plant cells contain fragmented and discrete mitochondria, indicating the dominance of mitochondrial fission in plants as opposed to fusion in many other eukaryotes (Logan, 2010). *Arabidopsis* possesses conserved and plant-specific mitochondrial fission factors, including the homologous DRP3A and DRP3B proteins that play dual roles in mitochondrial and peroxisomal fission (Hu et al., 2012). However, neither organelle fusion DRPs nor other components of the mitochondrial fusion apparatus have been identified in plants. Plant mitochondria do fuse, which may indicate the existence of a weak and plant-specific mitochondrial fusion machinery (Logan, 2010).

Cardiolipin (CL) is a key component of both prokaryotic and eukaryotic membranes, with unique structure and functions (Lewis and McElhaney, 2009). It is an anionic phospholipid with a dimeric structure, and contains a triple glycerol backbone

and four acyl groups, most of which are highly unsaturated. CL's acyl chain composition is quite simple, as almost all acyl chains in animal CL are composed of 18-carbon fatty acids, 80% of which being linoleic acid [18:2 (n-6)] (Schlame et al., 2005). This feature is rather unusual, because most other phospholipids, including CL's precursor PG, do not show an obvious preference for specific fatty acids. Although it is unknown how the acyl chain preference is determined in CL biosynthesis, the simple composition of acyl chains in CL apparently leads to a high degree of structural uniformity and molecular symmetry, which may facilitate the assembly of organized membrane domains and enhance the stability of mitochondrial membrane protein homodimers (Schlame et al., 2005).

In bacteria, CL-enriched membrane domains (CMDs) localize at the negatively-curved regions of the cell membrane, such as the poles of *Escherichia coli* (Renner and Weibel, 2011) and the septa of *Bacillus subtilis* undergoing spore formation, where decreasing CL levels causes reduced rate of sporulation (Kawai et al., 2004). CMDs also co-localize with *E. coli* cell division proteins like DivIVA and MinD (Lenarcic et al., 2009; Renner and Weibel, 2012), and facilitate the function of the cell fission protein FisB in *B. subtilis* (Doan et al., 2013). In eukaryotes, although the exact distribution pattern of CL on mitochondria has not been fully characterized, biochemical analysis revealed that ~75% of total CL localizes in the mitochondrial inner membrane and ~25% are in the outer membrane (Osman et al., 2011).

In yeast and animals, CL promotes mitochondrial fusion by affecting the enzymatic processing and/or aggregation of fusion DRPs (DeVay et al., 2009; Tadato et al., 2010; Joshi et al., 2012a). CL tends to concentrate in curved membrane regions,

promoting the formation of hexagonal membrane structures, which can be the intermediate state of double membrane in fission and fusion (Ortiz et al., 1999). However, under reduced CL levels caused by deletion of a positive regulator of CL, yeast mitochondria are more fragmented, indicating a stronger impact of CL on mitochondrial fusion (Tamura et al., 2009). In addition, CL contributes to the bioenergetics and biogenesis of mitochondria in animals and yeasts by enhancing the organization, stabilization, and/or activity of several protein complexes involved in respiration and protein import (Osman et al., 2011). CL also regulates the early events of apoptotic programmed cell death (PCD) in animals by providing an activating platform for Bcl-2 family proteins, factors required for inducing outer membrane permeabilization, which leads to the release of mitochondrial cytochrome c and other proapoptotic molecules (Lutter et al., 2000; Kuwana et al., 2002; Kagan et al., 2005; Gonzalez and Gottlieb, 2007; Montessuit et al., 2010). In humans, changes in CL levels can cause various pathological conditions, including Barth syndrome, aging, and heart failure (Chicco and Sparagna, 2007).

A previous study in the yeast *Pichia pastoris* discovered CL to constitute 2-4% of the phospholipids in peroxisomal membranes (Wriessnegger et al., 2007), raising the possibility that CL may also be involved in the dynamics and function of peroxisomes, essential organelles linked to mitochondria through metabolism and sharing fission DRPs with mitochondria (Schrader and Yoon, 2007; Hu et al., 2012). This finding, together with the distinct morphology of plant mitochondria from that of animals and yeasts prompted us to investigate CL's role in the dynamics of mitochondria and possibly other organelles in plants. In addition, although the well characterized protein

machinery that controls apoptosis in animals is not conserved in plants, plants possess caspase-like activities and Bcl-like proteins (Lord and Gunawardena, 2012). Plant programmed cell death (PCD) is a highly regulated cell death process that shares some morphological hallmarks with apoptosis, such as increased number of vesicles, cytoplasmic condensation, plasma membrane shrinkage, DNA fragmentation, and cytochrome *c* release (Gadjev et al., 2008). However, plant PCD network is poorly characterized at the molecular level. To this end, it was important to investigate CL's role in plant stress responses as well.

Recent studies of the *Arabidopsis* cardiolipin synthase (CLS) T-DNA insertion mutants demonstrated defects of the mutants in embryo development, growth and reproduction, mitochondrial ultrastructure and respiratory function, and protoplast response to UV light and heat shock stresses (Katayama and Wada, 2012; Pineau et al., 2013). In this study, we investigated the role of CL in mitochondrial dynamics, especially fission, and explored CL's function in stress response at the whole organism level. Subcellular distribution of CL and targeting and membrane topology of cardiolipin synthase (CLS) were determined, and *Arabidopsis cls* T-DNA mutant and artificial microRNA lines were characterized for defects in mitochondrial morphology and plant response to stresses that induce PCD. Our study revealed novel aspects of CL biology in organelle dynamics and plant stress response.

2.3 Results

2.3.1 Mitochondrial localization of CL and CLS in plant cells

To understand the role of CL in plant organelle dynamics, we first determined the subcellular distribution of CL and explored the possibility that it may also be present in other organelles such as peroxisomes. *Arabidopsis* seedlings containing a mitochondrial marker (*Saccharomyces cerevisiae* COX4-Yellow Fluorescent Protein or COX4-YFP) (Nelson et al., 2007) or a peroxisomal marker (YFP-Peroxisomal Targeting Signal 1 or YFP-PTS1) (Fan et al., 2005) were stained with the CL-specific fluorescent dye, 10-*N*-nonyl-acridine orange (NAO) (Mileykovskaya and Dowhan, 2000; Kawai et al., 2004; Kaewsuya et al., 2007; Renner and Weibel, 2011), which gives consistent and specific staining patterns under our experimental conditions. Confocal laser scanning microscopic analysis showed that, whereas peroxisomes were negatively stained for NAO, all fluorescent signals co-localized with the mitochondrial marker (Fig. 2.1A). Somewhat similar to the polar distribution of CL on bacterial cell membranes (Kawai et al., 2004; Renner and Weibel, 2011), CL was particularly enriched at specific domains in mitochondria, a pattern that was obvious in both wild type the *drp3A-2 drp3B-2* double mutant that contained extremely elongated mitochondria (Zhang and Hu, 2009; Aung and Hu, 2012) (Fig. 2.1A, 2.1B). We concluded that in plants, CL localizes primarily, if not exclusively, to mitochondria and is enriched at specific mitochondrial regions, the CL-enriched mitochondrial domains (CMDs).

To further examine the distribution and biosynthesis of CL in plants, we analyzed the subcellular localization of cardiolipin synthase (CLS), which is conserved in diverse eukaryotic species (Fig. 2.2A). *Arabidopsis* CLS (At4g04870) is capable of catalyzing CL synthesis from cytidinediphosphate-diacylglycerol (CDP-DAG) and phosphatidylglycerol (PG) in *E.coli*, and CLS^{N terminus}-GFP localized to mitochondria in

onion epidermis (Katayama et al., 2004; Nowicki et al., 2005). To get a complete view of CLS localization, full-length CLS fused with a C-terminal YFP-Hemagglutinin (HA) tag was expressed under the 35S constitutive promoter in *Arabidopsis* plants containing the organelle marker COX4-Cyan Fluorescent Protein (COX4-CFP) or CFP-PTS1 (Aung and Hu, 2011). Confocal microscopic analysis showed that CLS-YFP-HA overlapped completely with the mitochondrial marker but not the peroxisomal marker (Fig. 2.1C). In contrast, CLS fused to an N-terminal YFP (YFP-CLS) was diffused in the cytosol when expressed in tobacco (*Nicotiana tabacum*) leaves (Fig. 2.1D), proving that the N terminus is vital for organelle targeting of CLS. Immunoblot analysis of proteins from tobacco plants expressing the cytosolic YFP-CLS protein or the mitochondrial CLS-YFP-HA protein detected the former as a single band, while the latter appeared as two bands, one of which was slightly smaller than the full-length protein (Fig. 2.3A). After fractionation by several centrifugation steps, only the smaller band was detectable in the pellet fraction enriched in mitochondria (Fig. 2.3B). These data suggested that an N-terminal signal peptide was cleaved from the CLS precursor of the mitochondrial localized CLS-YFP-HA, which is consistent with the target peptide processing mechanism for many mitochondrial inner membrane proteins (Teixeira and Glaser, 2013).

Although the catalytic domain is well conserved, the N-terminal region of plant CLS homologs is divergent from those in non-plant CLS sequences (Fig. 2.2B, 2.2C). To dissect this plant-specific region, we made a series of CLS deletion constructs (Fig. 2.4A) and transiently expressed the 35S-driven truncated CLS-YFP proteins together with COX4-CFP in tobacco. Confocal microscopic analysis revealed that, as predicted,

mitochondrial targeting signals reside at the N terminus, as the C terminus of CLS (CLS¹⁴¹⁻³⁴¹) mis-targeted the fusion protein to compartments such as the plasma membrane, ER and Golgi (Fig. 2.4B, 2.4C). Interestingly, two separate regions at the N terminus seemed to contain mitochondrial targeting signals. Signal 1 (aa 1-20) was sufficient to target the protein to mitochondria. However, when signal 1 was deleted, signal 2 (aa 42-140) could direct the protein to both mitochondria and chloroplasts (Fig. 2.4B). Since both signals are fairly well conserved in plant CLS sequences (Fig. 2.4C), they may represent plant-specific targeting mechanisms for CLS and possibly some other proteins as well, although further investigations will be needed to clearly address this aspect of targeting *in planta*.

2.3.2 Membrane association and topology of CLS

In animals and yeasts, CL biosynthesis occurs in the mitochondrial inner membrane (Osman et al., 2011), but the membrane topology of the key enzyme CLS was unknown. To address this issue, mitochondria were isolated from transgenic plants co-expressing CLS-YFP-HA and COX4-YFP, and the purity of mitochondria was determined by immunoblot analysis using organelle-specific antibodies (Fig. 2.5A). The presence of CLS-YFP-HA fusion protein in mitochondria was confirmed by its detection with the GFP antibody (Fig. 2.5A). After treatments with TE, high concentrations of salt (NaCl), and Na₂CO₃, CLS-YFP-HA was detected in the pellet after each treatment, suggesting that CLS is indeed a mitochondrial integral membrane protein (Fig. 2.5B).

We further dissected the localization and topology of CLS by performing protease protection assays with thermolysin, which degrades proteins on the surface of the

organelles, and trypsin, which can access the intermembrane space. For the controls, the outer membrane protein YFP-PMD1 was digestible by both proteases, whereas the inner membrane protein COXII and the matrix protein COX4-YFP were protected from both enzymes (Fig. 2.5C and 2.5D). CLS-YFP-HA was resistant to thermolysin but digestible by trypsin (Fig. 2.5C and 2.5D), favoring a topology in which CLS is anchored to the mitochondrial inner membrane with its C terminus facing the intermembrane space (Fig. 2.5E).

2.3.3 Disruption of CLS leads to defects in mitochondrial structure and fission

The localization pattern of NAO-stained CMDs shared some similarities with those of the mitochondrial/peroxisomal fission proteins DRP3A and DRP3B, i.e., at the tips and fission sites of the organelles (Arimura and Tsutsumi, 2002; Arimura et al., 2004a; Mano et al., 2004; Zhang and Hu, 2009), suggesting a possible role of CL in plant mitochondrial division. To test this prediction, we characterized the *cls-1* (SALK_049840) mutant, which has a T-DNA insertion in exon 5 (Fig. 2.6A). A previous report of the same *cls* mutant allele described extreme retardation in embryo development and plant growth, and low fertility of the mutant (Katayama and Wada, 2012), yet the molecular basis of the mutation was not fully characterized. Reverse transcription PCR analysis revealed that *cls-1* contained three truncated *CLS* transcripts (Fig. 2.6B). Sequencing of the RT-PCR products showed that transcript 1 and 2 each retained partial sequence of exon 5 and were still in frame, thus may encode truncated proteins lacking part of the catalytic domain, whereas transcript 3 was missing the entire exon 5 (Fig. 2.6A). Consistent with the previously reported growth phenotypes of *cls* T-

DNA insertion mutants (Katayama and Wada, 2012; Pineau et al., 2013), *cls-1* was severely dwarfed (Fig. 2.6C, Fig. 2.7A) and produced very small siliques that contained non-viable seeds (Fig. 2.7B). The homozygous *cls-1* seeds produced by heterozygous plants were significantly delayed in germination (Fig. 2.6D). These phenotypes are in agreement with the expression pattern of *CLS*, which shows an elevation during seed development and peaks in dry seeds, followed by a quick decrease to the basal level after germination (Fig. 2.8A, 2.8B). The mutant phenotypes could be rescued by $35S_{\text{pro}}:\text{CLS-YFP-HA}$ (Fig. 2.6E and 2.6F, Fig. 2.7C), confirming the essential role of CL in plant development and the proper function of the CLS-YFP-HA fusion protein.

Liquid chromatography followed by mass spectrometry analysis (LC/MS) of lipids from leaf tissue revealed a ~70% reduction of CL in *cls-1*, which was restored by overexpression of CLS-YFP-HA (Fig. 2.6G). In *cls-1*, there was a ~2-fold accumulation of the two major species of PG, substrates for CLS; however, PG levels in the complemented *cls-1* lines were even higher than in the mutant (Fig. 2.6H), possibly reflecting the complex regulation of phospholipid levels in the CLS-overexpression lines.

To investigate CL's role in plant mitochondrial dynamics, COX4-YFP was transformed into *cls-1*. Confocal microscopy of various cell types in transgenic plants showed that in *cls-1*, mitochondria were remarkably elongated and sometimes enlarged, and these phenotypes could be largely rescued by CLS-YFP-HA (Fig. 2.9A, 2.9B). Similar to the *cls-1* mutant, the *drp3A-2 drp3B-2* double mutant (Zhang and Hu, 2009; Aung and Hu, 2012) also displayed significantly elongated and frequently enlarged mitochondria (Fig. 2.9C), suggesting that both mitochondrial elongation and enlargement appeared to be a direct consequence of the fission defect caused by the

absence of DRP3 functions. In contrast, consistent with the lack of detection of CL in peroxisomes, peroxisome morphology exhibited no obvious changes in *cls-1* (Fig. 2.7D). Based on these observations, we concluded that, opposite to what occurs in animals and yeasts, reduced CL level in plants has a much stronger impact on mitochondrial fission than fusion. It is less likely that CL inhibits mitochondrial fusion in plants, because CL has the intrinsic property to promote membrane curvature and hexagonal structure, an intermediate step required for the fission and fusion processes (Osman et al., 2011).

Transmission electron microscopy (TEM) further revealed that, in addition to the abnormal mitochondrial shape and size, inner mitochondrial membrane structure in *cls-1* was also significantly altered (Fig. 2.10). In contrast to the wild type (Fig. 2.10A, 2.10B), most mitochondria in the mutant contained markedly long or enlarged/bubble-like cristae structures and decreased abundance of cristae (Fig. 2.10C-2.10G), supporting the crucial role of CL in maintaining the structural integrity of mitochondria. The disruption of cristae structure may also cause mitochondrial swelling/enlargement, as these two morphological changes are often found to occur concurrently in conditions such as isolated mitochondria, disease conditions, and chemical-treated cell lines (Malamed, 1965; Myron and Connelly, 1971; Faller, 1978; Mannella et al., 2001; Sun et al., 2007; Magdalan et al., 2009). Taken together, our results demonstrated that CL plays a positive role in mitochondrial morphogenesis, including fission of the organelle and cristae formation in the inner membrane.

2.3.4 Cardiolipin regulates mitochondrial fission through DRP3 proteins

The similarities between *cls-1* and *drp3* mutants in mitochondrial fission defects suggested that, in plants, CL promotes mitochondrial fission and may exert this function via key mitochondrial division factors, such as DRP3. To elucidate the link between CL and DRP3, we expressed 35S_{pro}:CFP-DRP3 in COX4-YFP-containing *cls-1*, to see whether the mitochondrial fission defects could be partially rescued. Compared with the *cls-1* control (Fig. 2.11A), *cls-1* lines expressing 35S_{pro}:CFP-DRP3 contained more fragmented mitochondria, decreased levels of elongated and enlarged mitochondria, and an increased number of mitochondria per cell (Fig. 2.11B, 2.11C, and 2.11D). This result provided genetic evidence that DRP3 acts downstream from CL in mitochondrial fission. It is not surprising that CFP-DRP3 overexpression could not fully complement the *cls-1* defect in mitochondrial morphology and plant development to the wild-type levels, as CL is a membrane structural component that is involved in multiple aspects of mitochondrial morphogenesis besides DRP3-mediated fission.

In animals and yeasts, CL physically binds to fusion and fission DRPs (DeVay et al., 2009; Tadato et al., 2010; Montessuit et al., 2010). DRP3 and the human mitochondrial and peroxisomal fission DRP, DRP1, belong to the same DRP subclade, in which most members have dual functions in the division of mitochondria and peroxisomes (Miyagishima et al., 2008). Human DRP1 interacts with CL and stimulates oligomerization of the Bcl-2-family protein, Bax, in the initiation of apoptosis; R247, a positively-charged residue exposed on the surface of DRP1, was shown to mediate this interaction (Montessuit et al., 2010). Sequence alignment of fission DRPs from diverse species showed that this Arg is conserved in mitochondrial fission DRPs, but not in *Arabidopsis* ARC5 (DRP5B) (Fig. 2.12), which is localized to chloroplasts and

peroxisomes (Gao et al., 2003; Zhang and Hu, 2010). Comparison of protein tertiary structure of the GTPase domain revealed structural similarities between human DRP1 and *Arabidopsis* DRP3s, including the surface-exposed region in which the conserved Arg is located (Fig. 2.13A). These observations strongly suggested that in *Arabidopsis*, CL also interacts with DRP3 and the conserved Arg on DRP3 is likely required for this interaction.

We then tested the hypothesis that the conserved R273 on DRP3A and R258 on DRP3B, which presumably mediate the interaction with CL, also impact DRP3's function in mitochondrial fission. CFP fusions with DRP3A^{R273E} and DRP3B^{R258E}, in which the conserved CL-interacting residue Arg was substituted by a negatively charged residue, Glu, were generated. Tobacco cells transiently co-expressing DRP3^{R->E} with N- or C-terminal CFP and COX4-YFP showed strong inhibition of mitochondrial fission and, as a result, dramatic reduction of the total number of mitochondria per cell, which is in stark contrast to cells expressing wild-type DRP3s (Fig. 2.14A, 2.14B, and 2.14C, Fig. 2.13B). As expected, no morphological changes were observed for peroxisomes by co-expressing the mutant DRP3 proteins and the peroxisomal marker (Fig. 2.13C, 2.13D). Similar to the phenotype caused by DRP3^{R->E} in wild-type tobacco cells, CFP-DRP3A^{R273E} transiently expressed in *Arabidopsis* leaves of *drp3A-2* seedlings by the Fast Agro-mediated Seedling Transformation (FAST) method (Li et al., 2009) strongly enhanced the mitochondrial fission defect in *drp3A-2* to the level of the *drp3A-2 drp3B-2* double mutant (Fig. 2.15A). Transgenic plants expressing CFP-DRP3^{R->E} showed similar mitochondrial phenotypes and were dwarfed, somewhat similar to *drp3A drp3B* double and *drp3A drp3B drp5B* triple mutants (Aung and Hu, 2012) (Fig. 2.14D). These

data together argued strongly that the proper function of DRP3 in mitochondrial fission is CL dependent.

Previous studies showed that residues K38, S39, and T59 on human DRP1 are important for protein function; K38A and S39N reduced GTP binding and T59A decreased GTP hydrolysis. When ectopically expressed, mutant forms of hDRP1 led to fission inhibition and thus dramatic elongation of mitochondria. In contrast, overexpression of DRP1^{K38A} did not affect the distribution of peroxisome in the cell (Smirnova et al., 2001). A following report showed that overexpression of DRP1^{K38A} caused mild peroxisome elongation. When co-overexpressed with PEX11 β , peroxisome fission was strongly inhibited by DRP1^{K38A} (Koch et al., 2003). Overexpression of DRP1^{S39N} and DRP1^{T59A} resulted in reduced abundance of peroxisomes. Besides, peroxisome elongation was also caused by overexpression of DRP1^{S39N} (Li and Gould, 2003; Thoms and Erdmann, 2005). These three residues are also conserved in *Arabidopsis* organelle division DRPs; for example, K72, S73, and T93 on DRP3A are conserved respectively with hDRP1 K38, S39, and T59 (Fig. 2.12). To compare the inhibitory effects of DRP3A^{R273E} on mitochondrial division with those caused by CFP-DRP3A^{K72A}, CFP-DRP3A^{S73N} and CFP-DRP3A^{T93A}, we made 35S_{pro}:CFP-DRP3A constructs that contained K72A, S73N, and T93A, respectively. When transiently expressed in *Arabidopsis drp3A-2* plants and tobacco leaves, CFP-DRP3A^{K72A}, CFP-DRP3A^{S73N} and CFP-DRP3A^{T93A} caused mitochondrial morphological alterations comparable to those caused by CFP-DRP3A^{R273E} (Fig. 2.15A, 2.15C). In contrast, morphology or abundance of peroxisomes did not show obvious changes (Fig. 2.15B, 2.15D), somewhat consistent with the aforementioned data from overexpressing human

DRP1 mutant proteins. Furthermore, CFP-DRP3A^{R273E}, but not CFP-DRP3A^{K72A}, CFP-DRP3A^{S73N} or CFP-DRP3A^{T93A}, complemented the peroxisome phenotype in *drp3A-2* (Fig. 2.15B), suggesting that disrupting CL-DRP3 interaction does not interfere with DRP3's role in peroxisome fission, yet reducing DRP3's GTPase activity would abolish its function in the division of both peroxisomes and mitochondria. Taken together, our data reinforce the idea that CL is much more important to DRP3's role in mitochondrial fission than peroxisome fission.

2.3.5 Cardiolipin stabilizes the mitochondrial-associated DRP3 protein complex

To further determine the impact of CL on DRP3 at the mechanistic level, we analyzed the localization of the DRP3 proteins in mitochondria in tobacco plants co-expressing various forms of CFP-DRP3 and COX4-YFP. Wild-type CFP-DRP3 proteins were found to be frequently associated with mitochondria (Fig. 2.16A). Although some CFP-DRP3A^{R273E} and CFP-DRP3B^{R258E} proteins still localized to the massively elongated mitochondria, the total number of fluorescent spots per cell and the percentage of mitochondrial-associated fluorescent spots were significantly reduced (Fig. 2.16B, 2.16C, and 2.16D). These data suggested that CL is likely required for the stabilization of DRP3A and DRP3B proteins (oligomers) on mitochondria.

To detect the formation of the DRP3 protein complexes, we performed blue native gel electrophoresis (BN-PAGE) of proteins from tobacco leaves expressing YFP-DRP3 or YFP-DRP3^{R->E}, followed by immunoblot analysis. YFP-DRP3^{R->E} monomers remained at a similar level to that of the wild-type DRP3, but the level of the higher-order protein complex was greatly reduced (Fig. 2.17A). Consistent with this result, the

total protein levels of YFP-DRP3^{R->E} were also significantly reduced (Fig. 2.17B). To examine the possibility that the reduction of DRP3^{R->E} higher-order complex was due to impaired DRP3 self-interacting ability, co-immunoprecipitation (co-IP) was performed with HA- and YFP-tagged wild-type and mutant DRP3 proteins expressed in tobacco leaves. No obvious defects in self-interaction were observed for any of the DRP3 pairs (Fig. 2.18A), indicating that CL's role in DRP3 function was likely to stabilize the DRP3 oligomers.

To further support this view that CL can stabilize DRP3 oligomers, we analyzed the formation of the endogenous DRP3 complex in the *cls-1* mutant, using BN-PAGE followed by immunoblot analysis with DRP3 peptide antibodies. In our previous study, these antibodies had been able to detect the DRP3 higher-order complex but not monomers, possibly due to the low level of endogenous DRP3 monomers (Aung and Hu, 2012). As expected, there was a marked reduction in the level of the DRP3 higher-order complex in *cls-1* (Fig. 2.17C), while no obvious decrease was noted for the *DRP3* transcripts in the mutant (Fig. 2.18B). To further determine the specificity of this stabilization effect, we analyzed the complex formation of endogenous COXII (mitochondrial inner membrane) and VDAC (mitochondrial outer membrane) proteins, using BN-PAGE followed by immunoblot analysis. The complex pattern of these two proteins on the BN-PAGE gel did not show significant differences between wild type and *cls-1* (Fig. 2.17D), suggesting that the reduction of the DRP3 complex in *cls-1* is relatively specific. In addition, endogenous DRP3 and COXII were also analyzed using SDS-PAGE followed by immunoblot. The total protein amount was not obviously altered in *cls-1*. Nevertheless, DRP3 total protein amount was slightly diminished in comparison

with COXII (Fig. 2.17E). These results led us to the conclusion that CL can stabilize the mitochondrial-associated DRP3 protein complex.

2.3.6 Cardiolipin plays a role in plant responses to programmed cell death (PCD)-inducing stresses

The significant role of CL in mammalian apoptosis prompted us to explore the function of CL in plant PCD, a process that shares morphological and biochemical features with apoptosis (see Introduction). In fact, UV-C light and heat shock treatments had been found to cause increased cell death in protoplasts from a *cls* mutant (a different allele from *cls-1*), supporting CL's role in plant stress response (Pineau et al., 2013). To address this question in whole plants, we first treated wild-type and CL-deficient plants with heat, one of the most effective PCD stimuli in plants (Gadjev et al., 2008). The *cls-1* mutant was severely inhibited in growth and weak, therefore not suitable for physiological analysis. To this end, we generated artificial micro RNA (*amiRNA*) lines, and selected two lines in which the levels of the *CLS* transcripts were significantly reduced (Fig. 2.19). These *CLS amiRNA* lines did not show growth defects, but exhibited obvious changes in mitochondrial morphology (Fig. 2.20A).

To determine the optimal length of time for the heat treatment, we first placed wild-type Col-0 plants at 65°C and analyzed genomic DNA fragmentation, a feature of late-stage PCD (Collins et al., 1997). DNA fragmentation was detected after 30 min heat treatment (Fig. 2.20B). As CL presumably exerts its function in the early stage of PCD, we selected 10 min at 65°C as the PCD-inducing condition, and analyzed responses in both wild-type and *CLS* deficient seedlings after the treatment. Whereas wild-type Col-0

did not show strong differences in appearance, *CLS* deficient mutants displayed leaf chlorosis and shriveling, and even plant death (Fig. 2.19B, 2.19C), despite their lack of apparent growth deficiencies under normal conditions (see plants in Fig. 2.19B at 0 hr). To detect the level of PCD in the plants, we used the Terminal Deoxynucleotidyl Transferase Mediated dUTP Nick End Labeling (TUNEL) assay to stain fragmented DNA in wild type and the amiRNA-1 line, which exhibited stronger chlorosis than amiRNA-2 in response to heat (Fig. 2.19B). Three hours after the heat treatment, a significant level of DNA fragmentation was detected in amiRNA-1, whereas wild-type plants stained negative for TUNEL (Fig. 2.19D), indicating a much earlier burst of PCD in the *CLS* deficient line. Plants were also treated with a longer and milder heat stress: 37°C for 24 hours. Accelerated formation of chlorotic lesions was evident in amiRNA lines, again indicating the faster buildup of PCD in these plants (Fig. 2.20C, 2.20D).

To determine whether CL plays a specific role in heat stress response or it is broadly involved in PCD, we applied another commonly known PCD-inducing stimulus, prolonged darkness (Gadjev et al., 2008), to the seedlings. Unlike the wild-type plants, *CLS* deficient lines started to demonstrate signs of senescence after four to five days in the dark (Fig. 2.19E, 2.19F). Our results from the heat and extended dark treatments and the TUNEL assays together provided strong evidence that CL plays a protecting role in plants against PCD-inducing stresses.

2.4 Discussion

2.4.1 Novel and plant-specific aspects of CL biology uncovered

Previous efforts have been devoted to understanding the function, biosynthesis, and regulation of CL in various non-plant model organisms, which led to the discovery of CL's pivotal roles in mitochondrial dynamics and integrity, and human health (Houtkooper and Vaz, 2008). CL's role in plants is just beginning to be revealed. As shown in the two previous studies (Katayama and Wada, 2012; Pineau et al., 2013) and in this study, CL is essential for normal plant growth and development, as illustrated by the severe developmental defects in strong *cls* mutants. Thus, the functions of CL in mitochondrial electron transport, ATP production, and protein import, are very likely to be conserved among eukaryotes. In this study, we also revealed aspects of CL biology that were previously uncharacterized or are unique to plants.

First, we observed a distinct pattern of CMDs in a significant portion of plant mitochondria, which is similar to the pattern shown for CL on bacterial cell membranes (Mileykovskaya and Dowhan, 2000; Kawai et al., 2004) but has not been reported in animal or yeast cells. However, CMDs have been defined in mammals biochemically as detergent-resistant membrane fractions (Sorice et al., 2009). That fluorescent microscopy only detected CMDs in plants and bacteria suggests that the number of CMDs might be lower in other eukaryotic systems.

Second, we showed that the N terminus of *Arabidopsis* CLS consists of two peptides with mitochondrial targeting signals: Signal 1 and Signal 2, of which Signal 2 is conserved in plant CLS proteins but divergent from CLSs from non-plant systems, suggesting a possible plant-specific targeting mechanism for this protein. It is possible that Signal 1 is a mitochondrial matrix targeting signal, which directs the precursor protein partially into the matrix, and Signal 2 targets the protein to the mitochondrial

intermembrane space (IMS) after Signal 1 is cleaved off. Together the N-terminal (putative) TMD and Signal 2 ensure that CLS resides in the inner membrane with the correct topology. Signal 2 by itself leads the fusion proteins to both mitochondria and chloroplasts, substantiating the importance of Signal 1 for initial mitochondrial targeting. At this point, we do not completely exclude the possibility that targeting of the protein to both organelles by Signal 2 was an artifact in our experiment; further investigations are needed to clarify this possibility.

Third, we determined the topology of CLS, which resides in the mitochondrial inner membrane with the C terminus facing the IMS. This suggests that the C-terminal catalytic domain might be in the IMS. However, a previous study using rat liver suggested that CL is synthesized on the matrix side of mitochondrial inner membrane (Schlame and Haldar, 1993), thus it is unlikely that the catalytic domain is solely in the IMS. Since several TM domains are predicted in the C-terminal region of CLS, we predict that the enzymatic domain of CLS may pass the inner membrane.

More importantly, we showed a specific role of CL in mitochondrial fission through the dynamin-related protein DRP3, and in protecting plants from some program cell death-inducing stresses (see below).

2.4.2 CL-mediated mitochondrial fission and fusion

The contrasting morphology of mitochondria in plant vs. yeast and animal cells suggests a highly unbalanced mitochondrial dynamics leaning towards fission in plants, as opposed to animals and yeasts. Consistent with this notion, plant mitochondria exhibit impaired fission upon CL deficiency, which is linked at least in part to CL's ability

to stabilize DRP3 higher-order complexes. Taking into consideration the positive impact of CL on fusion DRP functions in yeasts and animals, we predict that CL plays equally critical roles in mitochondrial fission and fusion. The ultimate outcome of CL deficiency in mitochondrial dynamics may be determined by the relative strengths of the antagonistic fusion and fission machineries in an organism. As such, when CL is deficient, the impairment of the dominant machinery is more pronounced, resulting in the shift of mitochondrial dynamics towards fission in animals and yeasts and towards fusion in plants.

In this study, we showed the similarities in mitochondrial morphological phenotypes caused by the loss of DRP3 and CLS, rescue of the mitochondrial phenotype in *cls-1* by overexpressing DRP3, and stabilization of DRP3 oligomers by CL, suggesting a direct role of CL in mitochondrial fission through DRP3. In yeast and mammals, CL is an important structural component of the mitochondrial membrane, involved in the organization, stabilization, and/or activity of several protein complexes involved in respiration, protein import, and fusion (see Introduction). Reduction in the level of respiratory chain complexes was also shown for an *Arabidopsis cls* mutant (Pineau et al., 2013). However, CL's role in mitochondria seems to be selective rather than non-selective, as shown by the lack of obvious reduction in the levels of the mitochondrial membrane protein complexes COXII and VDAC in *cls-1*. CL tends to be enriched in specific membrane domains and promotes the formation of hexagonal membrane structure, an intermediate step of the fission and fusion processes (see Introduction). It will be interesting to determine in the future whether CL is also important for the function of other proteins involved in mitochondrial division/morphogenesis, such

as FIS1, a conserved protein that recruits DRP3 to both mitochondria and peroxisomes (Scott et al., 2006; Lingard et al., 2008; Zhang and Hu, 2009); ELM1, a plant-specific factor that recruits DRP3A to mitochondria (Arimura et al., 2008); and PMD1, another plant-specific factor that regulates mitochondrial and peroxisome morphogenesis in a DRP3-independent manner (Aung and Hu, 2011).

We cannot completely rule out the possibility that significantly increased fusion of mitochondria may also contribute to the observed phenotype in *c/s* mutants. However, CL has been shown by multiple studies to play a positive role in the mitochondrial fusion process in non-plant systems. This is achieved not only by its role in stabilizing the oligomerization and enzymatic processing of the fusion DRPs, but also by a structural role in promoting membrane curvature and hexagonal structure (see Introduction). Although mitochondrial fusion machinery has not been discovered in plants and thus makes it difficult to address this question for now, it is unlikely that CL plays an inhibitory role in mitochondrial fusion in plants.

2.4.3 Different membrane lipid compositions of mitochondria and peroxisomes may contribute to the distinct modes of DRP3 functions on these organelles

DRP higher-order complexes form a ring structure that encircle the organelle fission site to mediate membrane fission (Chan, 2012). However, whether and how the same DRP functions in distinct organelles in different manners is still an open question. In this study, we showed that DRP3^{R->E} mutant proteins conferred a dominant negative effect on mitochondrial fission when overexpressed, possibly by competing with wild-type DRP3 proteins on the mitochondria and consequently significantly reducing the

interaction between DRP3 and CL, which stabilizes the DRP3 complex.

Ectopically expressed dominant negative forms of human DRP1 with impaired GTP hydrolysis or GTP binding led to dramatic morphological changes to mitochondria, and a weaker impact on peroxisomal morphology (Smirnova et al., 2001; Li and Gould, 2003; Thoms and Erdmann, 2005). In our study, transient expression of CFP-DRP3A containing changes of the corresponding conserved amino acids, i.e., CFP-DRP3A^{K72A}, CFP-DRP3A^{S73N} and CFP-DRP3A^{T93A}, also caused strong inhibition of mitochondrial fission, but virtually no changes to the number or morphology of peroxisomes (Fig. 2.15D). It is possible that the endogenous mitochondrial fission DRPs in plants retained enough competence to divide peroxisome even in the presence of ectopically expressed mutant DRP3 proteins. Nonetheless, CFP-DRP3A^{R273E}, but not the three GTPase activity-reduced dominant negative forms of DRP3A, attenuated the peroxisome elongation phenotype in *drp3A-2*, supporting the conclusion that CL is not as essential to peroxisome fission as to mitochondrial fission. It is well known that membrane lipid composition can modulate membrane-associated protein functions (Marsh, 2008; Vögler et al., 2008). Thus, the mitochondrial-specific presence of CL and CMDs may reflect a mechanism for DRP3 proteins to distinguish mitochondria from peroxisomes.

2.4.4 Cardiolipin may link mitochondrial fission to programmed cell death (PCD)

In apoptosis, CL on the outer membrane provides an anchor and activating platform for caspase-8 as well as BID, a factor required for activating Bax and Bak - proteins that induce outer membrane permeabilization and the release of cytochrome c

(Lutter et al., 2000; Kuwana et al., 2002; Gonzalvez and Gottlieb, 2007; Montessuit et al., 2010). CL also directly contributes to cytochrome *c* release. Prior to apoptosis, CL on the outer leaflet of mitochondrial inner membrane binds to cytochrome *c* to retain it in the cristae, and stress signals induce the peroxidation of CL by cytochrome *c*, which presumably allows for remodeling of the cristae and the subsequent release of cytochrome *c* (Kagan et al., 2005; Gonzalvez and Gottlieb, 2007).

Although whether mitochondrial fission plays a central role in plant PCD is still being debated (Chan, 2012), multiple studies in non-plant systems have linked mitochondrial fission to the onset of PCD. For example, inhibition of human DRP1 activity reduces apoptotic mitochondrial fission and cytochrome *c* release (Frank et al., 2001). Ectopic expression of *Caenorhabditis elegans* DRP1 induces both mitochondrial fission and cell death (Jagasia et al., 2005), and the *S. cerevisiae* fission DRP, Dnm1, was shown to promote cell death (Fannjiang et al., 2004). CL and CMDs are believed to provide an activating platform for the PCD pathway by recruiting/stabilizing Bcl-2 family proteins required for the release of cytochrome *c* and other pro-PCD molecules (Gonzalvez and Gottlieb, 2007). It is possible that during PCD, CL's interactions with fission DRP and Bcl-2 family proteins are both strengthened, leading to increased mitochondrial scission and rupture of mitochondrial outer membranes and thus promoting the initiation of PCD.

Plant PCD is involved in embryogenesis, tissue differentiation, reproductive organ formation, pollination, senescence, and serves as a response mechanism to some abiotic and biotic stresses (Lord and Gunawardena, 2012). It shares several morphological hallmarks with animal apoptotic PCD (Gadjev et al., 2008), although the

well characterized protein machinery that controls animal apoptosis is not obviously conserved in plants. It would be of great interest to focus future investigations on the role of CL and DRP3 proteins in plant PCD. Our finding that CLS deficient plants have increased susceptibility to heat stress and prolonged darkness treatment is a first step in this research direction.

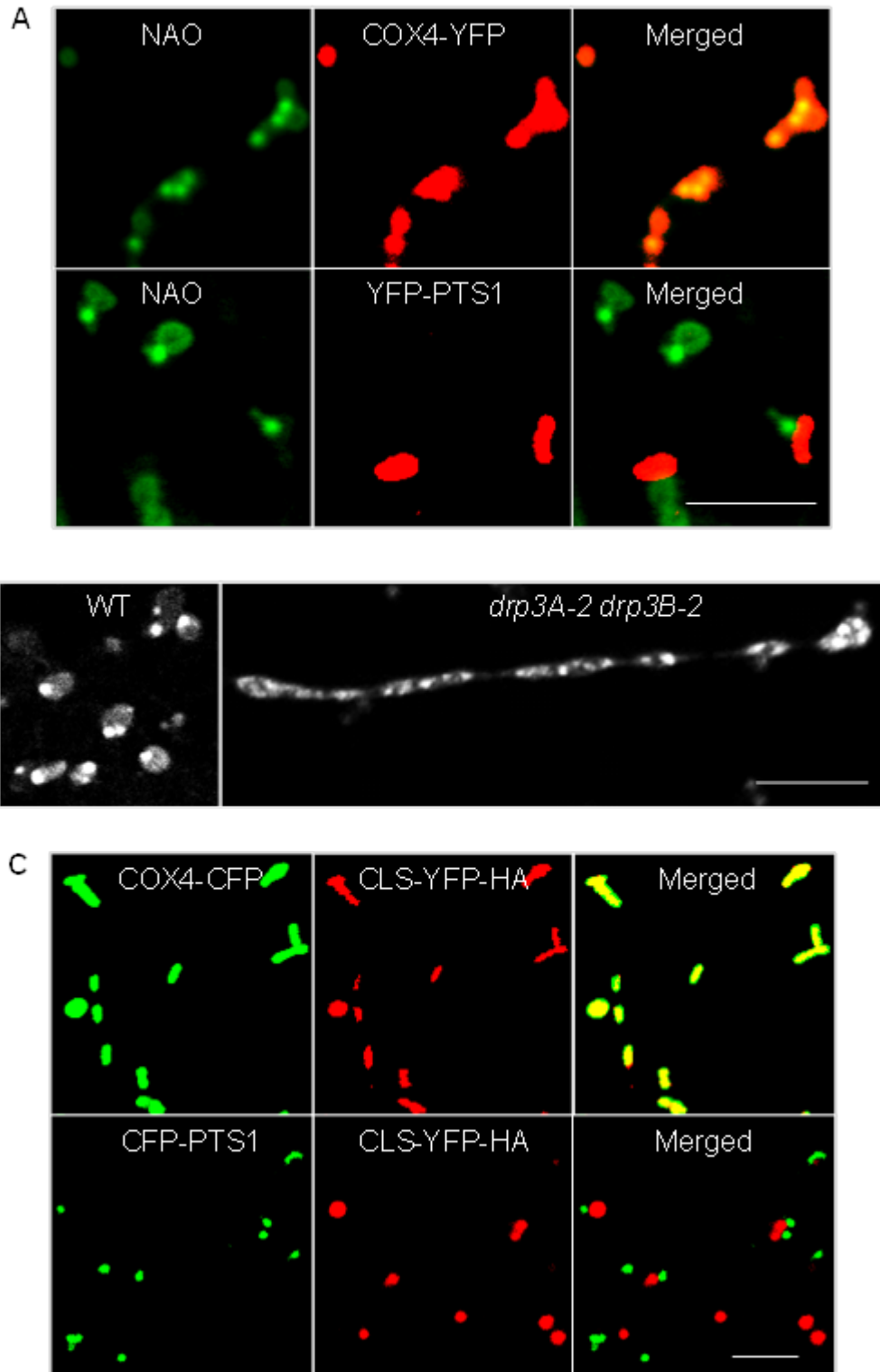
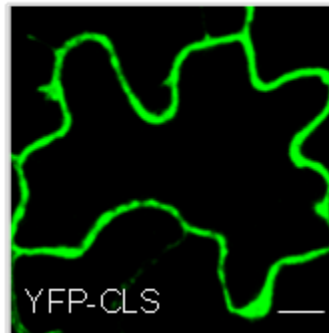


Figure 2.1. Subcellular localization of cardiolipin and CLS in plant cells.

Figure 2.1 (cont'd)

D



(A) Confocal images showing the localization of CL to mitochondria in *Arabidopsis*. Leaf epidermal cells of two-week-old T3 plants expressing COX4-YFP or YFP-PTS1 were stained with the CL-specific dye, NAO. Scale bar, 5 μm .

(B) Confocal images showing CMDs on mitochondria in leaf epidermal cells of two-week-old wild type and *drp3* double mutant stained with NAO. Scale bar, 5 μm .

(C) CLS localizes to mitochondria but not peroxisomes. Two-week-old T2 lines expressing CLS-YFP-HA and COX4-CFP or CLS-YFP-HA and CFP-PTS1 were used for analysis. Scale bar, 5 μm .

(D) Cytosolic diffusion of YFP-CLS transiently expressed in tobacco leaf epidermal cells. Scale bar, 10 μm .

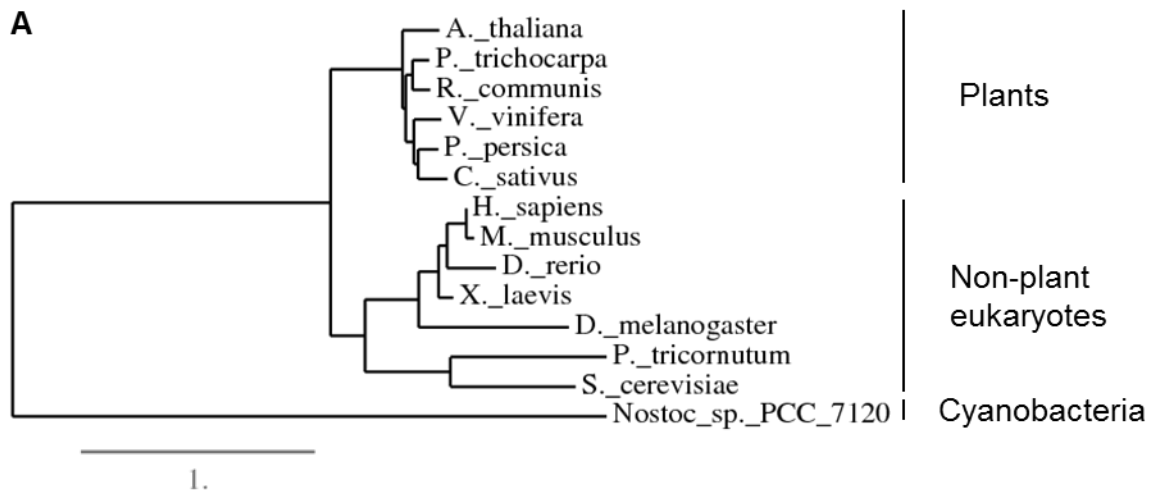


Figure 2.2. Sequence comparison of CLS proteins from different species.

Figure 2.2 (cont'd)

(A) A phylogenetic tree of CLS sequences from different species generated by the Phylogeny.fr program (<http://www.phylogeny.fr/version2.cgi/index.cgi>). The cyanobacterial CLS protein from *Nostoc sp. PCC 7120* shows low sequence similarity with those in eukaryotes. The plant species include *Arabidopsis thaliana*, *Ricinus communis*, *Populus trichocarpa*, *Vitis vinifera*, *Prunus persica*, and *Cucumis sativus*. The non-plant species include *Homo sapiens*, *Mus musculus*, *Danio rerio*, *Xenopus laevis*, *Drosophila melanogaster*, *Phaeodactylum tricornutum*, and *Saccharomyces cerevisiae*. Scale bar, 1.0 amino acid substitutions per site.

(B and C) Sequence alignment between *Arabidopsis* CLS and CLS homologs from non-plant species (B) and plant species (C). Sequence alignment was performed using the ClustalW2 program. Signal 1 and signal 2 on *Arabidopsis* CLS, which direct the protein to mitochondria and mitochondria/chloroplasts, respectively, are highlighted. The conserved enzymatic activity domain (CDP-alcohol phosphatidyltransferase) is underlined by blue dashed lines.

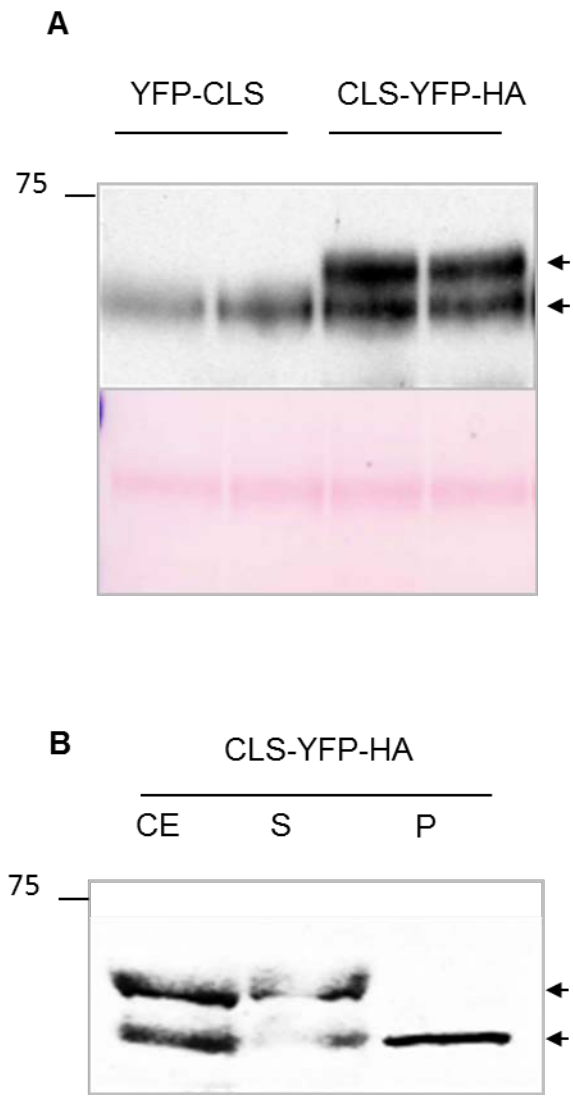


Figure 2.3. CLS-YFP-HA is processed upon mitochondrial targeting.

Figure 2.3 (cont'd)

(A) Immunoblot analysis of transiently expressed YFP-CLS and CLS-YFP-HA proteins in tobacco leaves, using α -GFP antibodies. Arrow heads point to the putative precursor and mature form of CLS-YFP-HA. Loading control, large subunit of Rubisco stained by Ponceau S.

(B) Immunoblot analysis of CLS-YFP-HA in different subcellular crude fractions. Tobacco leaves transiently expressing CLS-YFP-HA were homogenized on ice in grinding buffer (450 mM Sucrose, 1.5 mM EGTA, 0.2% BSA, 0.6% PVP-40, 10 mM DTT, 0.2 mM PMSF, and 15 mM MOPS/KOH, pH7.4). The homogenized solution is considered crude extract (CE). Chloroplasts and other organelles and particles were sedimented by centrifugation for 10 min at 3,500 g (5 min each time) and 5 min at 6,000 g. Finally, the solution was centrifuged for 10 min at 17,000 g to get a supernatant fraction (S) and a pellet fraction (P) enriched in mitochondria. Arrow heads point to the putative precursor and mature form of CLS-YFP-HA.

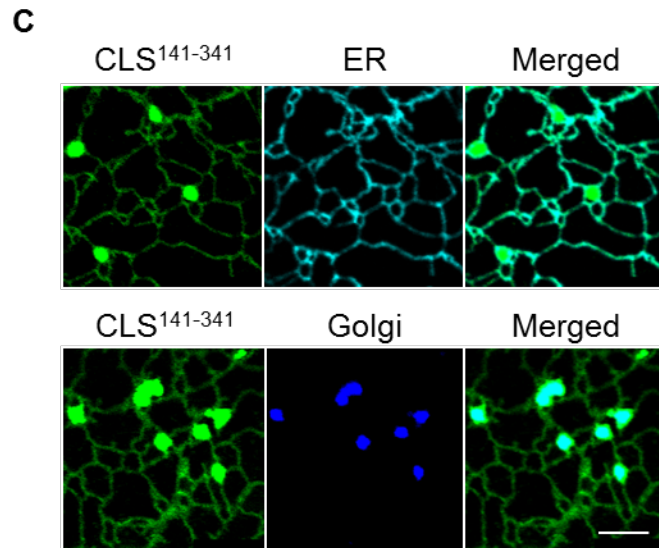
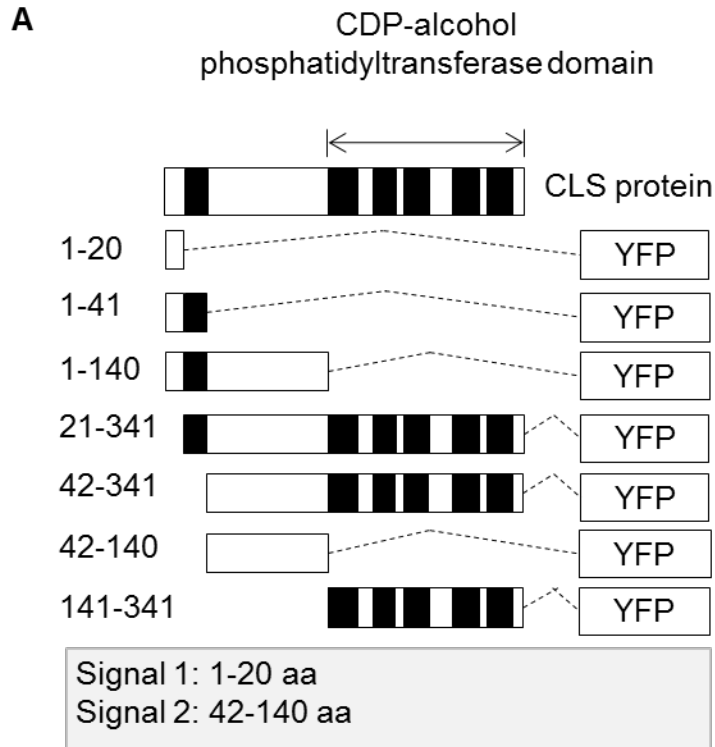


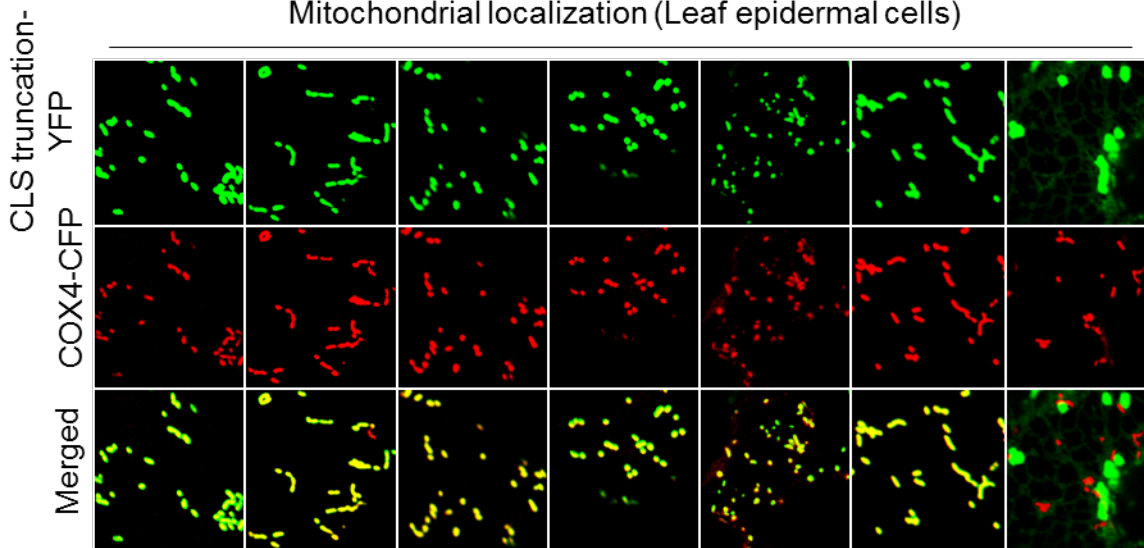
Figure 2.4. Analysis of organelle targeting signals on CLS.

Figure 2.4 (cont'd)

B

CLS region 1-20 1-41 1-140 21-341 42-341 42-140 141-341

Mitochondrial localization (Leaf epidermal cells)



Chloroplast localization (Leaf mesophyll cells)

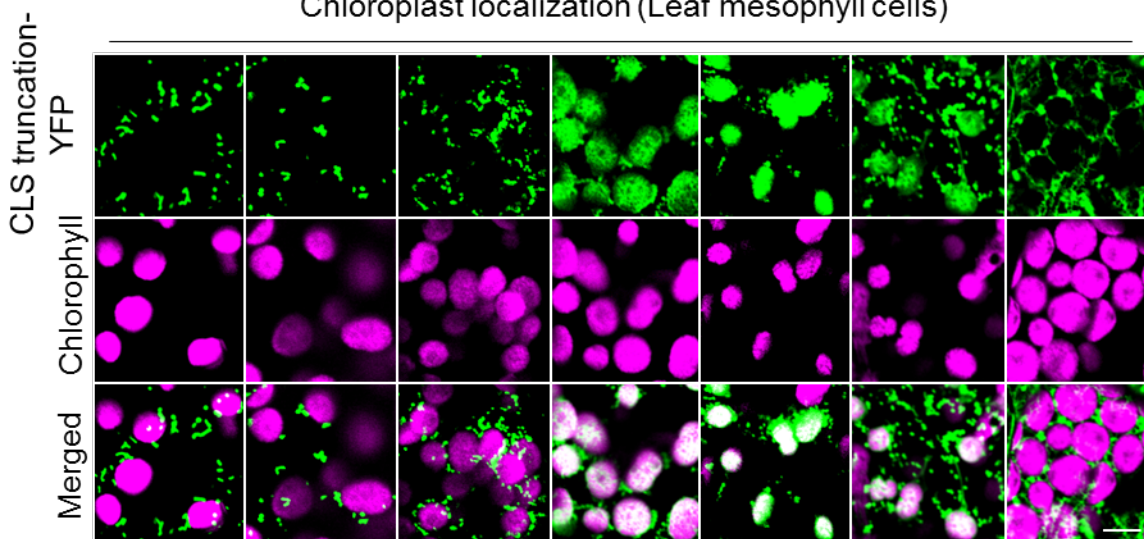


Figure 2.4 (cont'd)

(A) Schematics of the CLS protein and deletion constructs. Black box, transmembrane helices predicted by TMHMM server (<http://www.cbs.dtu.dk/services/TMHMM/>).

(B) Confocal images of the localization of fusion proteins between various CLS fragments and YFP transiently expressed in tobacco leaves together with the mitochondrial marker COX4-CFP. Co-localization between COX4-CFP and CLS-YFP fusion proteins were examined in epidermal cells. Co-localization between chloroplast autofluorescent signals and CLS-YFP fusion proteins were examined in mesophyll cells. Scale bars, 5 μm .

(C) Localization of CLS¹⁴¹⁻³⁴¹-YFP to the ER and Golgi. The YFP fusion protein was transiently expressed in tobacco leaves with the ER marker AtWAK2-CFP or Golgi marker GmMan1-CFP (Nelson et al., 2007). Scale bar, 5 μm .

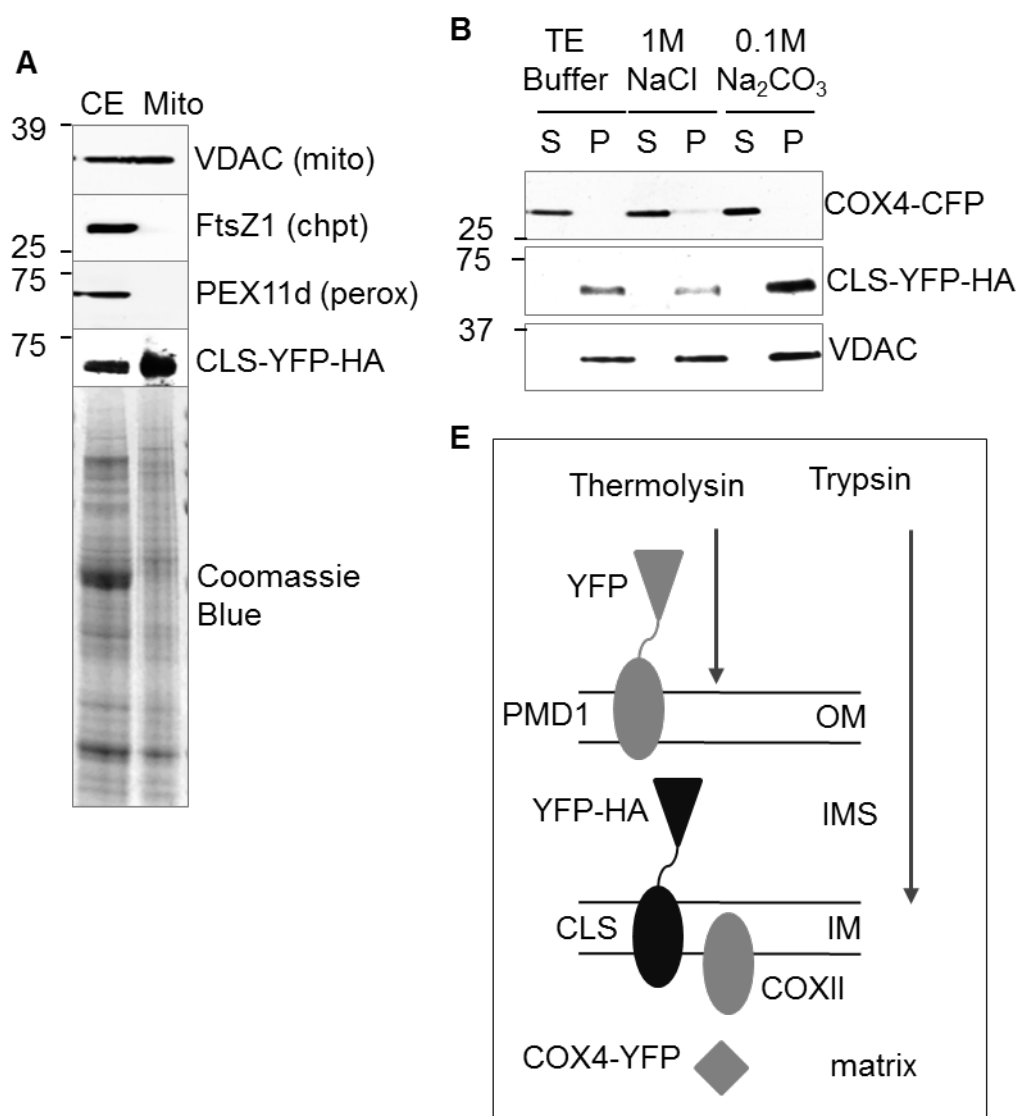


Figure 2.5. Analyses of mitochondrial membrane association and topology of CLS.

Figure 2.5 (cont'd)

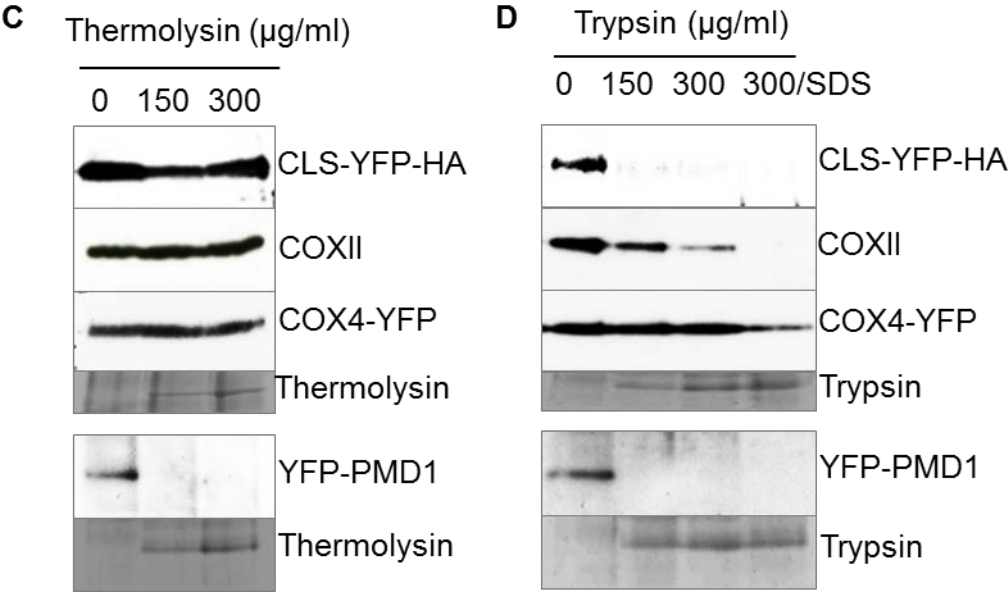


Figure 2.5 (cont'd)

(A) Immunoblot analysis to assess the purity of mitochondria isolated from leaf tissue of *Arabidopsis* transgenic plants. Organelle-specific antibodies used were against plant VDAC (mitochondria), FtsZ1 (chloroplasts) and PEX11d (peroxisomes), respectively. The presence of CLS-YFP-HA is confirmed by detection with the GFP antibody. CE, crude extract.

(B) Membrane association of CLS. Purified mitochondria were treated with TE, sodium chloride (NaCl), or sodium carbonate (Na₂CO₃, pH 11.0) respectively and later separated into soluble (S) and pellet (P) fractions by centrifugation. Immunoblot analyses were performed on the proteins using α -GFP (for CFP and YFP fusions) and α -VDAC antibodies. COX4-YFP and VDAC (voltage-dependent anion channel) were controls for matrix and membrane proteins, respectively.

(C and D) Protease protection assays to determine the membrane topology of CLS. Antibodies used were α -GFP and α -COXII. Mitochondria used for the detection of YFP-PMD1 were isolated independently from *Arabidopsis* plants expressing 35S_{pro}:YFP-PMD1 (Aung and Hu, 2011).

(E) Illustration of the digestive ability of thermolysin and trypsin. PMD1, COXII and COX4-YFP are controls for distinct sub-compartments of mitochondria. OM, outer membrane; IMS, intermembrane space; IM, inner membrane.

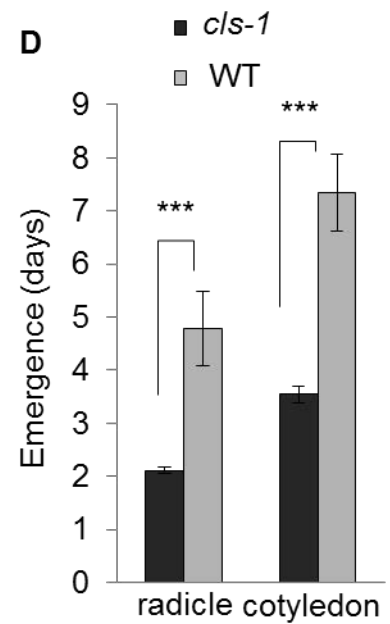
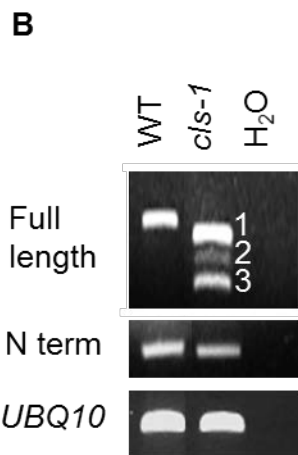
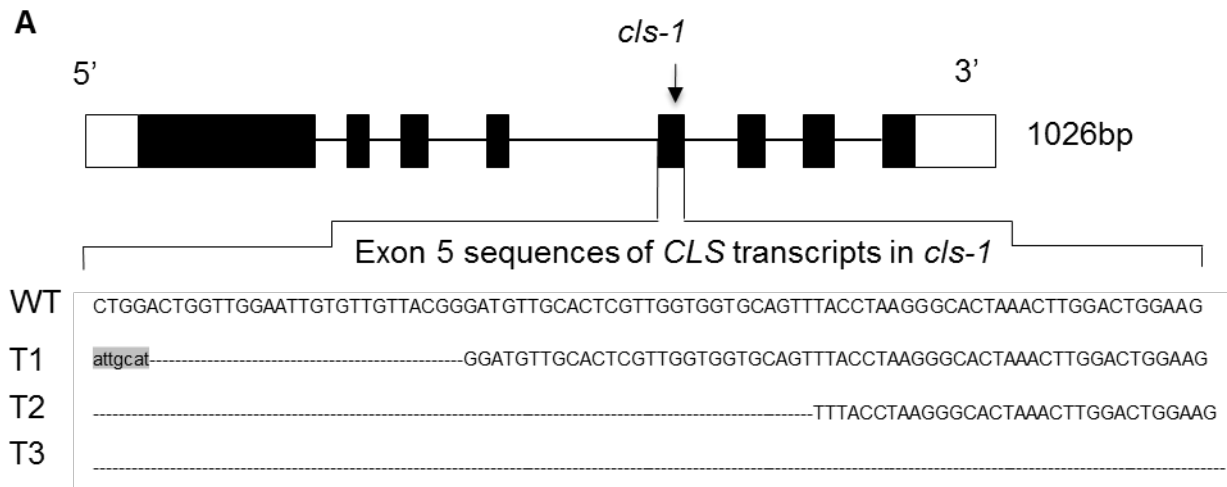


Figure 2.6. Molecular, phenotypic and biochemical analyses of the *cls-1* mutant and rescued lines.

Figure 2.6 (cont'd)

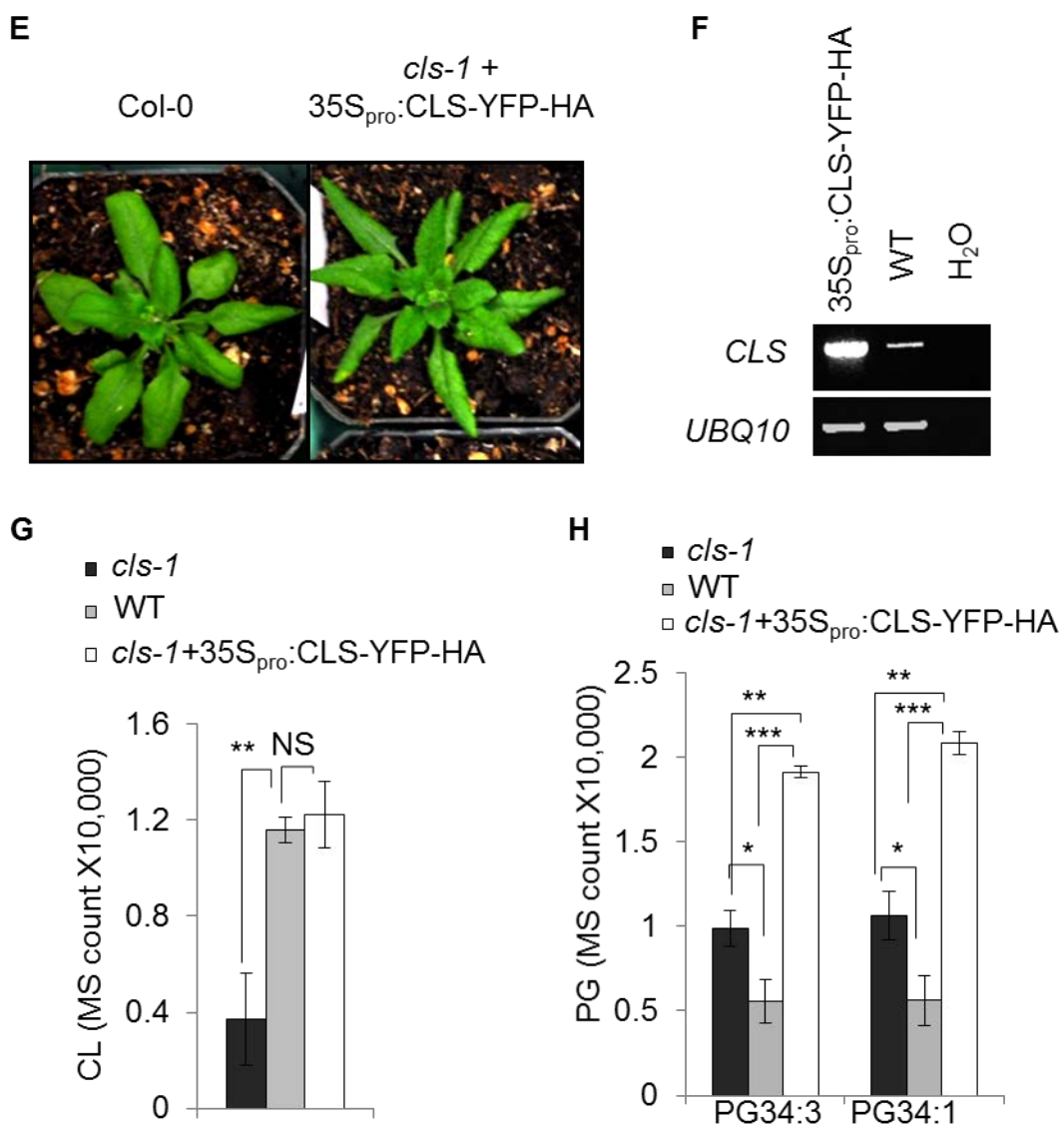


Figure 2.6 (cont'd)

(A) Schematics of the *Arabidopsis* *CLS* gene, and exon 5 sequences in the three *CLS* transcripts (T1-T3) in *cls-1* as a result of the T-DNA insertion. Open box, UTR; black box, exon; line, intron. Dashed lines indicate deletions from exon 5 in the three transcripts in *cls-1*. Nucleic acids in lower cases are foreign sequences introduced by the T-DNA insertion.

(B) Semi-quantitative RT-PCR analysis of RNA from four-week-old *cls-1*. N term, 500 bp of the N terminus of the *CLS* cDNA. *UBQ10* (ubiquitin 10) was used as a loading control. 1-3 represents transcripts 1-3.

(C) Three-week-old wild-type and *cls-1* plants.

(D) Delayed germination of *cls-1* seeds produced by heterozygotes. Average numbers of days required for the appearance of radicles and the two green cotyledons were quantified. Error bars, s.d.; n=5. Triple asterisks indicate $p < 0.001$ in *t*-test.

(E) Three-week-old Col-0 and a *cls-1* plant rescued by $35S_{pro}:CLS-YFP-HA$.

(F) RT-PCR analysis of *CLS* mRNA in the *CLS* overexpression line shown in (E). *UBQ10* was used as the loading control.

(G and H) Liquid chromatography-mass spectrometry analysis of CL (G) and PG (H) levels in wild type, *cls-1* and complemented *cls-1* line. MS counts normalized to total protein content were used for quantifications. Error bars, s.d.; n=4. NS, not significant ($p > 0.05$); double asterisks, $p < 0.01$; triple asterisks, $p < 0.001$. Total CL was used in (G), and two major PG species were used in (H).

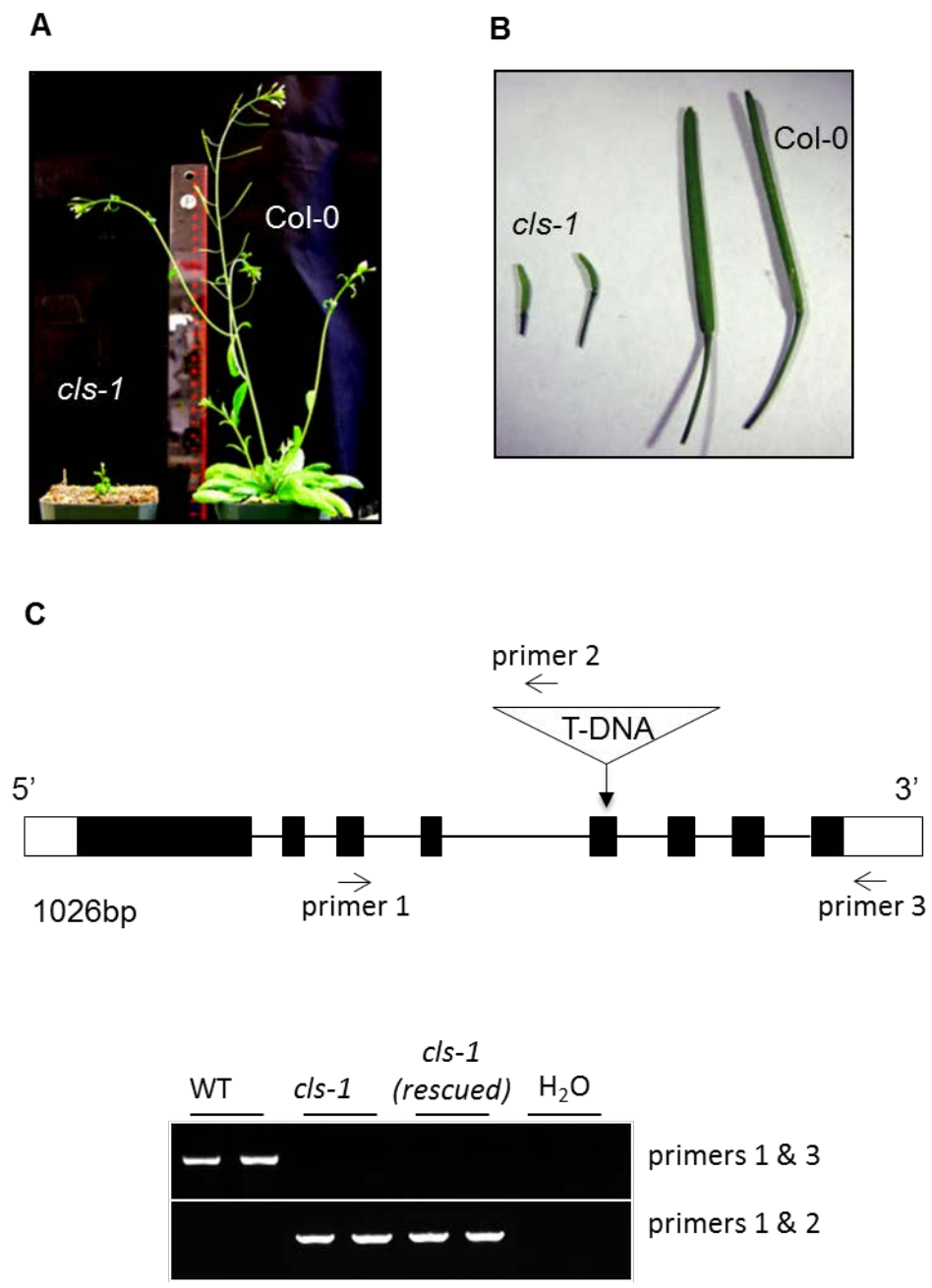
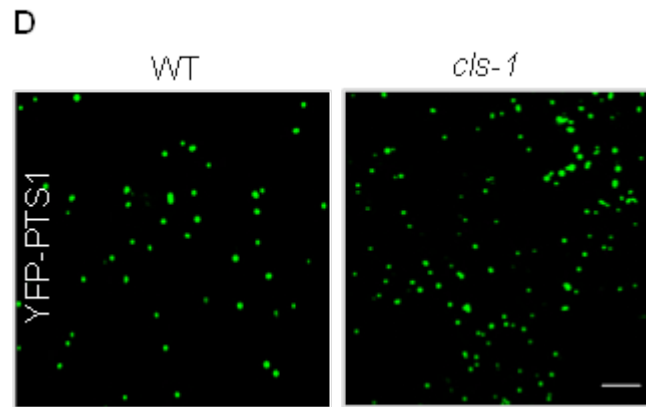


Figure 2.7. More characterization of *cls-1*.

Figure 2.7 (cont'd)



(A-B) Five-week-old plants (A) and siliques (B).

(C) Genotyping of *cls-1* mutant and rescued lines. Schematics of the *Arabidopsis CLS* gene, position of the T-DNA insertions in *cls-1*, and primers used in the genotyping are shown on the left. Genotyping of two independent lines for each genotype is shown on the right.

(D) Peroxisomal morphology in five-week-old *cls-1* and wild-type plants expressing the peroxisome marker YFP-PTS1 (SKL). Confocal images were taken from leaf mesophyll cells. Scale bar, 10 μ m.

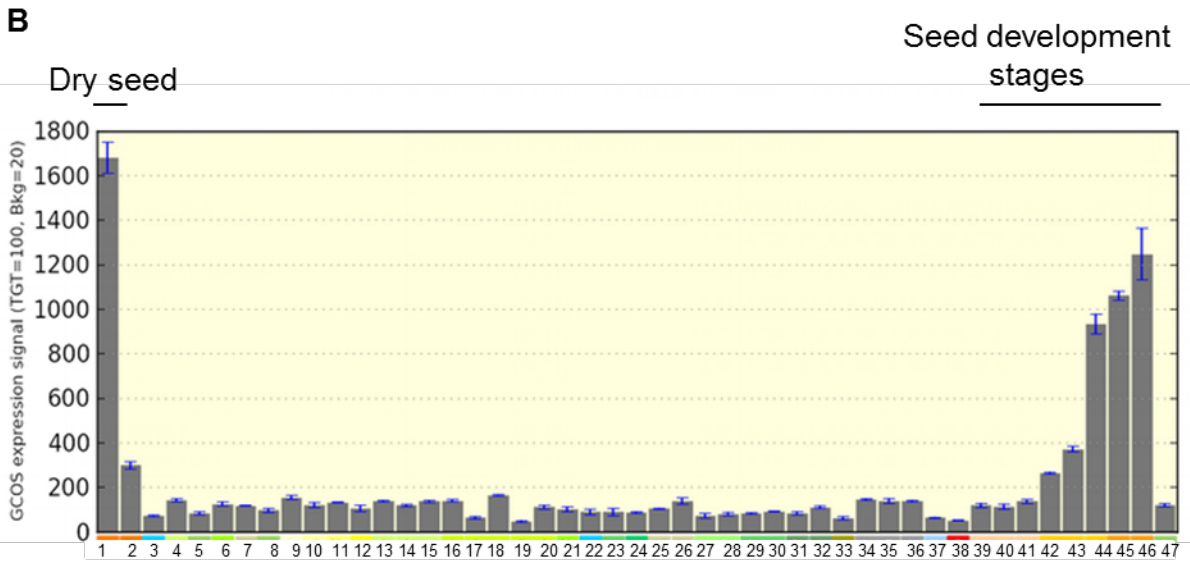
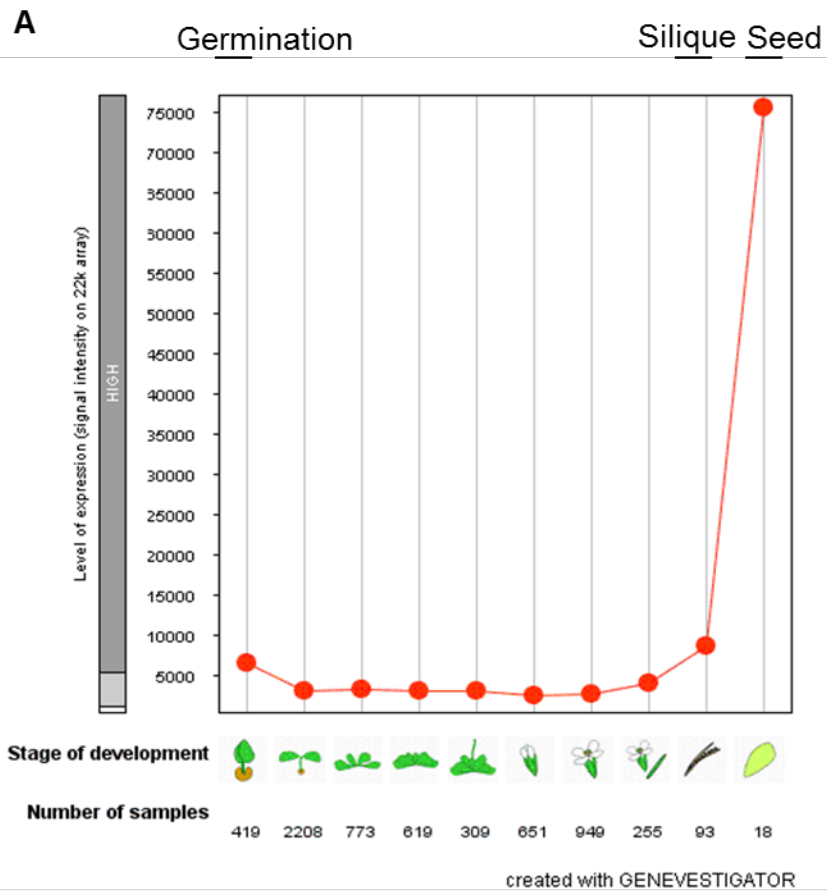


Figure 2.8. Expression profile of the *Arabidopsis* CLS gene.

Figure 2.8 (cont'd)

(A) *CLS* expression data from Genevestigator (<https://www.genevestigator.com/>).

(B) *CLS* expression data from *Arabidopsis* eFP browser (bar.utoronto.ca).

Developmental stages include: 1, Dry seed; 2, Imbibed seed, 24 h; 3, 1st Node; 4, Flower Stage 12, Stamens; 5, Cauline Leaf; 6, Cotyledon; 7, Root; 8, Entire Rosette After Transition to Flowering; 9, Flower Stage 9; 10, Flower Stage 10/11; 11, Flower Stage 12; 12, Flower Stage 15; 13, Flower Stage 12, Carpels; 14, Flower Stage 12, Petals; 15, Flower Stage 12, Sepals; 16, Flower Stage 15, Carpels; 17, Flower Stage 15, Petals; 18, Flower Stage 15, Sepals; 19, Flower Stage 15, Stamen; 20, Flowers Stage 15, Pedicels; 21, Leaf 1 + 2; 22, Leaf 7, Petiole; 23, Leaf 7, Distal Half; 24, Leaf 7, Proximal Half; 25, Hypocotyl; 26, Root; 27, Rosette Leaf 2; 28, Rosette Leaf 4; 29, Rosette Leaf 6; 30, Rosette Leaf 8; 31, Rosette Leaf 10; 32, Rosette Leaf 12; 33, Senescing Leaf; 34, Shoot Apex, Inflorescence; 35, Shoot Apex, Transition; 36, Shoot Apex, Vegetative; 37, Stem, 2nd Internode; 38, Mature Pollen; 39, Seeds Stage 3 w/ Siliques; 40, Seeds Stage 4 w/ Siliques; 41, Seeds Stage 5 w/ Siliques; 42, Seeds Stage 6 w/o Siliques; 43, Seeds Stage 7 w/o Siliques; 44, Seeds Stage 8 w/o Siliques; 45, Seeds Stage 9 w/o Siliques; 46, Seeds Stage 10 w/o Siliques; 47, Vegetative Rosette.

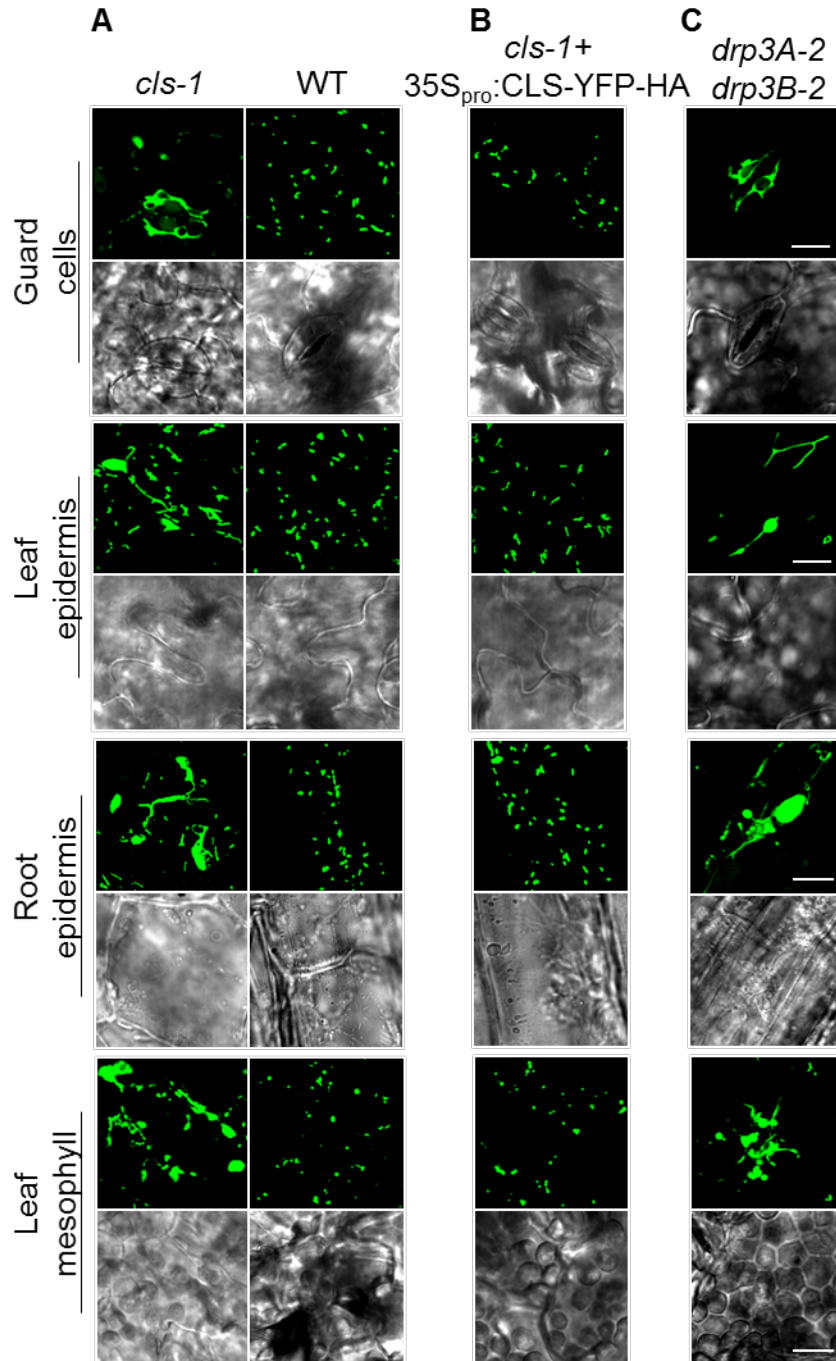


Figure 2.9. Mitochondrial morphology in *cls-1*.

Confocal images show mitochondrial morphologies in different cell types in wild type and *cls-1* (A), *cls-1* complemented by 35S_{pro}:CLS-YFP-HA (B), and *drp3* double mutant (C). All lines are expressing COX4-YFP. Scale bars, 10 μ m.

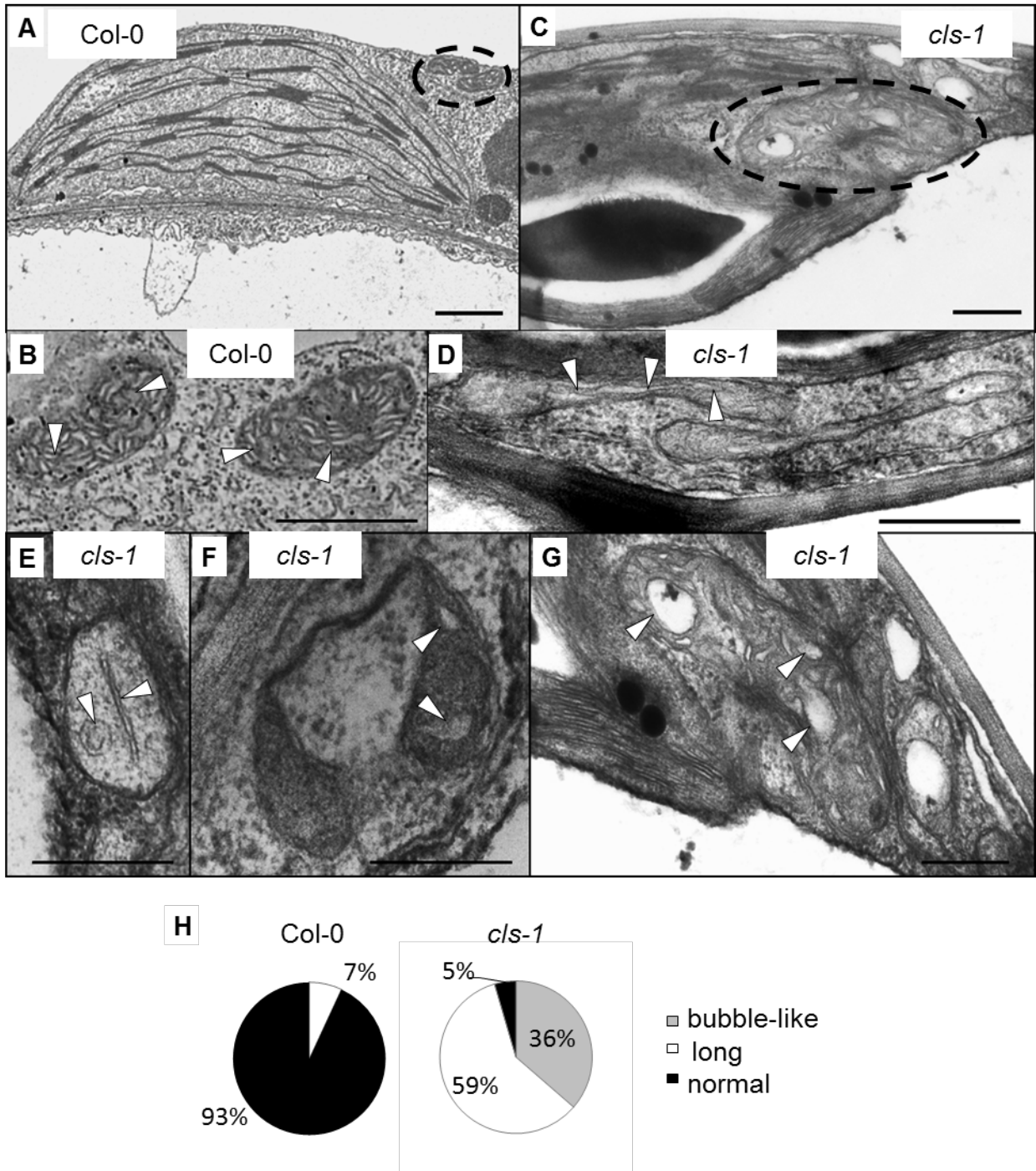


Figure 2.10. Transmission electron microscopic (TEM) analysis of mitochondrial structure from four-week-old wild-type and *cls-1* leaves.

Figure 2.10 (cont'd)

(A-F) TEM images with arrowheads indicating mitochondrial inner membrane and cristae structure. Dotted circles in (A) and (C) indicate individual mitochondria. Scale bars, 1 μm .

(G) Quantification of mitochondrial cristae structure with different morphologies in *c/s-1*. Data were collected from 22 mitochondria in the mutant. Long cristae is defined as >0.4 μm in length, and bubble-like cristae is defined as bubble-shaped and >0.2 μm in diameter.

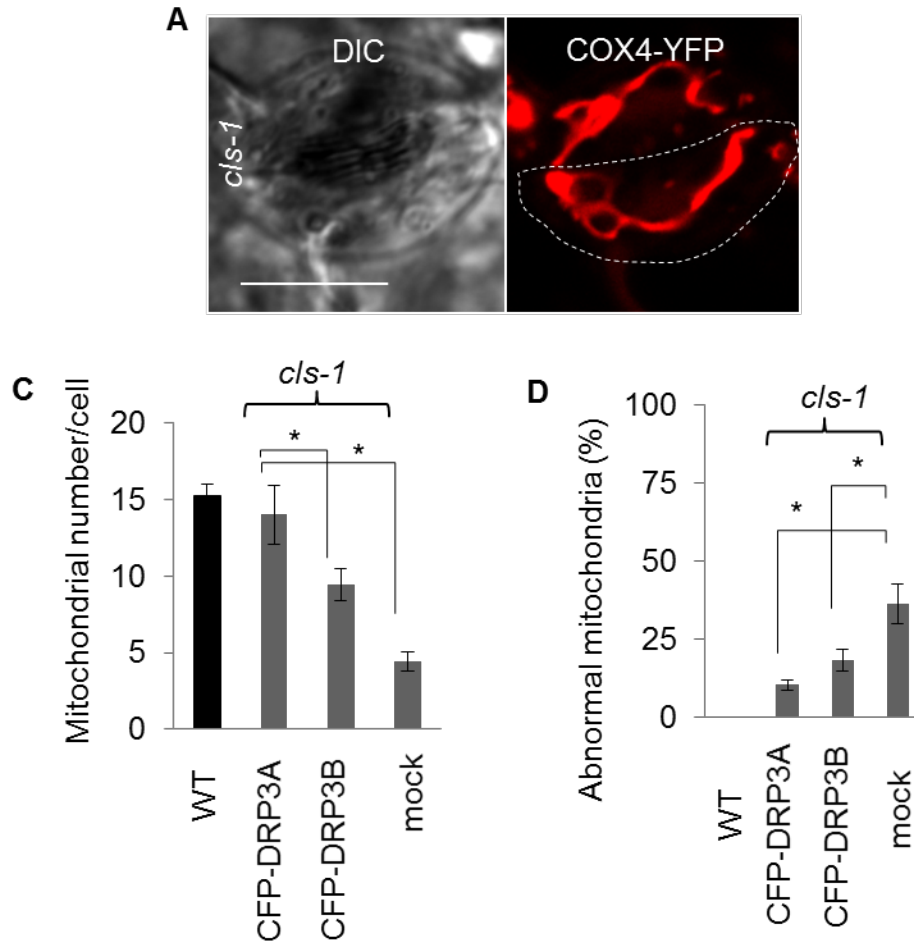


Figure 2.11. Partial complementation of the mitochondrial morphological phenotype in *c/s-1* by DRP3 proteins.

Figure 2.11 (cont'd)

B

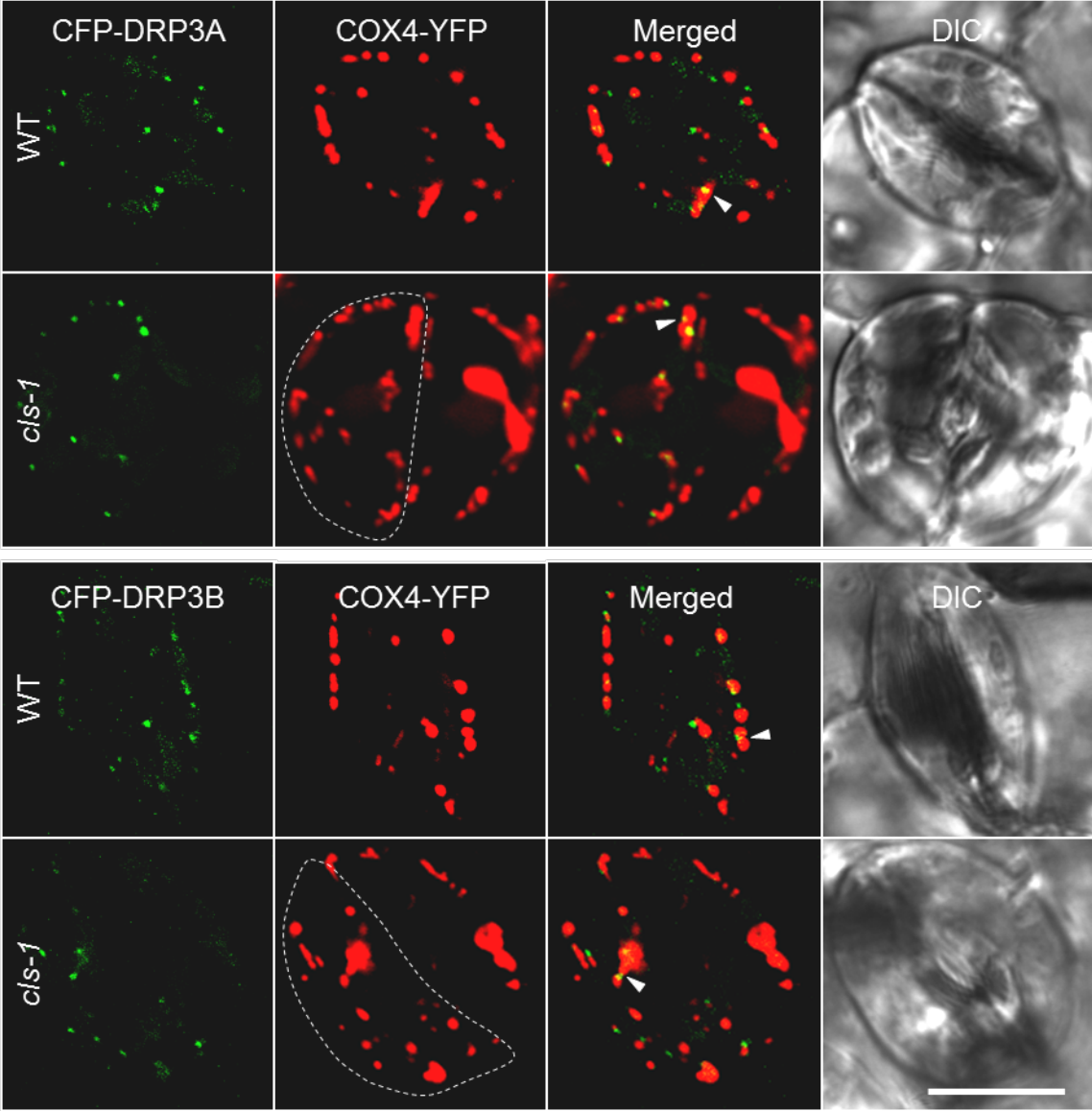


Figure 2.11 (cont'd)

(A) Mitochondrial morphology in *cls-1* guard cells. Scale bar = 10 μm .

(B) Mitochondrial morphology in wild-type and *cls-1* guard cells expressing 35S_{pro}:CFP-DRP3A or 35S_{pro}:CFP-DRP3B. Scale bar, 10 μm . Arrowheads point to some mitochondrial-associated DRP3 proteins. Dashed lines delineate single guard cells.

(C and D) Quantification of the rescue of mitochondrial fission defects in *cls-1* by CFP-DRP3 overexpression. Independent mitochondria per guard cell were quantified. Abnormal mitochondria include enlarged and elongated mitochondria, where enlarged mitochondria have diameters $>2 \mu\text{m}$ and elongated mitochondria have lengths $>4 \mu\text{m}$. Error bars, s.e.m.; n=6 (number of cells analyzed). Asterisks indicate $p<0.05$ in *t*-test.

```

atDRP3A  MTIEEVSGETPPSTPPSSSTPSPSSSTTNAAPLGSSVIPIVNLQDIFAQLGSQS--TIA  58
atDRP3B  MSVDDLP-----PSSASAVT---PLGSSVIPIVNLQDIFAQLGSQS--TIA  42
hsDLP1   -----MEALIPVINKLQDVFNVTVGAD---IIQ  24
mmDRP1   -----MEALIPVINKLQDVFNVTVGAD---IIQ  24
dmDRP1   -----MEALIPVINKLQDVFNVTVGSD---SIQ  24
scDNM1   -----MASLEDLIPTVINKLQDVMYDSGID---TLD  27
scVPS1   -----MDEHLISTINKLQDALAPLGGGSQSPID  28
atARC5   -----ATARCMAEVSAKSVTVEEMAEEDDAAIEERWSLYEAYNELHALAQELETPE  52

atDRP3A  LPQVVVVGSSGKSSVLEALVGRDFLPRGNDICTRRPLVLQQLQTKS-----RAN  109
atDRP3B  LPQVAVVVGSSGKSSVLEALVGRDFLPRGNDICTRRPLRLQLVQTKP-----SSD  93
hsDLP1   LPQIVVVGTSQSSGKSSVLESVGRDLLPRGTGIVTTRRPLILQLVHVSQ-----EDKRKTT  79
mmDRP1   LPQIVVVGTSQSSGKSSVLESVGRDLLPRGTGVVTRRPLILQLVHVSP-----EDKRKTT  79
dmDRP1   LPQIVVLGSSGKSSVIESVGRSFLPRGTGIVTTRRPLVLQLIYSPL-----DDRENRS  79
scDNM1   LPILAVVVGSSGKSSILETLVGRDFLPRGTGIVTTRRPLVLQLNINISPNPLIEEDDNSV  87
scVPS1   LPQITVVVGSSGKSSVLENIVGRDFLPRGTGIVTTRRPLVLQLINRRPKKSEHAKVNQTA  88
atARC5   APAVLVVGQQTGKSSALVEALMGFQFNHVGGGTTKTRRPITLHMKYDPQ-----  100

atDRP3A  GGSD-----DEWGEFR-HLPETRFYDFSEIRREIEAET  141
atDRP3B  GGSD-----EEWGEFLHHPVRRRIYDFSEIRREIEAET  126
hsDLP1   GEEN-----GVEAEWGWKFL-HTKNKLYTDFDEIRQEIENET  115
mmDRP1   GEENDPATWKNRSH-----LSKGVEAEWGWKFL-HTKNKLYTDFDEIRQEIENET  128
dmDRP1   AENG-----TSNAEWEGRFL-HTK-KCFTDFDEIRKEIENET  114
scDNM1   NPHDEVTKISGFEGTKPLEYR--GKERNHADEWGEFL-HIPGKRFYDFDDIKREIENET  144
scVPS1   NELIDLNINDDDKKDESGKHQNEGQSEDNKEEWEWGEFL-HLPGKKFYNFDEIRKEIVKET  147
atARC5   -----CQFPLCHLGSDD-DPSVSLPKSLSQIQAYIEAEN  133

atDRP3A  NRLVGE-NKGVADTQIRLKISSPNVLNITLVDLPGITKVP--VGDQPSDIEARIRTMILS  198
atDRP3B  NRVSGE-NKGVSDIPIGLKIFSPNVLDISLVDLPGITKVP--VGDQPSDIEARIRTMILT  183
hsDLP1   ERISGN-NKGVSEPIHLKIFSPNVNLTlVDLPGMTKVP--VGDQPKDIELQIRELILR  172
mmDRP1   ERISGN-NKGVSEPIHLKVFSNVNLTlVDLPGMTKVP--VGDQPKDIELQIRELILR  185
dmDRP1   ERAAGS-NKGICPEPINLKI FSTHVNLTlVDLPGITKVP--VGDQPEDIEAQIKELVLK  171
scDNM1   ARIAGK-DKGISKIPINLKVFSPHVNLTLVDLPGITKVP--IGEQQPDIEKQIKNLILD  201
scVPS1   DKVTGA-NSGISSVPINLRIYSPHVLTLTLVDLPLGLTKVP--VGDQPPDIERQIKDMLLK  204
atARC5   MRLEQEPSPFSAKEIIVKVQYKYCPNLTIIDTPGLIAPAPGLKNRALQVQARAVEALVR  193

atDRP3A  YIKQDTCILILAVTPANTDLANSDALQIASIVDPDGHRITIGVITKLDIMDKGTDARKLLLG  258
atDRP3B  YIKEPSCILILAVSPANTDLANSDALQIAGNADPDGHRITIGVITKLDIMDRGTDARNHLLG  243
hsDLP1   FISNPNSIILAVTAANTDMATSEALKISREVDPDGRRTLAVITKLDLMDAGTDAMDVLGM  232
mmDRP1   FISNPNSIILAVTAANTDMATSEALKISREVDPDGRRTLAVITKLDLMDAGTDAMDVLGM  245
dmDRP1   YIENPNSIILAVTAANTDMATSEALKLAKDVPDGRRTLAVVTKLDLMDAGTDAIDILCG  231
scDNM1   YIATPNCLILAVSPANVDLVNSESLLKAREVDPQKRTIGVITKLDLMDSGTNALDILSG  261
scVPS1   YISKPNAILSVNAANTDLANS DGLKLAREVDEPGRTRTIGVLTKVLDLMDQGTDIVIDILAG  264
atARC5   AKMQHKEFIILCLEDSSDWSIATTRRIVMQVDEPELSRTIVVSTKLDTKIPQFSCSSDVEV  253

atDRP3A  NVVPLRLGYGVVNVNQCQEDILLNRTVKEALLAEKFFRSHPVYHGLAD--RLGVPQLAKK  316
atDRP3B  KTIPLRLGYGVVNVNSQEDILMNRSIKDALVAEEKFFRSRPVYSGLTD--RLGVPQLAKK  301
hsDLP1   RVIPVKLGIIGVVNNSQLDINNKKSVTDSIRDEYAFLOKQK--YPSLAN--RNGTKYLART  288
mmDRP1   RVIPVKLGIIGVVNNSQLDINNKKSVTDSIRDEYAFLOKQK--YPSLAN--RNGTKYLART  301
dmDRP1   RVIPVKLGIIGVMNNSQKDIMDQKHIDDQMKDEAAFLQRK--YPTLAT--RNGTPYLAKT  287
scDNM1   KMYPLKLGFGVVNNSQQDIQLNKTVEESLDKEEDYFRKHPVYRTIST--KCGTRYLAKL  319
scVPS1   RVIPLRYGYIPVINEGQKDIEHKKTIREALENERKFFENHPSYSSKAH--YCGTPYLAKK  322
atARC5   FLSPPASALDSSLGDSPPFTSVPSGRVGYGQDSVYKSNDEFKQAVSLREMEDIASLEKK  313

```

Figure 2.12. Alignment of the N terminus (containing the GTPase domain) of mitochondrial/peroxisome division DRP proteins from various species.

Figure 2.12 (cont'd)

The conserved CL-interacting Arg and the three other conserved residues, Lys, Ser and Thr, in the GTPase domain are highlighted. Sequence alignment was performed using the ClustalW2 program.

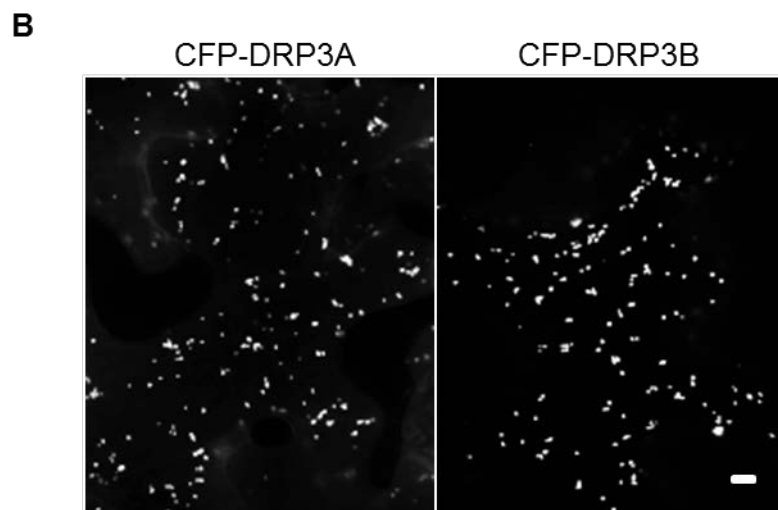
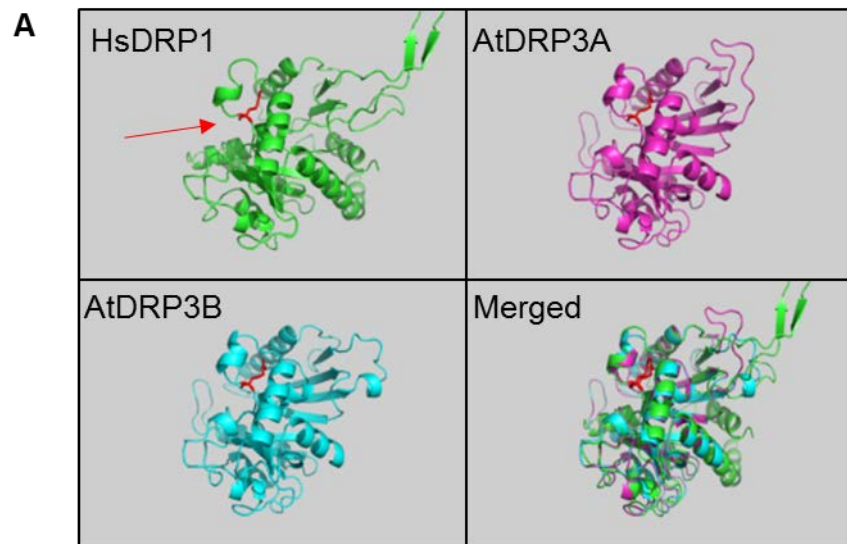


Figure 2.13. Functional association of CL and DRP3 in mitochondrial fission.

Figure 2.13 (cont'd)

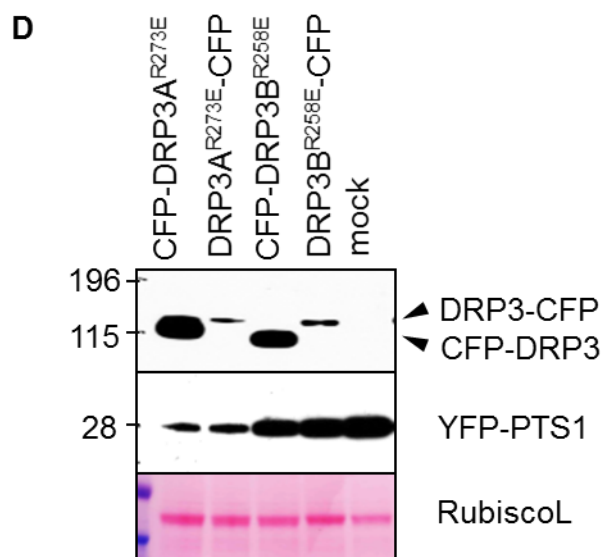
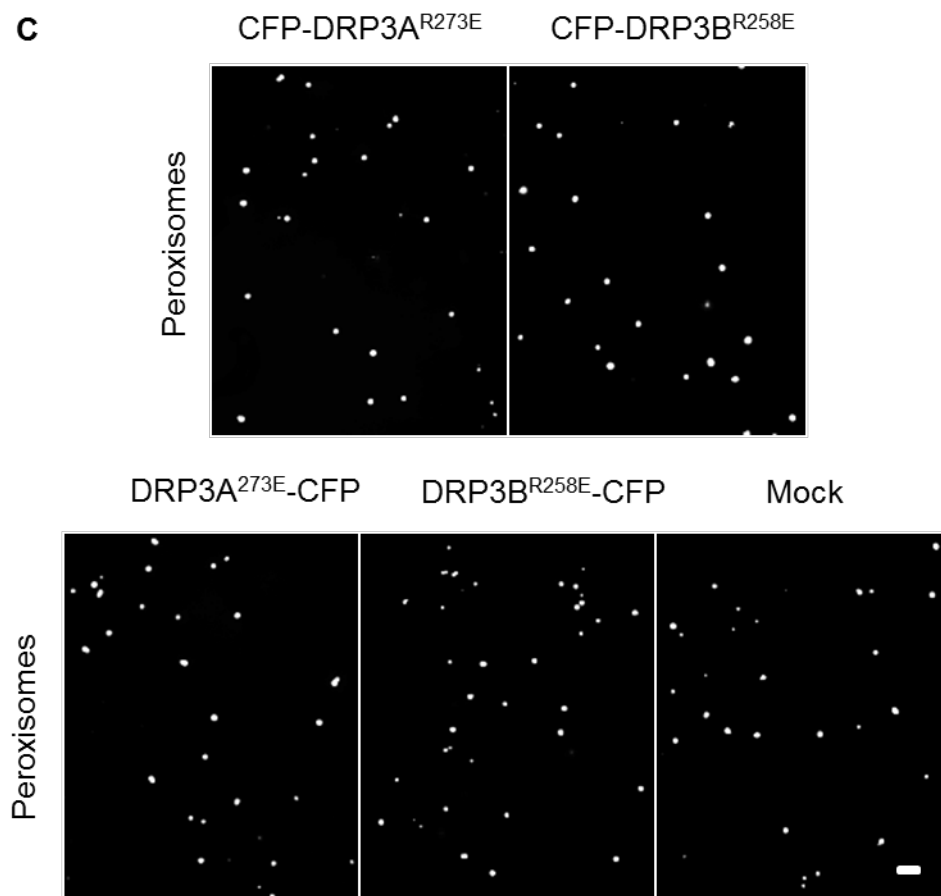


Figure 2.13 (cont'd)

(A) Structural modeling of the GTPase domain from *Arabidopsis* DRP3A (60 to 321 aa) and DRP3B (44 to 306 aa) and human DRP1 (2 to 314 aa). The protein model was generated by SWISS-MODEL (<http://swissmodel.expasy.org>), based on the structure of Dynamin 3 GTPase domain, and visualized with the PyMOL software. The cardiolipin-interacting Arg (R247) is shown in red and indicated by an arrow.

(B) Epifluorescent images showing mitochondrial morphology in tobacco leaf epidermal cells transiently overexpressing wild-type CFP-DRP3A or CFP-DRP3B, together with the mitochondrial marker COX4-YFP. Scale bar, 10 μm .

(C) Epifluorescent images showing peroxisome morphology in tobacco leaf epidermal cells transiently overexpressing DRP3A^{R273E}-CFP, DRP3B^{R258E}-CFP, CFP-DRP3A^{R273E}, or CFP-DRP3B^{R258E}, together with the peroxisomal marker YFP-PTS1. Scale bar, 10 μm .

(D) Immunoblot analysis of DRP3 fusion proteins in crude protein extracts from tobacco leaves co-expressing each CFP-DRP3 (or DRP3-CFP) fusion protein and the peroxisomal marker YFP-PTS1. The proteins were detected by the GFP antibody.

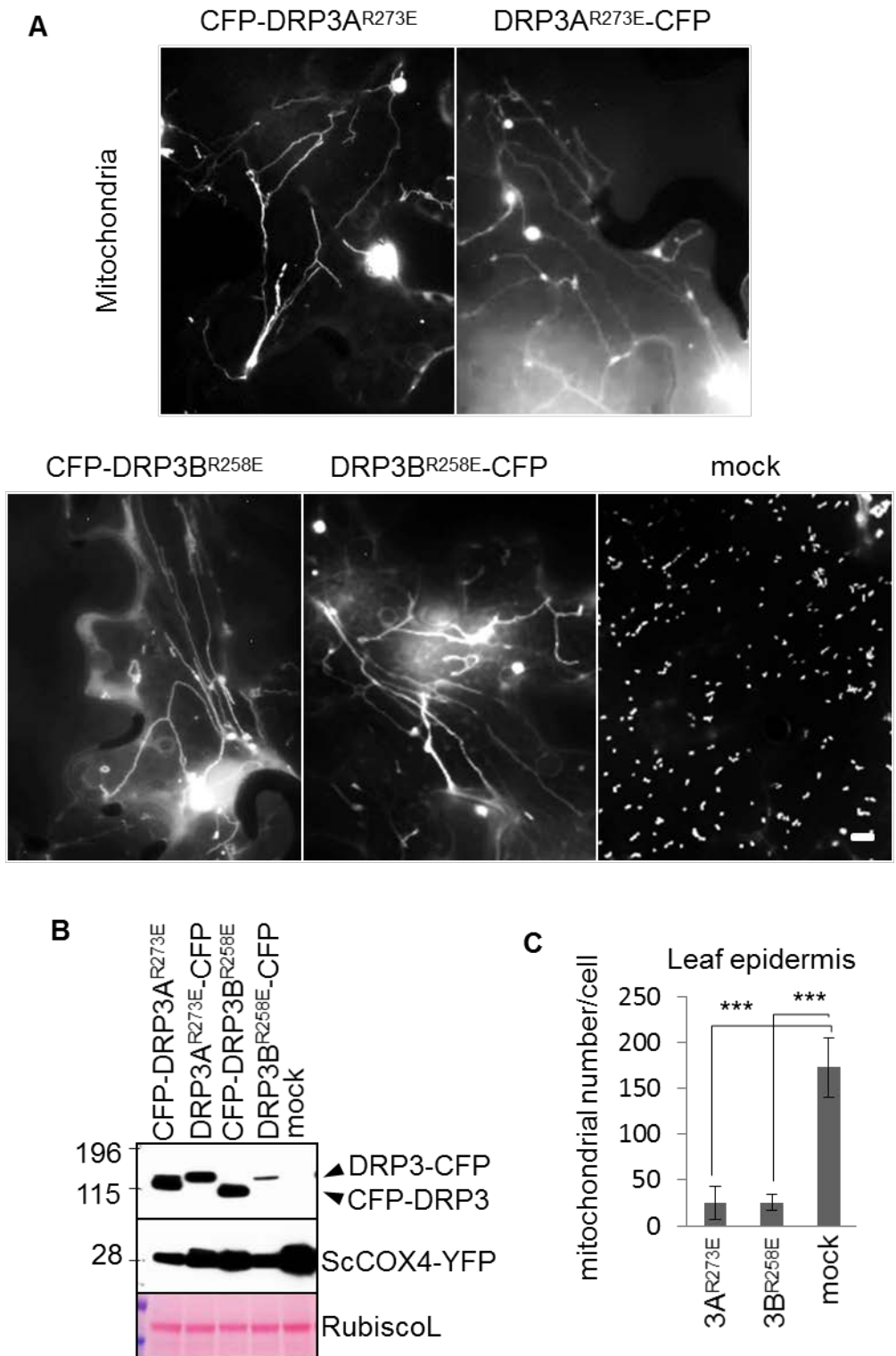
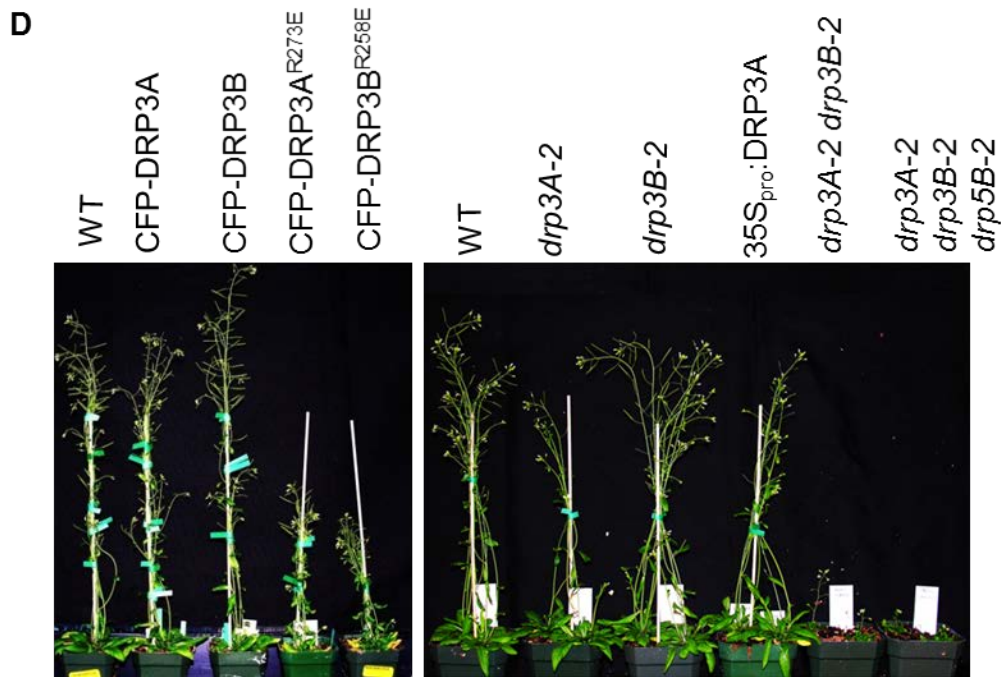


Figure 2.14. DRP3's function in mitochondrial fission depends on interaction with CL.

Figure 2.14 (cont'd)



(A) Epifluorescent images of tobacco leaf epidermis co-expressing CFP-DRP3^{R->E} (or DRP3^{R->E}-CFP) and the mitochondrial marker COX4-YFP. Scale bar, 10 μ m.

(B) Immunoblot analysis of the expression of DRP3 fusion proteins in crude protein extracts from tobacco leaves co-expressing CFP-DRP3 (or DRP3-CFP) and COX4-YFP. Proteins were detected by the GFP antibody. The large subunit of Rubisco stained by Ponceau S was shown as a protein loading control.

(C) Quantification of the number of independent mitochondria in cells expressing CFP-DRP3A^{R273E} or CFP-DRP3B^{R258E}. Error bars, s.d.; n=5. Triple asterisks indicate $p < 0.001$.

(D) Six-week-old plants overexpressing CFP-DRP3 or CFP-DRP3^{R->E}, and various DRP3 loss- and gain-of-function lines.

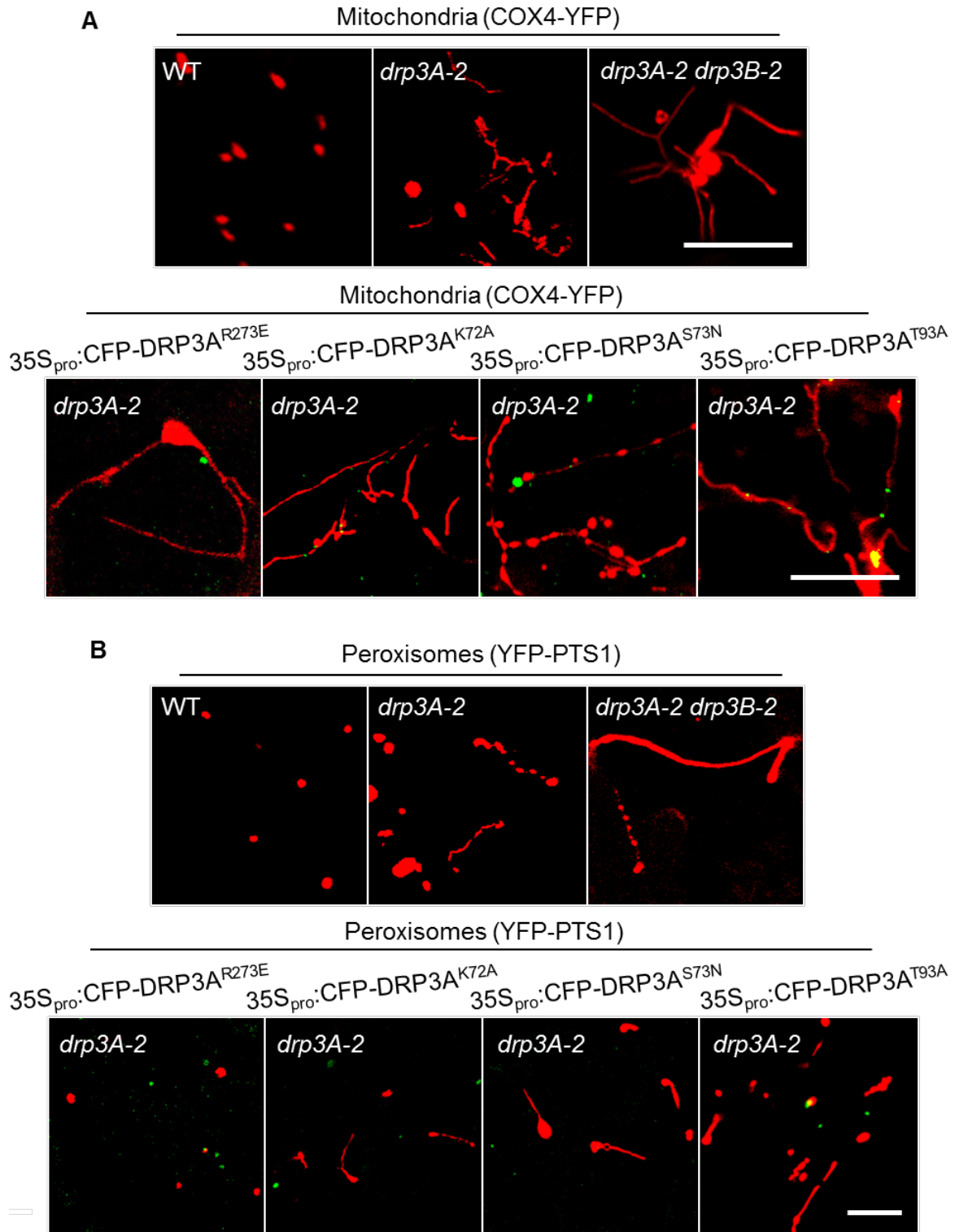
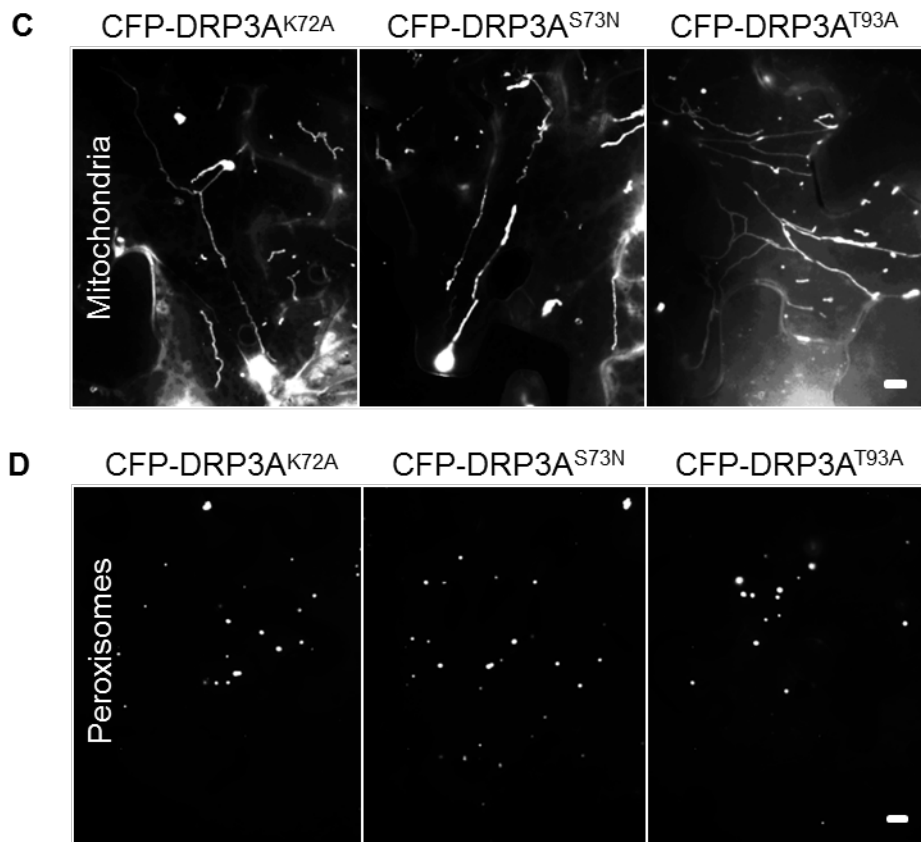


Figure 2.15. Analysis of the role of a few conserved residues in mitochondrial and peroxisomal fission.

Figure 2.15 (cont'd)



(A-B) Mitochondrial (A) and peroxisomal (B) morphologies in leaves of *Arabidopsis* plants in various genetic background (left) or in *drp3A-2* transiently expressing mutant CFP-DRP3A proteins (right).

(C-D) Tobacco leaf epidermis overexpressing CFP-DRP3A^{K72A}, CFP-DRP3A^{S73N} or CFP-DRP3A^{T93A} and the mitochondrial (C) or peroxisomal (D) marker.

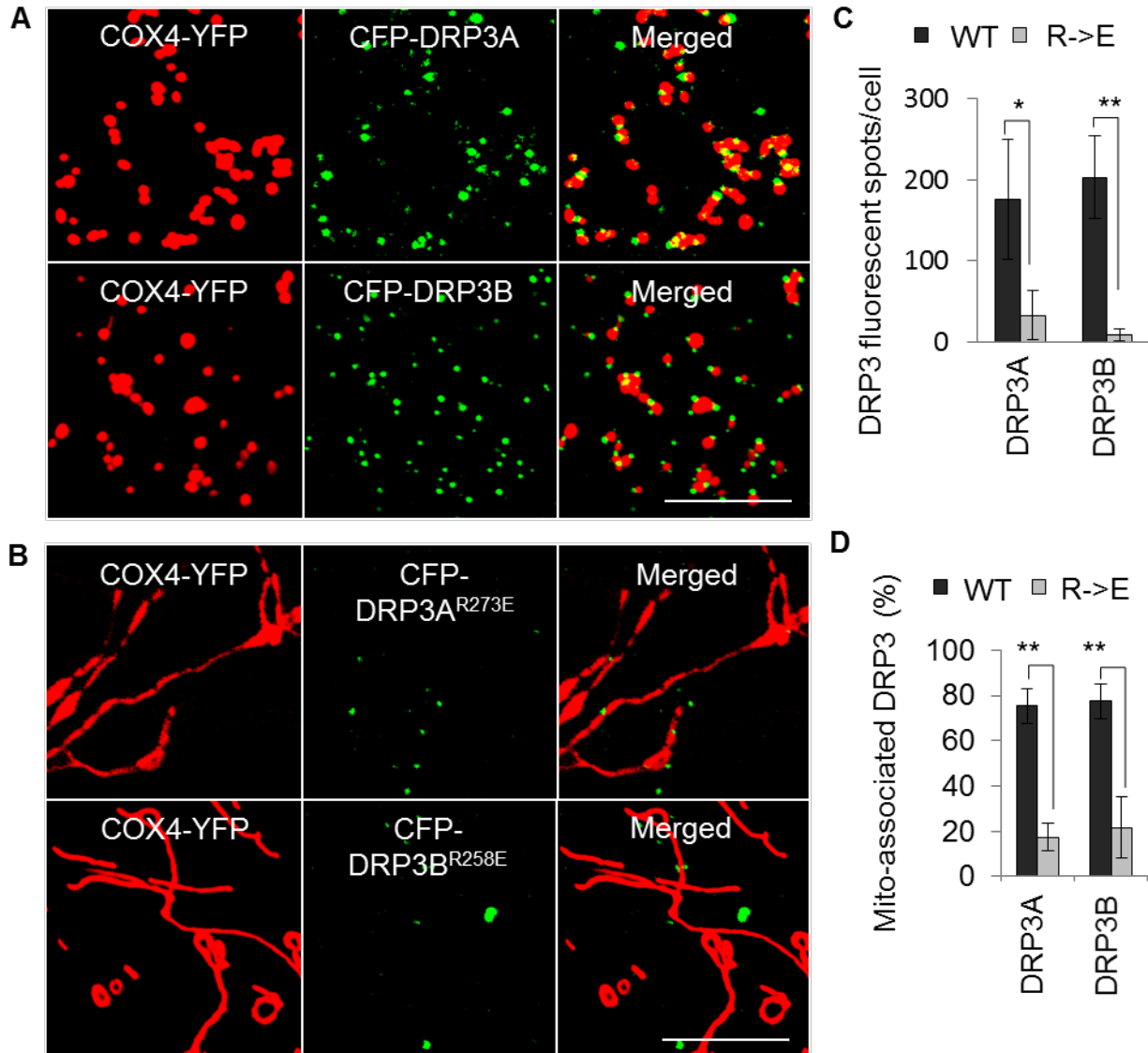


Figure 2.16. Association of CFP-DRP3 and CFP-DRP3^{R->E} proteins with mitochondria.

(A and B) Confocal analysis of the association of CFP-DRP3 and CFP-DRP3^{R->E} with mitochondria in tobacco leaf epidermis expressing COX4-YFP. Scale bar, 10 μ m.

(C and D) Quantification of the number of CFP-DRP3 fluorescent spots and their mitochondrial association. Error bars, s.d.; n=4. Single asterisk, $p < 0.05$; double asterisks, $p < 0.01$.

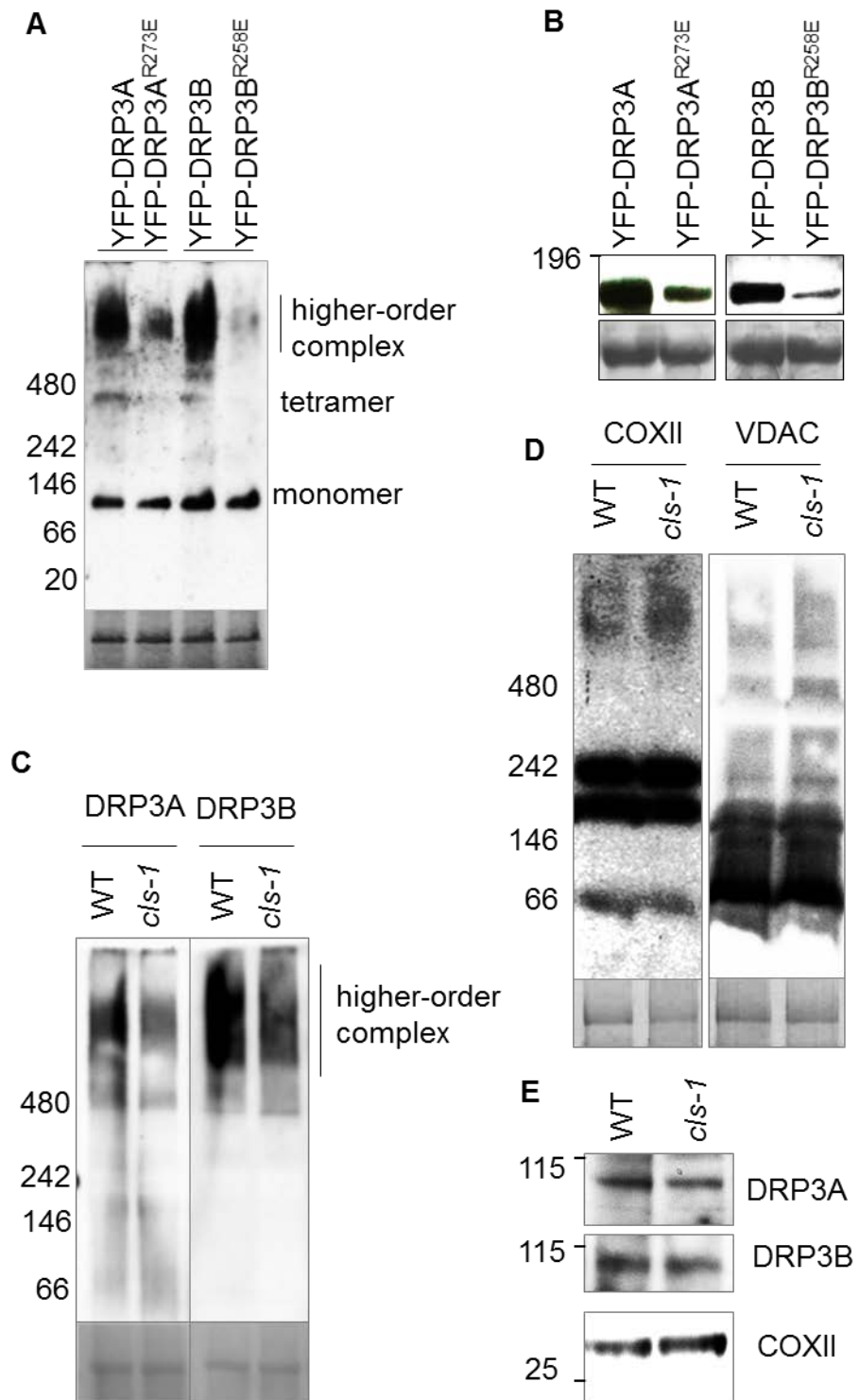


Figure 2.17. Cardiolipin stabilizes DRP3 protein complexes.

Figure 2.17 (cont'd)

(A) BN-PAGE followed by immunoblot analysis to detect the level of oligomerization of DRP3 proteins overexpressed in tobacco leaves. Crude protein extracts were analyzed and the α -GFP antibody was used to detect YFP-DRP3 proteins. Coomassie Blue staining of Rubisco is shown at bottom as the loading control.

(B) SDS-PAGE followed by immunoblot analysis of DRP3 fusion proteins analyzed in (A), detected by α -GFP antibodies. Loading control, large subunit of Rubisco stained by Ponceau S.

(C and D) BN-PAGE followed by immunoblot analysis to detect the level of complex formation for DRP3 (C) and COXII and VDAC proteins (D) in *cls-1*. Crude protein extracts from leaves were used, and endogenous DRP3A, DRP3B, COXII, and VDAC proteins were detected by their respective antibodies. Coomassie Blue staining of Rubisco is shown as the loading control.

(E) SDS-PAGE followed by immunoblot analysis of endogenous DRP3 and COXII in *cls-1*, detected by their respective antibodies.

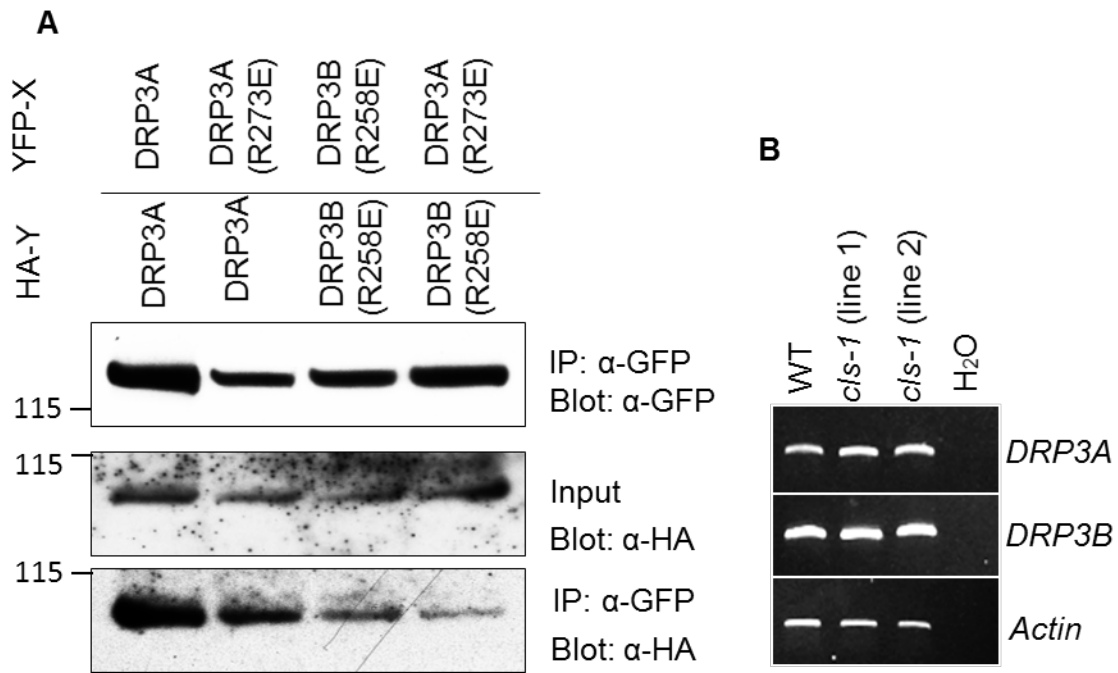


Figure 2.18. Analyses of $DRP3^{R \rightarrow E}$ protein self-interaction in tobacco and *DRP3* transcript levels in *cls-1*.

(A) Co-IP analysis of YFP- and HA-tagged *DRP3* proteins co-expressed in tobacco leaves. IP, immunoprecipitation. Blot, immunoblot.

(B) RT-PCR analysis of *DRP3A* and *DRP3B* transcripts in wild-type and *cls-1* plants.

Actin mRNA level was included as a loading control.

Figure 2.19 (cont'd)

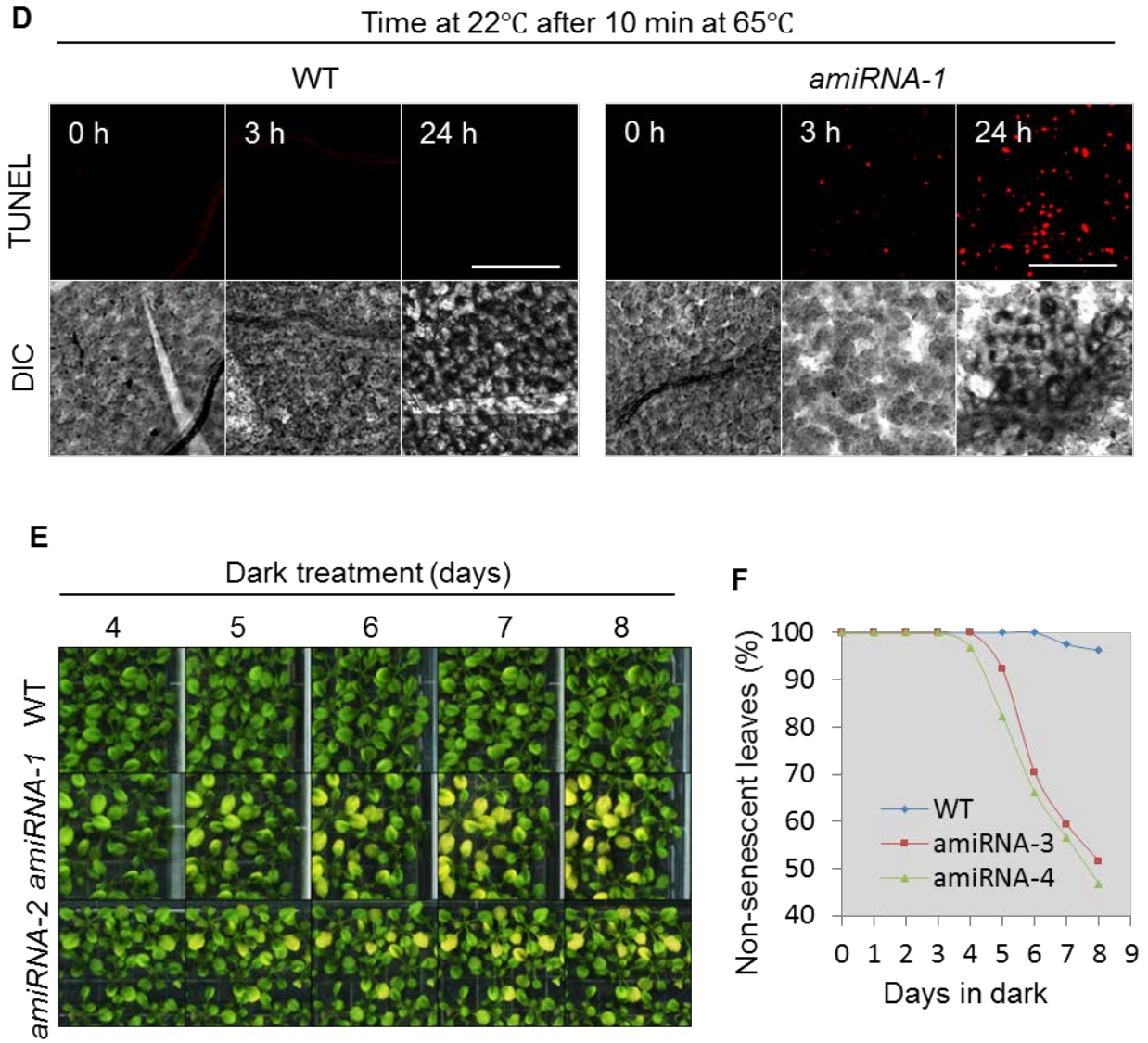


Figure 2.19 (cont'd)

(A) RT-PCR analysis of *CLS* mRNA levels in four-week-old plants.

(B) Appearance of three-week-old *Arabidopsis* plants treated with 65°C heat for 10 min and left to recover at 22°C for varied lengths of time.

(C) Quantitative analysis of the tolerance of wild-type and *cls* mutants to heat stress. Percentage of healthy leaves showing no chlorosis or withering was calculated. Error bars, s.e.m; n=2.

(D) TUNEL staining of fragmented DNA in leaf epidermal cells from wild type and *CLS* amiRNA-1 lines treated by heat. Scale bars, 100 µm.

(E) Accelerated induction of senescence in dark-treated *CLS* deficient mutants. Three-week-old seedlings were subjected to dark treatment for 8 days, during which the plates were brought to light for imaging before being placed back to the dark.

(F) Quantitative analysis of the number of senescent leaves in wild-type and *cls* mutants shown in (E). Percentage of healthy leaves showing no visible signs of senescence was calculated.

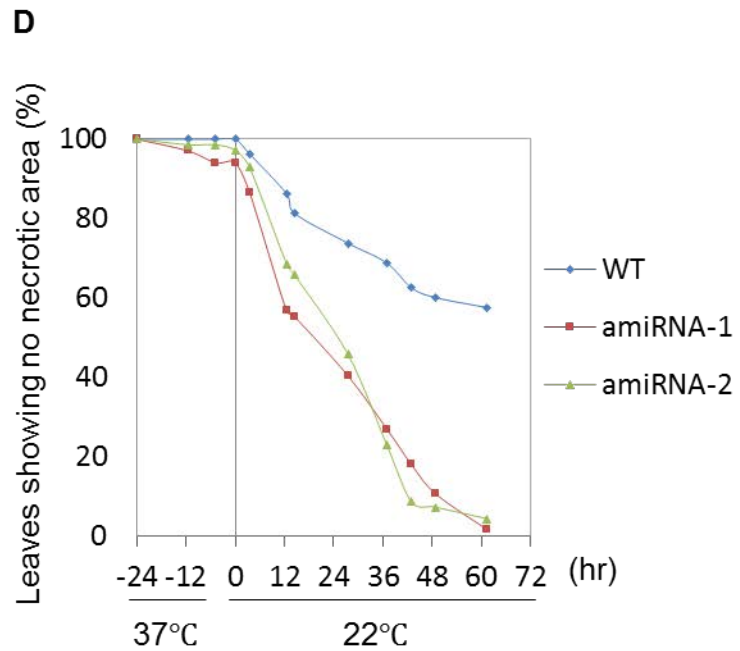
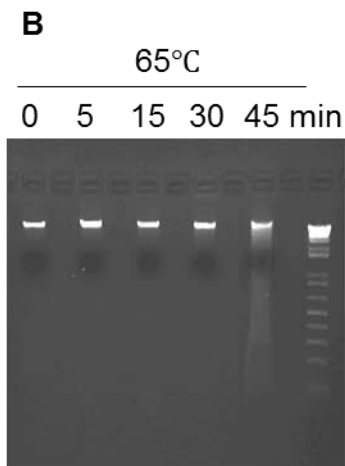
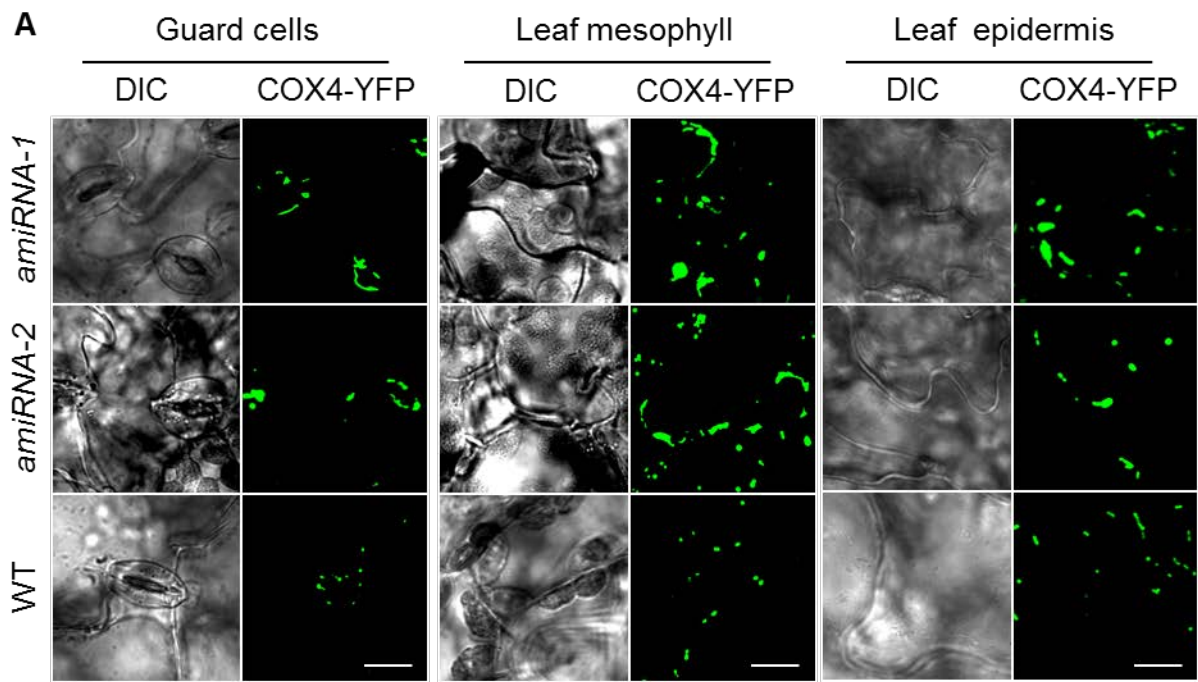
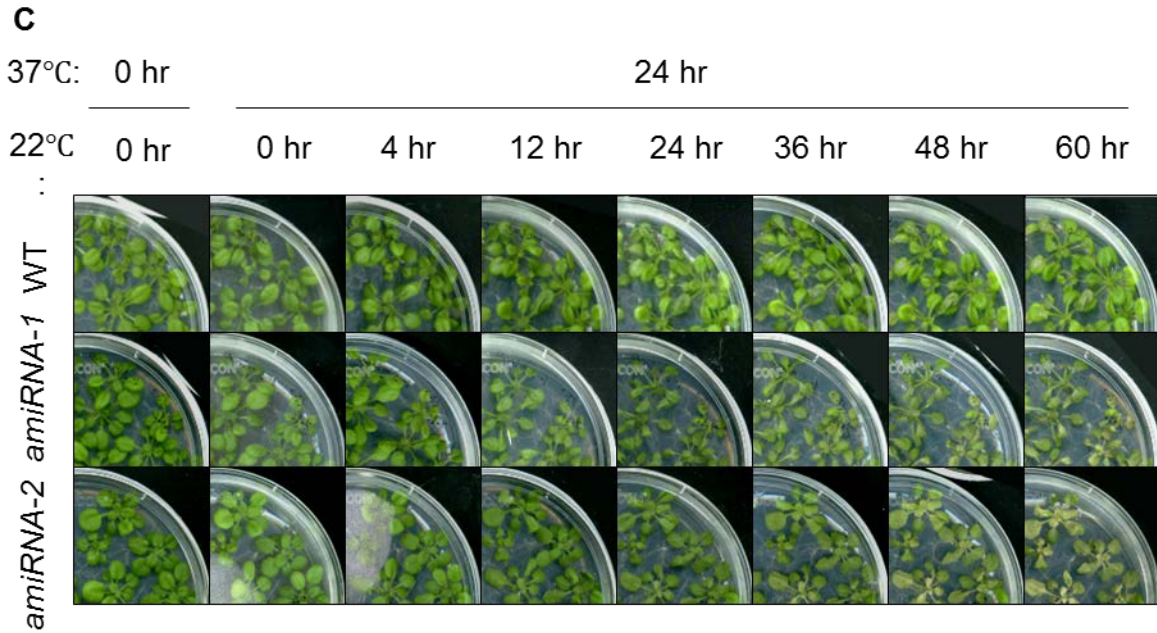


Figure 2.20. Mitochondrial phenotypes of *CLS* amiRNA lines and characterization of CL's role in plant response to PCD-inducing stresses.

Figure 2.20 (cont'd)



(A) Confocal images showing mitochondrial morphology in the two amiRNA lines used in this study. Scale bars, 10 μm .

(B) Electrophoresis of genomic DNA from wild-type plants incubated at 65°C for various lengths of time.

(C) Three-week-old *Arabidopsis* seedlings subjected to 37°C heat treatment for 24 hours and then left at 22°C.

(D) Quantitative analysis of the susceptibility of wild type and *cls* mutants to 24-hr heat stress at 37°C. Percentage of leaves showing no signs of chlorosis or withering was calculated.

Table 2.1. DNA primers used in Chapter 2.

Primer	Sequence (5'-3')
CLS-Fw-AttB1	ggggacaagttgtacaataaaagcaggcttcatggcgatttacagatctctaag
CLS-Re-AttB2-N	ggggaccactttgtacaagaaagctgggtcctatgatctcttaatcatagatatagg
CLS-Re-front	cgccattgatatcatattcgg
CLS-Re-AttB2-C	ggggaccactttgtacaagaaagctgggtctgatctcttaatcatagatatagg
DRP3A-Fw-attB1	ggggacaagttgtacaataaaagcaggcttcatgactattgaagaagttccg
DRP3A-Fw-attB2-N	ggggaccactttgtacaagaaagctgggtcttagaatccgatccattttggtg
DRP3A-Re-attB2-C	ggggaccactttgtacaagaaagctgggtcgaatccgatccattttggtg
DRP3B-Fw-attB1	ggggacaagttgtacaataaaagcaggcttcatgtccgtcgacgatctccc
DRP3B-Re-attB2-N	ggggaccactttgtacaagaaagctgggtcttacatataagccgtccgttc
DRP3B-Re-attB2-C	ggggaccactttgtacaagaaagctgggtccatataagccgtccgttc
CLS-partial -Re-1	ggggaccactttgtacaagaaagctgggtctggcttgtttccggtgattg
CLS-partial-Re-2	ggggaccactttgtacaagaaagctgggtcgaacaacggcgaaaactgcggtgg
CLS-partial-Re-3	ggggaccactttgtacaagaaagctgggtcaaaactctgactaattttccacc
CLS-partial-Fw-4	ggggacaagttgtacaataaaagcaggcttcatgagaccattcttcaccgccgctac agc
CLS-partial-Fw-5	ggggacaagttgtacaataaaagcaggcttcatgccgttgtcccacatttctcac
CLS-partial-Fw-6	ggggacaagttgtacaataaaagcaggcttcatgaagagttttgtaatgtgccg
DRP3A-R273E-Fw	gtaaatagagtgccaggaggatattttgctaaaccg
DRP3A-R273E-Re	ctggcactcatttacaactcccacgatccaagtc
DRP3B-R258E-Fw	gagttgtaaatagagtgcaagaggatattttgatg
DRP3B-R258E-Re	tcctcttgactctcatttacaactcccacgatcc
CLS I miR-s	gattacacaccgataagaaccctctcttttgtattcc
CLS II miR-a	gagggttcttatcgggtgtgtaatacaagagaatcaatga
CLS III miR*s	gaggattcttatcggctgtgtattcacaggctcgatgatg
CLS IV miR*a	gaatacacagccgataagaatcctctacatatatattcct
UBQ10-1	tcaattctcttaccgtgatcaagatg
UBQ10-2	ggtgtcagaactctccacctcaagag
RT-3A-F	gctgcaaatgcgagtgatacaaggtggg
RT-3A-R	caactcatctagtgtcctgtaagcttgc
RT-3B-F	ctgcaccagctggaagcacaagctggag
RT-3B-R	ccgattcagcttctaacggcagctcgtc
P67_Act7_FP	ttcaatgtccctgccatga
P68_Act7_RP	tgaacaatcgatggacctga
PR-1-LB1	atgaattttactggctattc
PR-1-RB1	aaccacatgttcacggcgga
PR-2-LB1	gcttccttctcaaccccaca
PR-2-RB1	ctgaacctccttgagacgga
eIF1 α -LB1	gcacagtcattgatgccccca
eIF1 α -RB1	cctcaagaagagttggctcct
CLS-genotyping-1	cgtaccttgatcctcttgacag

Table 2.1 (cont'd)

Primer	Sequence (5'-3')
CLS-genotyping-2	atTTGccgatttcggaac
CLS-genotyping-3	ttagcgagggaacatgTTTTg
DRP3A-K72A-fw	cagTggcgcgTctagcgtcctTgaagcactcgtcg
DRP3A-K72A-re	cgctagacgcgccactgctTggctccaacaac
DRP3A-S73N-fw	ggcaagaatagcgtcctTgaagcactcgtcggccg
DRP3A-S73N-re	gacgctattctTgccactgctTggctccaacaac
DRP3A-T93A-fw	atctgcgcgcgtcgtcctctTgtctccagctcc
DRP3A-T93A-re	acgacgcgcgcagatatcattaccacgaggag

Table 2.2. Vectors used in Chapter 2.

Vector and reference	Construct	Plant selection
pDonor 207 (Invitrogen)	all donor plasmids	
pEarleyGate 100 (Earley et al., 2006)	amiRNA CLS	BASTA
pEarleyGate 101 (Earley et al., 2006)	YFP-CLS.	BASTA
pEarleyGate 104 (Earley et al., 2006)	CLS-YFP-HA	BASTA
pEarleyGate 201 (Earley et al., 2006)	HA-DRP3A	BASTA
pDest-35S-6xHis-YFP-X (Reumann et al., 2009)	YFP-DRP3A, YFP-DRP3B, YFP-DRP3A ^{R273E} , YFP-DRP3B ^{R258E}	Kanamycin
pDest-35S-X-YFP-6xHis (Reumann et al., 2009)	CLS ¹⁻²⁰ -YFP, CLS ¹⁻⁴¹ -YFP, CLS ¹⁻¹⁴⁰ -YFP, CLS ²¹⁻³⁴¹ -YFP, CLS ⁴²⁻³⁴¹ -YFP, CLS ⁴²⁻¹⁴⁰ -YFP, CLS ¹⁴¹⁻³⁴¹ -YFP	Kanamycin
pGWB544 (Nakagawa et al., 2007)	CFP-DRP3A, CFP-DRP3B, CFP-DRP3A ^{R273E} , CFP-DRP3B ^{R258E} , CFP-DRP3A ^{K72A} , CFP-DRP3A ^{S73N} , CFP-DRP3A ^{T93A}	Hygromycin
pGWB545 (Nakagawa et al., 2007)	DRP3A ^{R273E} -CFP, DRP3B ^{R258E} -CFP	Hygromycin

2.5 Methods

2.5.1 Plant material and transformation

Plants were grown at 22°C with 70% humidity, 70 to 80 $\mu\text{mol m}^{-2} \text{s}^{-2}$ of white light for 14 h per day. Col-0 was used as the wild type. Seeds for the T-DNA insertion mutant *cls-1* (SALK_049840) were provided by the Arabidopsis Biological Resource Center (ABRC), and homozygous mutants were identified by PCR of genomic DNA. Organelle marker lines were either generated in our previous studies or obtained from other sources, as cited in the text. Transgenic *Arabidopsis* plants were generated via simplified flora dipping method (<http://entomology.wisc.edu/~afb/protocol.html>) using *Agrobacterium tumefaciens* strain GV3101 (pMP90). To screen for transformants with BASTA, T1 plants were grown on soil and sprayed at 7 days and 9 days after germination with 0.1% (v/v) of Basta (Finale; Farnam Companies, Phoenix, AZ, USA) with 0.05% (v/v) Silwet L-77. For other transformants, T1 seeds were plated on 0.5 Linsmaier and Skoog (1/2 LS) medium containing 50 $\mu\text{g/ml}$ kanamycin, or 50 $\mu\text{g/ml}$ hygromycin (see Supplemental Table S2). Transient gene expression in tobacco (*Nicotiana tabacum*) plants was performed as described previously (Aung and Hu, 2011). Information on the primers and vectors used is provided in Supplemental Table S1 and S2.

2.5.2 Gene cloning, plasmid construction, and RT-PCR

The coding sequences of specific genes were amplified with Gateway compatible primers (Supplemental Table S1) by Phusion polymerase (NEB), using cDNA made

from total RNA of *Col-0* plants. The PCR products were cloned into pDonor207 vector and various destination vectors (Supplemental Table S2) via a standard Gateway cloning system (Invitrogen, <http://www.invitrogen.com/>). To generate point mutations of DRP3A^{R273E}, DRP3A^{K72A}, DRP3A^{S73N}, DRP3A^{T93A} and DRP3B^{R258E}, overlapping PCR was performed (<http://gfp.stanford.edu/protocol/index5.html>) with primers containing the mutation sites.

To clone the artificial microRNA construct, amiRNA *CLS* (5'-TTACACACCCGATAAGAACCC-3') was designed by WMD3-Web MicroRNA Designer (<http://wmd3.weigelworld.org/cgi-bin/webapp.cgi>). Overlapping PCR was used to clone the amiRNA according to the WMD3-Web MicroRNA Designer (http://wmd3.weigelworld.org/downloads/Cloning_of_artificial_microRNAs.pdf). The precursor miRNA was amplified by Gateway-compatible primers (Supplemental Table 1) and cloned into pEarley100 (Supplemental Table S2).

To analyze gene expression level in plants, semi-quantitative RT-PCR was performed as previously described (Aung and Hu, 2011).

2.5.3 Protein preparation and immunoblot analysis

For crude plant protein extraction, 50 mg fresh tissue from *Arabidopsis* or tobacco plants were ground with plastic pestles using liquid nitrogen and 500 μ l extraction buffer (60 mM Tris-HCl pH 8.8, 2% SDS, 2.5% glycerol, 0.13 mM EDTA pH 8.0, and 1X protease inhibitor cocktail complete from Roche). The tissue lysates were vortexed for 30 s, heated at 70°C for 10 min, and centrifuged at 13,000 g twice for 5 min at room temperature. The supernatants were then transferred to new tubes. 15 μ l of the

supernatant mixed with 5 μ l 4X LDS sample buffer was loaded onto SDS-PAGE. To prepare mitochondrial proteins for SDS-PAGE analysis, 15 μ l purified mitochondria (see below) mixed with 5 μ l 4X LDS sample buffer were heated at 70 °C for 10 min, before loaded onto SDS-PAGE.

To prepare crude native protein extracts, 100 mg fresh weight of *Arabidopsis* or tobacco leaves was homogenized with a pestle in liquid nitrogen. Total native proteins were isolated using a NativePAGE™ Sample Prep Kit (Invitrogen, Carlsbad, CA, USA). 400 μ l 1X TBS buffer containing 2% Triton X-100 was added to the homogenized samples before the mixture was incubated on ice for 30 min and later centrifuged at 17,000 g two times (15 min/each) at 4 °C. 25 μ L of the supernatant was transferred to a new tube, mixed with 3 μ l 5% G-250, and then separated on a 4%-16% Native PAGE™ according to the product manual.

After separation on the gel, proteins were transferred to a PVDF membrane. For native gels, the PVDF membrane was fixed by 8% acetic acid, rinsed, air dried, and washed with methanol, as described in the product manual. The membrane was blocked with 5% milk in 1x TBST (50 mM Tris-base, 150 mM NaCl, 0.05% Tween 20, pH 8.0) for 1 h at room temperature, and then incubated for 1 h at room temperature with primary antibody prepared in the blocking buffer as follows: 1:20000 for α -GFP (Abcam), 1:5000 for α -Actin (Sigma), 1:1,000 for α -PEX11d (Orth et al., 2007), 1:5,000 for α -VDAC (Reumann et al., 2009), 1:3000 α -FtsZ1 (provided by Dr. Kathy Osteryoung, MSU), 1:250 α -COXII (a stock from the former lab of Dr. Lee McIntosh, MSU), 1:2000 for α -HA (Cell signaling) and 1:400 for α -DRP3A and α -DRP3B (Aung and Hu, 2012). The probed membrane was washed with 1x TBST three times at 5min each time,

followed by incubation with the secondary antibody (i.e., 1:20,000 goat anti-rabbit IgG or 1:20,000 goat anti-mouse IgG, Millipore) at room temperature, washed four times with 1x TBST for 10 min each time, and then visualized with SuperSignal West Dura Extended Duration Substrate (Pierce Biotechnology).

2.5.4 NAO staining and microscopy

For NAO staining, an NAO (Invitrogen, cat. a-1372) stock solution of 2 mg/ml in 100% ethanol was prepared. 10-day-old seedlings were incubated with 10 µg/ml NAO in ddH₂O (diluted from the stock) in the dark for 10 min at room temperature. A leaf from the treated seedlings was used for fluorescence microscope analysis, using a Zeiss Axio Imager upright epifluorescence microscope and an Olympus Fluoview FV1000 confocal laser scanning microscope.

For confocal microscopy, NAO was excited with a 458 nm laser and detected at 575-620 nm. For epifluorescence microscopy, NAO was excited and detected with the same setting as CFP. CFP, YFP, and chlorophyll auto-fluorescence were excited with 458, 515, and 515 nm lasers respectively and detected at 475–500 nm, 531–580 nm and 655–755 nm, as previously described (Aung and Hu, 2011). Fluorescent mitochondrial, Golgi, and ER makers used were from a previously study (Nelson et al., 2007). The mitochondrial marker ScCOX4-YFP is a fusion of the first 29 aa of the yeast *S. cerevisiae* cytochrome *c* oxidase IV and YFP. The Golgi marker GmMan1-CFP contains the first 49 aa of soybean α-1,2-mannosidase I, which includes the cytoplasmic tail and transmembrane domain. The ER marker AtWAK2-CFP contains the signal

peptide of *Arabidopsis* wall-associated kinase 2 (AtWAK2) at the N terminus of the CFP and the ER retention signal His-Asp-Glu-Leu at the C terminus of CFP.

To observe the ultrastructure of organelles in mesophyll cells, four-week-old wild-type and *cls-1 Arabidopsis* plants were subjected to transmission electron microscopy analysis, using methods previously described (Fan et al., 2005; Aung and Hu, 2011).

2.5.5 Total lipid extraction

Lipid extraction was performed following a modified protocol from Kansas Lipidomics Research Center (<http://www.k-state.edu/lipid/lipidomics/index.htm>). Approximately 50 mg of *Arabidopsis* leaf tissue was collected and quickly immersed in 3 ml 75°C (preheated) isopropanol with 0.01% BHT (butylated hydroxytoluene, Sigma B1378) for 15 min. After adding 1.5 ml chloroform and 0.6 ml water, the mixture was briefly vortexed and then incubated 1 hr at room temperature with agitation. After the liquid portion was transferred to a new glass tube, 4 ml chloroform/methanol (2:1) with 0.01% BHT was added to the tube with the leaf tissue and agitated for 30 min at room temperature. This step was repeated until the tissue turned white. Then 1 ml 1 M aqueous KCl was added to the combined lipid extract. After a brief vortex, the sample was centrifuged at 1000 g for 5 min. After the upper phase was discarded, 2 ml water was added. After another brief vortex, the mixture was centrifuged again at 1000 g for 5 min. After discarding the upper phase, the organic extract was evaporated to dryness with blowing nitrogen in a 37°C water bath. Finally, the dried residue was dissolved in 1 ml chloroform and the tube was filled with nitrogen to protect the sample from oxidation.

2.5.6 LC/MS analysis

Analyses of lipids were performed using a Waters LCT Premier mass spectrometer interfaced to Shimadzu LC-20 HPLC pumps and a Shimadzu SIL-5000 autosampler. A 10- μ l aliquot of each reconstituted lipid extract was injected onto a Supelco Ascentis Express C18 column (2.1 x 50 mm, 2.7 μ m particles), and gradient elution was performed using a total flow rates of 0.4 ml/min and gradients based on solvent A (10 mM aqueous ammonium formate, pH 2.7) and solvent B (acetonitrile/2-propanol 1:2 v/v) as follows (A/B): 0-4 min (90/10), linear gradient to 20/80 at 15 min, linear gradient to 1/99 at 20 min and held at these conditions until 28 min, at which time the solvent composition was returned to the initial condition. Mass spectra were acquired using W-mode ion optics (mass resolution at full width half-maximum = 9000) using negative-ion mode electrospray ionization over m/z 100-2000. Mass spectra were acquired in five quasi-simultaneous functions using aperture 1 potential settings of 20, 35, 50, 65, and 80 volts to generate non-selective ion fragmentation using a protocol known as multiplexed collision-induced dissociation (Gu et al., 2010; Stagliano et al., 2010) that provides additional evidence of lipid structure from fragment ion masses. Levels of cardiolipin were quantified by integration (Waters QuanLynx software) of the extracted ion chromatogram for m/z 1401.98, corresponding to $[M-H]^-$ of the most abundant form of cardiolipin (with two 16-carbon and two 18-carbon fatty acids and a total of 3 double bonds. Amounts of other forms of cardiolipin relative to the major form remained constant across all wild-type and mutant extracts. An external standard of 1',3'-bis[1,2-dioleoyl-*sn*-glycero-3-phospho]-*sn*-glycerol (Avanti) was used for method development and quantitative analysis.

2.5.7 Co-immunoprecipitation (Co-IP)

Tobacco leaves (~1 g fresh weight) transiently expressing the YFP-DRP3 and HA-DRP3 fusion proteins were homogenized in 4 ml RIPA buffer (Thermo) with 1x complete protease inhibitor cocktail (Roche), and lysed on a rotator for 1 hr at 4°C. After the lysed tissue was centrifuged at 13,000 g for 10 min, the supernatant was incubated with 20 µl agarose conjugated anti-GFP (MBL) on a rotator at 4°C for 1 hour to pull-down the YFP fusion proteins. The agarose beads were spun down at 3000 g for 15 sec and washed three times with RIPA buffer. YFP-interacting proteins were eluted by adding 1x NuPAGE LDS sample buffer (Invitrogen) and heating at 75°C for 10 min. The eluted proteins were subjected to immunoblot analysis as described above.

2.5.8 Mitochondrial isolation and determination of protein membrane association and topology

Mitochondria were isolated from rosette leaves of four-week-old transgenic plants expressing 35S_{pro}:YFP-PMD1 or 35S_{pro}:CLS-YFP-HA and the mitochondrial marker, COX4-YFP, using a previously published protocol (Aung and Hu, 2011). The purity of mitochondrial preparations was determined using immunoblot analyses and organelle-specific antibodies as described above. Mitochondrial membrane association was tested using previously described methods (Nakagawa et al., 2007).

To determine the topology of CLS on the mitochondrial membrane, protease protection assays were employed using proteases thermolysin and trypsin. For thermolysin treatment, 200 µl purified mitochondria was treated with 0, 150 or 300 µg/ml

of thermolysin in an incubation buffer containing 50 mM Hepes/NaOH, pH 7.5, 0.33 M sorbitol, and 0.5 mM CaCl₂. The reactions were carried out at 4°C for 1 h, and stopped by incubating on ice for 5 min with 5 mM EDTA. For trypsin treatment, 200 µl purified mitochondria was treated with 0, 150 or 300 µg/ml of trypsin in an incubation buffer containing 50 mM Hepes/NaOH, pH 7.5, and 0.33 M sorbitol. As a control, mitochondria were also treated with 1% SDS and 300 µg/ml trypsin, in which SDS served to permeabilize the membrane to cause the loss of protection of inner membrane proteins against trypsin. The reactions were carried out at 4°C for 30 min, and stopped by incubating on ice for 5 min with 0.5 mM PMSF. Immunoblot analysis was then performed as described above.

2.5.9 TUNEL assay

Whole *Arabidopsis* seedlings were fixed overnight in 4% paraformaldehyde in PBS, pH 7.4, and washed with PBS for 10 min. Samples were then permeabilized by immersing them in 0.1% (v/v) Triton X-100 in 0.1% sodium citrate for 2min on ice, washed with PBS for 10 min, and then incubated with 4% pectinase and 2% cellulase for 30 min. Treated samples were washed with PBS for 10 min before being used for the TUNEL assay with protocols provided by the manufacturer (Roche).

2.5.10 Statistical analysis

Quantitative analysis results are presented as the means ± s.d. (or s.e.m) from repeated experiments as indicated in the Figure legends. Pairwise Student's *t*-test was used to analyze statistical significance.

2.6 Acknowledgements

The authors would like to thank Dr. Christoph Benning for comments on the manuscript, Drs Weili Yang, Henrik Tjellström, Min Zhang, and John Froehlich for technical assistance, and Dr. Tsuyoshi Nakagawa for providing the pGWB544 and pGWB545 vectors. This work was supported by grants from the Chemical Sciences, Geosciences and Biosciences Division, Office of Basic Energy Sciences, Office of Science, U.S. Department of Energy (DE-FG02-91ER20021), and National Science Foundation (MCB 1330441) to JH, and by Michigan AgBioResearch to ADJ.

CHAPTER 3

The *Arabidopsis* mitochondrial membrane-bound ubiquitin protease UBP27 contributes to mitochondrial morphogenesis

The work presented in this chapter has been published:
Ronghui Pan, Navneet Kaur, and Jianping Hu. (2014)
The Plant Journal 78: 1047–1059.
doi:10.1111/tpj.12532.

3.1 Abstract

Mitochondria are essential organelles with dynamic morphology and function. Post-translational modifications (PTMs), including protein ubiquitination, are critically involved in animal and yeast mitochondrial dynamics. How PTMs contribute to plant mitochondrial dynamics is just beginning to be elucidated, and mitochondrial enzymes involved in ubiquitination have not been reported from plants. In this study, we identified an *Arabidopsis* mitochondrial localized ubiquitin protease, UBP27, through a screen combining bioinformatics and fluorescent fusion protein targeting analysis. We characterized UBP27 with respect to its membrane topology and enzymatic activities, and analyzed the mitochondrial morphological changes in *UBP27* T-DNA insertion mutants and overexpression lines. We have shown that UBP27 is embedded in the mitochondrial outer membrane with an N_{in}-C_{out} orientation and possesses ubiquitin protease activities *in vitro*. UBP27 demonstrates similar subcellular localization, domain structure, membrane topology and enzymatic activities with two mitochondrial deubiquitinases, yeast ScUBP16 and human HsUSP30, indicating that these proteins are functional orthologs in eukaryotes. Although loss-of-function mutants of *UBP27* do not show obvious phenotypes in plant growth and mitochondrial morphology, *UBP27* overexpression can change mitochondrial morphology from rod to spherical shape and reduce the mitochondrial association of dynamin-related protein 3 (DRP3) proteins, large GTPases that serve as the main mitochondrial fission factors. Thus, our study has uncovered a plant ubiquitin protease that plays a role in mitochondrial morphogenesis possibly through modulation of the function of organelle division proteins.

3.2 Introduction

The ATP-generating respiratory function of mitochondria is essential to cellular maintenance and organismal growth in eukaryotes (Friedman and Nunnari, 2014; Genova and Lenaz, 2014; Schwarzländer and Finkemeier, 2013; Trounce, 2000). In plants, mitochondria are involved in the metabolism of carbon, nitrogen, phosphorus and sulfur, and play an important role in plant stress response (Jacoby et al., 2012; Schwarzländer and Finkemeier, 2013). Mitochondria are dynamic and can adjust their morphology, abundance, and contents in response to developmental and environmental cues (Carrie et al., 2013; Palikaras and Tavernarakis, 2014; Palmer et al., 2011b; Wiedemann et al., 2004).

Mitochondrial morphology and number are largely determined by the relative strength of two topologically opposite processes, fission and fusion (Palmer et al., 2011b). In yeasts and animals, both mitochondrial fission and fusion employ dynamin-related GTPases present on the outer and inner mitochondrial membranes (Chan, 2012). In plants however, mitochondrial fission seems to be dominant over fusion and the fusion machinery has not been discovered. In *Arabidopsis thaliana*, mitochondrial fission is mainly executed by the homologous dynamin-related proteins (DRPs) DRP3A and DRP3B, both of which are also involved in peroxisome division (Arimura et al., 2004a; Arimura and Tsutsumi, 2002; Aung and Hu, 2012; Fujimoto et al., 2009; Logan, 2010; Mano et al., 2004; Zhang and Hu, 2009). Other plant mitochondrial fission factors include: FISSION1A (FIS1A) and FIS1B, C-terminal-tail-anchored proteins dual-localized to the surface of mitochondria and peroxisomes with a rate-limiting role in organelle fission (Scott et al., 2006; Zhang and Hu, 2008a, 2009); ELONGATED

MITOCHONDRIA1 (ELM1), a protein specifically involved in mitochondrial division that recruits DRP3A to the organelle (Arimura et al., 2008); and PEROXISOME AND MITOCHONDRIAL DIVISION FACTOR1 (PMD1), another dual localized membrane protein involved in the division of peroxisome and mitochondria but acting independently from ELM1, FIS1, or DRP3 (Aung and Hu, 2011).

As revealed in yeasts and animals, mitochondrial dynamics is subjected to various modes of regulation, including post translational modifications (PTMs), which represent an essential step toward the maturation, diversification, or degradation of proteins. PTMs are achieved by the addition of small molecules, such as phosphate, methyl, or acetyl groups, or by the covalent attachment of small proteins, such as ubiquitin and ubiquitin-like proteins, to the protein substrates (Kerscher et al., 2006). Take the mammalian mitochondrial/peroxisomal division protein Drp1 as an example, this protein is regulated by protein phosphorylation (Cereghetti et al., 2008; Chang and Blackstone, 2007; Cribbs and Strack, 2007; Han et al., 2008; Taguchi et al., 2007), ubiquitination (Karbowski et al., 2007; Nakamura et al., 2006; Wang et al., 2011; Yonashiro et al., 2006), SUMOylation (Braschi et al., 2009; Figueroa-Romero et al., 2009; Harder et al., 2004; Zunino et al., 2007), and S-Nitrosylation (Cho et al., 2009), resulting in alterations in Drp1's dimerization, GTPase activity, targeting to or association with mitochondria, or protein stability. Genome-wide proteomic experiments identified multiple phosphorylation sites on Arabidopsis DRP3A and DRP3B (Durek et al., 2010; Heazlewood et al., 2008; Mayank et al., 2012; Nakagami et al., 2010; Sugiyama et al., 2008; Wang et al., 2013), although the consequences of these phosphorylation events have not been determined. DRP3A and DRP3B were reported

to undergo mitotic phosphorylation at unidentified sites, leading to the induction of mitochondrial fission during mitosis (Wang et al., 2012).

Among the PTMs, ubiquitination is a key regulatory mechanism in multiple cellular pathways (Komander and Rape, 2012) and in both fission and fusion of mitochondria in animals and yeasts (Palmer et al., 2011b). Ubiquitinations may occur as the attachment of a single ubiquitin molecule or a multi-molecule chain that may vary in the number of ubiquitin molecules, branch patterns, and/or 3D structures, granting various fates to the substrates (Vierstra, 2009). Recent studies in plants indicated key roles of ubiquitination in the biogenesis and/or function of chloroplasts (Ling et al., 2012) and peroxisomes (Kaur et al., 2013; Lingard et al., 2009), two organelles functionally linked to mitochondria.

A critical feature of ubiquitination is its reversibility mediated by de-ubiquitination enzymes (DUBs), most of which are cysteine proteases and some are metalloproteases. Based on the catalytic domain configuration, DUBs are further classified into two major groups that include ubiquitin C-terminal hydrolases (UCHs) and ubiquitin-specific proteases (UBPs, or USPs in mammals), and two non-canonical groups that include ovarian tumor proteases (OTUs) and Machado–Joseph disease protein domain proteases (MJDs). UCHs are suggested to process short multi-ubiquitin chains and ubiquitin precursors, whereas UBPs can hydrolyze the peptide or isopeptide bond between ubiquitins and other proteins (Clague et al., 2012; Eletr and Wilkinson, 2014; Reyes-Turcu et al., 2009).

Bioinformatic analyses identified at least 90 DUBs in human, 17 in the yeast *Saccharomyces cerevisiae*, and 64 in *Arabidopsis* (Amerik and Hochstrasser, 2004; Liu

et al., 2008; Nijman et al., 2005). There are two reported mitochondrial outer membrane (MOM)-localized UBP-type DUBs, ScUBP16 from yeast (Kinner and Kölling, 2003) and HsUSP30 from human (Nakamura and Shigehisa, 2008). Suppression of HsUSP30 function leads to enhanced mitochondrial elongation and inter-connection, demonstrating a positive role of de-ubiquitination in mitochondrial fission (Nakamura and Shigehisa, 2008), whereas removal or overexpression of ScUBP16 did not cause noticeable changes to mitochondrial morphology or inheritance (Kinner and Kölling, 2003). Beyond the three highly conserved catalytic residues, i.e., one cysteine (Cys) and two histidines (His), UBPs share low sequence similarities and possess variant domain compositions, implying diversity in their localization, regulation and/or substrate specificity (Amerik and Hochstrasser, 2004; Nijman et al., 2005). Out of the 27 predicted Arabidopsis UBPs (Liu et al., 2008), several nuclear, cytosolic, or plastid UBPs have been shown to contribute to diverse developmental processes (Chandler et al., 1997; Cui et al., 2013; Doelling et al., 2001; Ewan et al., 2011; Luo et al., 2008; Moon et al., 2005; Schmitz et al., 2009; Zhao et al., 2013); none was reported to associate with mitochondrial morphogenesis or function.

The role of post-translational modifications in plant mitochondrial dynamics is beginning to be revealed. We recently showed that cardiolipin, a mitochondrial specific phospholipid, promotes mitochondrial fission in Arabidopsis by stabilizing the supercomplex of DRP3 proteins on mitochondria (Pan et al., 2014a). To determine whether ubiquitination plays a role in plant mitochondrial dynamics, we searched the Arabidopsis genome for mitochondrion-localized proteins potentially involved in ubiquitination or de-ubiquitination. Here we report the identification of Arabidopsis

UBP27 as a mitochondrial specific DUB with deubiquitinase activities. We also provide evidence that UBP27 plays a role in mitochondrial morphogenesis and reduces the association of DRP3 proteins with mitochondria, possibly facilitating the recycling of DRP3 proteins from mitochondria to the cytosol.

3.3 Results

3.3.1 *Arabidopsis* UBP27 is localized to mitochondria

To determine whether de-ubiquitination is involved in plant mitochondrial dynamics, we searched the 27 predicted *Arabidopsis* UBPs (Liu et al., 2008) for those localized to mitochondria. Based on literature mining and bioinformatic analysis using tools that predict subcellular localization and transmembrane domains (TMDs) (Claros and Vincens, 1996; Emanuelsson et al., 2000; Guda et al., 2004; Höglund et al., 2006; Hua and Sun, 2001; Small et al., 2004), UBP17, UBP25 and UBP27 were each predicted by at least two programs to have a strong likelihood to be mitochondrial; among them only UBP27 contained a predicted TMD (Fig. 3.1).

To examine the subcellular localization of UBP17, UBP25, and UBP27, N-terminal and C-terminal YFP fusions of their full-length proteins were co-expressed in *Nicotiana tabacum* (tobacco) with the mitochondrial marker cytochrome c oxidase 4-Cyan Fluorescent Protein (COX4-CFP), which is a fusion of the first 29 amino acids of the yeast *S. cerevisiae* COX4 and CFP (Nelson et al., 2007) and has been successfully used in our previous studies (Aung and Hu, 2011, 2012; Pan et al., 2014a). Confocal microscopy analysis of tobacco leaf epidermal cells revealed that, whereas UBP17 and

UBP25 did not seem to associate with mitochondria as either C- or N-terminal YFP fusions (Fig. 3.2A), both UBP27-YFP and YFP-UBP27 showed localization to mitochondria (see below).

Transgenic plants co-expressing COX4-CFP and UBP27-YFP or COX4-CFP and YFP-UBP27 were generated to further confirm the mitochondrial localization of UBP27. Confocal microscopy analysis of transgenic plants demonstrated that UBP27-YFP formed a ring structure on the surface of mitochondria (Fig. 3.3A) and tended to aggregate at the conjunction of non-separated mitochondria (Fig. 3.2B), suggesting that the protein is localized to MOM. Although many YFP-UBP27 proteins also localized to mitochondria, a significant amount was diffused in the cytosol (Fig. 3.2B, 3.2C), suggesting that blocking the N terminus markedly decreased the mitochondrial targeting specificity of UBP27. To determine the targeting specificity of UBP27, we also made transgenic plants expressing YFP-UBP27 or UBP27-YFP together with the peroxisome marker CFP-PTS1 (peroxisomal targeting signal type 1, SKL). Peroxisomal association was not observed for either protein (Fig. 3.2D), consistent with UBP27's specific localization to mitochondria.

Yeast ScUBP16 and human HsUSP30 are MOM-localized DUBs that share low sequence identities but similar domain structures (Kinner and Kölling, 2003; Nakamura and Shigehisa, 2008). Despite low overall sequence similarities with ScUBP16 and HsUSP30, UBP27 also contained a predicted TMD near the N terminus and a long ubiquitin C-terminal hydrolase (UCH) domain (Fig. 3.4A, Fig. 3.3B). Phylogenetic analysis using all the predicted Arabidopsis UBPs, ScUBP16, and HsUSP30 grouped UBP27 in the same subclade with the two mitochondrial DUBs (Fig. 3.3C), suggesting

that UBP27 may be the plant ortholog of ScUBP16 and HsUSP30.

3.3.2 Analysis of UBP27's mitochondrial targeting sequence and membrane topology

The exclusive mitochondrial targeting of UBP27-YFP as opposed to YFP-UBP27 suggested that the mitochondrial targeting signal resided at the N terminus of UBP27. The mitochondrial targeting of N-terminal tail-anchored proteins often depends on an N-terminal TMD and the flanking regions that contain positively charged residues (Nakamura and Shigehisa, 2008; Rapaport, 2003). To dissect the mitochondrial targeting signal of UBP27, C-terminal YFP fusion proteins of various UBP27 segments (Fig. 3.5A) were co-expressed with COX4-CFP in tobacco leaves. Like the full-length (FL) protein, UBP27¹⁻⁷¹, which contained the TMD and its two flanking regions, targeted the fusion protein to mitochondria, while UBP27⁷²⁻⁵⁰⁵-YFP was diffused in the cytosol (Fig. 3.5B). Hence, the N terminus contained the mitochondrial targeting signal. By contrast, N-terminal segments that lacked the TMD and one of the flanking regions, i.e., UBP27¹⁻²⁶, UBP27¹⁻⁴⁹, UBP27²⁷⁻⁷¹, and UBP27⁵⁰⁻⁷¹, lost or reduced the ability to recognize mitochondria (Fig. 3.5B), suggesting the importance of TMD and the two flanking regions for mitochondrial targeting. Notably, a significant fraction of UBP27²⁷⁻⁷¹ still localized to mitochondria (Fig. 3.5B), indicating that the TMD's C-terminal flanking region plays a stronger role than the N-terminal flanking region in UBP27's mitochondrial targeting.

Both ScUBP16 and HsUSP30 are integral MOM proteins with the catalytic domain facing the cytosol (Kinner and Kölling, 2003; Nakamura and Shigehisa, 2008).

Hydropathy plot analysis using TMHMM (www.cbs.dtu.dk/services/TMHMM/) likewise suggested UBP27 to be N-terminally anchored to the mitochondrial membrane with the catalytic domain exposed in the cytosol (Fig. 3.4B). To experimentally test the topology of UBP27 on mitochondrial membrane, we isolated mitochondria from leaf tissue of transgenic Arabidopsis lines co-expressing UBP27-YFP and COX4-CFP. The purity of the isolated mitochondria was confirmed by immunoblot analysis, which did not detect contamination from peroxisomal protein PEX14 (Fig. 3.6A). The presence of UBP27-YFP in the mitochondrial fraction was shown by immunoblotting using the GFP antibody (Fig. 3.6B). The isolated mitochondria were treated with the TE buffer, high concentration salt solution (1M NaCl), and alkaline carbonate (Na₂CO₃, pH11.0) respectively. UBP27 was detected solely in the pellet after each treatment followed by centrifugation (Fig. 3.6C), supporting the conclusion that UBP27 is an integral membrane protein of mitochondria.

The topology of UBP27 on mitochondrial membrane was further determined by protease protection assays with thermolysin, which degrades proteins unprotected by the organelle membrane. UBP27-YFP was degraded by thermolysin, but the MOM protein VDAC, which was largely embedded in the membrane, the inner membrane protein COXII, and the matrix protein COX4-CFP were all protected (Fig. 3.6D). These data provided evidence that UBP27 passes MOM in an N_{in}-C_{out} orientation (Fig. 3.6E).

3.3.3 UBP27 hydrolyses casein and possesses ubiquitin protease activity *in vitro*

To determine UBP27's enzymatic activity, we first performed a preliminary universal protease activity assay, using *Escherichia coli*-expressed GST-UBP27, in

which UBP27's first 49 amino acids that contained TMD were removed. Despite protein instability (Fig. 3.7A), GST-UBP27 demonstrated protease activity on the substrate casein, as measured colorimetrically by the release of Tyr from casein (Fig. 3.7B). To confirm that UBP27 is a functional deubiquitinase that can cleave covalently attached ubiquitin molecules, we conducted an *in vitro* assay. A His-tagged quaternary polyubiquitin of Arabidopsis UBQ14 (His-AtUBQ14) was generated as a test substrate, and either expressed alone or co-expressed with GST-UBP27 in *E. coli* cells. Immunoblotting with anti-ubiquitin as well as anti-His antibodies showed that 8 hours after protein induction, His-UBQ14 was accumulated at a comparable level in cell lines with or without GST-UBP27. Forty-eight hours later, lines co-expressing GST-UBP27 displayed accumulation of cleaved ubiquitin products, significantly faster degradation of His-UBQ14, and appearance of free single ubiquitin molecules (Fig. 3.8). Therefore, UBP27 is a *bona fide* deubiquitinase capable of processing polyubiquitin *in vitro*.

3.3.4 UBP27 affects mitochondrial morphogenesis

To look into UBP27's role in mitochondrial dynamics, we identified four *UBP27* T-DNA insertion lines: *ubp27-1*, *ubp27-2*, *ubp27-3* and *ubp27-4* (Fig. 3.9A), none of which exhibited apparent abnormalities in growth compared with the wild type (Fig. 3.10A). Semi-quantitative RT-PCR did not detect full-length *UBP27* transcripts in *ubp27-1* or *ubp27-3* nor did it detect the 5' 550 bp of the transcript in *ubp27-3* (Fig. 3.9B), suggesting that these two alleles do not encode fully functional UBP27 proteins and that *ubp27-3* is possibly a null mutant.

The mitochondrial marker COX4-YFP and peroxisomal marker YFP-PTS1 were

introduced into the *ubp27* mutants respectively by floral dipping. Confocal microscopy analysis of T2 lines did not identify significant alterations in mitochondrial, peroxisomal, or chloroplast morphology in the mutants (Fig. 3.9C, Fig. 3.10B, 3.10C). Thus, this mutant analysis did not reveal an essential role of UBP27 in mitochondrial morphogenesis and plant development.

To further explore the role of UBP27 in mitochondrial dynamics, we expressed *UBP27* under the control of the 35S constitutive promoter in tobacco leaves. In plants such as Arabidopsis and tobacco, mitochondria appear as discrete and mostly rod-shaped structures. However, in tobacco epidermal cells overexpressing UBP27 together with the mitochondrial marker COX4-YFP (Fig. 3.11A), the number of rod-shaped mitochondria (>1µm long) was reduced to ~4% and most of the mitochondria became spherical (< 1µm long), although the total number of mitochondria remained similar (Fig. 3.11B, 3.11c). To compare the phenotype caused by overexpressing UBP27 with those caused by ectopic expression of mitochondrial fission factors, 35S-CFP-DRP3A and 35S-CFP-DRP3B were also expressed in tobacco along with the mitochondrial marker. A significant change in mitochondrial morphology from rod-shape to sphere-shape also occurred (Fig. 3.11B, 3.11C). When UBP27 and CFP-DRP3 were co-expressed, mitochondrial were also highly spherical, but the massive mitochondrial aggregation in some cells prevented us from quantifying these organelles (Fig. 3.12A).

Consistent with the phenotype caused by overexpressing *UBP27*, mitochondria were also mostly spherical in Arabidopsis transgenic plants expressing 35S-UBP27-YFP, whereas mitochondria in transgenic lines overexpressing YFP-TOM22, a MOM protein involved in protein import, UBP27¹⁻⁷¹-YFP, the mitochondrial localized N terminus of

UBP27, or UBP27⁷²⁻⁵⁰⁵-YFP, the non-mitochondrial localized catalytic domain of UBP27, did not show discernible morphological differences from the wild type (Fig. 3.12B). These data led us to the conclusion that UBP27 is involved in mitochondrial morphogenesis. We further predicted that UBP27 possibly functions through the division process that involves DRP3.

3.3.5 UBP27 reduces the mitochondrial association of DRP3

To determine whether UBP27 affects the localization of DRP3, the mitochondrial association of CFP-DRP3 in tobacco cells overexpressing UBP27 was compared with cells that did not express UBP27. When UBP27 was co-expressed, CFP-DRP3's mitochondrial association was reduced to ~20% for both DRP3A and DRP3B (Fig. 3.13A, 3.13B). These results indicated that UBP27 may promote the dissociation of DRP3 proteins from mitochondria. To see whether the opposite phenotype could be observed in *ubp27* mutants, YFP-DRP3 was transformed into *ubp27-3*. YFP-DRP3's mitochondrial association in transgenic plants did not seem to show obvious differences compared with that of the wild type (Fig. 3.14).

As a first step to determine whether DRP3 proteins might be targets of UBP27 for deubiquitination, SDS-PAGE followed by immunoblot analysis was performed on the *UBP27* loss- and gain-of-function lines. Endogenous DRP3 proteins detected by DRP3A and DRP3B peptide antibodies (Aung and Hu, 2012; Pan et al., 2014a) did not show apparent alterations in these lines both in terms of protein levels and protein mobility (Fig. 3.15), the latter of which might be a reflection of DRP3's PTM. Due to instability of recombinant UBP27 proteins, we have not been able to prove direct interaction between

UBP27 and DRP3 proteins in co-immunoprecipitation assays. Thus, although we have discovered UBP27 as a mitochondrial ubiquitin protease that affects mitochondrial dynamics, further investigations will be needed to determine whether DRP3 proteins, or other mitochondrial proteins, are subjected to deubiquitination by UBP27.

3.4 Discussion

3.4.1 Evidence for the presence of a mitochondrial deubiquitinase in plants

In this study, we asked the question whether the ubiquitin system plays a role in mitochondrial dynamics. We characterized the Arabidopsis UBP27 protein with respect to its subcellular targeting, membrane topology, enzymatic activities, and analyzed the mitochondrial morphological changes in *UBP27* loss-of-function and gain-of-function plants. Bioinformatic predictions, fluorescence microscopy, sub-fractionation and protease protection assays led to the conclusion that UBP27 is a MOM protein with an N_{in}-C_{out} topology. The universal protease and ubiquitin protease activities of UBP27 were verified *in vitro* using recombinant UBP27 proteins. Lastly, our analysis of *UBP27* gain-of-function phenotypes suggested that UBP27 affects mitochondrial morphogenesis and dynamics possibly by promoting the dissociation of DRP3 from mitochondria. In summary, we have identified Arabidopsis UBP27 as a mitochondrial de-ubiquitination enzyme that affects mitochondrial morphogenesis possibly through the division process.

Yeast ScUBP16 and human HsUSP30 are mitochondrial DUBs that share the same domain structure with UBP27 despite little sequence similarities. The exact

function has not been assigned to ScUBP16 (Kinner and Kölling, 2003), whereas HsUSP30 is suggested to be involved in mitochondrial fission (Nakamura and Shigehisa, 2008). Our phylogenetic analysis suggested that, within all the Arabidopsis UBPs, UBP27 is most closely related to ScUBP16 and HsUSP30, arguing for UBP27 as the plant ortholog of these two mitochondrial UBPs. Thus, the mitochondrial ubiquitin system appears to be conserved across diverse eukaryotic systems to regulate mitochondrial dynamics. Furthermore, it is highly likely that plant mitochondrial ubiquitin ligases are also present, even though proteins with obvious sequence similarities to the non-plant mitochondrial ubiquitin ligases have not been reported in plants. In summary, our study takes a first step towards getting a comprehensive picture of the role of protein ubiquitination in modulating plant mitochondrial morphogenesis and function.

3.4.2 UBP27's role in plant mitochondrial dynamics and morphogenesis

Mitochondrial morphology varies in different species and cell types, depending on the balance between fission and fusion. In yeast and mammalian cells, mitochondria are often highly tubular and inter-connected (Chan, 2012). In plant cells, mitochondria are highly fragmented and often appear as discrete rod-shaped entities, yet the biological significance and mechanism for maintaining mitochondrial fragmentation and the rod shape in plants is still unclear.

HsUSP30 was suggested to play a positive role in mitochondrial fission, because down-regulation of *USP30* expression by RNAi induced mitochondrial elongation and inter-connection (Nakamura and Shigehisa, 2008). Here, we show that *UBP27* overexpression effectively changed mitochondrial morphology from rod-shaped to

spherical, and similar changes can be achieved by overexpressing CFP-DRP3. Similarly, overexpressing human Drp1 caused fragmented mitochondrial network in human HeLa cells (Stojanovski et al., 2004). Therefore, UBP27 appears to play a positive role in changing rod-shaped to round mitochondria through division. The strong mitochondrial aggregation phenotype seen in this study in cells co-expressing UBP27 and CFP-DRP3, but not in cells where each protein was overexpressed alone is, to some extent, similar to previous observations of cells overexpressing organelle fission factors such as *Arabidopsis* PMD1 (Aung and Hu, 2011) or DRP1's organelle anchor FIS1 in human (Stojanovski et al., 2004). Although this aggregation might have been caused by a functional interaction between UBP27 and CFP-DRP3, it may also have been an artifact caused by high levels of two membrane-associated proteins. Overexpression of some fluorescently tagged MOM proteins was shown to cause mitochondrial aggregation to one pole of the cell or heterogeneous changes in mitochondrial morphology (Duncan et al., 2011). As such, although we are in favor of a positive role for UBP27 in converting mitochondria from rod to spherical shape based on the uniform alteration of mitochondrial morphology in cells overexpressing *UBP27*, we cannot completely rule out the possibility that the mitochondrial shape alterations were artifacts from ectopic expression of a MOM protein.

In contrast to the mitochondrial fission defects caused by the suppression of HsUSP30 in human (Nakamura and Shigehisa, 2008), loss of UBP27 function did not cause any obvious defects in mitochondrial morphology in *Arabidopsis*. These different phenotypes between *ubp27* and *Hsusp30* mutants may reflect the different relative strength between mitochondrial fission and fusion processes in plants and mammals.

Since mitochondrial fusion machinery is stronger in human cells, HsUSP30's function in mitochondrial fission may be required to achieve the balance between fusion and fission under normal conditions. In plant cells where mitochondrial fission is predominant over fusion, this pro-fission activity of UBP27 may not be essential to balance the fusion machinery that is already weak. This may explain why *UBP27* gain-of-function but not loss-of-function plants display altered mitochondrial morphology. However, neither knockout nor overexpression of the putative yeast ortholog ScUBP16 led to obvious changes to mitochondrial morphology (Kinner and Kölling, 2003). Therefore, AtUBP27, ScUBP16, and HsUSP30 may have diverged in their function during evolution. Meanwhile, other possibilities, such as the presence of a mitochondrial protein with redundant function to UBP27, cannot be excluded.

3.4.3 Is the function of DRP3 directly modulated by UBP27?

DRP proteins are core components of the mitochondrial fission and fusion machinery and are highly dynamic in localization and oligomerization (Legesse-Miller et al., 2003; Westermann, 2008). The function of the mammalian mitochondrial/peroxisomal fission DRP, Drp1, is regulated by ubiquitination (see Introduction), yet there has been no direct evidence to support the regulation of DRP by ubiquitination in plants.

Our study revealed a significant reduction in DRP3's association with mitochondria when UBP27 was over-expressed, suggesting that UBP27 may promote the dissociation of DRP3 from mitochondria in a direct or indirect manner. UBP27 may act to accelerate the recycling of DRP3 from MOM to the cytosol, which is necessary to

maintain DRP3's optimal function in mitochondrial division. In *UBP27* overexpressing cells, although the dissociation of DRP3 from mitochondria is accelerated, DRP3 still functions normally in organelle division during its attachment to mitochondria, thus no deficiency in mitochondrial fission was observed. As such, ectopic expression of *UBP27* may have caused further division of rod-shaped to spherical mitochondria, but the total number of mitochondria remains the same as a result of a feed-back mechanism to control the total volume of mitochondria in the cell. Alternatively, assuming that mitochondrion-localized DRP3 provides a force to maintain the rod shape of mitochondria by a yet-unknown mechanism, *UBP27* overexpression, which decreases mitochondrion-associated DRP3, may cause the morphological changes of mitochondria from rod to round shape. These possibilities will need to be rigorously tested in the future.

One critical question is whether DRP3 is a direct target of *UBP27* for deubiquitination. We have not been able to prove direct interaction between *UBP27* and DRP3 proteins, as a result of the extreme instability of recombinant *UBP27* proteins. In this study, when we attempted to use DRP3A and DRP3B-specific peptide antibodies to analyze DRP3 proteins in *UBP27* loss- and gain-of-function plants by immunoblot, we did not detect PTM forms of DRP3. One possibility is that DRP3 proteins are not targeted for deubiquitination by *UBP27*. Alternatively, these DRP3 antibodies were not specific enough to detect the modified DRP3 proteins when the amount of the modified proteins is very low. Thus, it will be necessary to use more sensitive methods such as quantitative mass spectrometry to compare the level of DRP3 protein ubiquitination in these lines.

Although it is critical to determine whether DRP3 and UBP27 interact, whether DRP3 ubiquitination differs in wild-type and *ubp27* plants, and whether DRP3 is a direct target of deubiquitination by UBP27, it is equally possible that UBP27 has an impact on DRP3's association with mitochondria in an indirect manner. UBP27 may directly affect the function of mitochondrial proteins involved in other aspects of mitochondrial functions besides mitochondrial dynamics. Therefore, although DRP3 and other mitochondrial fission factors are candidates for UBP27's substrates, other possible substrates also exist.

Accession #	Protein name	Subcellular Localization prediction							membrane domain prediction	Previous experiment evidence	
		MitoPred	Mitoprot 2	MultiLoc	PeroxpP	Predotar	SubLoc	TargetP			
AT2G32780	AtUBP1	x	x	x	x	x	nu	x	No	x	
AT1G04860	AtUBP2	x	x	x	x	x	nu	x	No	pt	proteomics
AT4G39910	AtUBP3	x	x	x	x	x	ct	x	No	nu	sub-fractionation
AT2G22310	AtUBP4	x	x	x	x	x	ct	x	No	nu	sub-fractionation
AT2G40930	AtUBP5	x	x	x	x	x	nu	x	No	x	
AT1G51710	AtUBP6	x	x	x	x	x	nu	x	No	plasmodesma	proteomics
AT3G21280	AtUBP7	x	x	x	x	x	nu	x	No	x	
AT5G22030	AtUBP8	x	x	x	x	x	ct	mt	No	x	
AT4G10570	AtUBP9	x	x	x	x	x	nu	x	No	x	
AT4G10590	AtUBP10	x	x	x	x	x	nu	x	No	x	
AT1G32850	AtUBP11	x	x	x	x	x	nu	x	No	x	
AT5G06600	AtUBP12	x	x	x	x	x	ct	x	No	ct	proteomics
AT3G11910	AtUBP13	x	x	x	x	x	ct	x	No	ct & plasmodesma	proteomics
AT3G20630	AtUBP14	mt	x	x	x	x	ct	x	No	ct	proteomics
AT1G17110	AtUBP15	x	x	pt	x	er	nu	ex	Yes	ct & nu	fluorescent tag
AT4G24560	AtUBP16	x	x	pt	x	er	nu	ex	Yes	x	
AT5G65450	AtUBP17	mt	mt	mt	x	mt	nu	mt	No	x	
AT4G31670	AtUBP18	x	x	x	x	x	nu	ex	Yes	x	
AT2G24640	AtUBP19	x	x	x	x	x	nu	ex	Yes	x	
AT4G17890	AtUBP20	mt	x	x	x	x	nu	x	No	x	
AT5G46740	AtUBP21	x	x	pt	x	x	nu	pt	No	x	
AT5G10790	AtUBP22	mt	x	x	x	x	nu	x	No	x	
AT5G57990	AtUBP23	x	x	x	px	x	nu	pt	No	x	
AT4G30890	AtUBP24	x	x	x	x	x	nu	x	No	x	
AT3G14400	AtUBP25	mt	mt	mt	x	mt	nu	mt	No	x	
AT3G49600	AtUBP26	x	x	x	x	x	nu	x	No	nucleolus	proteomics
AT4G39370	AtUBP27	mt	x	x	x	x	nu	mt	Yes	x	

Figure 3.1. Predicted and experimentally confirmed localization, and TMD prediction for all *Arabidopsis* UBPs.

Figure 3.1 (cont'd)

The sub-cellular localization and TMD were predicted with online bioinformatics tools (see Results). Some localization information was from literature (Kleffmann et al., 2004; Chandler et al., 1997; Fernandez-Calvino et al., 2011; Ito et al., 2011; Liu et al., 2008; Pendle et al., 2005). mt, mitochondrion; pt, plastid; nu, nucleus; er, endoplasmic reticulum; px, peroxisome; ex, extracellular; ct, cytosol.

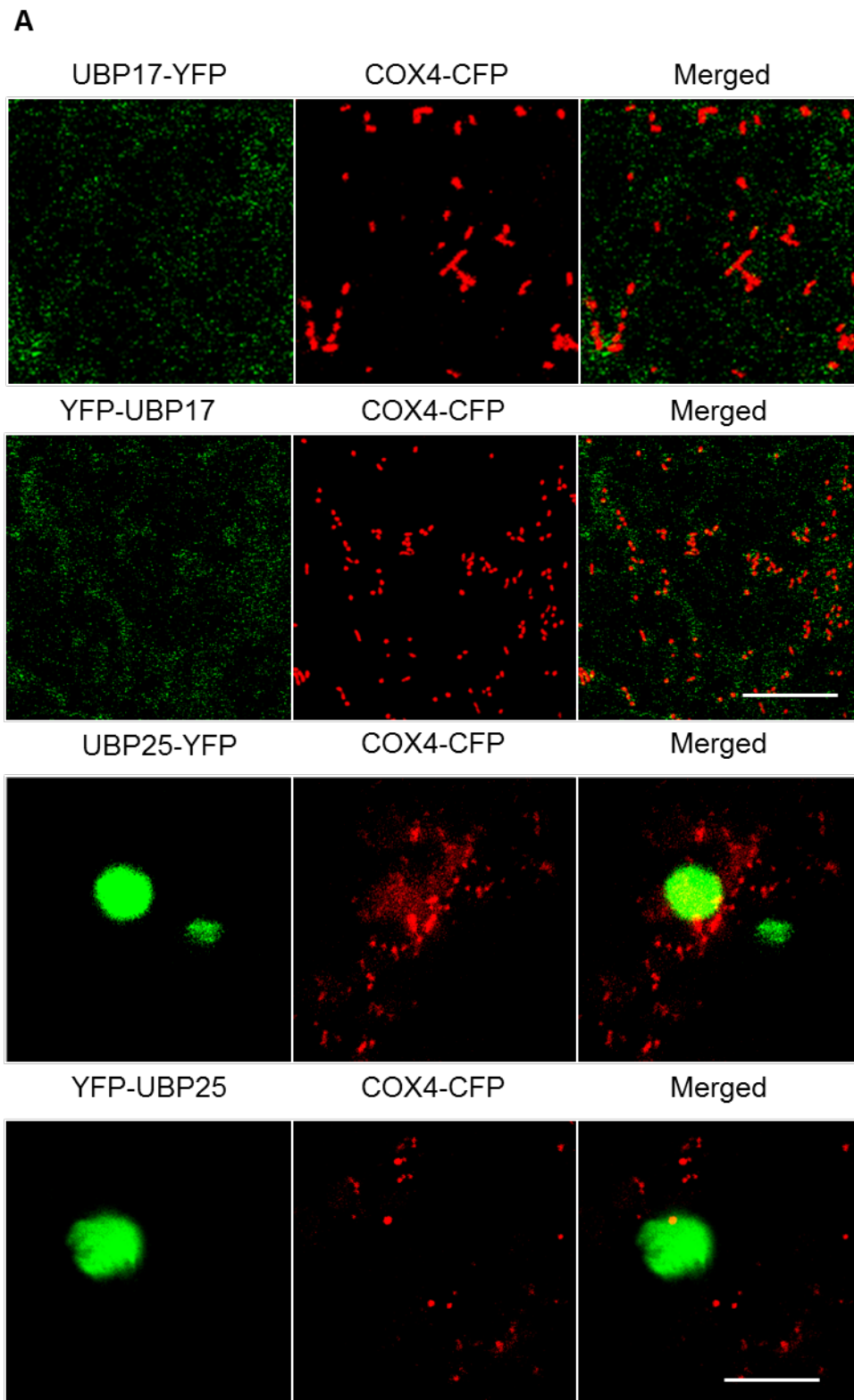


Figure 3.2. Analysis of the sub-cellular localization of UBP17, UBP25 and UBP27.

Figure 3.2 (cont'd)

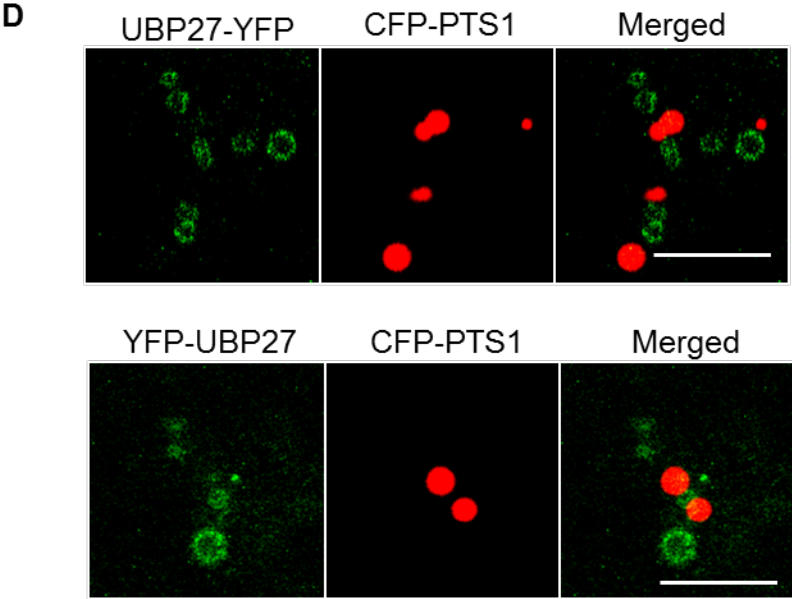
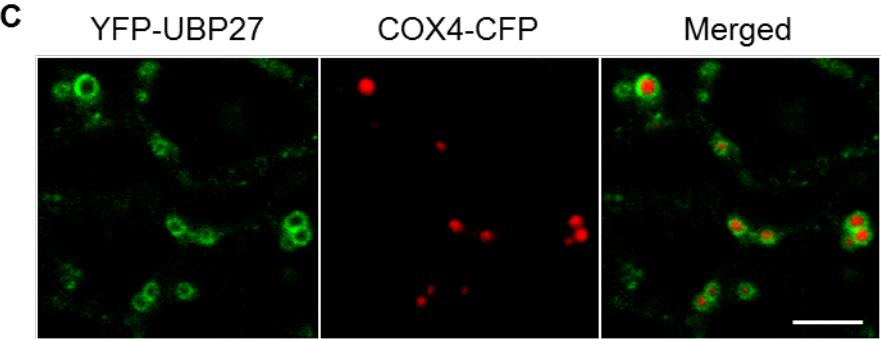
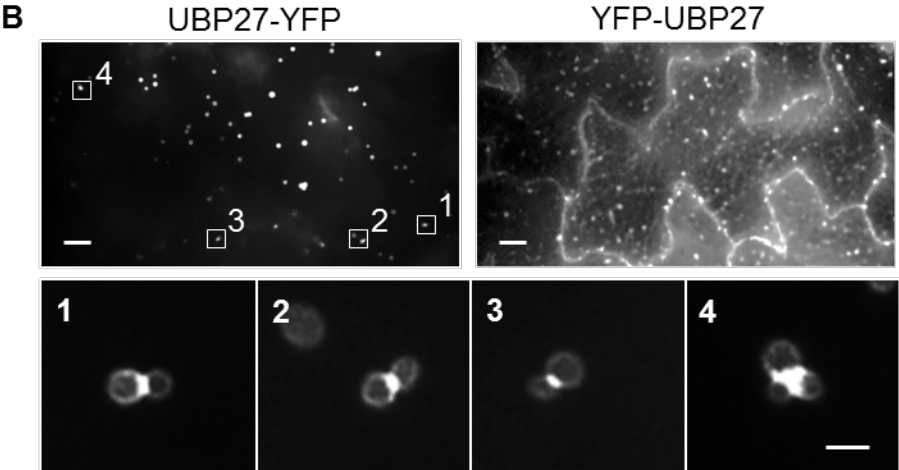


Figure 3.2 (cont'd)

(A) Confocal images of tobacco epidermal cells co-expressing the mitochondrial marker COX4-CFP and YFP fusions of UBP17 or UBP25. Scale bars = 10 μm .

(B) Epifluorescent images comparing the specificity of UBP27-YFP and YFP-UBP27 localization. Leaf epidermal cells of two-week-old *Arabidopsis* plants expressing the mitochondrial marker and UBP27-YFP or YFP-UBP27 were used for the analysis. Unseparated mitochondria in the boxed areas are magnified below. Scale bars = 5 μm for the upper panel, = 1 μm for the lower panel.

(C) Confocal images of leaf epidermal cells in transgenic *Arabidopsis* plants co-expressing YFP-UBP27 and the mitochondrial marker COX4-CFP. Scale bars = 5 μm .

(D) Confocal images of leaf epidermal cells in transgenic *Arabidopsis* plants co-expressing YFP fusions of UBP27 and the peroxisomal marker CFP-PTS1. Scale bars = 5 μm .

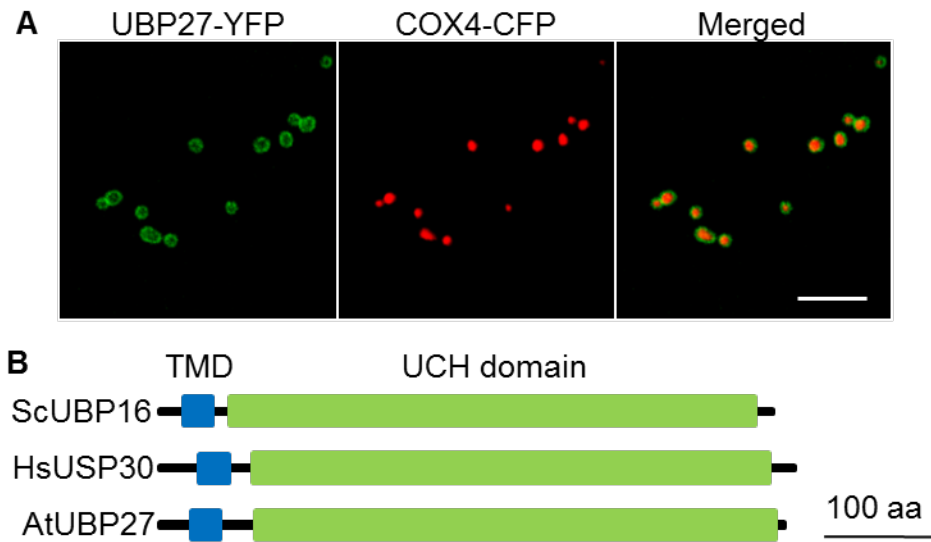


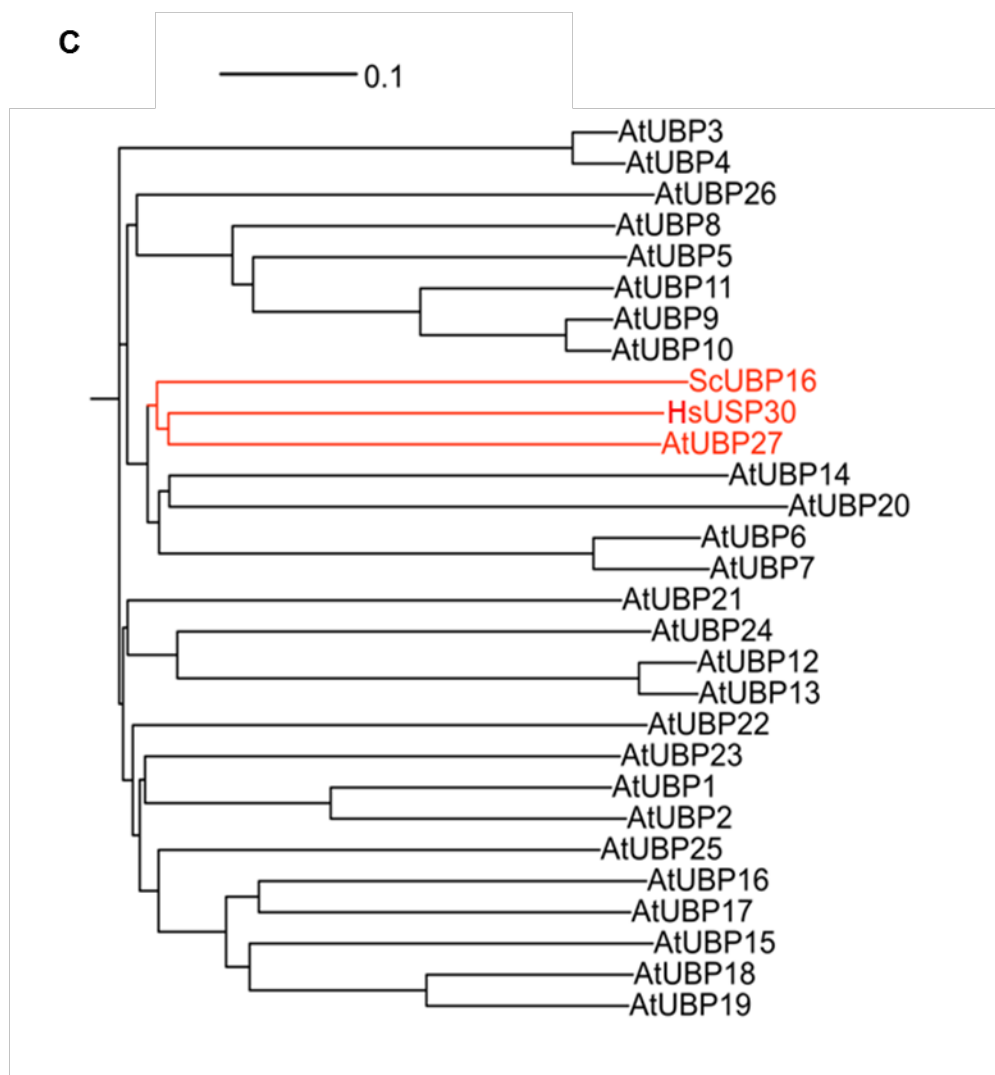
Figure 3.3. UBP27 is a putative ortholog of the mitochondrial UBPs ScUBP16 and HsUSP30.

(A) Confocal images showing the localization of UBP27-YFP on the surface of mitochondria. Leaf epidermal cells of two-week-old *Arabidopsis* plants co-expressing UBP27-YFP and COX4-CFP were used for the analysis. Scale bar = 5 μ m.

(B) Domain structure comparison of UBP27 and the mitochondrial UBPs ScUBP16 and HsUSP30. TMD, transmembrane domain; UCH, ubiquitin C-terminal hydrolase.

(C) Phylogenetic analysis of the relationship between *Arabidopsis* UBPs and the two known mitochondrial UBPs. Scale bar, 0.1 amino acid substitution per site.

Figure 3.3 (cont'd)



A

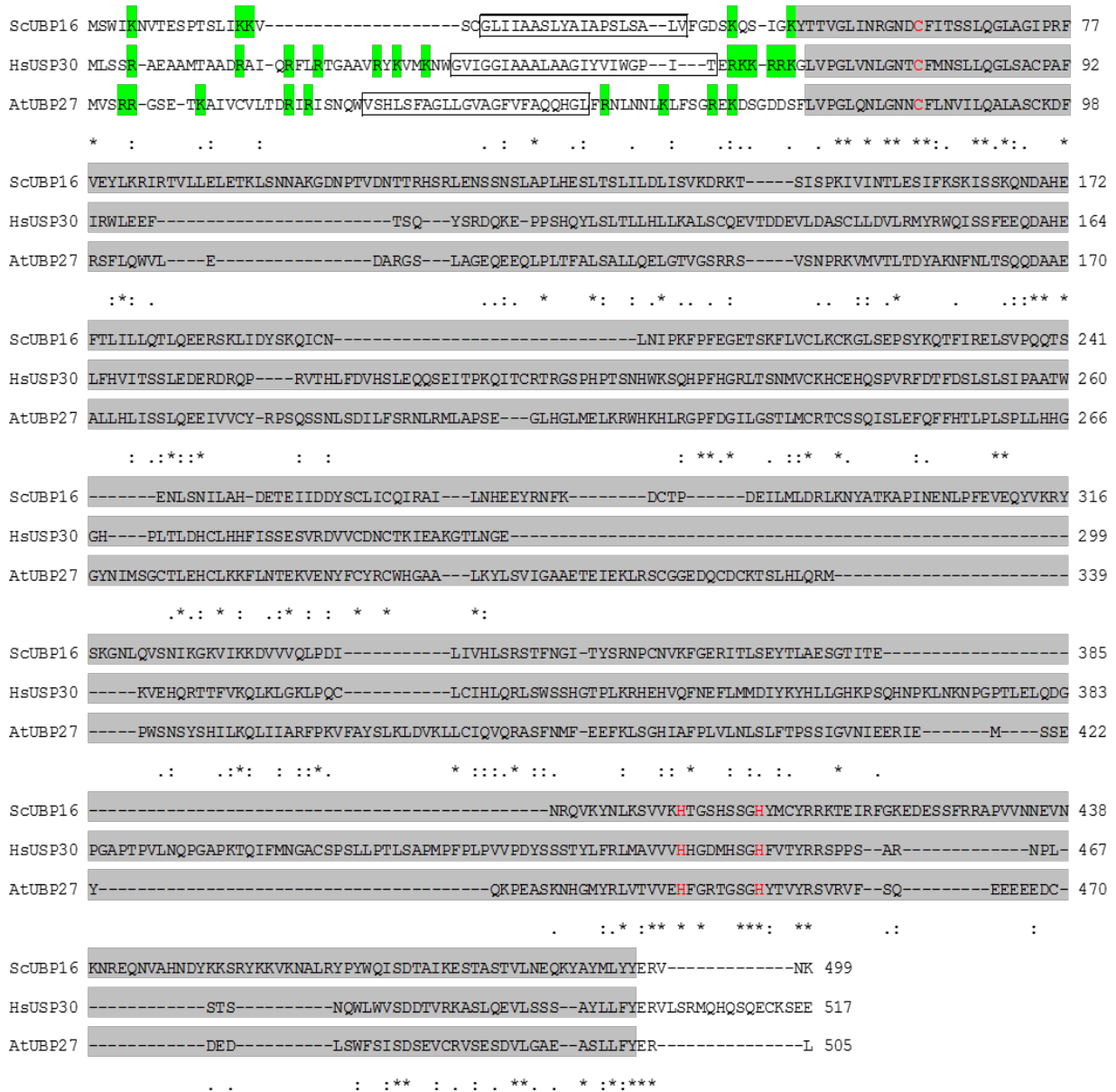
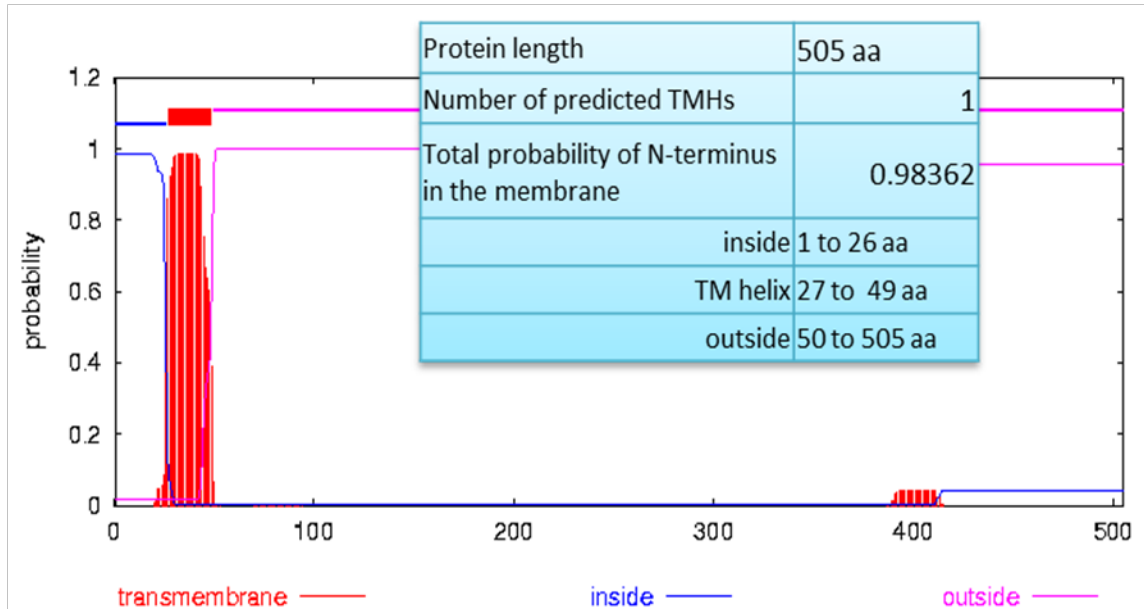


Figure 3.4. Sequence comparison of mitochondrial UBP proteins from different species and topology prediction for UBP27.

Figure 3.4 (cont'd)

B



(A) Sequence alignment between UBP27 from *Arabidopsis thaliana*, UBP16 from *Saccharomyces cerevisiae* and USP30 from *Homo sapiens*. The predicted TMDs are in boxes. The UCH domain is highlighted in grey. Positively charged residues in the flanking regions of the N-terminal TMD are highlighted in green. The three residues of the conserved catalytic triad are marked with red.

(B) Membrane topology of UBP27 predicted by the TMHMM software (<http://www.cbs.dtu.dk/services/TMHMM/>).

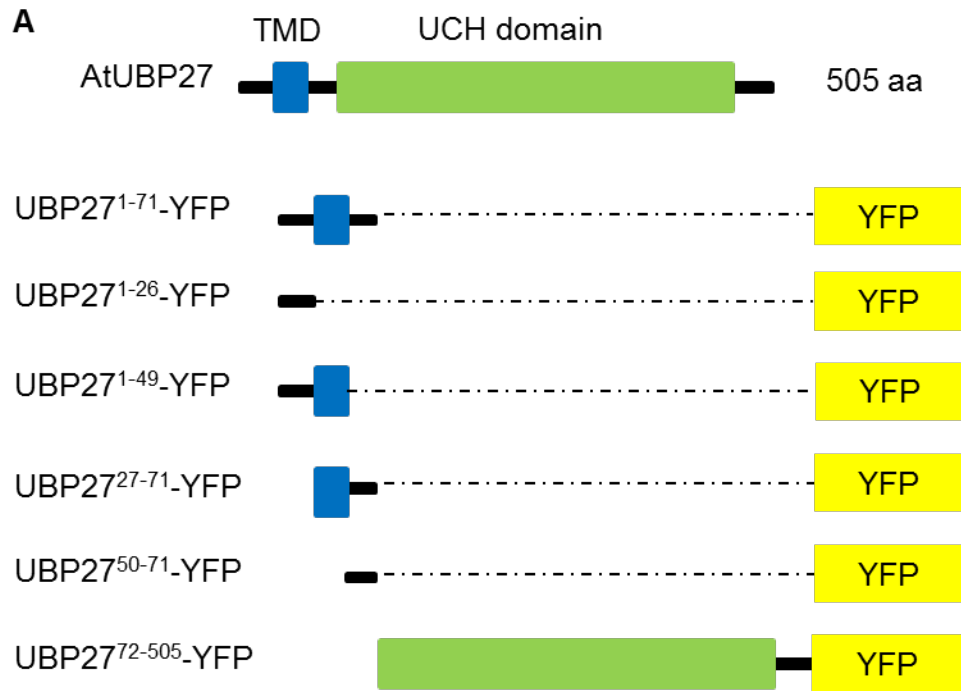
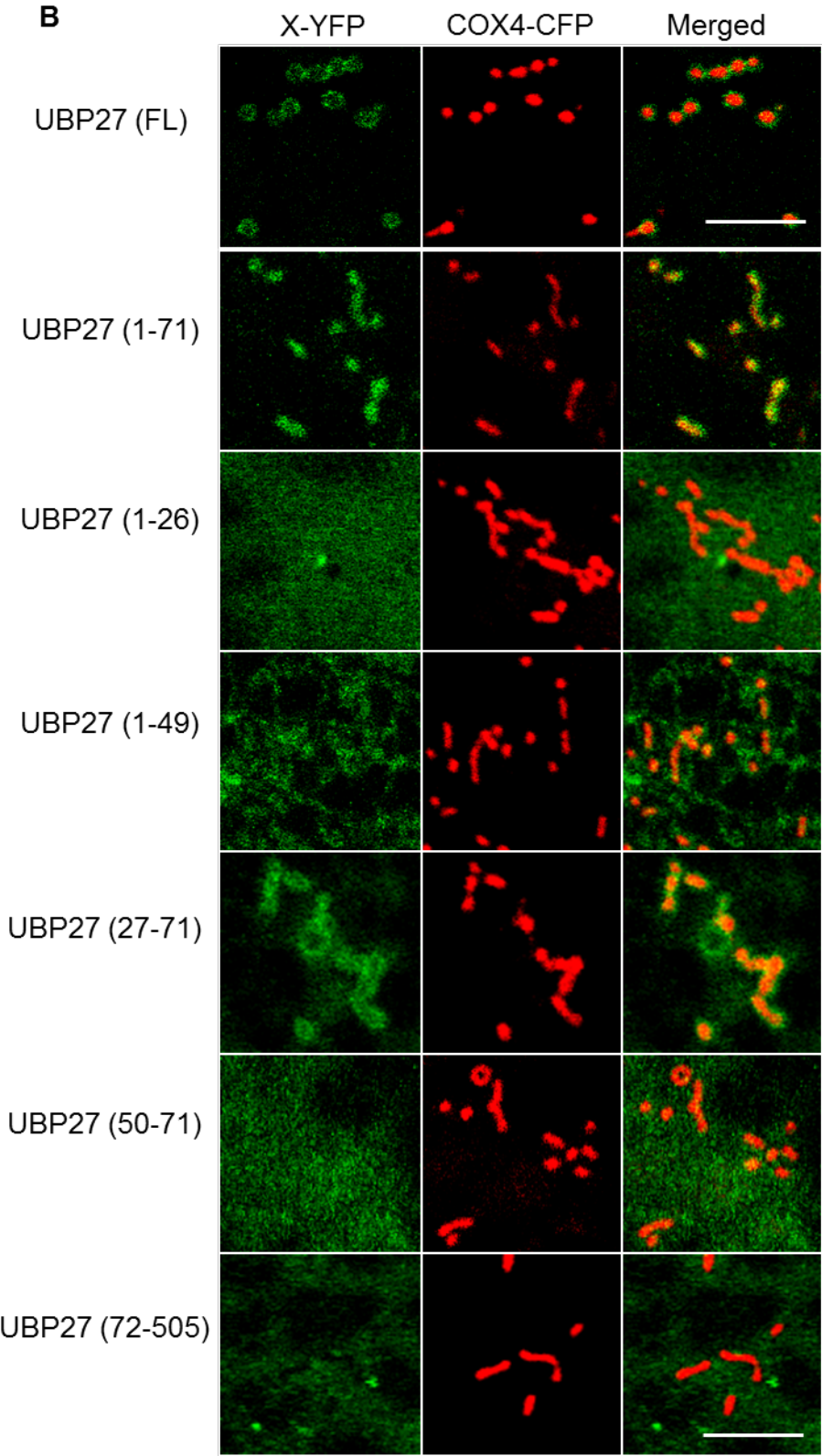


Figure 3.5. Analysis of mitochondrial targeting signals on UBP27.

(A) Schematic of the UBP27-YFP protein and deletion constructs. TMD, transmembrane domain. UCH, ubiquitin C-terminal hydrolase.

(B) Confocal images of the localization of various UBP27 fragments fused to YFP. Co-localization between COX4-CFP and the YFP fusions were examined in epidermal cells of tobacco leaves transiently expressing the two proteins. Scale bar = 5 μ m. FL, full length.

Figure 3.5 (cont'd)



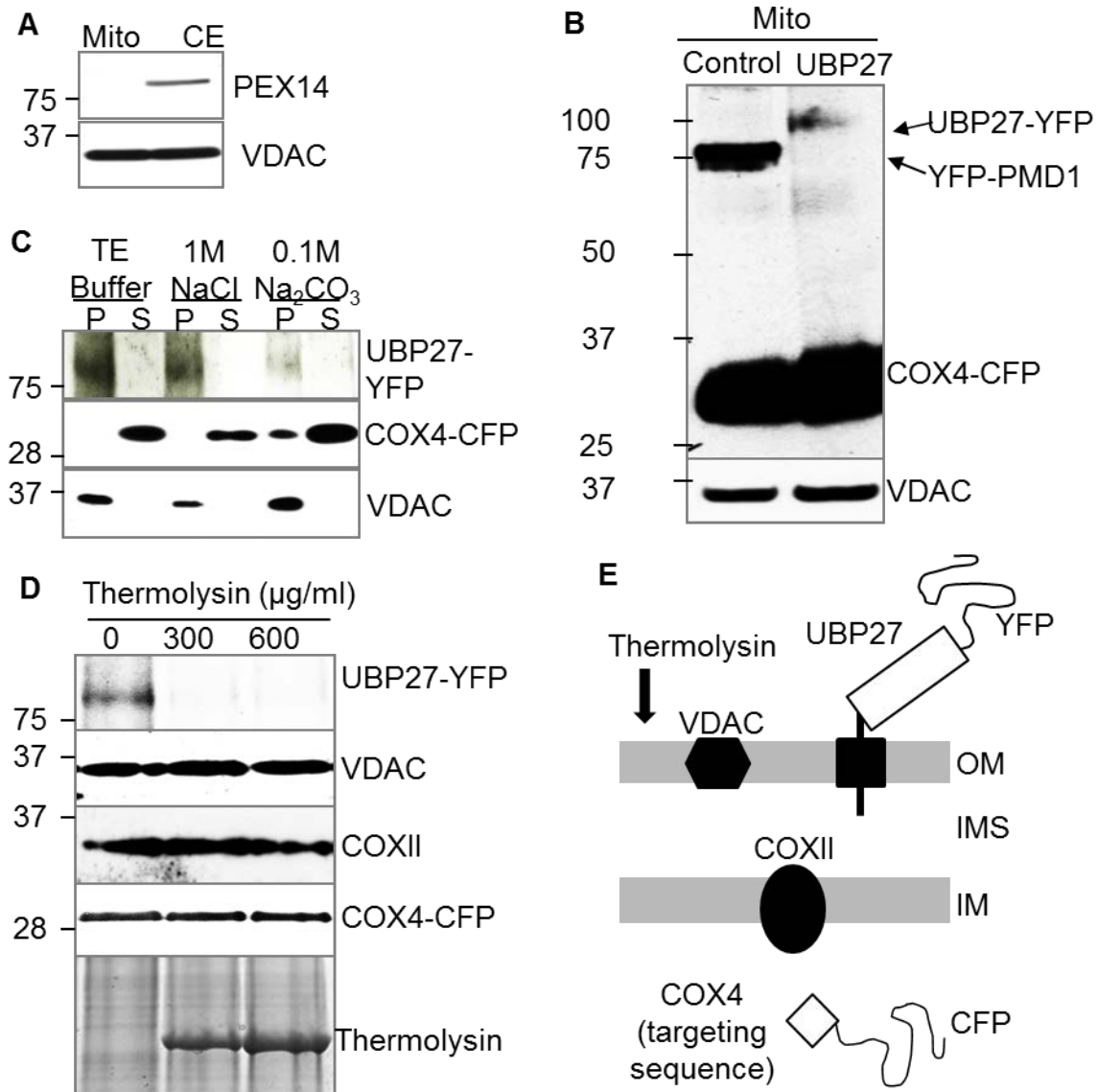


Figure 3.6. Immunoblot analyses of the mitochondrial membrane association and topology of UBP27.

(A) Assessment of the purity of isolated mitochondria from the leaf tissue of Arabidopsis transgenic plant expressing UBP27-YFP and COX4-CFP. Antibodies used were against maize voltage-dependent anion selective channel (VDAC for mitochondria) and Arabidopsis PEX14 (for peroxisomes). Mito, isolated mitochondria. CE, crude extract. Numbers on the left are molecular weight markers in kDa.

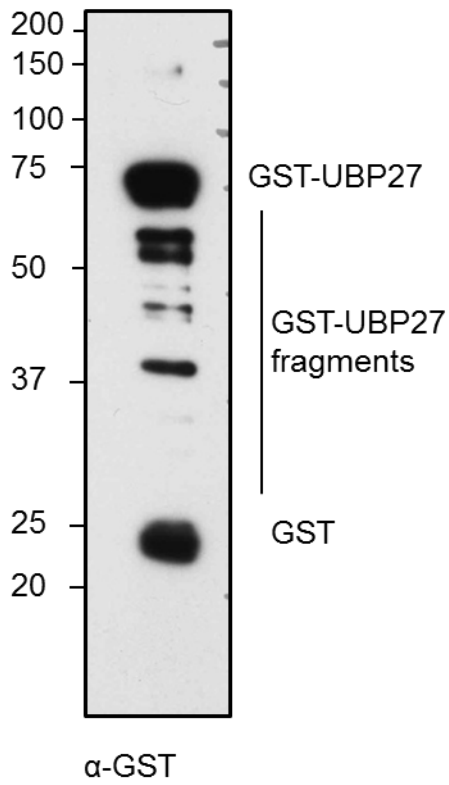
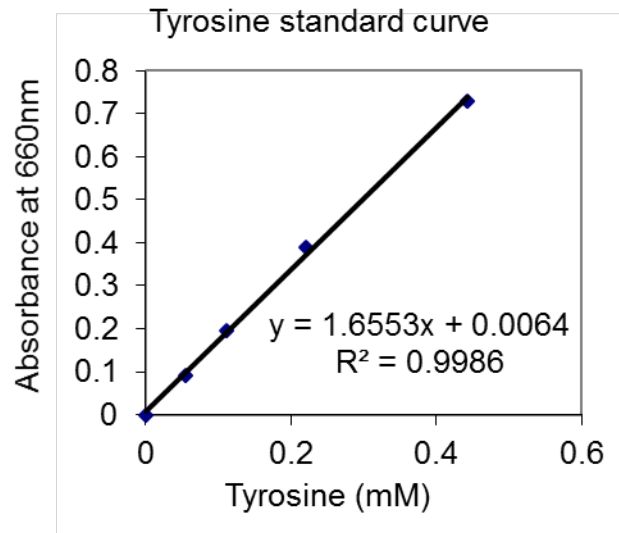
Figure 3.6 (cont'd)

(B) Confirmation of the presence of UBP27-YFP in isolated mitochondria shown in (a), using the GFP antibody. Isolated mitochondria from plants co-expressing YFP-PMD1 and COX4-CFP ([Aung and Hu, 2011](#)) were used as the control (CON). VDAC was the control for protein loading.

(C) Mitochondrial membrane association of UBP27-YFP. Purified mitochondria were treated with TE, NaCl, or Na₂CO₃ (pH 11.0) respectively and separated into soluble (S) and pellet (P) fractions by centrifugation. UBP27-YFP and COX4-CFP were detected by α -GFP, and COX4 and VDAC were controls for matrix and integral membrane proteins, respectively.

(D) Protease protection assay to determine the membrane topology of UBP27. Isolated mitochondria from plants co-expressing UBP27-YFP and COX4-CFP were treated with thermolysin followed by immunoblot analysis using α -GFP, α -VDAC, and α -COXII antibodies, respectively.

(E) Diagram showing the digesting ability of thermolysin. VDAC, COXII, and COX4-CFP are controls for distinct sub-compartments of mitochondria. OM, outer membrane; IMS, intermembrane space; IM, inner membrane.

A**B**

$$x=0.003866$$

$$\text{Activity}=(x*2.2)/0.2*10*0.4=0.01063$$

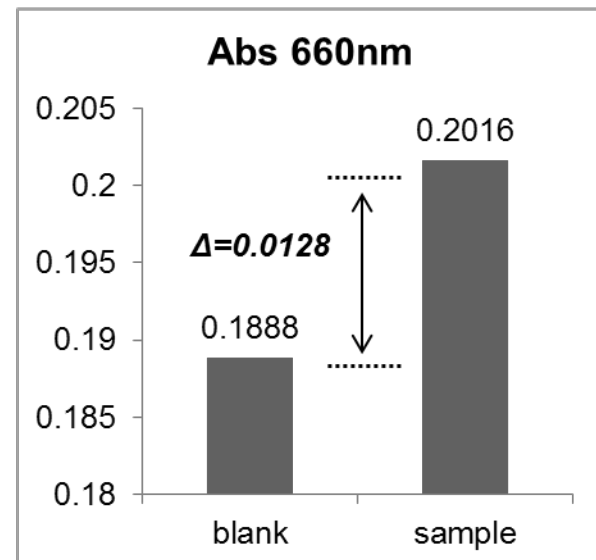


Figure 3.7. GST-UBP27 hydrolyzes casein.

Figure 3.7 (cont'd)

(A) Purified GST-UBP27 (deleted for aa 1-49 that contains the TMD) from *E. coli* is unstable. Anti-GST antibody was used to detect GST-UBP27. GST-UBP27 degradation fragments are indicated. Molecular weight markers in kDa are indicated on the left of the blot.

(B) GST-UBP27 has protease activity on the substrate casein. GST-UBP27 was incubated with casein, and the release of Tyr was quantified colorimetrically using Folin's reagent. Absorbance value obtained from GST-UBP27 hydrolysis of casein was compared to a Tyr standard curve to finally calculate specific activity (U/ml). Units/mL of enzyme = $(\mu\text{mole Tyr released})(\text{Total Vol. of assay})/(\text{Vol. used in colorimetric assay})(\text{Vol. of enzyme})(\text{Time of assay})$.

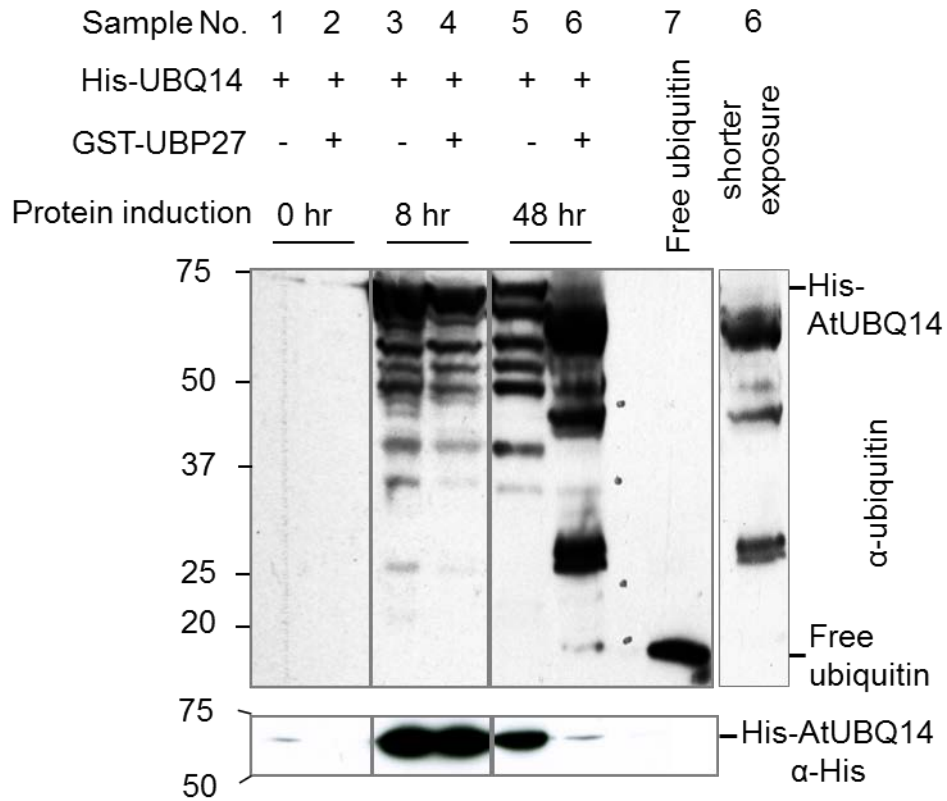


Figure 3.8. UBP27 possesses de-ubiquitinase activity *in vitro*.

The substrate 6xHis-AtUBQ14 was either expressed alone (lanes 1, 3, 5) or co-expressed with GST-UBP27 (lanes 2, 4, 6) in *E. coli* Rosetta (DE3) strain for the indicated periods of time. 6xHis-AtUBQ14 and its breakdown products were detected by anti-ubiquitin antibody. Lane 7 contains pure free ubiquitin as a control for the ubiquitin antibody and used to determine the mobility of monomeric ubiquitin. Lower panel shows the intact AtUBQ14 polyubiquitin quaternary structure detected by the anti-His antibody. Molecular weight makers in kDa are shown on the left of the immunoblots.

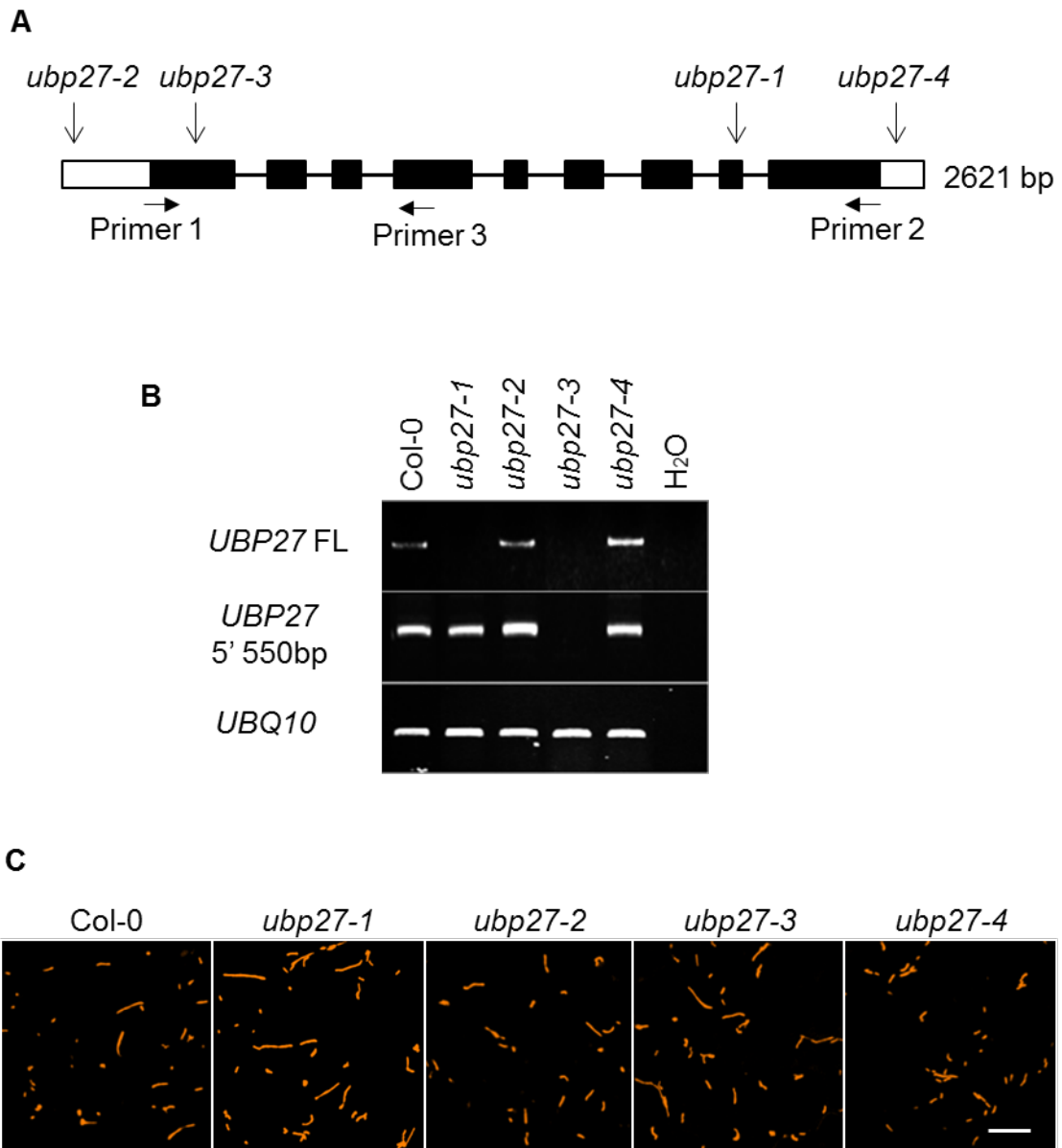


Figure 3.9. Characterization of the *UBP27* T-DNA insertion lines.

Figure 3.9 (cont'd)

(A) Schematic of the *UBP27* gene. Open box, UTR; black box, exon; line, intron. Arrows indicate the T-DNA insertion sites. Primers 1 and 2 were used to amplify the full-length *UBP27* and primers 1 and 3 were used to amplify the 5' 500 bp of the *UBP27* transcript.

(B) Semi-quantitative RT-PCR analysis of RNA from four-week-old *UBP27* T-DNA insertion lines. FL, full length. *Ubiquitin 10 (UBQ10)* was used as the loading control.

(C) Confocal images showing mitochondrial morphology in epidermal cells of six-week-old *Arabidopsis* plants expressing the mitochondrial marker COX4-YFP. Scale bar = 10 μm .

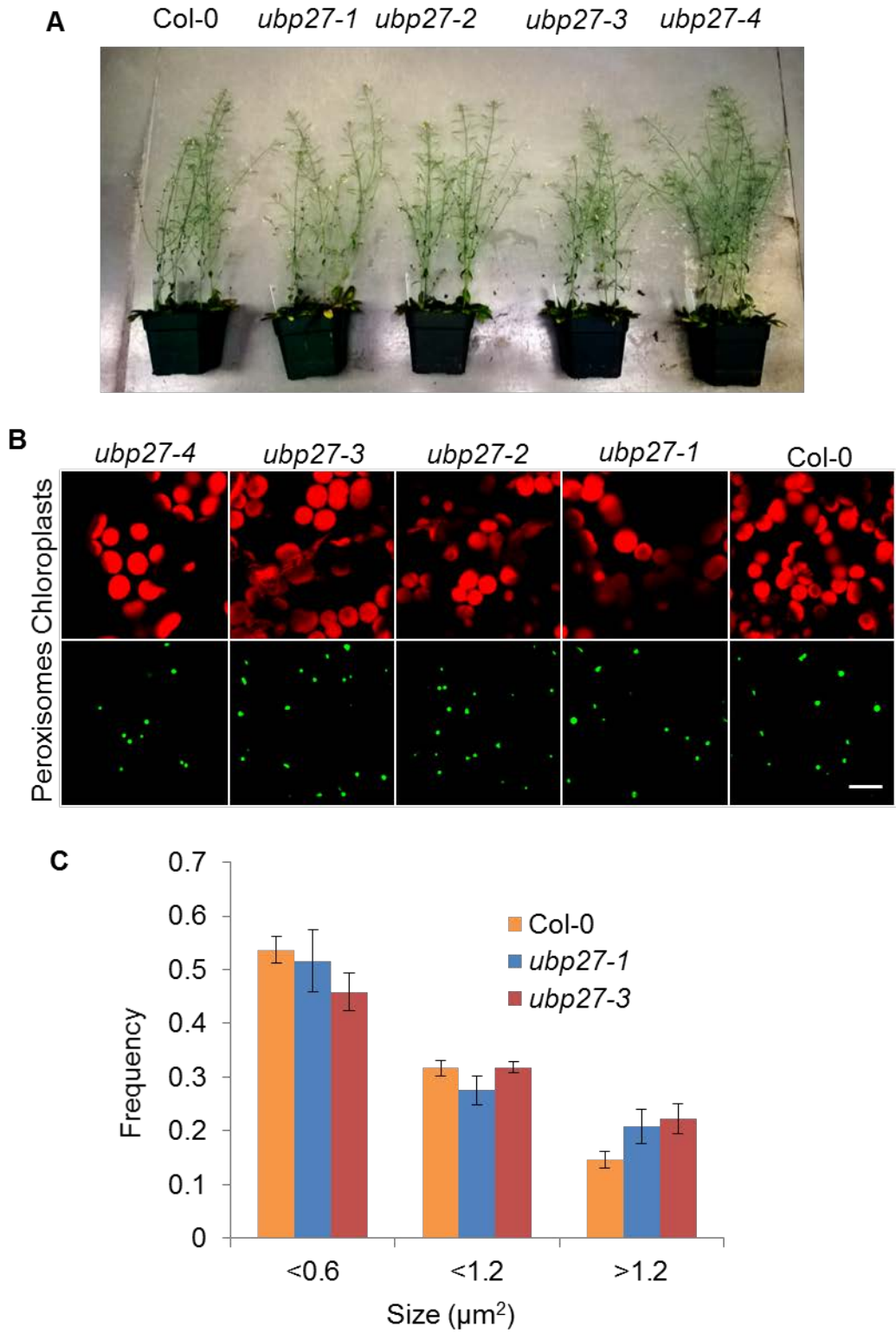


Figure 3.10. Additional characterization of the *UBP27* T-DNA insertion lines.

Figure 3.10 (cont'd)

(A) Growth phenotype of 6-week old *UBP27* T-DNA insertion lines.

(B) Confocal images showing chloroplast and peroxisome morphology in mesophyll cells of *Arabidopsis* plants expressing the peroxisome marker YFP-PTS1. Chloroplasts were marked by chlorophyll autofluorescence. Scale bar = 10 μm .

(C) Quantitative analysis of mitochondria size distribution in Col-0 and *ubp27* loss-of-function mutants expressing COX4-YFP. Mitochondrial size in a $4.9 \times 10^3 \mu\text{m}^2$ confocal image was quantified with Image J software. No statistical significance in mitochondrial size was detected between the samples. Error bar, s.e.m.; n=4.

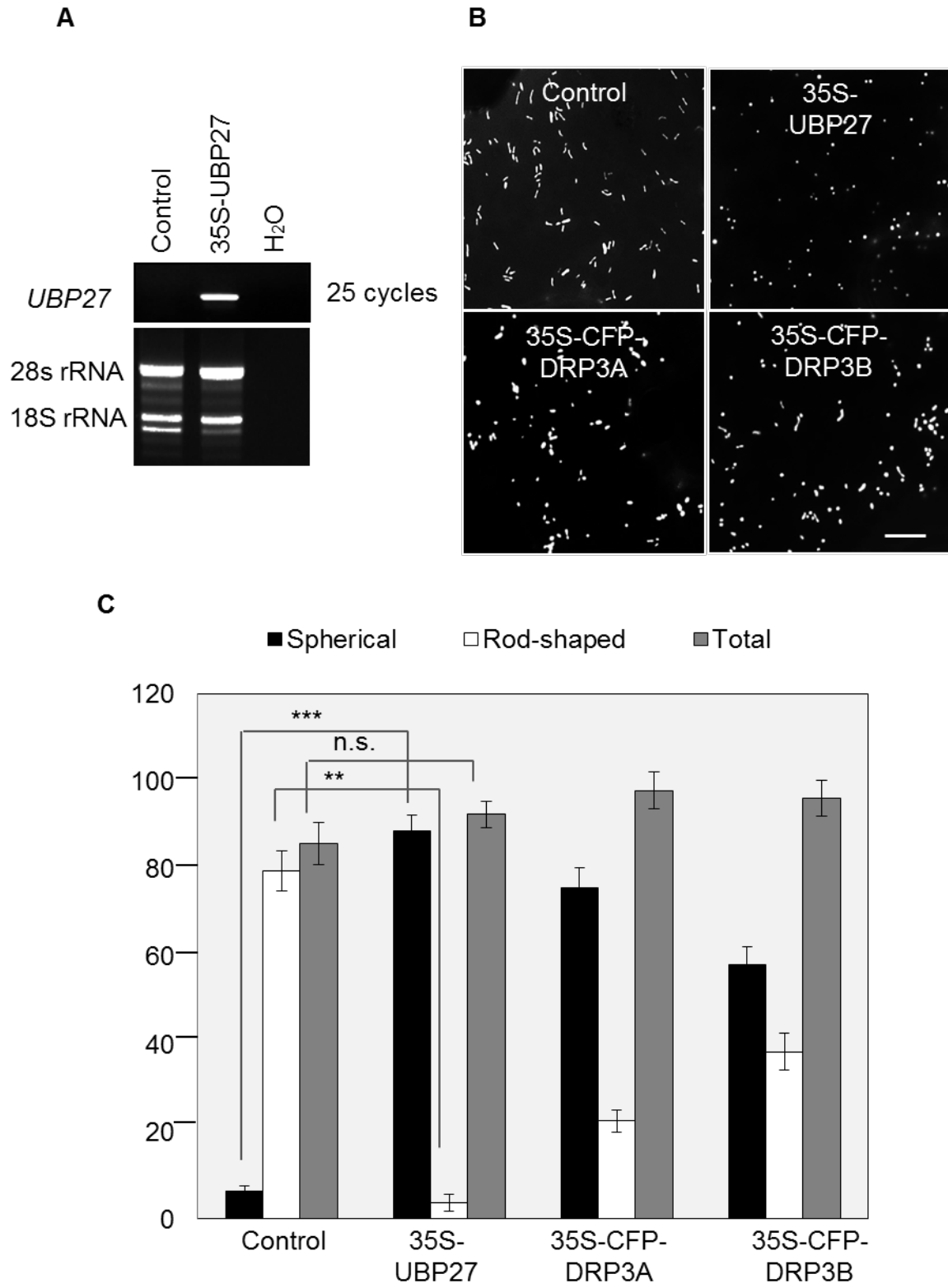


Figure 3.11. UBP27 overexpression leads to mitochondrial morphological changes.

Figure 3.11 (cont'd)

(A) Semi-quantitative RT-PCR analysis of RNA from tobacco leaf tissue transiently overexpressing UBP27 and the mitochondrial marker COX4-YFP or only COX4-YFP (control). Primers 1 and 2 shown in Figure 5a were used to amplify full-length *UBP27* transcript. Total RNA was used as the loading control.

(B) Epifluorescent images showing mitochondrial morphology in tobacco leaf epidermal cells transiently overexpressing UBP27 or CFP-DRP3 and the mitochondrial marker COX4-YFP. Control, COX4-YFP alone. Expression of CFP-DRP3 was evidenced by the detection of CFP signals under the fluorescent microscope. Scale bar, 10 μm .

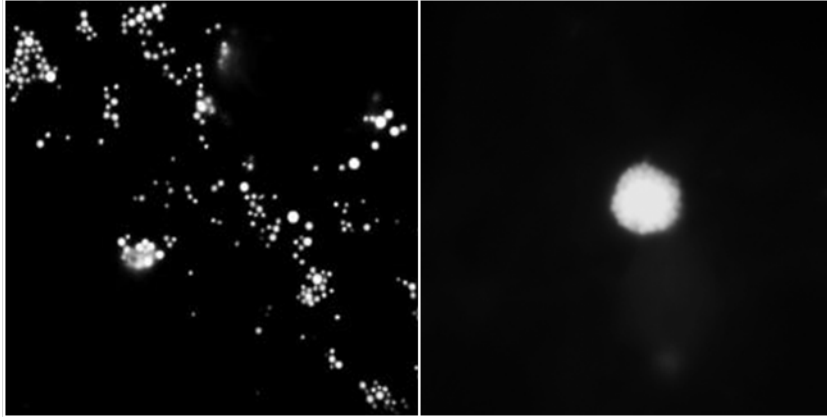
(C) Quantification of the mitochondria with different shapes in tobacco leaf epidermal cells shown in (b). Error bars, s.e.m.; n=6. ***, $p < 0.001$; **, $p < 0.01$; n.s., not significant. Rod and spherical mitochondria are defined as $>1 \mu\text{m}$ and $<1 \mu\text{m}$ in length respectively. Y axis indicates the number of mitochondria in $3.6 \times 10^3 \mu\text{m}^2$ of analyzed area.

A

35S-UBP27 & 35S-CFP-DRP3A

Weak aggregation

Strong aggregation



35S-UBP27 & 35S-CFP-DRP3B

Weak aggregation

Strong aggregation

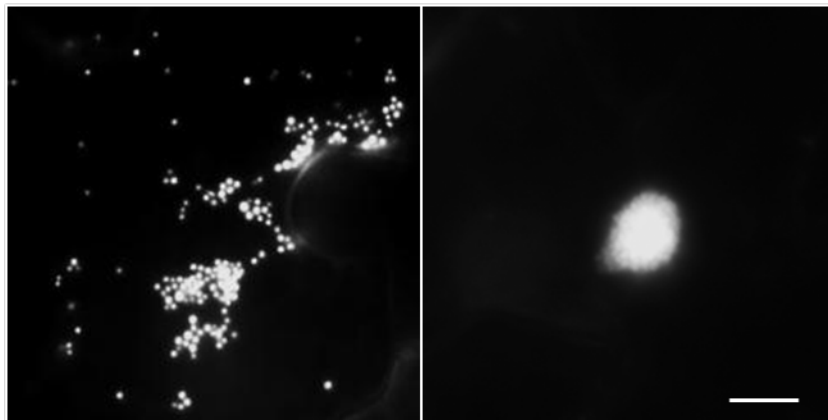
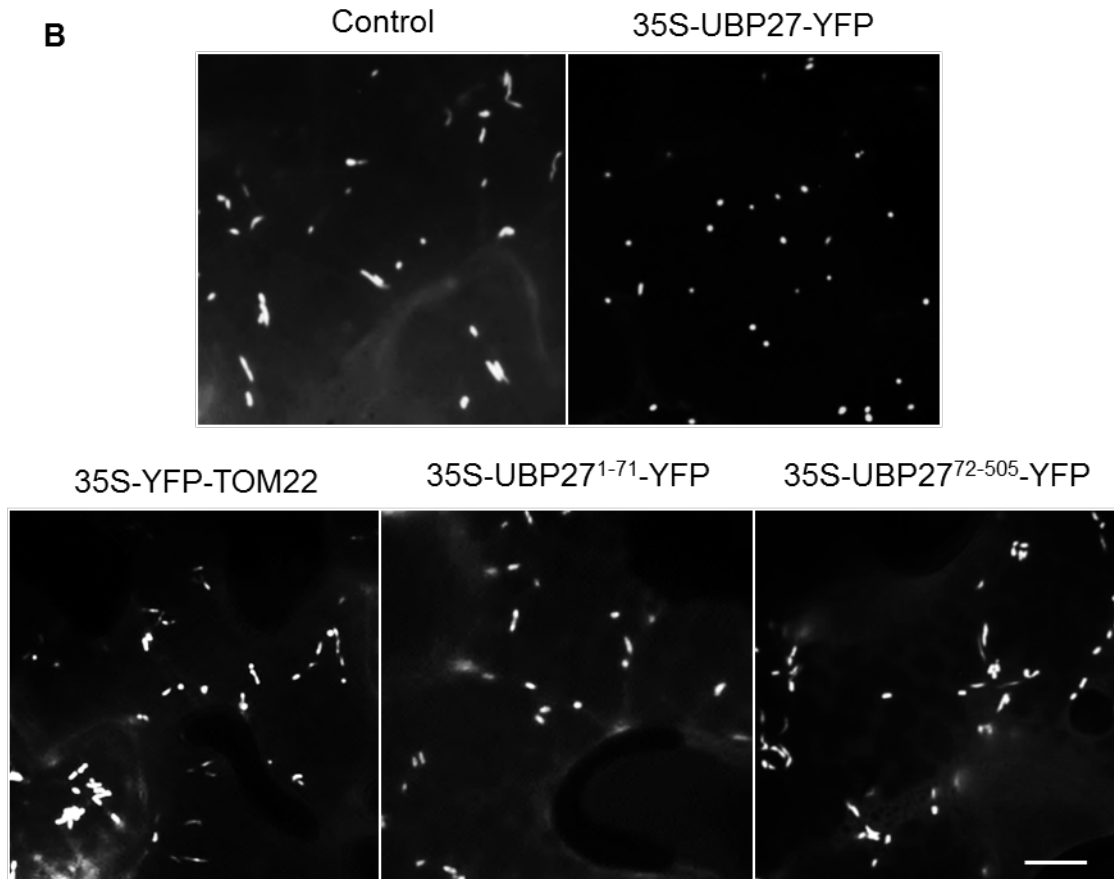


Figure 3.12. Mitochondrial phenotypes caused by *UBP27* overexpression.

Figure 3.12 (cont'd)



(A) Epifluorescent images showing mitochondrial aggregation in tobacco leaf epidermal cells co-expressing 35S-UBP27 and 35S-CFP-DRP3. Scale bar = 10 μ m.

(B) Epifluorescent images comparing mitochondrial morphology in *Arabidopsis* T2 plants overexpressing UBP27-YFP, YFP-TOM22, UBP27¹⁻⁷¹-YFP and UBP27⁷²⁻⁵⁰⁵-YFP. Scale bar = 10 μ m. Control, plants only expressing the mitochondrial marker COX4-CFP.

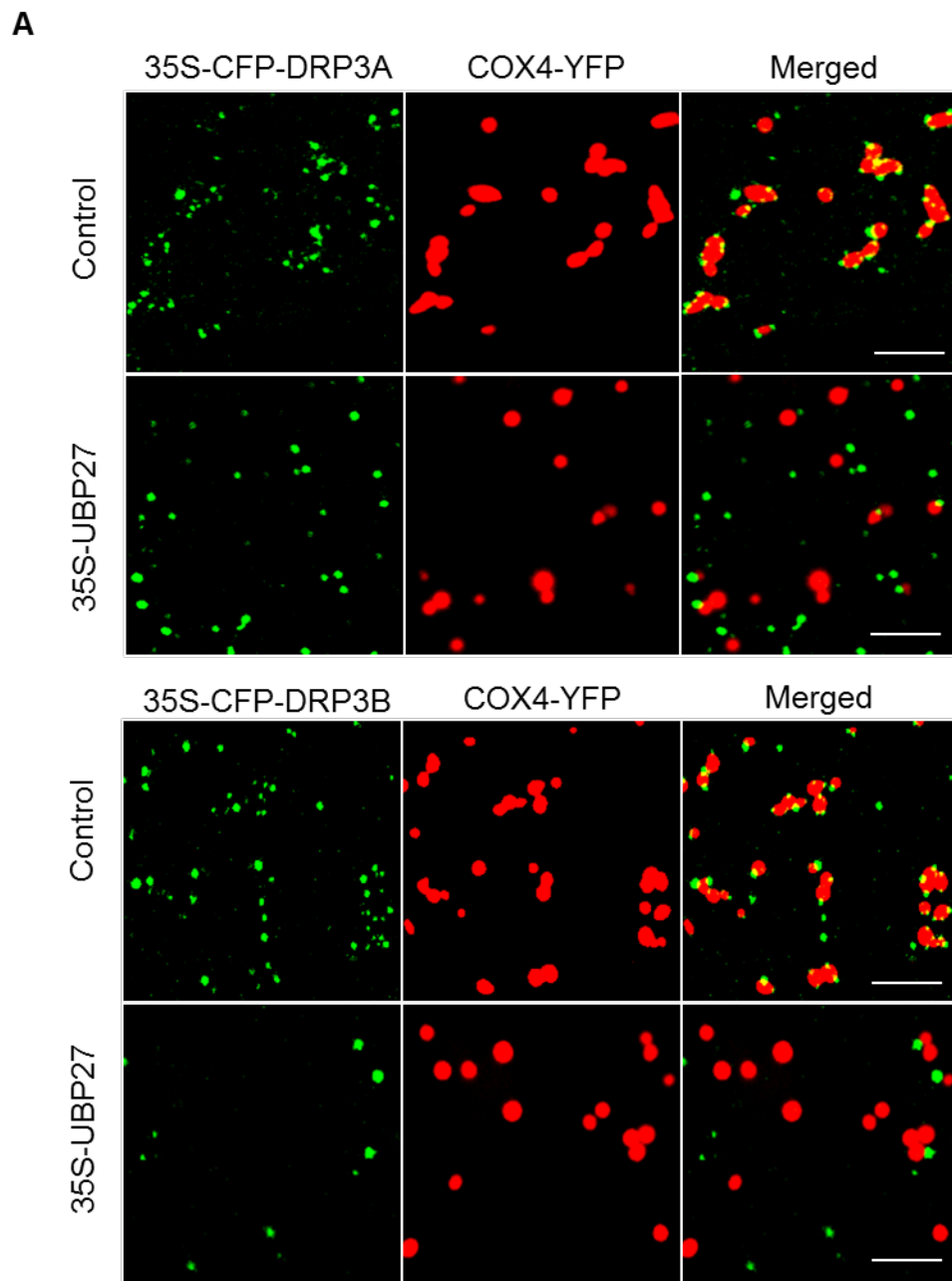
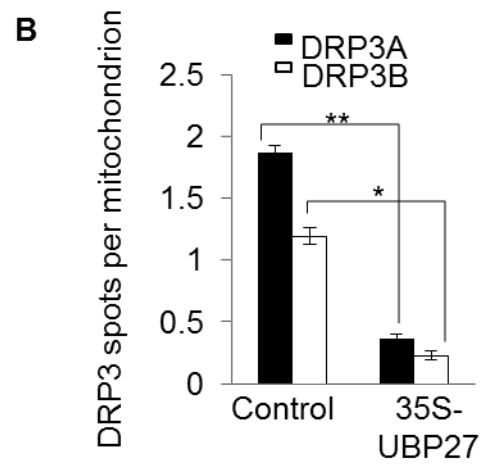


Figure 3.13. UBP27 overexpression reduces the association of DRP3 with mitochondria.

Figure 3.13 (cont'd)



(A) Confocal images showing the association of CFP-DRP3 with mitochondria in tobacco leaf epidermis expressing COX4-YFP (control) or COX4-YFP and 35S-UBP27. Scale bars = 5 μ m.

(B) Quantification of the mitochondrial association of CFP-DRP3 in tobacco leaf epidermis expressing CFP-DRP3 alone or co-expressing CFP-DRP3 and UBP27. Error bars, s.e.m.; n=4. **, p<0.01; *, p<0.05; n.s., not significant.

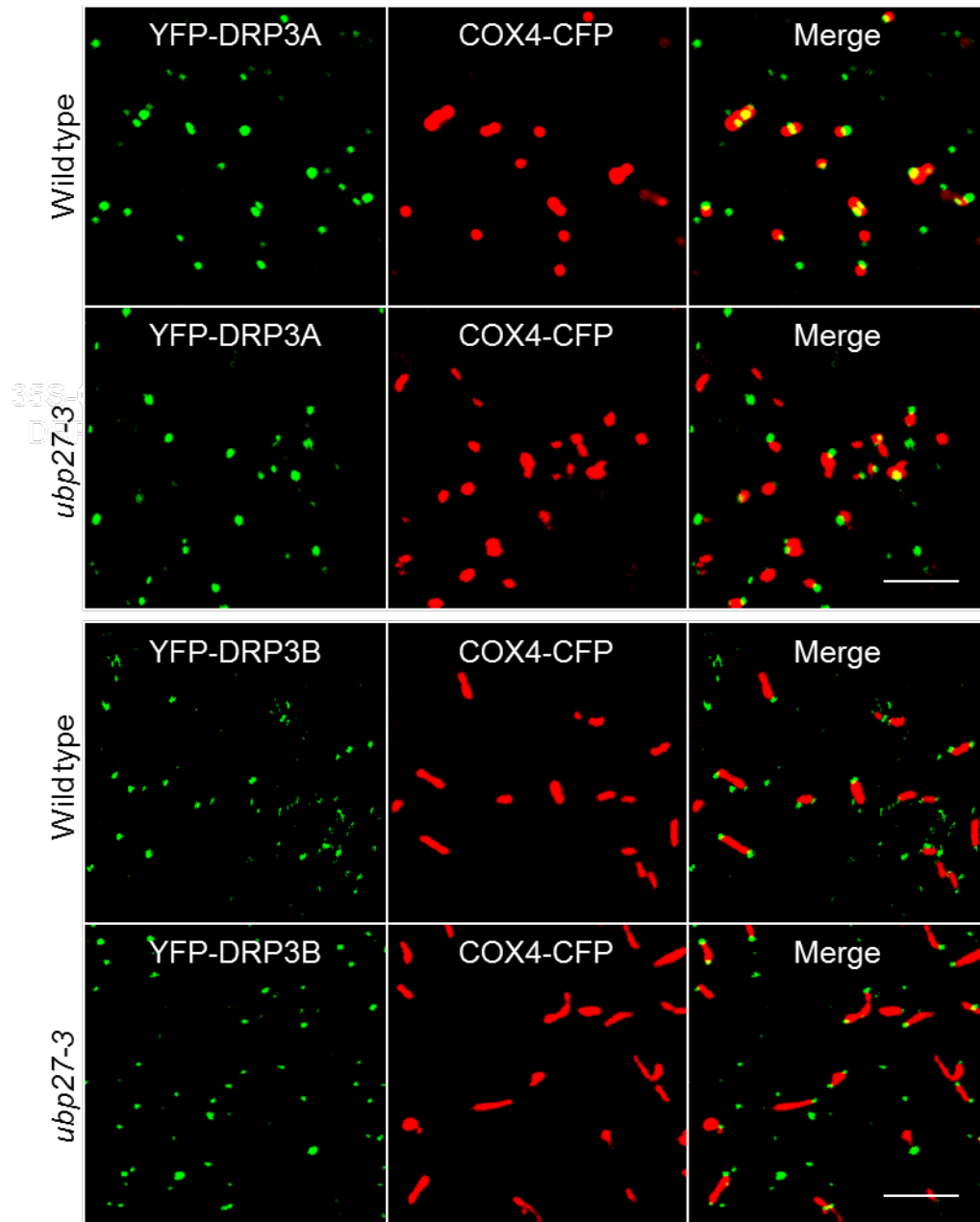


Figure 3.14. Mitochondrial association of DRP3 is not changed in *ubp27* loss-of-function mutant.

Confocal images showing the association of YFP-DRP3 with mitochondria in Arabidopsis leaf epidermis expressing COX4-CFP in wild-type or *ubp27-3* background.

Scale bars = 5 μ m.

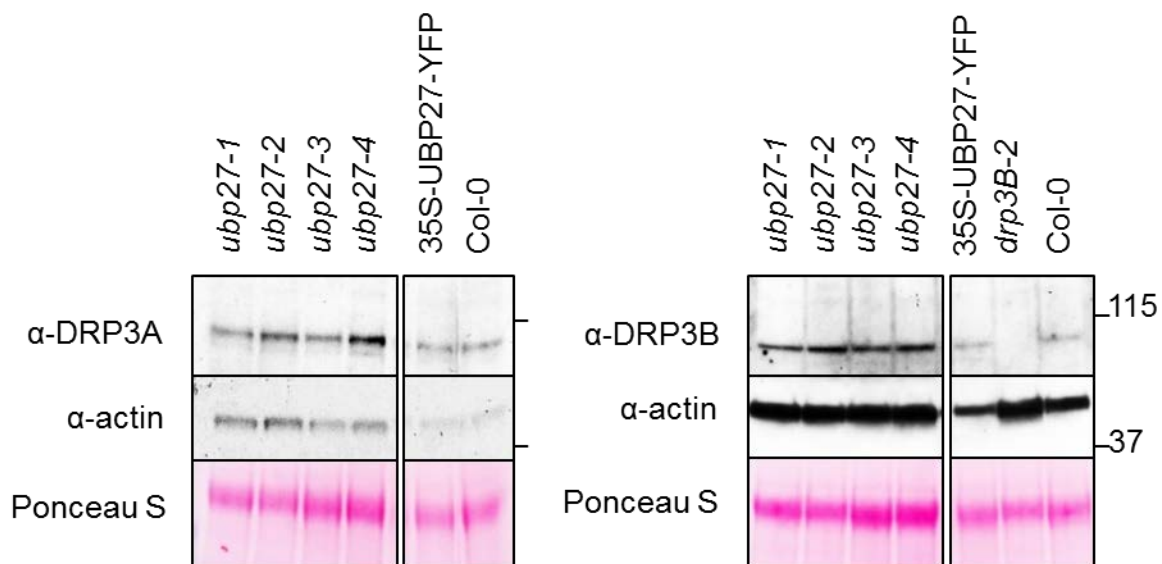


Figure 3.15. Immunoblot analysis of endogenous DRP3A and DRP3B proteins in wild-type, *UBP27* loss-of-function mutants and gain-of-function lines.

DRP3A and DRP3B were detected by specific peptide antibodies. Immunoblot using α -actin antibody and Ponceau S staining were used as loading controls. Numbers on the right are molecular weight markers in kDa.

Table 3.1. DNA primers used in this study.

Primer	Sequence
UBP17-Fw-AttB1	ggggacaagttgtacaaaaaagcaggcttcatgatgtggtttttcttctgattcg
UBP17-Re-AttB2-N	ggggaccactttgtacaagaaagctgggtctcaatcaaacgtttgagatttattatg
UBP17-Re-AttB2-C	ggggaccactttgtacaagaaagctgggtcatcaaacgtttgagatttattatgacg
UBP25-Fw-AttB1	ggggacaagttgtacaaaaaagcaggcttcatgggatttaaactgcagatg
UBP25-Re-AttB2-N	ggggaccactttgtacaagaaagctgggtctcacgagtacttcttcttgc
UBP25-Re-AttB2-C	ggggaccactttgtacaagaaagctgggtccgagtacttcttcttctgtaaatctcc
UBP27-Fw-AttB1	ggggacaagttgtacaaaaaagcaggcttcatggttctagaagaggctccg
UBP27-Re-AttB2-N	ggggaccactttgtacaagaaagctgggtctcaaagccttcatagaagagc
UBP27-Re-AttB2-C	ggggaccactttgtacaagaaagctgggtcaagccttcatagaagagcaagc
<i>ubp27-1</i> -genotyping-1	tcaatccaatgaaaaccaagc
<i>ubp27-1</i> -genotyping-2	ctccatcacgggtggttacaac
<i>ubp27-2</i> -genotyping-1	caggcttgagagctaatacgag
<i>ubp27-2</i> -genotyping-2	tacctggaggatgacgttgag
<i>ubp27-3</i> -genotyping-1	aagatgaagaagggcttctgc
<i>ubp27-3</i> -genotyping-2	tgtgatgaaataccgtgattcc
<i>ubp27-4</i> -genotyping-1	tgaaacagttaatcatcgccc
<i>ubp27-4</i> -genotyping-2	aggctattccactttccatcg
UBP27-partial -Re-1	ggggaccactttgtacaagaaagctgggtcaaaagaatcgtctccggagtc
UBP27-partial-Re-2	ggggaccactttgtacaagaaagctgggtcccattgattagagatcctaattc
UBP27-partial-Re-3	ggggaccactttgtacaagaaagctgggtctagaccgtgctgttgggcaaatac
UBP27-partial-Fw-4	ggggacaagttgtacaaaaaagcaggcttcatggttctgcatttcttctgc
UBP27-partial-Fw-5	ggggacaagttgtacaaaaaagcaggcttcatgttccgcaactaaacaactaaaac
UBP27-partial-Fw-6	ggggacaagttgtacaaaaaagcaggcttcatgctctgactctgccttcaaaatc
UBQ14-1	gaattcgaatttccaagcgattaatc
UBQ14-2	gtcgacgtcgacgataagtttttagaaccac
TOM22-1	ggggacaagttgtacaaaaaagcaggcttcatggcgcttaagaaaatcgg
TOM22-2	ggggaccactttgtacaagaaagctgggtcttagagcatcgaccgaccgg

Table 3.2. Vectors used in this study.

Vector and reference	Construct	Plant selection
pDonor 207 (Invitrogen)	all donor plasmids	N/A
pEarleyGate 100 (Earley et al., 2006)	35S-UBP27	BASTA
pEarleyGate 101 (Earley et al., 2006)	YFP-UBP27, YFP-UBP17, YFP-UBP25, YFP-TOM22	BASTA
pEarleyGate 104 (Earley et al., 2006)	UBP27-YFP, UBP17-YFP, UBP25-YFP	BASTA
pDEST15 (Invitrogen)	GST-UBP27	N/A
pET28a (Novagen)	His-UBQ14	N/A
pDest-35S-X-YFP-6xHis (Reumann et al., 2009)	UBP27 ¹⁻⁷¹ -YFP, UBP27 ¹⁻²⁶ -YFP, UBP27 ¹⁻⁴⁹ -YFP, UBP27 ²⁷⁻⁷¹ -YFP, UBP27 ⁵⁰⁻⁷¹ -YFP, UBP27 ⁷²⁻⁵⁰⁵ -YFP, UBP27-YFP (used in tobacco)	Kanamycin
pGWB544 (Nakagawa et al., 2007)	CFP-DRP3A, CFP-DRP3B	Hygromycin

3.5 Methods

3.5.1 Plant material

Plants were grown at 22°C with 70% humidity, 70 to 80 $\mu\text{mol m}^{-2} \text{s}^{-1}$ white light for 14 h per day. Col-0 was used as the wild type. Seeds for the T-DNA insertion mutant *ubp27-1* (SAIL_399_F01), *ubp27-2* (SALK_067020), *ubp27-3* (SALK_027968) and *ubp27-4* (SALK_023358) were provided by the Arabidopsis Biological Resource Center (ABRC), and homozygous mutants were identified by PCR of genomic DNA. Peroxisome marker lines CFP-PTS1 and YFP-PTS1 were generated in our previously study (Fan et al., 2005). Mitochondrial marker lines COX4-YFP and COX4-CFP were generated in a previous study (Nelson et al., 2007) and obtained from ABRC.

3.5.2 Plant transformation

Transgenic Arabidopsis plants were generated via a simplified floral dipping method (Clough and Bent, 1998) using *Agrobacterium tumefaciens* strain GV3101 (pMP90). To screen for transformants with BASTA, T1 plants were grown on soil and sprayed at 7 days and 9 days after germination with 0.1% (v/v) BASTA (Finale; Farnam Companies, Phoenix, AZ, USA) with 0.05% (v/v) Silwet L-77. For other transformants, T1 seeds were plated on 0.5 Linsmairer and Skoog (1/2 LS) medium containing 50 $\mu\text{g/ml}$ kanamycin. Transient gene expression in tobacco (*Nicotiana tabacum*) plants was performed as described previously (Aung and Hu, 2011). Information of the primers and vectors used is provided in Tables 3.1 and 3.2.

3.5.3 Gene cloning, plasmid construction, and RT-PCR

The coding sequences of specific genes were amplified with Gateway-compatible primers (Table S1) by Phusion polymerase (NEB), using cDNA made from total RNA of Col-0 plants. The PCR products were cloned into pDonor207 vector and various destination vectors (Table S2) via a standard Gateway cloning system (Invitrogen, <http://www.invitrogen.com/>). Substrate polyubiquitin *AtUBQ14* (At4g02890) was similarly amplified and cloned in EcoR1/Sal1 sites of pET28a using primers UBQ14-1/HU5795 and UBQ14-2/HU5796 (sequences shown in Table 3.1).

To analyze gene expression level in plants, RT-PCR was performed as previously described (Aung and Hu, 2011).

3.5.4 Plant protein preparation

Protein sample was prepared as previously described (Pan et al., 2014a). For crude plant protein extraction, 50 mg fresh tissue from *Arabidopsis* or tobacco plants were ground with plastic pestles using liquid nitrogen and 500 μ l extraction buffer (60 mM Tris-HCl pH 8.8, 2% SDS, 2.5% glycerol, 0.13 mM EDTA pH 8.0, and 1X protease inhibitor cocktail complete from Roche). The tissue lysates were vortexed for 30 s, heated at 70°C for 10 min, and centrifuged at 13,000 g twice for 5 min at room temperature. The supernatants were then transferred to new tubes. 15 μ l supernatant mixed with 5 μ l 4X LDS sample buffer was loaded onto SDS-PAGE.

To prepare mitochondrial proteins for SDS-PAGE analysis, 15 μ l purified mitochondria mixed with 5 μ l 4X LDS sample buffer were heated at 70 °C for 10 min, before loaded onto SDS-PAGE.

3.5.5 Immunoblot analysis

After separation on the gel, proteins were transferred to a PVDF membrane. The membrane was blocked with 5% milk in 1x TBST (50 mM Tris-base, 150 mM NaCl, 0.05% Tween 20, pH 8.0) for 1 h at room temperature.

For immunoblot using α -ubiquitin antibody (polyclonal rabbit, 1:100, Sigma-aldrich), nitrocellulose membrane was used instead of PVDF membrane. After transfer, the nitrocellulose membrane was immersed in distilled water and autoclaved for 30 min in liquid cycle setting. Then excessive water was removed, and the nitrocellulose membrane was autoclaved for 15min in dry cycle setting and blocked the same way as the PVDF membrane.

After blocking, the membrane was incubated for 1 h at room temperature with primary antibody prepared in the blocking buffer as follows: 1:20000 for α -GFP (Abcam), 1:2,500 for α -PEX14 (Lingard and Bartel, 2009), 1:5,000 for α -VDAC (Reumann et al., 2009), 1:250 for α -COXII (Moellering and Benning, 2010), 1:10,000 for α -GST (Invitrogen), 1:150 for α -ubiquitin (Sigma-Aldrich), 1:2000 for α -His (Invitrogen) and

1:400 for α -DRP3A and α -DRP3B (Aung and Hu, 2012). Then the membrane was washed with 1x TBST three times for 5 min each time, and incubated with the secondary antibody (i.e., 1:20,000 goat anti-rabbit IgG or 1:20,000 goat anti-mouse IgG, Millipore) at room temperature. After that, the membrane was washed four times with 1x TBST for 10 min each time, and then visualized using the SuperSignal West Dura Extended Duration Substrate (Pierce Biotechnology).

3.5.6 Microscopy

Fluorescence microscopy analysis was performed using a Zeiss Axio Imager upright epifluorescence microscope or an Olympus Fluoview FV1000 confocal laser scanning microscope. For confocal microscopy, CFP, YFP, and chlorophyll autofluorescence were excited with 458, 515, and 515 nm lasers and detected at 465–490 nm, 505–555 nm and 655–755 nm, respectively.

3.5.7 Mitochondrial isolation, and determination of protein membrane association and topology

Mitochondria were isolated from rosette leaves of four-week-old transgenic plants expressing 35S_{pro}:UBP27-YFP-HA and the mitochondrial marker, COX4-CFP, using a previously published protocol (Aung and Hu, 2011). The purity of mitochondrial preparations was determined using immunoblot analyses and organelle-specific antibodies as described above. Mitochondrial membrane association was tested using previously described methods (Nakagawa et al., 2007).

To determine the topology of UB27 on the mitochondrial membrane, protease protection assays were employed using thermolysin. 200 μ l purified mitochondria was treated with 0, 300 or 600 μ g/ml of thermolysin in an incubation buffer containing 50 mM HEPES/NaOH, pH 7.5, 0.33 M sorbitol, and 0.5 mM CaCl₂. The reactions were carried out at 4°C for 30 min, and stopped by incubating on ice for 5 min with 5 mM EDTA. Immunoblot analysis was then performed as described above.

3.5.8 Determination of mitochondrial size distribution

Confocal images were analyzed with the software ImageJ

(<http://rsb.info.nih.gov/ij/download.html>), using the protocol modified from the automatic determination of particle size distribution (<http://www.microscopy.ethz.ch/downloads/particle-size.pdf>). First, using Image>Color>Split Channels, the color channels of the image were split and a single channel image was used for further analysis. Second, using Analyze>Set Scale, image magnification was calibrated by setting a scale. Third, using Image>Adjust>Threshold, the threshold was adjusted to filter noise signals and to make the mitochondria appear as dots in the black and white mode. Fourth, using Analyze>Analyze Particles, mitochondrial size was analyzed. The analysis result was copied to Microsoft Excel software and subjected to a histogram analysis (http://mesa.ac.nz/?page_id=3813) to show the distribution of the mitochondrial size.

3.5.9 Phylogenetic tree construction

Protein sequences were aligned using Clustal Omega (<http://www.ebi.ac.uk/Tools/msa/clustalo/>). Sequence alignment was subjected to phylogenetic analysis using ClustalW2 – Phylogeny (http://www.ebi.ac.uk/Tools/phylogeny/clustalw2_phylogeny/). The phylogenetic tree was generated by the Tree of Life V1.0 software (<http://itol.embl.de/itol.cgi>).

3.5.10 Universal protease activity assay

Protease activity assay was performed using casein as a substrate according to instructions on colorimetric protease assays posted on the Sigma website (<http://www.sigmaaldrich.com/life-science/learning-center/life-science-video/universal-protease.html>). Briefly, to exclude the TMD, the N-terminal 49 amino acids were removed when expressing the GST-UBP27 fusion in *E. coli*. 1 µg of GST-UBP27 was incubated with 0.65% solution of casein (5 ml) at 37 °C for 10 min. A second set (Blank) omitting the protease was run in parallel. Both sets were treated with 5 ml TCA (Trichloroacetic acid) to precipitate the protein. 1 µg of GST-UBP27 was added to the

Blank set after the addition of TCA. Following 30 min incubation at 37°C, solutions from both sets were filtered. Folin's reagent (1 ml) and 500 mM sodium carbonate solution (5 ml) was added to the filtrate (2 ml) and incubated at 37°C for 30 minutes. Absorbance at 660 nm was recorded and value of the Blank sample subtracted from the Absorbance of the protease samples was plotted on a tyrosine standard curve to determine specific activity.

3.5.11 *In vitro* deubiquitinase activity assay

His-tagged AtUBQ14 was co-expressed with GST-UBP27 in *E. coli* strain Rosetta DE3 (Novagen) and protein induction was carried out with 0.1mM IPTG at 20 °C for various lengths of time. Sonicated lysates were analyzed by western blots. Purified bovine erythrocytes ubiquitin (Sigma-aldrich) was used as a control.

3.5.12 Statistical analysis

Quantitative analysis results are presented as the means \pm s.d. (or s.e.m.) from repeated experiments as indicated in the figure legends. Pairwise Student's *t*-test was used to analyze statistical significance.

3.6 Acknowledgements

We would like to thank Melinda Frame for help with confocal microscopy and Kyaw Aung for technical assistance. This work was supported by grants to JH from the Chemical Sciences, Geosciences and Biosciences Division, Office of Basic Energy Sciences, Office of Science, U.S. Department of Energy (DE-FG02-91ER20021), and National Science Foundation (MCB 1330441).

CHAPTER 4

Characterization of a small family of RING domain proteins associated with *Arabidopsis* energy organelles

4.1 Abstract

Eukaryotic cells are defined by the presence of membrane-delineated organelles. In plants, three organelles – chloroplasts, mitochondria and peroxisomes – are essential for energy capture, conversion, storage and metabolism. These organelles behave very dynamically in function, morphology, abundance, distribution and protein content, in response to stimuli from both inside and outside of plant cells. Post-translational modifications (PTMs), including protein ubiquitination, are critical in the regulation of animal and yeast mitochondrial dynamics. How ubiquitination contributes to the dynamics of plant chloroplasts, mitochondria and peroxisomes are just beginning to be addressed. Here, we report the characterization of a small family of RING domain-containing proteins composed of SP1, SPL1 and SPL2. Many RING domain proteins are ubiquitin E3 ligases, and this activity has been previously tested in vitro for SP1. In this work, I show that SP1 and SPL1 localize to chloroplasts, mitochondria and peroxisomes, while SPL2 localizes to only chloroplasts and mitochondria. I preliminarily characterized the targeting signal, membrane association and loss-of-function and gain-of-function mutant phenotypes of these RING domain proteins, and revealed different characteristics in these aspects. My results suggest that these three proteins probably regulate different aspects of organelle dynamics. Since the SP1/SPL1 family members associates with multiple plant energy organelles, these proteins may be able to coordinately regulate the dynamics of chloroplast, mitochondria and peroxisomes.

4.2 Introduction

To create an optimal environment for specific biochemical reactions, eukaryotic cells contain numerous membrane-bounded compartments, among which are peroxisomes, mitochondria and chloroplasts – organelles that cooperate in various metabolic pathways, such as photorespiration, lipid metabolism, and hormone biosynthesis (Peterhansel et al., 2010; Millar et al., 2008; Hu et al., 2012). Peroxisomes, mitochondria and chloroplasts are considered energy organelles in plants because of their essential roles in energy capture, conversion, storage and/or metabolism. Peroxisomes are bounded by a single membrane and host many important metabolic processes, such as lipid mobilization, photorespiration, detoxification, hormone biosynthesis and metabolism, and pathogen defense in plants (Hu et al., 2012). Mitochondria are enclosed by double membranes and participate in many vital tasks, including energy metabolism, programmed cell death, and intracellular calcium homeostasis, and are considered the power house in the cell because of their ability to provide ATP (Millar et al., 2008). Chloroplasts, the chlorophyll-containing plastids, are surrounded by two membranes - the inner envelope membrane (IEM) and outer envelope membrane (OEM). Chloroplasts also contain a network of internal membranes called thylakoids, where major photosynthetic machinery components reside (Jarvis and López-Juez, 2013). In addition to photosynthesis, chloroplasts also carry out the synthesis of fatty acids and amino acids, the metabolism of nitrogen and sulfur, and other functions (Neuhaus and Emes, 2000).

Peroxisomes can bud from the endoplasmic reticulum and multiply from pre-existing peroxisomes via division through partially overlapping steps including

elongation, membrane constriction and fission (Yan et al., 2005; Hu et al., 2012). In *Arabidopsis*, three protein families are the major known division factors: PEX11a to –e for elongation (Lingard and Trelease, 2006; Orth et al., 2007), DRP3A and DRP3B for membrane scission (Fujimoto et al., 2009; Mano et al., 2004; Aung and Hu, 2012; Zhang and Hu, 2009) and FIS1A and FIS1B presumably for recruiting DRP3 (Zhang and Hu, 2008b). DRP5B, which was originally identified as a chloroplast division factor, was recently found to be engaged in peroxisome division as well (Zhang and Hu, 2010). As descendants of endosymbiotic α -proteobacteria (Lane and Martin, 2010), mitochondria can only divide by binary fission (Friedman and Nunnari, 2014). In spite of differences in membrane structure and evolutionary origins, peroxisomes and mitochondria share two groups of division factors, DRP3 and FIS1. This is not very surprising due to the highly interconnected functions of these two organelles. DRPs (Dynamin-Related Protein) play a key role in the fission process, in which these dimerized large GTPases dynamically localize at the fission sites, form spiral-like structure via higher order assembly, and promote membrane fission through assembly-driven and GTP hydrolysis-driven constrictions (Hoppins et al., 2007). In addition to FIS1 and DRPs, there are several lineage-specific or organelle-specific factors, such as WD40 domain-containing proteins MDV1/CAF4 in yeasts, Mff in human, and ELM1 and PMD1 in *Arabidopsis* (Motley et al., 2008; Gandre-Babbe and Bliiek, 2008; Arimura et al., 2008; Aung and Hu, 2011). Among them, MDV1/CAF4, Mff and PMD1 are also shared by mitochondria and peroxisomes. Similar to mitochondria, chloroplasts are propagated by binary fission. Chloroplast fission is mediated by several concentric rings, i.e., a Z-ring and an inner PD-ring on the stromal side and an outer PD-ring and a discontinuous

DRP5B ring on the cytosolic side (Jarvis and López-Juez, 2013; Gao et al., 2003). The Z-ring is formed by FtsZ1 and FtsZ2, two homologous tubulin-like GTPases (TerBush and Osteryoung, 2012). The inner PD-ring has yet uncertain composition, whereas the outer PD-ring comprises polyglucan filaments (Yoshida et al., 2010).

Due to the endosymbiotic origin, mitochondria and chloroplasts contain their own genomes (Millar et al., 2008; Friedman and Nunnari, 2014; Green, 2011) as well as transcriptional and translational machinery. However, the proteomes of mitochondria and chloroplasts are almost all encoded by nuclear genes and imported from the cytosol (Millar et al., 2005; Cánovas et al., 2004; Strittmatter et al., 2010). In contrast, peroxisomes do not contain any genomic information. They can be generated de novo from specific ER subdomains (Hu et al., 2012). ER is an important source of peroxisome membrane phospholipids and some peroxisome membrane proteins (Schlüter et al., 2006; Mullen and Trelease, 2006). Peroxisome matrix proteins are all imported from the cytosol (Hu et al., 2012). Thus, protein import is essential to the biogenesis and functions of these plant energy organelles. The mitochondrial and chloroplast matrix protein import is initiated by protein translocation across their outer membranes, which is mediated by the TOM machinery at the mitochondrial outer membrane and the TOC machinery at the outer envelope of chloroplasts, respectively (Duncan et al., 2013; Strittmatter et al., 2010). In *Arabidopsis*, the TOC machinery is composed of the channel protein TOC75, the receptors for photosynthetic proteins TOC33 and TOC159, and the receptors for housekeeping proteins TOC34 and TOC132/TOC120 (Shi and Theg, 2013; Strittmatter et al., 2010). The *Arabidopsis* TOM machinery mainly consists of the conserved proteins TOM40 and METAXIN, as well as

the plant specific proteins TOM20, TOM9, and OM64 (refer to Fig. 1.1 in Chapter 1) (Duncan et al., 2013; Braun and Schmitz, 1999). For *Arabidopsis* peroxisomes, the cargo proteins are first recognized by the receptors PEX5 and PEX7, which dock to the import apparatus formed by membrane proteins PEX13 and PEX14. Then the cargo proteins translocate into the matrix, after which the receptors are recycled. At least in yeasts and mammals, the recycling of PEX5 depends on a ubiquitin system consisting of a ubiquitin-conjugating enzyme PEX4, three ubiquitin-protein ligases PEX2, PEX10, and PEX12, as well as two AAA ATPases PEX1 and PEX6. In *Arabidopsis*, PEX4 is anchored to the membrane by PEX22, whereas PEX1 and PEX6 are tethered to the membrane by APEM9 (refer to Fig. 1.2 in Chapter 1) (Hu et al., 2012).

The morphology and abundance of mitochondria and peroxisomes are very dynamic depending on the physiological and environmental conditions, so the fission machinery must be regulated effectively. Multiple regulatory mechanisms are employed for this purpose. In *Arabidopsis*, PEX11b is regulated by light through the far-red light receptor phyA and the bZIP transcription factor HYH (Hu and Desai, 2008; Desai and Hu, 2008). Besides regulation at the transcriptional level, regulation of the division machinery may also be achieved at the post-translational modification (PTM) level. Multiple aspects of the fission DRP proteins, such as the GTPase activity, translocation from cytosol to the organelle division site, interaction with other factors, and polymer assembly, may be influenced by PTMs. The human peroxisome/mitochondrion division factor DRP1 can be modified via phosphorylation, SUMOylation, ubiquitination and S-nitrosylation, which enhance or repress the function of this protein in mitochondrial division (Chang and Blackstone, 2010). However, peroxisomes are either not affected

or not yet verified to be affected by these modifications. To date, there is no evidence that any of these DRP modification mechanisms are conserved from mammals to plants or yeasts. However, phosphorylation of the *Arabidopsis* DRP3A and DRP3B proteins was discovered by multiple proteomics studies (Heazlewood et al., 2008; Sugiyama et al., 2008; Durek et al., 2010; Nakagami et al., 2010; Mayank et al., 2012; Wang et al., 2013). The effects of these phosphorylation events on the function of DRP3 are not known yet. In addition, DRP3A and DRP3B were reported to be phosphorylated at unidentified positions during mitosis, which may induce mitochondrial fission (Wang et al., 2012).

As an important form of PTM, ubiquitination is defined as the covalent attachment of ubiquitin, a small 76-amino acid protein, usually to the lysine residues of the target proteins (Sadanandom et al., 2012; Vierstra, 2009). Ubiquitination may occur as the attachment of a single ubiquitin molecule or a multi-ubiquitin chain, the latter of which can vary in the number of ubiquitin molecules, branch patterns, and/or 3D structures. The nature of ubiquitin linkage and position of the modified residue determine the fate of the substrates. In most cases, the substrate is degraded by the 26S proteasome, the major proteolytic machinery in eukaryotic cells (Vierstra, 2009). The ubiquitin-proteasome system (UPS) adjusts the abundance of key regulatory proteins and enzymes to control various cellular pathways (Sadanandom et al., 2012; Vierstra, 2009). It was estimated that proteins involved in the UPS pathway take approximately 5~6% of the *Arabidopsis* proteome (Smalle and Vierstra, 2004). Most (~1406) of these proteins are, or predicted to be, E3 ligases. E3 ligase is a component in the triad ubiquitination cascade, which consists of ubiquitin-activating enzyme (E1),

ubiquitin-conjugating enzyme (E2), and ubiquitin-ligase (E3) (Sadanandom et al., 2012). The tremendous diversity of E3 ligases is consistent with E3s' key roles in defining substrate specificity. Based on the types of the enzymatic domain, the *Arabidopsis* E3 ligases can be classified into several groups, such as HECT, RING and U-BOX (Sadanandom et al., 2012; Vierstra, 2009). The RING-type E3s can either function by itself or dependent on a multi-subunit anaphase-promoting complex (APC) Skp1-Cullin-F-box (SCF). The RING domain is named due to its initial identification in a protein called Really Interesting New Gene (Freemont et al., 1991). Similar to the DNA-binding zinc finger domain, the RING domain contains a cysteine-rich motif that coordinates two zinc atoms. However, RING domain interacts with proteins rather than DNA (Borden, 2000; Lovering et al., 1993). Stone, S. *et al* identified 469 *Arabidopsis* RING-type E3s based on bioinformatics analysis, and confirmed the ubiquitination activity for many of them *in vitro* (Stone et al., 2005). RING-type E3s have been shown to mediate various pathways in plants, such as auxin signaling, photomorphogenesis, defense, the secretory pathway and seed development (Serrano and Guzmán, 2004; Xu and Li, 2003; Xie et al., 2002; Molnár et al., 2002; Holm et al., 2002; Hardtke et al., 2002; Matsuda et al., 2001).

In mammalian cells, the UPS apparatus plays an important role in the quality control of mitochondrial proteome as well as in the regulation of mitochondrial dynamics. The identified components of the mammalian mitochondrial UPS apparatus comprises E3 ligases MUL1, MITOL (or MARCH-V) and Parkin, and deubiquitinase (DUB) USP30 (Livnat-Levanon and Glickman, 2011). Recent studies in *Arabidopsis* demonstrated that ubiquitin E3 ligases play critical roles in the biogenesis and/or function of chloroplasts

(Ling et al., 2012) and peroxisomes (Lingard et al., 2009; Kaur et al., 2013). However, no component of the triad ubiquitination cascade has yet been found to associate with the other plant energy organelle, mitochondria. Our discovery of a mitochondrial outer membrane-bound DUB named UBP27 strongly supports the presence of plant mitochondrial UPS (Pan et al., 2014; Chapter 3 of this thesis).

To look for additional factors in plant mitochondrial UPS, particularly E3s, we searched the *Arabidopsis* genome for mitochondrion-localized proteins that could potentially be involved in ubiquitination. Here, we report the identification of a small protein family of three RING domain-containing proteins, SP1, SPL1 and SPL2. These three proteins were previously found to localize to chloroplasts, with SP1 mediating the ubiquitination and degradation of multiple components of the TOC machinery (Ling et al., 2012). In this study, we show that all three members of this protein family localize to mitochondria as well as chloroplasts, and SP1 and SPL1 also localize to peroxisomes. These three E3s appear to possess distinct characteristics in regulating the dynamics of the three plant organelles. I hypothesize that plants possibly use SP1/SPL-mediated ubiquitination events to coordinate the dynamics and thus the functions of chloroplasts, mitochondria and peroxisomes.

4.3 Results and discussion

4.3.1 Subcellular localization of members of a small RING-type E3 protein family in *Arabidopsis*

In a previous genome-wide study, approximately 1406 proteins were predicted to be ubiquitin RING-type E3s in *Arabidopsis* (Stone et al., 2005). From this list of proteins, we searched for potential mitochondrial localized E3s, using bioinformatic predictions for protein subcellular localizations compiled in the SubCellular Proteomic Database (SUBA) (<http://suba.plantenergy.uwa.edu.au/>). A small protein family of three RING-type E3s, namely SP1, SPL1 and SPL2, were predicted to be associated with mitochondria.

We then experimentally analyzed their subcellular localization with YFP fusion proteins. Transgenic *Arabidopsis* lines expressing these fusion proteins under the 35S constitutive promoter were generated, using the floral dipping method in wild type plants expressing the mitochondrial marker COX4-CFP or the peroxisomal marker CFP-PTS1. The leaf tissue of T2 plants was used for confocal analysis. All three proteins targeted to chloroplasts (Fig. 4.1), consistent with a previous report (Ling et al., 2012). The SP/SPL-YFP proteins all seemed to be more concentrated on smaller chloroplasts, yet with different distribution patterns. Specifically, SP1 and SPL1 signals were relatively low and formed numerous tiny spots on the chloroplasts (Fig. 4.1A, 4.1B), probably indicating that SP1 and SPL1 are part of some small protein complexes. However, SPL2 signals were stronger throughout chloroplasts and formed much fewer but bigger spots (Fig. 4.1C), suggesting that SPL2 are probably part of very big protein complexes.

Interestingly, SP1, SPL1 and SPL2 were all present on mitochondria (Fig. 4.2). SP1 distributed evenly on mitochondria (Fig. 4.2A). SPL1 signals were very low throughout mitochondria and in addition appeared as numerous bright spots associated with mitochondria (Fig. 4.2B). SPL2 spread all over mitochondria and formed a few large foci on mitochondria (Fig. 4.2C). These observations strongly support the

presence of a mitochondrial associated ubiquitin ligase system in *Arabidopsis*. The different distribution patterns of these proteins suggest that members of this family may play distinct functions on mitochondria.

In addition to chloroplasts and mitochondria, SP1 and SPL1 also localized to peroxisomes (Fig. 4.3). SP1 often appeared as bright spots (Fig. 4.3A), while SPL1 signals were relatively low and evenly distributed on most peroxisomes (Fig. 4.3B). Different from SP1 and SPL1, SPL2 did not localize to peroxisomes (Fig. 4.3C), indicating that SPL2 may be functionally more divergent from SP1 and SPL1.

4.3.2 Protein sequence analysis of SP1/SPL family members

Within the SP1/SPL family, SP1 and SPL1 share a 58% amino acid identity, and SPL2 is more divergent with 22% sequence identity to SP1 and 23% to SPL1 (Fig. 4.4). Hydropathy plot analysis using TMHMM Server v. 2.0 (<http://www.cbs.dtu.dk/services/TMHMM/>) showed that SP1 and SPL1 are likely to contain one transmembrane domain (TMD) with a predicted probability around 0.6 (Fig. 4.5A, 4.5B). In comparison, SPL2 contained two TMDs, both with a predicted probability higher than 0.8 (Fig. 4.5C). One SPL2 TMD was at the similar position to that of SP1 and SPL1, but the other SPL2 TMD was at the very N-terminus (Fig. 4.6A). The N-termini of SP1 and SPL1 had very low probability to contain TMDs, but instead they were predicted to contain signal peptides (Fig. 4.6A) by the SignalP 4.1 Server, which predicts the presence and location of signal peptide cleavage sites in protein amino acid sequences (<http://www.cbs.dtu.dk/services/SignalP/>). These analyses are consistent with SPL2's different organelle association pattern from SP1 and SPL1.

Studies in mammals identified several mitochondrial ubiquitin E3s, including Parkin, MITOL and MUL1 (Livnat-Levanon and Glickman, 2011). MUL1 was also reported to be an E3 for small ubiquitin-like modifier (SUMO) (Braschi et al., 2009). MUL1 is a RING-type protein (Li et al., 2008) showing 27%, 26% and 23% sequence identity to *Arabidopsis* SP1, SPL1 and SPL2 respectively. We also searched against the rice genome using the BLAST tool for proteins with similar sequences to *Arabidopsis* SP1/SPL family and human MUL1. Based on a phylogenetic analysis of these proteins, SP1, SPL1 and MUL1 were more closely related, and SP1 had a close homologue in rice (Fig. 4.6B). SPL2, as well as its homologue in rice, was more distantly related to SP1 and SPL1 (Fig. 4.6B). Therefore, SP1 and SPL1 are probably functionally distinct from SPL2. Additional blast analyses identified homologous proteins for both SP1 and SPL2 in other plant species, such as *Brassica napus*, *Citrus sinensis*, *Nicotiana tomentosiformis*, *Vitis vinifera*, *Glycine max*, *Prunus mume*, *Zea mays*, *Oryza sativa* and others. Thus, the functions of the SP1/SPL family proteins are very likely conserved across different plant species.

4.3.3 SP1 is integral to the mitochondrial and peroxisomal membranes

SP1, as well as SPL1, was predicted to contain one TMD. SP1 was shown by Ling *et al* to be integral to the chloroplast membrane (Ling et al., 2012). To analyze the membrane association of SP1 to mitochondria and peroxisomes, we isolated these two organelles from *Arabidopsis* leaf tissue stably expressing SP1-YFP together with either COX4-CFP or CFP-PTS1. The purity of these isolated organelles was determined by immunoblot analysis using organelle specific antibodies: VDAC for mitochondria and

PEX14 for peroxisomes (Fig. 4.7A). The presence of SP1-YFP and the organelle markers on mitochondria and peroxisomes was confirmed by immunoblot with GFP antibody (Fig. 4.7A). To separate integral membrane proteins from total proteins, the isolated organelles were treated with Tris–EDTA (TE) buffer, high concentration salt solution (1 M NaCl), and alkaline carbonate (Na_2CO_3 , pH 11.0) respectively. Integral membrane proteins were concentrated into the pellet after centrifugation. SP1-YFP, as well as the mitochondrial membrane protein VDAC and the peroxisomal membrane protein PEX14, was detected in the pellet after each treatment (Fig. 4.7B, 4.7C), suggesting that SP1 is indeed an integral membrane protein of both mitochondria and peroxisomes.

SP1 was previously reported to localize to the chloroplast outer envelope, where SP1 mediates the ubiquitination and degradation of multiple components of the TOC complexes (Ling et al., 2012). It is possible that the mitochondrial/peroxisomal SP1, as well as SPL1, is topologically similar to SP1 on chloroplasts. Further, it is also possible that SP1 and SPL1 modulate the function of the protein import machineries on the mitochondrial outer membrane and peroxisome membrane. These hypotheses will need to be tested in the future to dissect the membrane topology and identify the substrates for SP1 and SPL1. The topology of SPL2 on chloroplast and mitochondrial membrane will also need to be experimentally tested.

4.3.4 Analysis of SP1 and SPL1 targeting signals

The localization of SP1 and SPL1 to all three energy organelles indicates that the SP1/SPL-mediated UPS apparatus may play a regulatory role to simultaneously

coordinate the dynamics and/or functions of chloroplasts, mitochondria and peroxisomes. An intriguing question is how a protein recognizes three different subcellular compartments. To dissect the targeting information on SP1 and SPL1, we generated a series of SP1 and SPL1 deletion constructs to make C-terminal YFP fusion proteins. These 35S-driven YFP fusion proteins were transiently expressed in tobacco (*Nicotiana tabacum*) together with the mitochondrial marker COX4-CFP or the peroxisome marker CFP-PTS1.

As described above, the first 24 amino acids of SP1 and SPL1 were predicted to form targeting peptides. In tobacco leaf cells, SP1¹⁻²⁴-YFP and SPL1¹⁻²⁴-YFP targeted to chloroplasts, but not mitochondria and peroxisomes (Fig. 4.8A, 4.9A). Therefore, these N-terminal peptides, SP1¹⁻²⁴ and SPL1¹⁻²⁴, contain chloroplast targeting information. On the other hand, SP1²⁵⁻³⁴⁷-YFP and SPL1²⁵⁻³³⁸-YFP, which contained the full-length protein deleted for the N-terminal peptide, localized to mitochondria and peroxisomes, but not chloroplasts (Fig. 4.8D, 4.9D). These results suggest that the N-terminal peptides are sufficient and necessary for the chloroplast targeting of SP1 and SPL1. SP1¹⁻²⁴⁹-YFP and SPL1¹⁻²⁴⁷-YFP, which contained the N-terminal peptide and the TMD, localized to all three organelles (Fig 4.8C, 4.9C). Additionally, SP1¹⁻²²⁵-YFP and SPL1¹⁻²²⁴-YFP localized to chloroplasts, but not mitochondria and peroxisomes (Fig. 4.8B, 4.9B). Thus, the TMD appeared to be necessary for mitochondrial and peroxisome localization.

In summary, the N-terminal peptides of SP1 and SPL1 contain the necessary chloroplast targeting information for these two proteins, and the TMD is required for the mitochondrial and peroxisomal localization. Different from SP1 and SPL1, SPL2 does

not contain the N-terminal signal peptide, so SPL2 might use a different targeting mechanism for chloroplasts, a hypothesis that needs to be tested in the future. Human MUL1 is more closely related to SP1 and SPL1 than SPL2, but does not contain the N-terminal signal peptide either (Fig. 4.6A). It is possible that the N-term peptides evolved in this gene family in plants after the split of plant and animal lineages.

4.3.5 SP1 and SPL1 play a different role from MUL1 in regulating mitochondrial dynamics

In mammalian cells, MUL1 was reported to be a positive regulator of mitochondrial fission. Overexpression of MUL1-YFP induced mitochondrial clustering and fission, possibly because of its ability to stabilize human DRP1 (Braschi et al., 2009). However, overexpression of SP1-YFP and SPL1-YFP in transgenic *Arabidopsis* lines did not cause noticeable increases in mitochondrial fission (Fig. 4.10).

MUL1 was reported to mediate the SUMOylation of DRP1 (Braschi et al., 2009). The N-terminal YFP fusion protein of human SUMO1 (YFP-hSUMO1) localized to mitochondrial fission sites and the two tips in a punctate manner similar to human DRP1, and hSUMO1 physically interacts with DRP1 in yeast-two-hybrid assays (Y2H) (Harder et al., 2004). There are four expressed SUMO paralogues (SUMO1, 2, 3 & 5) in *Arabidopsis* (Kurepa et al., 2003; Saracco et al., 2007). To check the subcellular localization of these *Arabidopsis* SUMOs, we generated constructs to express N-terminal YFP fusion proteins of SUMOs driven by the 35S promoter. Transgenic *Arabidopsis* lines stably expressing these YFP-SUMOs were generated using floral dipping method and analyzed by confocal microscopy. However, the subcellular

distribution pattern of *Arabidopsis* SUMOs indicate that they are mostly in the cytosol and/or nuclei, but not associated with mitochondria (Fig. 4.11A). Furthermore, to test whether *Arabidopsis* SUMOs physically associate with DRP3, we conducted Y2H assays using the Matchmaker two-hybrid system. *Arabidopsis* SUMO1, SUMO2, SUMO3, SUMO5 and DRP3A were cloned into the pGilda and pB42AD vectors to create protein fusions with the DNA binding domain (BD) and the activation domain (AD) respectively. When AD-DRP3A and BD-DRP3A were coexpressed in the yeast strain EGY48, yeast cells grew abundantly in medium lacking Ura, Trp, His, and Leu (SD/galactose-UTHL) and turned blue in the presence of 5-bromo-4-chloro-3-indolyl- β -D-galactopyranoside, confirming the well-known self-interaction of DRP3 (Fig. 4.11B). However, yeast cells expressing the combinations of DRP3A and any one of the SUMOs did not grow on SD/galactose-UTHL medium (Fig. 4.11B). Therefore, in Y2H, no interactions between *Arabidopsis* SUMOs and DRP3s were detected. Based on the observations above, we conclude that the regulatory role of MUL1 in mitochondrial dynamics by SUMOylation in metazoan is very likely not conserved in its homologous proteins in plants.

To further analyze the functions of endogenous SP1 and SPL1 proteins, four T-DNA insertion mutants were obtained from the Arabidopsis Biological Resource Center (ABRC) (Fig. 4.12A). Homozygous plants were isolated after PCR genotyping of genomic DNA. The gene transcription level was also analyzed using Semi-quantitative reverse transcription polymerase chain reaction (RT-PCR). Full length SP1 transcripts were not detectable in *sp1-1*, *sp1-2*, or *spl1-1*, and were strongly decreased in *spl1-2* (Fig. 4.12B). Hence, *sp1-1*, *sp1-2* and *spl1-1* are null mutants, while *spl1-2* is a knock-

down mutant. A homozygous double mutant line was also generated by crossing *sp1-2* and *sp1-1*. The growth and development of these mutants were not significantly different from wild-type plants in normal growth conditions (Fig. 4.12C). To examine the mitochondrial morphology, mitochondrial marker COX4-YFP was introduced into *sp1*, *sp1/1* and the double mutants using floral dipping method. The mitochondrial morphology in the leaf tissue of these mutants was analyzed using confocal microscopy. No obvious abnormality was observed in these mutants in comparison to wild-type mitochondria (Fig. 4.12D).

To analyze the consequences caused by the overexpression of non-tagged SP1 and SPL1, we made constructs to overexpress these proteins under the 35S promoter. These constructs were transiently expressed in tobacco leaves together with organelle markers. However, no significant organelle abnormality was detected by confocal microscopy (Fig. 4.13D). We also generated similar constructs to overexpress point mutant forms of SP1 and SPL1. Five of the conserved residues in the RING domain were substituted (Cys by Ser, His by Tyr) (Fig. 4.13C). When the mutant forms of SP1 and SPL1 were expressed in tobacco leaves, no obvious changes of the organelle morphology occurred (Fig. 4.13D). Therefore, we conclude that, in contrast to hMUL1, *Arabidopsis* SP1 and SPL1 are very likely not essential factors in *Arabidopsis* mitochondrial fission process.

As described above, MUL1-mediated DRP1 SUMOylation promotes mammalian mitochondrial fission (Braschi et al., 2009). Nevertheless, SUMOylation very likely targets multiple proteins in mitochondria, rather than just DRP1 (Braschi et al., 2009; Harder et al., 2004). It is reported that overexpression of MUL1 caused a reduction in

mitochondrial fusion rate (Braschi et al., 2009). This in theory could cause MUL1-induced mitochondrial fragmentation. However, no homologous components of the non-plant mitochondrial fusion machinery are found in plants yet. It is possible that SUMOylation negatively regulates the mammalian fusion machinery, which are not conserved in plants. Moreover, mitochondria are often elongated and interconnected in mammalian and yeast cells, suggesting stronger activity of mitochondrial fusion than fission. In contrast, mitochondria are highly fragmented in plants, indicating the dominance of fission. Therefore, the need to further increase fission or decrease fusion by SUMOylation probably does not exist in plants.

4.3.6 SPL2 may function in mitochondrial distribution, movement or division

In contrast to the evident similarities between SP1 and SPL1 in amino acid sequence, domain composition and subcellular localization, SPL2 seems to be divergent from SP1 and SPL1. To analyze whether SPL2 is involved in mitochondrial dynamics, we generated artificial micro RNA (amiRNA) lines in the background of COX4-YFP plants to specifically reduce the transcript level of *SPL2*. RT-PCR analysis showed that the *SPL2* transcript level was significantly reduced (Fig. 4.12A, 4.13A). In contrast to SP1 and SPL1, *SPL2* deficiency mediated by amiRNA resulted in strong mitochondrial aggregation (Fig. 4.13B), suggesting that *SPL2* is probably important for the distribution, movement, or division of mitochondria.

To analyze the consequences caused by the overexpression of *SPL2*, we made a construct to overexpress *SPL2* under the 35S promoter. When expressed in tobacco leaves together with organelle markers, no significant organelle abnormality was

detected using confocal microscopy (Fig. 4.13D). We also generated a construct to overexpress a point mutant form of SPL2. Four of the conserved residues in the RING domain were substituted (Cys by Ser, His by Tyr) (Fig. 4.13C). In contrast to mutant forms of SP1 and SPL1, strong mitochondrial aggregation was induced by the overexpression of mutant SPL2 (Fig. 4.13D). Our results showed that the disruption of SPL2 functions by *SPL2* amiRNA and by the dominant negative form of SPL2 protein both result in strong mitochondrial aggregation. Hence, we conclude that SPL2 is an important factor in mitochondrial dynamics. In the future, SPL2 substrates will need to be identified and SPL2's mode of action in mitochondrial dynamics will need to be further elucidated.

4.3.7 Next steps in the elucidation of SP1/SPL functions

In this chapter, we characterized a small family of RING domain-containing proteins by analyzing their localization, domain structures, membrane association, targeting signals, and loss-of-function and gain-of-function mutants. We showed that these proteins are distinct from each other in some of the properties tested. SP1 and SPL1 are more similar to each other and localize to chloroplasts, mitochondria and peroxisomes. Since SP1 is known to be a regulator of protein import in chloroplasts, SP1 and SPL1 may also be involved in protein import for mitochondria and peroxisomes. SPL2 deficiency led to strong mitochondrial aggregation, and thus is probably involved in mitochondrial distribution, movement and/or fission. To better understand the functional mechanisms of SP1, SPL1 and SPL2, further studies will need to be done in the future, as described below.

SP1 has a known role in regulating chloroplast protein import. SP1-mediated regulation of TOC complex was uncovered because disrupting SP1 function partially suppressed the defects of *toc33* and *toc75* deficient mutants (Ling et al., 2012). Similar strategy can be applied to uncover the roles of SP1 and SPL1 in mitochondrial and peroxisomal protein import. For example, *sp1*, *spl1* and *sp1 spl1* double mutants can be crossed with *tom* and *pex* mutants, such as *tom20*, *tom40*, *metaxin* and *om64* for mitochondria and *pex13*, *pex14*, *pex5*, *pex6* and *pex7* for peroxisomes (refer to Fig. 1.1 and 1.2 in Chapter 1). Either suppression or escalation of the defects in these *tom* or *pex* mutants by disrupting SP1 and SPL1 can manifest the role of SP1 and SPL1 in the biogenesis of mitochondria and peroxisomes. Besides genetics, we can also employ Y2H screens using SP1 and SPL1 as baits to fish out their direct targets. Since they are integral membrane proteins, Y2H using the split ubiquitin system may be used to test membrane protein interactions (Fetchko and Stagljar, 2004; Iyer et al., 2005; Kittanakom et al., 2009; Thaminy et al., 2004). Additionally, by comparing the “ubiquitinomics” of isolated mitochondria from wild-type plants to those from *sp1* or *spl1* mutants using mass spectrometry, it is also possible to find their targets to help to illustrate the functions of SP1 and SPL1. Given that SP1 was found to be involved in the import of photosynthesis-related proteins (Ling et al., 2012), one possibility is that SP1 and SPL1 modulate the import of photorespiration apparatus into mitochondria and peroxisomes, thus to adjust the rate of photosynthesis in parallel with photorespiration. To this end, we may compare the behaviors of *sp1 spl1* mutants with wild-type plants under stresses that disturb the equilibrium of photosynthesis and photorespiration.

SPL2 is apparently a special member in this protein family, because of its uniqueness in organelle association pattern, predicted domain structure and loss-of-function/dominant negative mutant phenotypes. I propose a role of SPL2 in regulating mitochondrial distribution, movement and/or fission. Thus possible substrates may include proteins involved in these processes, such as fission factors like PMD1, DRP3 and FIS1. Another good candidate for SPL2's substrate is MIRO1/2, which is essential for mitochondrial motility (Yamaoka et al., 2011; Yamaoka and Leaver, 2008). In addition, since plant mitochondria mainly move on actin filament, the association between SPL2 and cytoskeletons will also need to be checked. To look into the function of SPL2, strategies like suppressor screening, Y2H screening and "ubiquitin-omics" analysis of mitochondria can be employed here as well.

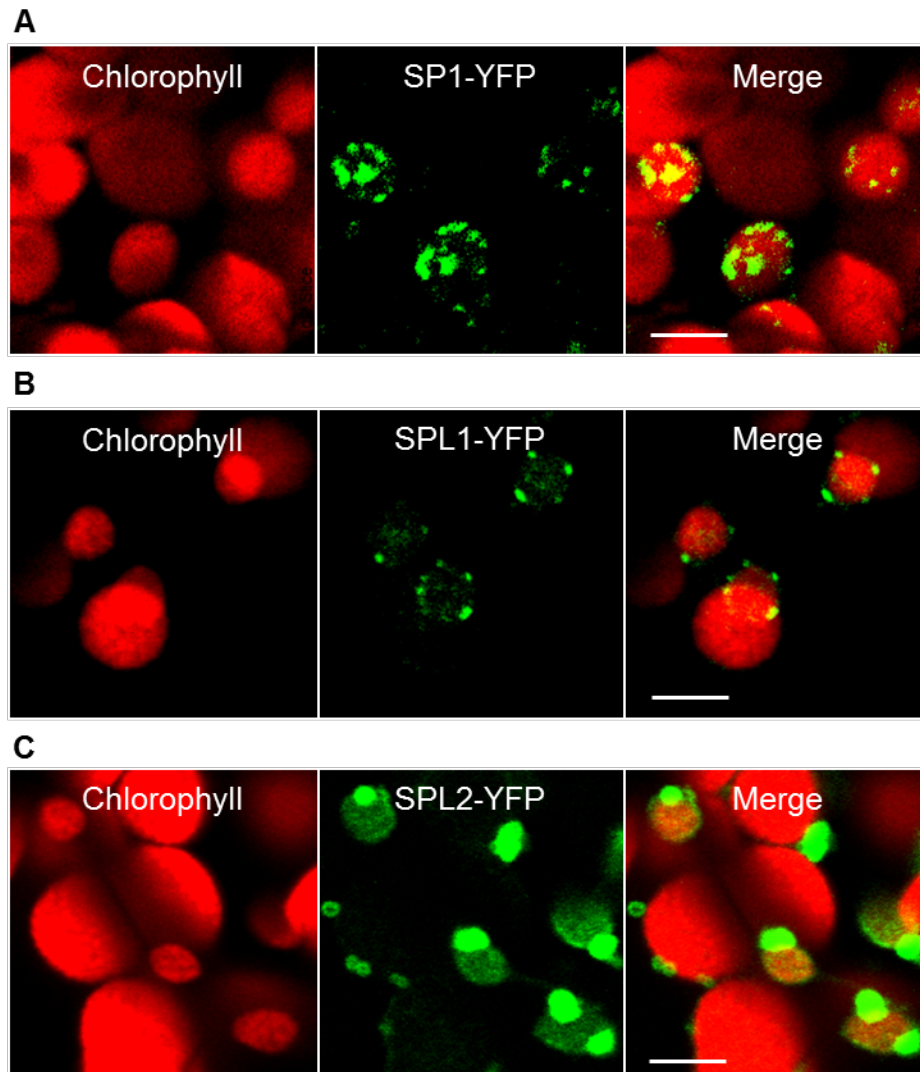


Figure 4.1. Chloroplast association of SP1, SPL1 and SPL2 in *Arabidopsis*.

Two-week-old T2 lines expressing SP1-YFP (A), SPL1-YFP (B) or SPL2-YFP (C) were used for analysis. Confocal images were taken from leaf mesophyll cells. Chloroplasts were marked by chlorophyll auto-fluorescence. Scale bar, 5 μm .

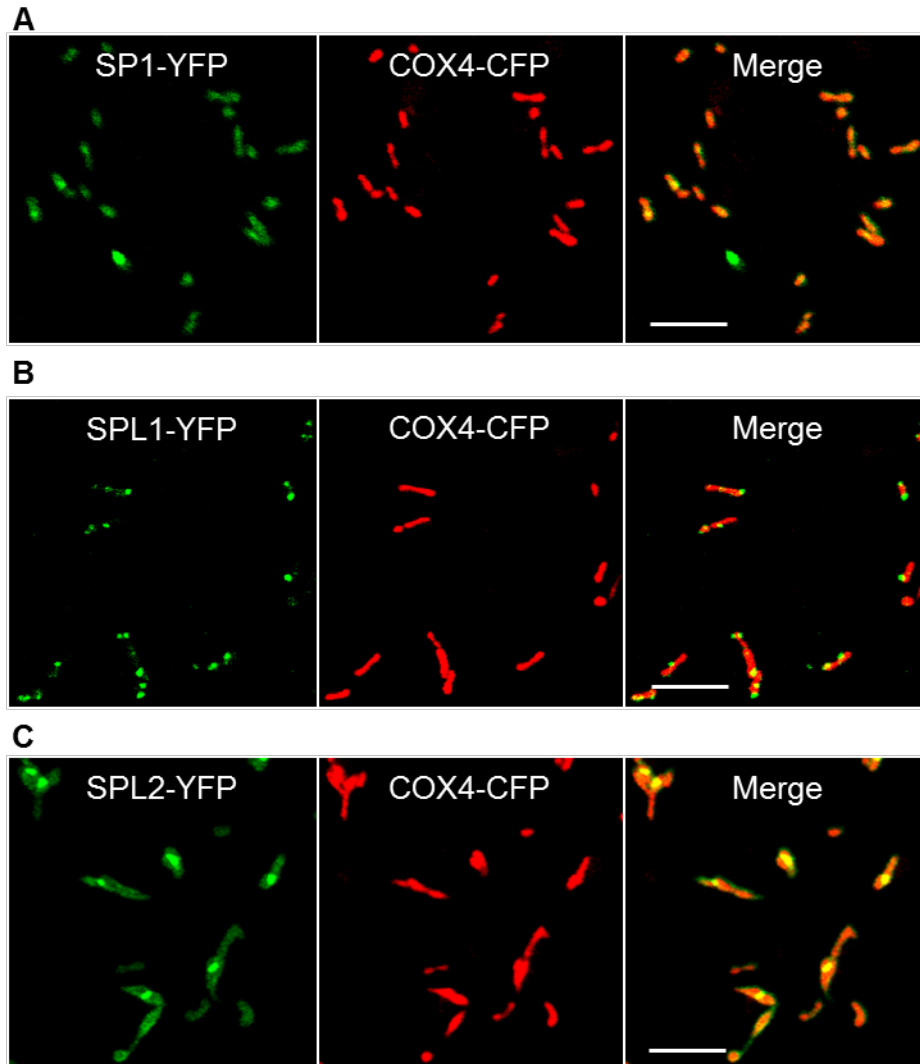


Figure 4.2. Mitochondrial association of SP1, SPL1 and SPL2 in *Arabidopsis*.

Two-week-old T2 lines expressing SP1-YFP (A), SPL1-YFP (B) or SPL2-YFP (C) were used for analysis. Confocal images were taken from leaf epidermal cells. Mitochondria were marked by mitochondrial targeted COX4-CFP, which was stably expressed in these lines. Scale bar, 5 μ m.

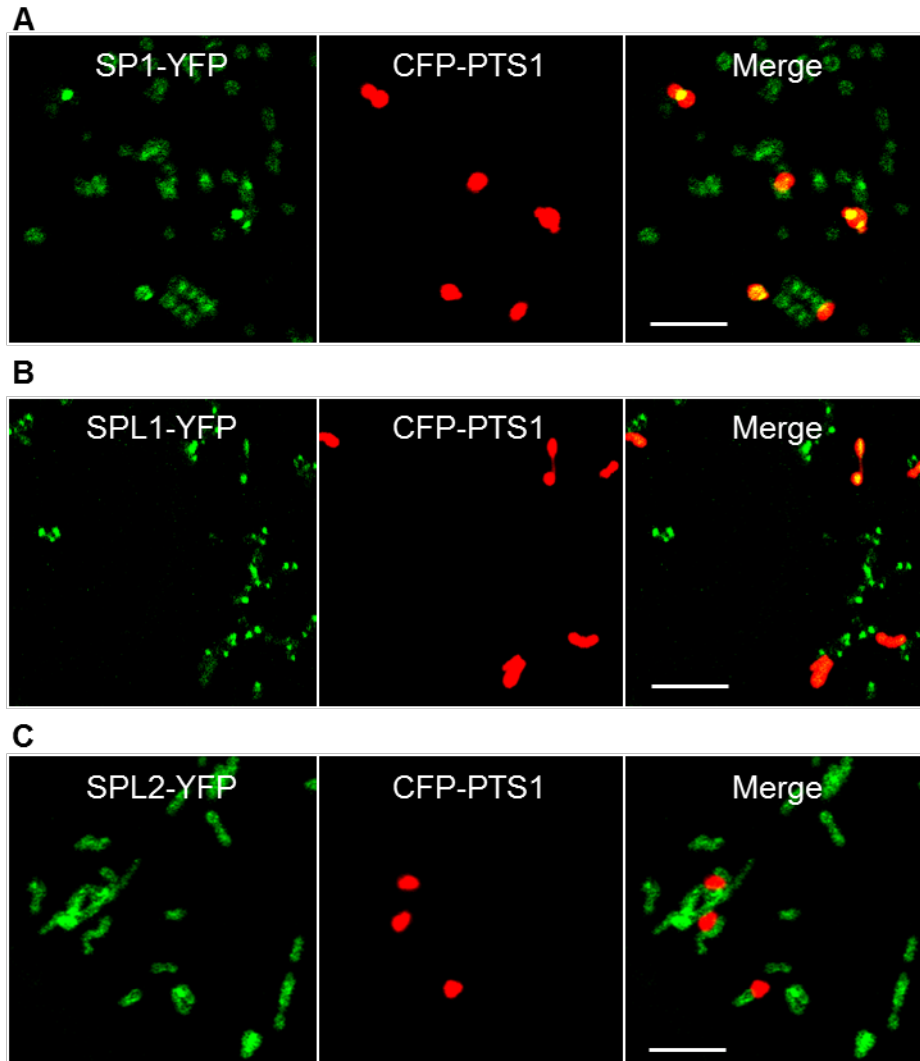


Figure 4.3. Peroxisomal association of SP1 and SPL1 in *Arabidopsis*.

Two-week-old T2 lines expressing SP1-YFP (A), SPL1-YFP (B) or SPL2-YFP (C) were used for analysis. Confocal images were taken from leaf epidermal cells. Peroxisomes were marked by peroxisome targeted CFP-PTS1, which was stably expressed in these lines. Scale bar, 5 μm.

```

SP1  MIP-----WGGVTCCLSAAALYLLGRSSGRDAEVLE
SPL1  MIH-----LAGFTCCLGGVALYLLTRSTGRDI---K
SPL2  MSSPERALLNLLTDIALSFDGAILGLTLAVSAVGSALKYASTNAALKKIK
      *                *. *  .:..... *   *:..   :

SP1  TVTRVNQLKELAQLLE-----LDSKILPFIVAVS
SPL1  SITRVYQLKDLEQLVE-----VESKVVPLIIAVS
SPL2  DAPEV-SISDLRSLLPASEDKSETNDRKSNDQRIVVVRGVVVKPKISGDE
      ..*  .:..:*  .*:                : . : * * . .

SP1  GRVGSETP-----IKCEHSGIRGVI---VEETAEQHFLKHNETG
SPL1  GDVGSETP-----IKCEHSYVLGVF---LKRTAEQQVLRNRWRF
SPL2  GYKNNNVLISPETGDKALIIQRTQTYVYSGWKRLFQSTGHRFMLERSLRK
      *   .:..   *:  ::  : .   .: *..:  .*.:.

SP1  SWVQDSALMLSMSKEVPWFLLDD-----GTS--RVHVMGARGATGFALTVG
SPL1  SWVRNSTLMQPMTKKEVPWYLDD-----GTG--RVNVDVSQGELGLALTVG
SPL2  H-----GADFTRTVPFVIVGKDQQSNSSFVAVNMDGSRQPLP--LT--
      ::: ** :  .   .:.  *::  ::   **

SP1  SEVFEEES-GRS--LVRGTLDYLQGLKMLGVKRIERVLPTGIPLTIVGEAV
SPL1  SDVFEEKAEPVS--LVQGALGYLKGFKILGVRHVERVVPIGTPLTVVGEAV
SPL2  -TVYNRLQPINSSFLQA---FLYPDYPVGLLDIEKILPPGKDITAVGIYS
      *::..   .   :::.   :*   :*   :*:::* * *   :* **

SP1  KDDIGE FRIQKPDRGPFYVSSKSLDQLISNLGKWSRLYKYASMGFTVLGV
SPL1  RDGMGNVRIQKPEQGFYVTYIPLDQLISKLGDLRFRKYASMGFTVLGV
SPL2  F-NNGVPEIKSCQDLPLYFSEMTKDKMIEDLMEQTN---FIFLGSVILGI
      . *  .*:.. :  *:::..  . *::*..*  . :.   :  :*  .:***:

SP1  FLITKHVIDSVLERR-----RRRQL--QKSCFCRVLDAAAKRAELESEG
SPL1  ILISKPVIEYILKRIEDTLERRRRQF-----ALKRVVDAAARRAKPVT--
SPL2  VSV--GILSYAAVRTWNKWKQWNHQRELPQRPNDVVDDE-----
      . :   ::.   *   .:*   *:*

SP1  SNGTRESISDSTKKEDAVP--DLCVICLEQEYNAVVFVPCGHMCCCTACSS
SPL1  -----GGGTSRDGTP--DLCVVCLDQKYNTAFVECGHMCCCTPCSL
SPL2  -----PEDADEIPDGELCVICVSRRRVPAFIPCGHVCCRCAS
      .. . *  :***:*:.. . .*:  ***:  ** * :

SP1  HLT-----SCPLCRRRIDLAVKTYRH
SPL1  QLR-----TCPLCRERIQQVLKIYRH
SPL2  TVERELNPKCPVCLQSIRGSMRVYYS
      :   .**:*  . *   :: *

```

Figure 4.4. Protein sequence comparison of *Arabidopsis* SP1, SPL1 and SPL2.

Figure 4.4 (cont'd)

The alignment was performed using the ClustalW2 program (<http://www.ebi.ac.uk/Tools/msa/clustalw2/>). Identical amino acids are marked with asterisks and similar amino acids are marked with dots.

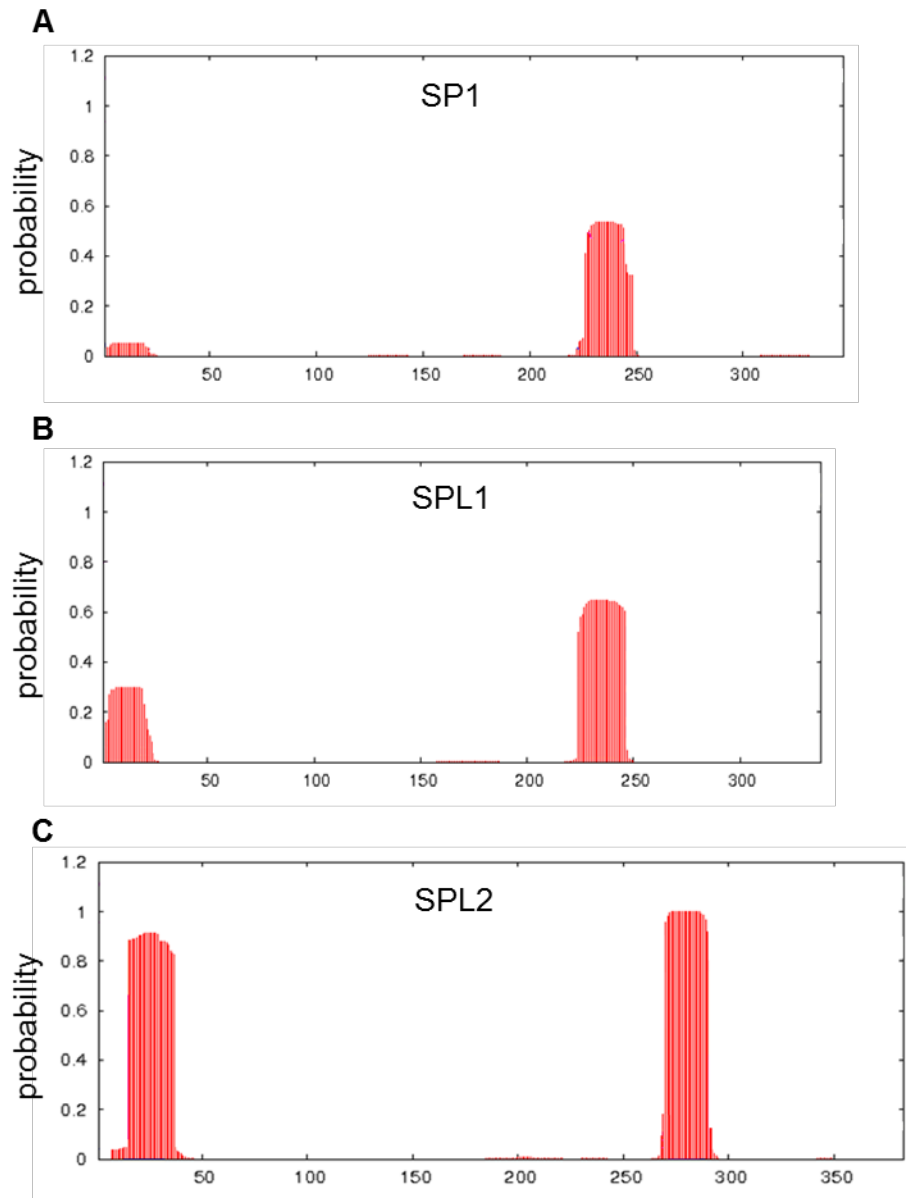


Figure 4.5. Transmembrane domain (TMD) prediction analysis of *Arabidopsis* SP1, SPL1 and SPL2.

Protein sequences of SP1 (A), SPL1 (B) and SPL2 (C) were analyzed by TMHMM server (<http://www.cbs.dtu.dk/services/TMHMM/>). Potential TMDs are indicated by red columns. Y-axis is the probability to be TMDs, and the X-axis is the amino acid number in the analyzed protein sequence.

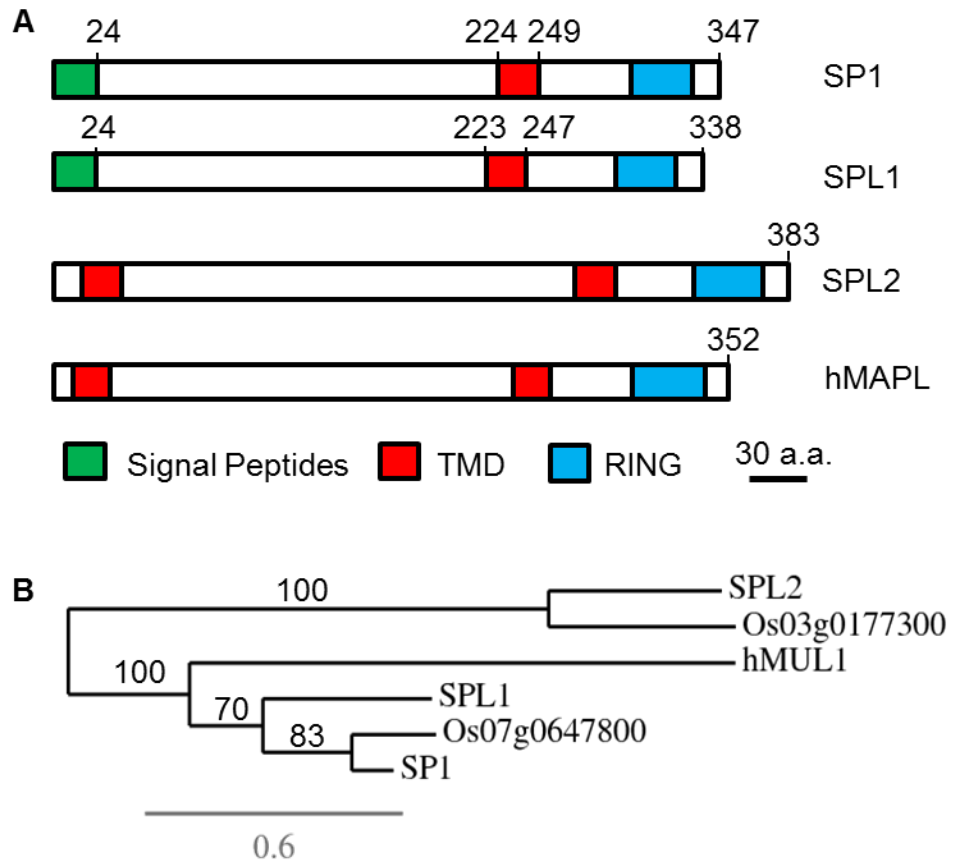


Figure 4.6. Bioinformatics analysis of *Arabidopsis* SP1, SPL1 and SPL2.

Figure 4.6 (cont'd)

(A) Domain structure comparison of SP1, SPL1, SPL2 and hMUL1. Red box, TMD predicted by TMHMM server, as shown in Fig. 5. Green box, signal peptide predicted by SignalP 4.1 Server (<http://www.cbs.dtu.dk/services/SignalP/>). Blue box, RING domain.

(B) Phylogenetic tree of *Arabidopsis* SP1, SPL1 and SPL2, human MUL1, and their homologues in rice *Oryza sativa Japonica Group*. Scale bar, 0.6 amino acid substitution per site. Branch support values are indicated. The phylogenetic analysis was performed using the Phylogeny.fr program (http://www.phylogeny.fr/version2_cgi/index.cgi).

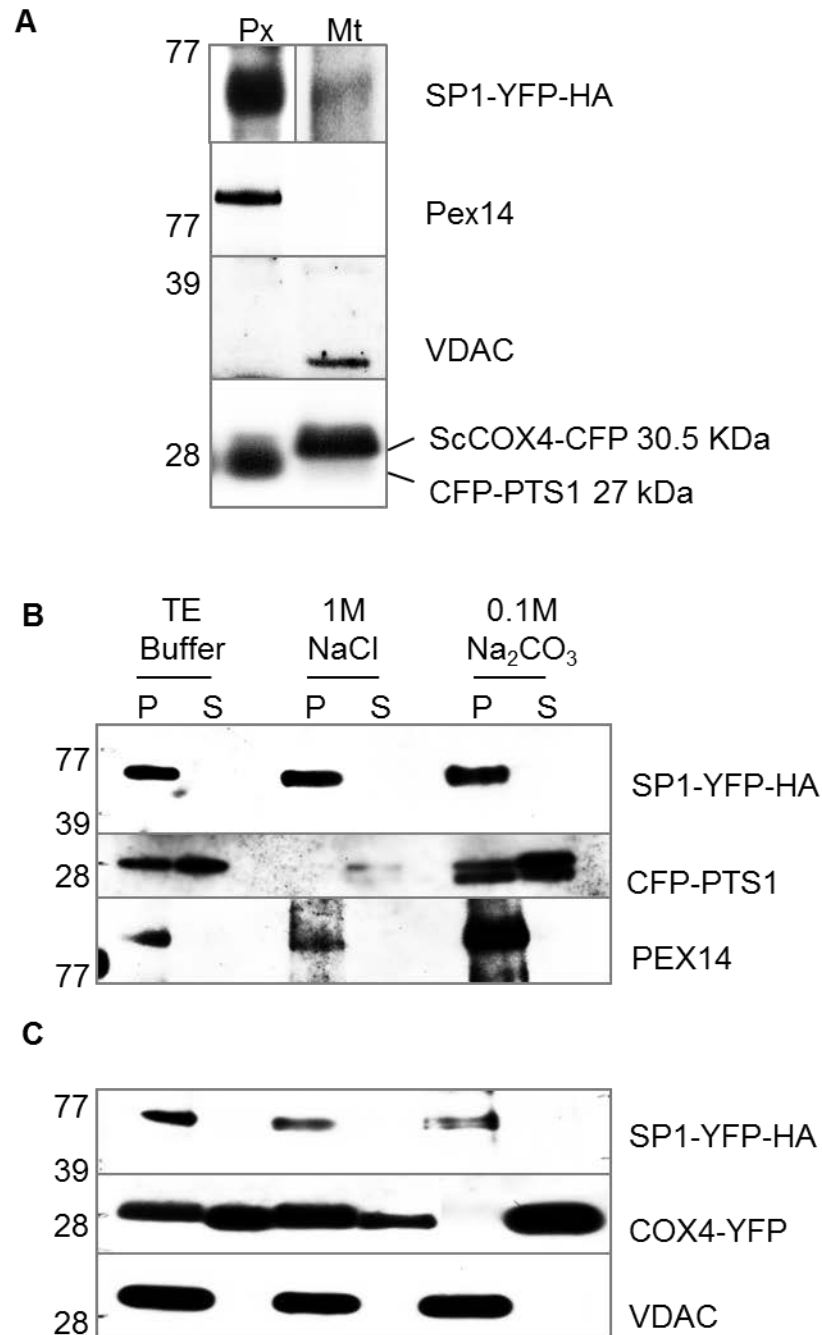


Figure 4.7. Immunoblot analyses of the mitochondrial and peroxisomal membrane association of SP1.

Figure 4.7 (cont'd)

(A) Assessment of the purity of isolated mitochondria and peroxisomes from the leaf tissue of *Arabidopsis* transgenic plant expressing SP1-YFP and the corresponding organelle marker COX4-CFP or CFP-PTS1. Antibodies used were against maize voltage-dependent anion selective channel (VDAC for mitochondria) and *Arabidopsis* PEX14 (for peroxisomes). The presence of SP1-YFP and the corresponding organelle markers in isolated mitochondria or peroxisomes was shown using the GFP antibody. Mt, isolated mitochondria. Px, isolated peroxisomes. Molecular weight markers in kDa are indicated on the left.

(B) Peroxisomal membrane association of SP1-YFP. Purified peroxisomes were treated with TE, NaCl, or Na₂CO₃ (pH 11.0) respectively and separated into soluble (S) and pellet (P) fractions by centrifugation. SP1-YFP and CFP-PTS1 were detected by α-GFP, and CFP-PTS1 and PEX14 were controls for matrix and integral membrane proteins, respectively.

(C) Mitochondrial membrane association of SP1-YFP. Purified mitochondria were treated with TE, NaCl, or Na₂CO₃ (pH 11.0) and separated into soluble (S) and pellet (P) fractions by centrifugation. SP1-YFP and COX4-CFP were detected by α-GFP, and COX4-YFP and VDAC were controls for matrix and integral membrane proteins, respectively.

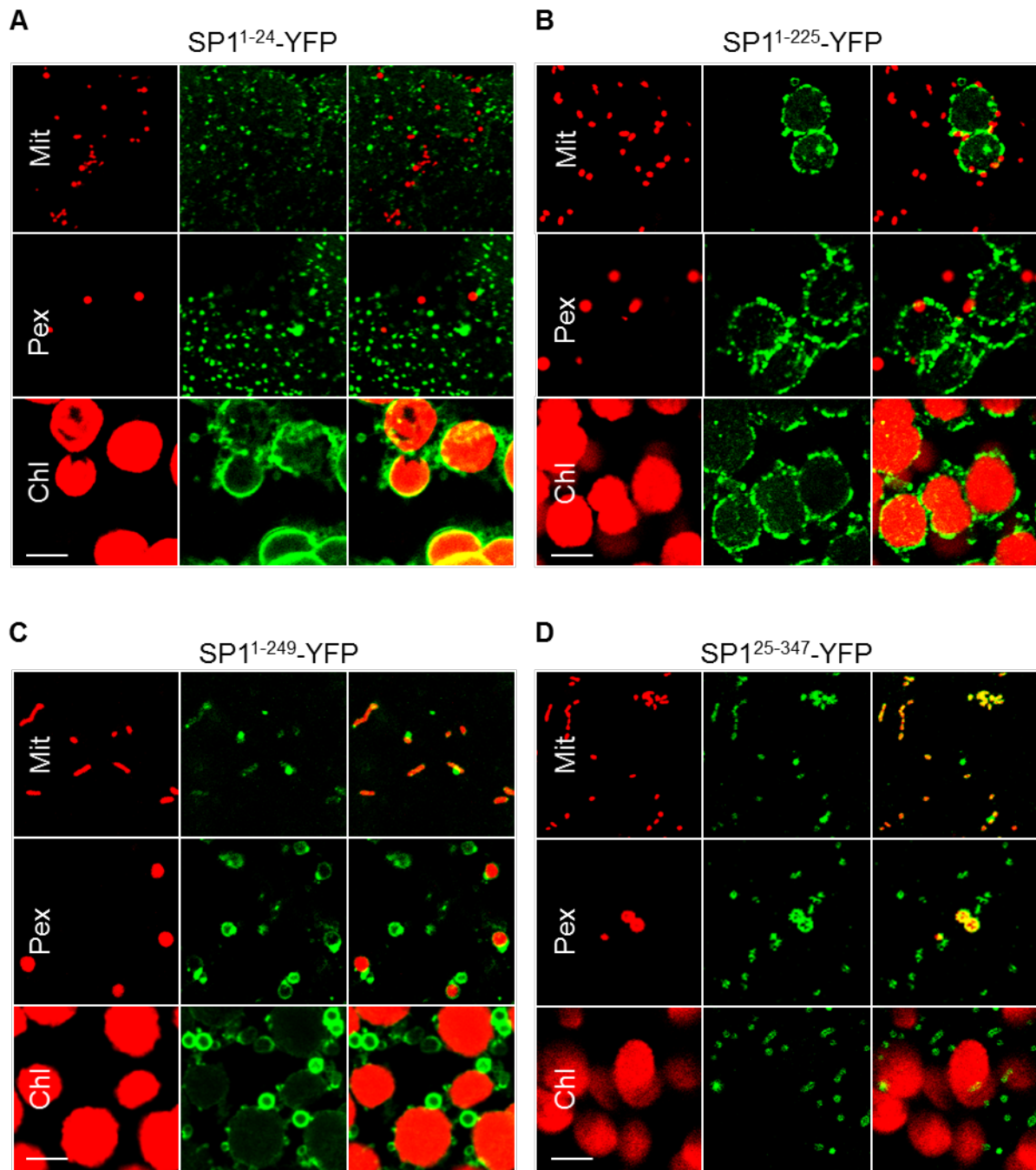


Figure 4.8. Analysis of organelle targeting signals on SP1.

Figure 4.8 (cont'd)

Confocal images of the localization of fusion proteins between various SP1 fragments and YFP transiently expressed in tobacco leaves together with the organelle markers. The amino acids included in SP1 fragments are indicated as superscripts (SP1 domain structure shown in Fig. 4.6A). Mit stands for mitochondria, labeled by COX4-CFP; Pex stands for peroxisomes, labeled by CFP-PTS1; and Chl stands for chloroplasts, marked by chlorophyll autofluorescence. Co-localization between COX4-CFP/CFP-PTS1 and SP1-YFP fusion proteins was examined using epidermal cells. Co-localization between chloroplast autofluorescent signals and SP1-YFP fusion proteins was examined in mesophyll cells. Scale bars, 5 μm .

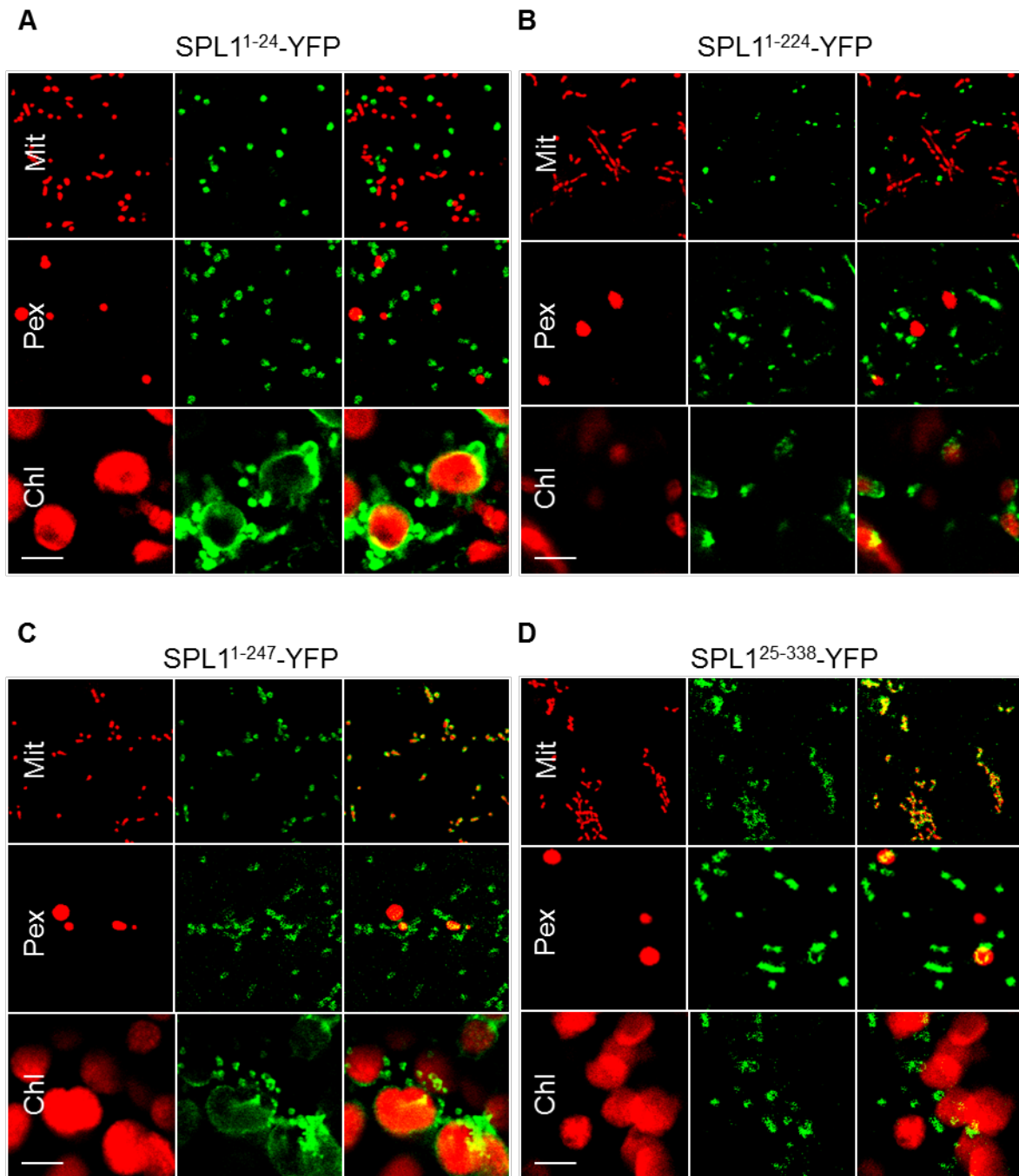


Figure 4.9. Analysis of organelle targeting signals on SPL1.

Figure 4.9 (cont'd)

Confocal images of the localization of fusion proteins between various SPL1 fragments and YFP transiently expressed in tobacco leaves together with the organelle markers. The amino acids included in SPL1 fragments are indicated as superscripts (SPL1 domain structure shown in Fig. 4.6A). Mit stands for mitochondria, labeled by COX4-CFP. Pex stands for peroxisomes, labeled by CFP-PTS1. Chl stands for chloroplasts, marked by chlorophyll autofluorescence. Co-localization between COX4-CFP/CFP-PTS1 and SPL1-YFP fusion proteins was examined in epidermal cells. Co-localization between chloroplast autofluorescent signals and SPL1-YFP fusion proteins was examined in mesophyll cells. Scale bars, 5 μm .

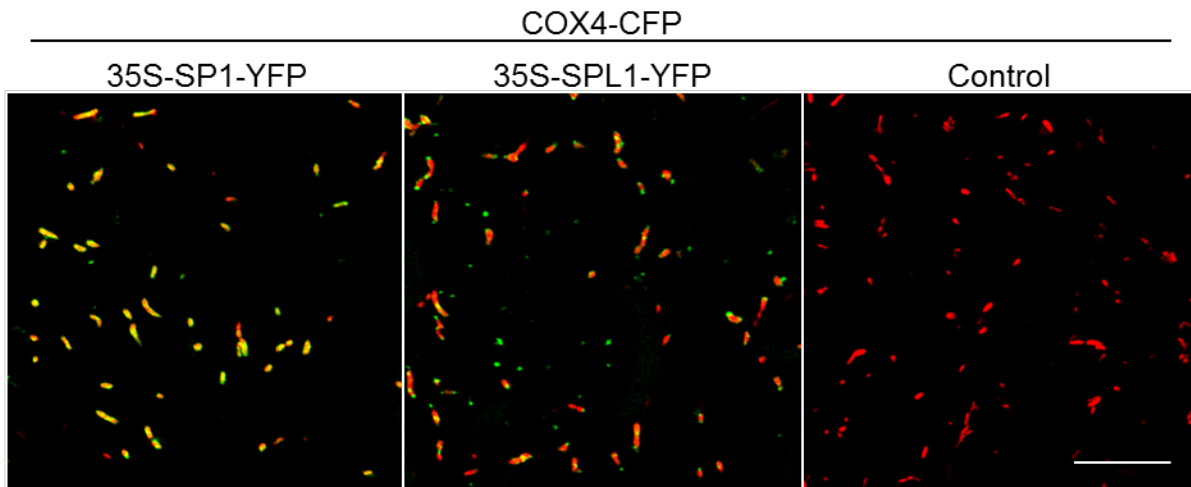
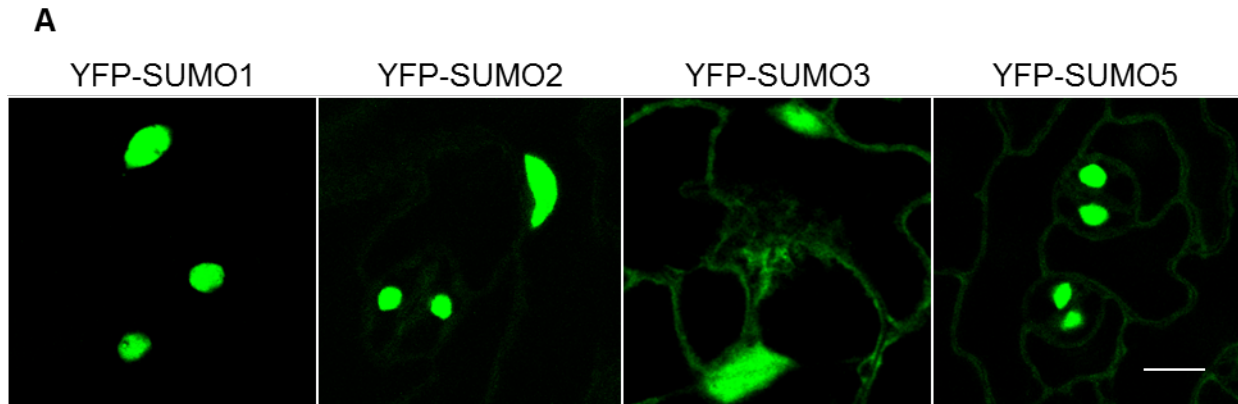


Figure 4.10. Mitochondrial morphology is not affected by overexpression of SP1 or SPL1.

Confocal images show the mitochondrial morphology in two-week-old T2 *Arabidopsis* lines with only the mitochondrial marker COX4-CFP, both COX4-CFP and SP1-YFP, or both COX-CFP and SPL1-YFP, all of which were driven by the 35S promoter. Images were taken in leaf epidermal cells. CFP fluorescence is shown in red. YFP fluorescence is shown in green. CFP and YFP images are merged for cells with SP1-YFP and SPL1-YFP. Scale bar, 10 μ m.



B

AD \ BD	DRP3A	SUMO1	SUMO2	SUMO3	SUMO5
DRP3A	+	-	-	-	-
SUMO1	-				
SUMO2	-				
SUMO3	-				
SUMO5	-				

Figure 4.11. Subcellular localization and yeast two hybrid (Y2H) analysis of *Arabidopsis* SUMO proteins.

Figure 4.11 (cont'd)

(A) Subcellular localization pattern of *Arabidopsis* SUMO proteins. Confocal images were taken in leaf epidermis from 2-week-old transgenic plants stably expressing YFP-SUMO1, YFP-SUMO2, YFP-SUMO3 and YFP-SUMO5. YFP signals are shown in green. Scale bar, 10 μ m.

(B) The *Arabidopsis* SUMO proteins did not interact with DRP3A in Y2H. Yeast transformation was done on SD/-UTH media. After transformation, the positive colonies were streaked on SD/-UTHL plus β -gal to check for protein interaction, as shown in the image. Growth of the colonies and the blue color together indicates positive protein interactions.

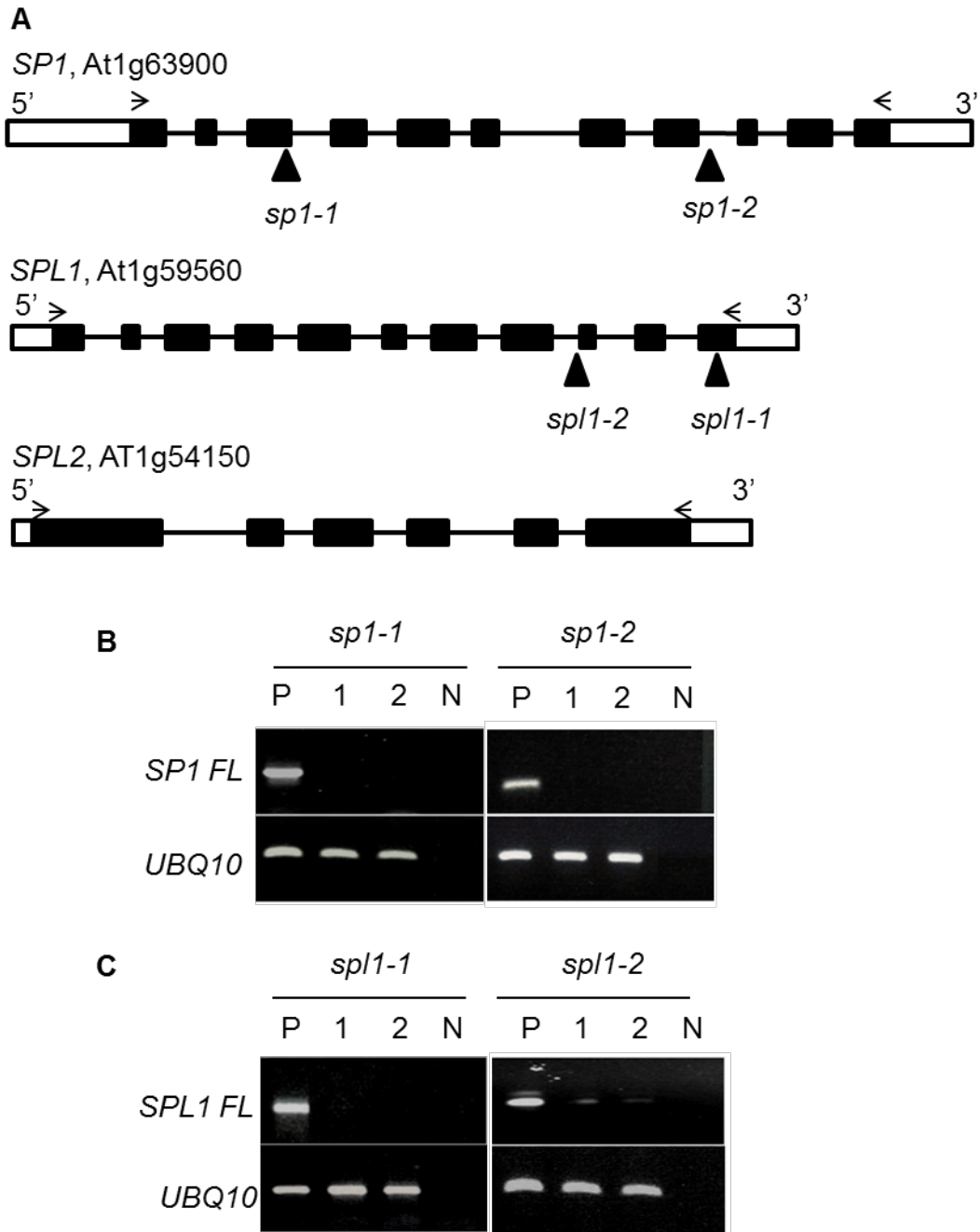


Figure 4.12. Molecular, phenotypic and mitochondrial morphology analyses of the *sp1* and *spl1* single and double mutants.

Figure 4.12 (cont'd)

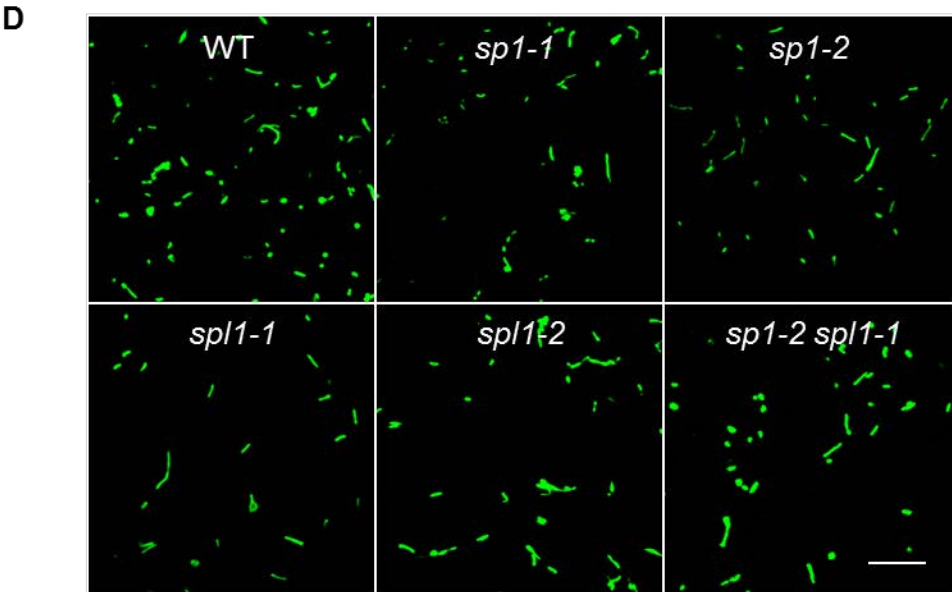
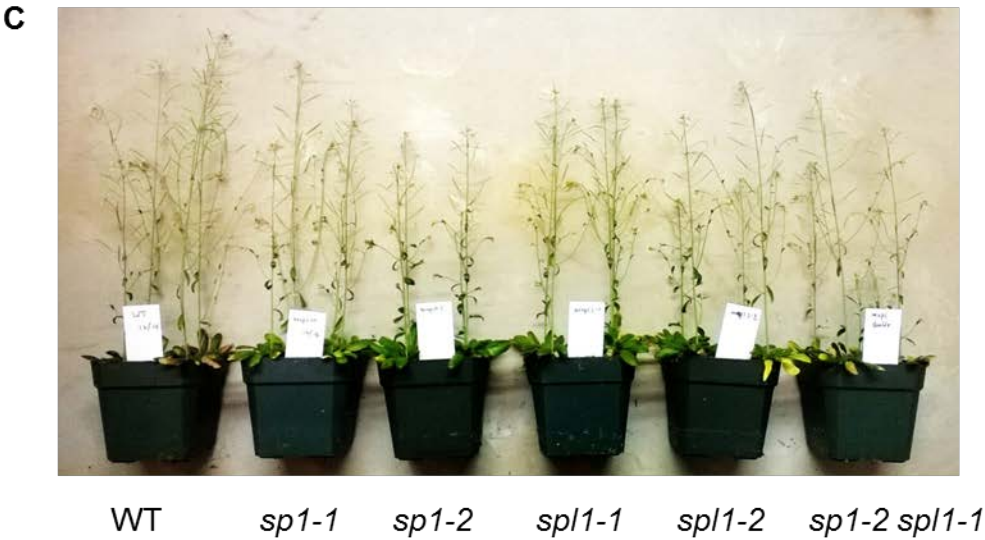


Figure 4.12 (cont'd)

(A) Schematics of the *SP1*, *SPL1* and *SPL2* genes. Open box, UTR; black box, exon; line, intron. Black triangles indicate the T-DNA insertion sites. Arrows indicate the primers used to amplify full length cDNAs.

(B) Semi-quantitative RT-PCR analysis of RNA from four-week-old *SP1* and *SPL1* T-DNA insertion lines. Two individual plants were analyzed for each mutant. P stands for wild-type sample and N stands for water (negative control). FL, full length. *UBQ10* (ubiquitin 10) was used as a loading control.

(C) Growth phenotype of 6-week-old *SP1* and *SPL1* T-DNA insertion lines.

(D) Confocal images showing mitochondrial morphology in epidermal cells of 2-week-old *Arabidopsis* plants expressing the mitochondrial marker COX4-YFP. Scale bar = 10 μm .

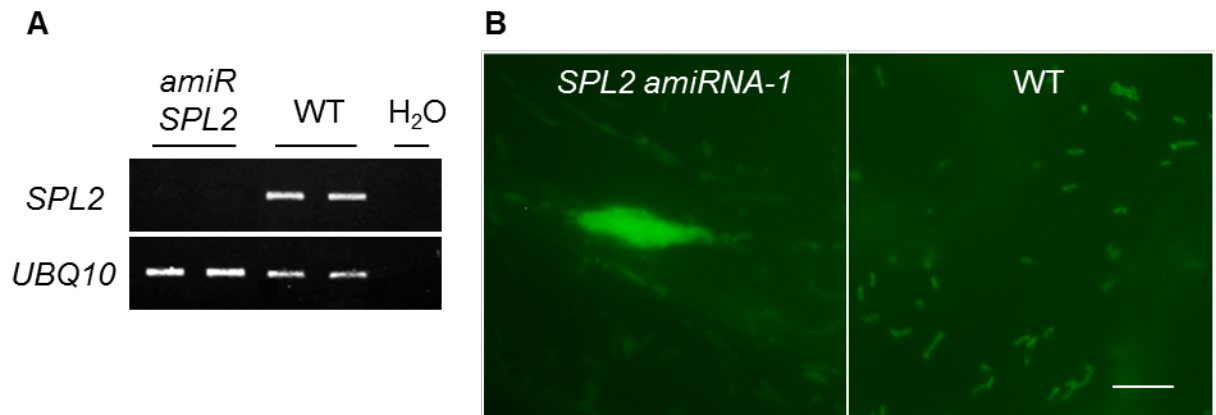


Figure 4.13. SPL2 plays a role in mitochondrial dynamics.

(A) RT-PCR analysis of *SPL2* mRNA level in 4-week-old *Arabidopsis* plants. *UBQ10* (ubiquitin 10) was used as a loading control. Two independent lines of wild-type and *amiR SPL2* are shown.

(B) Epifluorescent images showing mitochondrial morphology in epidermal cells of 4-week-old *Arabidopsis* plants expressing the mitochondrial marker COX4-YFP. Scale bar = 10 μm .

(C) The RING domain sequences of SP1, SPL1 and SPL2. The conserved active Cys and His residues are marked in red. The substituted residues in the point mutant protein forms are underlined with green lines.

(D) Epifluorescent images showing mitochondrial morphology in tobacco leaf epidermal cells transiently overexpressing each of the wild-type SP1, SPL1, SPL2 and their point mutant forms, together with the mitochondrial marker COX4-YFP. Scale bar, 10 μm .

Figure 4.13 (cont'd)

C

SP1: C V I C L E Q E Y N A V F V P C G H M C C C T A C S S H L T S C P L C

SPL1: C V V C L D Q K Y N T A F V E C G H M C C C T P C S L Q L R T C P L C

SPL2: C V I C V S R R R V P A F I P C G H V V C C R R C A S T V E R E L N P K C P V C

D

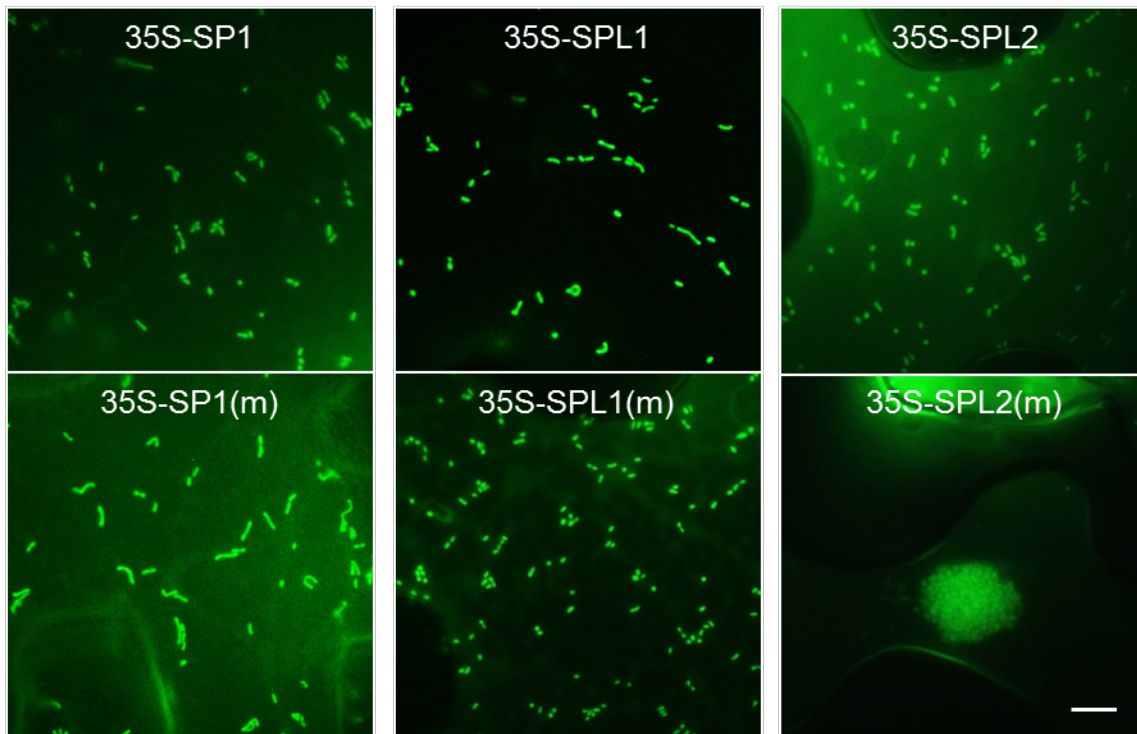


Table 4.1 DNA primers used in this study.

Primer	Sequence
SP1-Fw-AttB1	ggggacaagttgtacaaaaagcaggcttcatgattccttggggtggagttac
SP1-Re-AttB2-N	ggggaccactttgtacaagaaagctgggtctcagtgacgatatgtcttaaccg
SP1-Re-AttB2-C	ggggaccactttgtacaagaaagctgggtcgtgacgatatgtcttaaccgccag
SPL1-Fw-AttB1	ggggacaagttgtacaaaaagcaggcttcatgatacatttggctggatttac
SPL1-Re-AttB2-N	ggggaccactttgtacaagaaagctgggtctcaatggcggtaaatttc
SPL1-Re-AttB2-C	ggggaccactttgtacaagaaagctgggtcatggcggtaaatttcaaac
SPL2-Fw-AttB1	ggggacaagttgtacaaaaagcaggcttcatgtcctcgcggagcgtgctc
SPL2-Re-AttB2-N	ggggaccactttgtacaagaaagctgggtcctaagagtaatacacgcgatag
SPL2-Re-AttB2-C	ggggaccactttgtacaagaaagctgggtcagagtaatacacgcgatagatc
SUMO1-Fw-AttB1	ggggacaagttgtacaaaaagcaggcttcatgtctgcaaccaggag
SUMO1-Re-AttB2-N	ggggaccactttgtacaagaaagctgggtctcaggccgtagcaccaccac
SUMO2-Fw-AttB1	ggggacaagttgtacaaaaagcaggcttcatgtctaaccctcaagatgac
SUMO2-Re-AttB2-N	ggggaccactttgtacaagaaagctgggtcttaaagcccattatgatcg
SUMO3-Fw-AttB1	ggggacaagttgtacaaaaagcaggcttcatgtctgctactccggaagaag
SUMO3-Re-AttB2-N	ggggaccactttgtacaagaaagctgggtcctaaaagcagaagagcttcag
SUMO5-Fw-AttB1	ggggacaagttgtacaaaaagcaggcttcatggtgagttccacagacac
SUMO5-Re-AttB2-N	ggggaccactttgtacaagaaagctgggtctcaaggagtgaaggaccg
<i>sp1-1</i> -genotyping-1	aggatcattcaattccaacc
<i>sp1-1</i> -genotyping-2	attacatggacacggcttgc
<i>sp1-2</i> -genotyping-1	tattcgctgaatcgagcaaac
<i>sp1-2</i> -genotyping-2	gctgccatgtataacaggctg
<i>spl1-1</i> -genotyping-1	ttgggagattgtcaagggtg
<i>spl1-1</i> -genotyping-2	ggcttaattaagcccaacctg
<i>spl1-2</i> -genotyping-1	gcgttgggttatcttaaaggc
<i>spl1-2</i> -genotyping-2	aggctcttagtgcaggagc
SP1-partial -Re-1	ggggaccactttgtacaagaaagctgggtcgccactactccggccgag
SP1-partial-Re-2	ggggaccactttgtacaagaaagctgggtcataattgtacaaccttgacc
SP1-partial-Re-3	ggggaccactttgtacaagaaagctgggtcatacttgaacctccttgac
SP1-partial-Fw-4	ggggacaagttgtacaaaaagcaggcttcatgaggatgctgaagtactcg
SPL1-partial -Re-1	ggggaccactttgtacaagaaagctgggtcgctgtgctcctggtaag
SPL1-partial-Re-2	ggggaccactttgtacaagaaagctgggtcataattgtacaaccttgacc
SPL1-partial-Re-3	ggggaccactttgtacaagaaagctgggtcatacttgaacctccttgac
SPL1-partial-Fw-4	ggggaccactttgtacaagaaagctgggtcctctagaacagagtcaatgac
SP1-RingMutant-Fw	gtttgcocagtggttatatgagcagcagcaccgcatgctc
SP1-RingMutant-Re	gagcatgagggtgctgctcatataaccactcgggacaaac
SPL1-RingMutant-Fw	ctttgtgagagtggttatatgagcagcagcaccatgctc
SPL1-RingMutant-Re	gagcatggtgtgctgctcatataaccactctcaaaaaag
SPL2-RingMutant-Fw	cgtttattcccagtggtatgtagtaagtagcaggcgtatgctc
SPL2-RingMutant-Re	gcacatgcctgctacttactacatataccactgggaataaacg
SPL2-I miR-s	gatgttaactctcgttccggtctctctttgtattcc
SPL2-II miR-a	gaccgccaacgagaggttaaacatcaaagagaatcaatga
SPL2-III miR*s	gaccacggaacgagacttaaacctcacaggctcgtgatag
SPL2-IV miR*a	gaagtttaagctcgttccgtggtctacatatattcct

Table 4.2 Vectors used in this study.

Vector and reference	Construct	Plant selection
pDonor 207 (Invitrogen)	all donor plasmids	N/A
pEarleyGate 100 (Earley et al., 2006)	35S-SP1, 35S-SPL1, 35S-SPL2, 35S-SP1(m), 35S-SPL1(m), 35S-SPL2(m); amiRNA SPL2	BASTA
pEarleyGate 101 (Earley et al., 2006)	YFP-SUMO1; YFP-SUMO2; YFP-SUMO3; YFP-SUMO5;	BASTA
pEarleyGate 104 (Earley et al., 2006)	SP1-YFP; SPL1-YFP; SPL2-YFP;	BASTA
pDest-35S-X-YFP-6xHis (Reumann et al., 2009)	SP1 ¹⁻²⁴ -YFP; SP1 ¹⁻²²⁵ -YFP; SP1 ¹⁻²⁴⁹ -YFP; SP1 ²⁵⁻³⁴⁷ -YFP; SPL1 ¹⁻²⁴ -YFP; SPL1 ¹⁻²²⁴ -YFP; SPL1 ¹⁻²⁴⁷ -YFP; SPL1 ²⁵⁻³³⁸ -YFP;	Kanamycin
pGilda-GW (Clontech)	BD-DRP3A; BD-SUMO1; BD-SUMO2; BD-SUMO3; BD-SUMO5	N/A
pB42AD (Clontech)	AD-DRP3A; AD-SUMO1; AD-SUMO2; AD-SUMO3; AD-SUMO5	N/A

4.4 Methods

4.4.1 Plant materials

Arabidopsis plants were grown at 22°C, with 70% humidity, and 14-h 70 to 80 $\mu\text{mol m}^{-2} \text{s}^{-2}$ of white light per day. Tobacco (*Nicotiana tabacum*) plants were grown at 24°C, with 70% humidity and 14-h 50 $\mu\text{mol m}^{-2} \text{s}^{-2}$ of white light per day. The Col-0 ecotype of *Arabidopsis* was referred as the wild type. T-DNA insertion mutants, *sp1-1* (SALK_063571), *sp1-2* (SALK_002099), *sp1-1* (SALK_064720), and *sp1-2* (SALK_024744) were provided by Arabidopsis Biological Resource Center (ABRC; Columbus, OH, USA). Homozygous mutants were identified by PCR of genomic DNA followed by RT-PCR analysis as described previously (Zhang and Hu, 2010). Peroxisome marker lines CFP-PTS1 and YFP-PTS1 were generated in our previously study (Fan et al., 2005). Mitochondrial marker lines COX4-YFP and COX4-CFP were generated in a previous study (Nelson et al., 2007) and obtained from ABRC.

4.4.2 Plant transformation

All organelle markers and other constructs used in this study were transformed into plants via simplified floral dipping method (<http://entomology.wisc.edu/~afb/protocol.html>) with *Agrobacterium tumefaciens* strain GV3101 (pMP90). To screen for transformants with kanamycin resistance, T1 seeds were plated on 0.5 Linsmaier and Skoog (1/2 LS) medium containing 50 g/ml of kanamycin. To obtain BASTA-resistant transformants, T1 seeds were grown on soil and sprayed with 0.1% (v/v) Basta (Finale; Farnam Companies, Phoenix, AZ, USA) and

0.025% (v/v) Silwet L-77 after 7 days, for at least two times. To perform protein transient expression in tobacco plants, leaves of six to 8-week-old *Nicotiana tabacum* plants were infiltrated with resuspended *A. tumefaciens* cells harboring specific plasmids. *Agrobacterium* cells were grown in shakers for 24 h at 28°C with 200 rpm agitation. Then the cells were spun down and resuspended in water to an A600 of 0.05. Leaf areas subjected to infiltrations were cut off and used for confocal imaging.

4.4.3 Gene cloning, plasmid construction and RT-PCR

The coding sequences of specific genes were amplified with Gateway compatible primers by Phusion polymerase (NEB). The cDNA made from total RNA extracts of Col-0 plants was used as template. The PCR products were cloned into pDonor207 vectors and various destination vectors via standard Gateway cloning system (Invitrogen, <http://www.invitrogen.com/>). To generate dominant negative forms of SP1, SPL1 and SPL2, overlapping PCR was performed (<http://gfp.stanford.edu/protocol/index5.html>) with primers containing the mutation sites. All primers used in this study are shown in Table 4.1. All vectors used are shown in Table 4.2.

To clone the artificial microRNA construct, amiRNA SPL2 (5'-TGTTTAACTCTCGTTCCGCGG-3') was designed by WMD3-Web MicroRNA Designer (<http://wmd3.weigelworld.org/cgi-bin/webapp.cgi>). Overlapping PCR was used to clone the amiRNA according to the WMD3-Web MicroRNA Designer (http://wmd3.weigelworld.org/downloads/Cloning_of_artificial_microRNAs.pdf). The precursor miRNA was amplified by Gateway-compatible primers and cloned into pEarley100 vector.

To analyze gene expression level in plants, semi-quantitative RT-PCR was performed as previously described (Aung and Hu, 2011).

4.4.4 Immunoblot analysis

To prepare mitochondrial and peroxisomal proteins for SDS-PAGE analysis, 15 μ l purified mitochondria and peroxisomes mixed with 5 μ l 4X LDS sample buffer (Invitrogen) were heated at 70 °C for 10 min, before loaded onto SDS-PAGE. Proteins were transferred to a PVDF membrane after separation. The membrane was blocked with 5% milk in 1x TBST (50 mM Tris-base, 150 mM NaCl, 0.05% Tween 20, pH 8.0) for 1 h at room temperature, then incubated for 1 h at room temperature with primary antibody prepared in the blocking buffer as follows: 1:20000 for α -GFP (Abcam), 1:2,500 for α -PEX14 (Lingard and Bartel, 2009) and 1:5,000 for α -VDAC (Reumann et al., 2009). The probed membrane was washed with 1x TBST three times at 5 min each time, followed by incubation with the secondary antibody (i.e., 1:20,000 goat anti-rabbit IgG or 1:20,000 goat anti-mouse IgG, Millipore) at room temperature for 1 h. After that, the membrane was washed four times with 1x TBST for 10 min each time, and then visualized using the SuperSignal West Dura Extended Duration Substrate (Pierce Biotechnology).

4.4.5 Purification of peroxisomal and mitochondrial proteins

Rosette leaves from 4-week-old transgenic *Arabidopsis* plants expressing 35S-SP1-YFP and an organelle marker were used for organelle purification. Peroxisomes were isolated from the peroxisomal marker (CFP-PTS1) background as described

previously (Reumann et al., 2009). Mitochondria were isolated from the mitochondrial marker (COX4-CFP) background, using a previously published protocol (Aung and Hu, 2011; Kruff et al., 2001; Werhahn and Braun, 2002). The purity of mitochondrial preparations was determined using immunoblot analyses and organelle-specific antibodies as described above. Mitochondrial membrane association was tested using previously described methods (Nakagawa et al., 2007).

4.4.6 Microscopy

Two fluorescence microscopes, the Zeiss Axio Imager Upright Microscope and the Olympus Fluoview FV1000 confocal laser scanning microscope, were used. For confocal microscopy, CFP, YFP, and chlorophyll auto-fluorescence were excited with 458-, 515-, and 515-nm lasers respectively and detected at 465–490 nm, 505–555 nm and 655-755 nm respectively.

4.4.7 Yeast two-hybrid assay

The Matchmaker two-hybrid system (Clontech) was modified by introducing the gateway cassette (attR1-Cmr-ccdB-arrR2) into pGilda and pB42AD vectors. Specific gene constructs were transformed into yeast strain EGY48 and selected on standard Synthetic Dropout medium (SD/-Ura-Trp-His). The plasmid DNA was transformed using Frozen-EZ Yeast Transformation KitTM as recommended by the manufacturer (Zymo). Transformants were then transferred onto SD/-Ura-Trp-His-Leu medium that contains β -gal to test for protein interaction.

CHAPTER 5

CONCLUSION AND PERSPECTIVES

Eukaryotic cells contain numerous membrane-enclosed organelles, providing specific environments for various biochemical reactions. In plant cells, mitochondria, peroxisomes and chloroplasts are critically involved in many essential aspects of plant physiology, including energy capture, conversion, storage and metabolism. To achieve the ideal organismal physiology, these organelles alter their functions in response to changes from both inside and outside of the cell. Therefore, dissecting the mechanisms behind the dynamics of these organelles is important for fully understanding their functions.

In plants, the major protein machineries governing protein import and membrane fission of these organelles have been identified. However, the regulatory mechanisms of the functions of the major protein components are just beginning to be uncovered in plants and other systems. Their functions can be directly and promptly adjusted by covalent attachment of small molecules and by membrane lipids. In my dissertation research, I used the model plant *Arabidopsis* to further characterize the regulatory mechanisms of organelle dynamics, focusing on protein import and membrane fission (Fig. 5.1).

5.1 Membrane lipids

In Chapter 2, I showed that cardiolipin (CL), a negatively charged phospholipid, is involved in mitochondrial fission and plant stress response in *Arabidopsis*. CL is present in bacterial cell membranes and eukaryotic mitochondrial membranes. Its distribution pattern at the tips and fission sites of bacterial membrane resembles that of the key fission factor Dynamin-related Protein3 (DRP3), on mitochondria (Fujimoto et al., 2009;

Mano et al., 2004; Aung and Hu, 2012; Zhang and Hu, 2009). CL also supports the functions of bacterial division proteins, as reported in multiple studies (Renner and Weibel, 2011; Kawai et al., 2004; Lenarcic et al., 2009; Doan et al., 2013). Besides its predominant localization in mitochondria (Osman et al., 2011), CL was also reported to be in peroxisomes in a yeast study (Wriessnegger et al., 2007). Hence, we had hypothesized that CL may be a dual fission factor for mitochondria and peroxisomes. In this study, I characterized CL and Cardiolipin Synthase (CLS), and found both localized specifically to mitochondria. CL deficiency resulting from *CLS* gene disruption leads to mitochondrial elongation and enlargement, abnormal mitochondrial cristae, and plant susceptibility to various abiotic stresses. CL mediates mitochondrial fission at least partially through stabilizing the DRP3 higher-order complex. Our discovery of the role of CL in mitochondrial fission adds to its well-known function in mitochondrial fusion process, which had been shown in non-plant systems (Sesaki et al., 2006; Tamura et al., 2009).

At this point, we cannot exclude the possibility that CL also impacts the functions of other mitochondrial fission proteins, such as FIS1, ELM1 and PMD1 (Scott et al., 2006; Lingard et al., 2008; Zhang and Hu, 2009; Arimura et al., 2008; Aung and Hu, 2011). To test this, native protein gel can be used to analyze the formation of proteins complexes that contain these proteins in CL deficient mutants. In addition, protein-lipid interaction between CL and these proteins could be tested. It's also possible that CL plays a role in mitochondrial fusion in plants, too. However, the plant mitochondrial fusion machinery has not been identified yet, thus the interaction between fusion proteins and CL cannot be tested at present. A possible strategy to reveal the role of CL

in plant mitochondrial fusion is to generate a *drp3A drp3B cls* triple mutant, in which we may see less mitochondrial elongation if CL also promotes mitochondrial fusion.

In non-plant systems, CL is found to be crucial for multiple aspects of mitochondrial functions, including mitochondrial fusion, mitochondrial electron transport chain complex formation and mitochondrion-mediated programmed cell death (PCD) (Osman et al., 2011). The roles of CL in mitochondrial electron-transport chain complex formation and abiotic stress response are just beginning to be elucidated in plants. It is still unknown whether CL is also involved in biotic stress response in plants, which should be feasible to test using the loss-of-function mutants of *CLS*.

In mammalian apoptosis, CL contributes significantly to mitochondrial outer membrane permeabilization and cytochrome c release (Lutter et al., 2000; Kuwana et al., 2002; Gonzalez and Gottlieb, 2007; Montessuit et al., 2010). CL directly interacts with cytochrome c and pro-apoptotic Bcl-2 family proteins (Kagan et al., 2005; Gonzalez and Gottlieb, 2007). CL was also recently shown to mediate mitophagy in mammals (Chu et al., 2013). However, the roles of CL in plant PCD and mitophagy are still very obscure. Particularly, the plant PCD pathway, which lacks homologous proteins to almost all the mammalian apoptotic factors, is very different from that in mammals (van Doorn, 2011). The mitophagy pathway also has plant-specific features and is much less characterized in plants than in mammals (Li et al., 2014). In Chapter 2, we showed that CL is important for plant response to PCD-inducing abiotic stresses. Hence, it is probable that CL may be a conserved PCD and mitophagy factor across different kingdoms and thus will be worthwhile to test whether these two pathways are affected in CL deficient mutants.

Besides CL, other membrane lipids can also contribute to the dynamics of mitochondria. The remodeling of CL, such as the formation of monolysocardiolipin (MLCL) and the desaturation of CL acyl contents, may significantly impact CL functions. The regulation of CL distribution on both mitochondrial outer and inner membranes may also be important for CL functions. Apart from mitochondria, how membrane lipids contribute to the dynamics of peroxisomes and chloroplasts in plants still wait to be elucidated.

5.2 Post-translational modifications

In Chapters 3 and 4, I focused on protein ubiquitination, which has not been shown previously to occur in plant mitochondria. I identified a mitochondrial outer membrane associated deubiquitinase, UBP27. Overexpression of UBP27 reduces mitochondrial length and mitochondrial association of DRP3. Without identification of UBP27 substrates, we can propose different mechanisms to explain how UBP27 contributes to mitochondrial morphogenesis. First, it is possible that UBP27 directly regulates DRP3 localization and promotes the recycling of DRP3 back to the cytosol after mitochondrial fission. Second, UBP27 may be indirectly involved in mitochondrial morphogenesis. Since UBP27 localizes on mitochondrial outer membrane with the enzymatic domain facing the cytosol, it is possible that UBP27 actually regulates protein import by targeting the TOM machinery. Besides, UBP27 may target other proteins at the cytosolic side of mitochondrial outer membrane, such as proteins involved in mitochondrion-cytoskeleton interactions.

In Chapter 4, I reported characterizations of a small family of RING-domain

containing proteins composed of SP1, SPL1 and SPL2. The RING domain is one type of domains found in ubiquitin E3 ligases. The ubiquitination activity was previously confirmed *in vitro* for SP1. Intriguingly, I found that SP1 and SPL1 both associate with peroxisomes, mitochondria and chloroplasts - three metabolically linked organelles. SPL2 associates with two of them – mitochondria and chloroplasts. Since SP1 was previously reported to target chloroplast protein import machinery, it is possible that SP1 and SPL1 are involved in the protein import processes of mitochondria and peroxisomes. In this scenario, SP1 and SPL1 can coordinately modulate the biogenesis of all three organelles. Moreover, when *toc* mutants are combined with *sp1* loss-of-function mutant, the *toc* defects are ameliorated (Ling et al., 2012). Similar strategies can be employed to check if the disruption of *SP1* and *SPL1* affects the loss-of-function mutants of protein import machineries of mitochondria and peroxisomes.

No growth or organelle defects have been observed in the loss-of-functions mutants of *SP1* and *SPL1*. However, disrupting SPL2 function leads to strong mitochondrial aggregation, indicating SPL2's potential roles in mitochondrial movement, distribution, or fission/fusion. More in-depth analyses are needed to reveal the mechanism behind this mitochondrial aggregation phenotype. Proteins involved in mitochondrial movement and distribution can be tested as potential ubiquitination substrates of SPL2. Genome-wide screens, such as Y2H screening using UBP27 or SP1/SPL as baits, and mass spectrometry-based “ubiquitin-omics” analysis of isolated mitochondria, may also be employed.

The organelle dynamics machineries can be regulated by PTMs other than ubiquitination. For example, DRP3 was reported by multiple studies to be

phosphorylated, yet it is unknown whether these phosphorylation events affect DRP3 activity and the general plant physiology. To detect PTMs of DRP3 and other proteins, proteomics analyses of purified organelles can be performed. As suggested by the studies of mammalian DRP1 PTMs, the post-translational regulation of mitochondrial fission DRP and possibly other organelle dynamics proteins can be very specific to tissue types and developmental stages to meet the specific requirements of these conditions to fine tune organelle dynamics (see Chapter 1). Tissue and development differences should also be considered when analyzing the role of a specific type of protein PTMs in organelle dynamics in plants.

5.3 Broader impacts of this study

The dynamics of organelles are important for their functions. Peroxisomes, mitochondria and chloroplasts are essential for plant growth, general physiology, energy metabolism, biomass accumulation and stress response. Because these organelles are metabolically linked, it is also important to keep their functions coordinated. Changing the functions of each plant energy organelles as well as their functional coordination by adjusting organelle dynamics can potentially contribute to agriculture and biofuel production. Thus, it is important to analyze the major protein machineries governing organelle dynamics and the regulatory mechanisms of these major machineries.

Cardiolipin is important not only for mitochondrial dynamics but also for plant stress response. The exact roles of cardiolipin in plant stress response and programmed cell death (PCD) are still unclear. The study of cardiolipin will also reveal the overall mechanism of plant PCD as well as how mitochondria are involved in this

process. PCD is critically involved in plant embryogenesis, tissue differentiation, reproductive organ formation, pollination, senescence, and serves as a response mechanism to some abiotic and biotic stresses (Lord and Gunawardena, 2012). Hence, the study of the role of mitochondria and CL in PCD is also a critical step toward improving plant health and stress defense.

Ubiquitination regulates the dynamics of plant chloroplasts and peroxisomes. In this dissertation research, I discovered mitochondrial ubiquitin specific protease and ubiquitin E3 ligases as well. In particular, members of the RING domain E3 ligase family SP1/SPL are associated with multiple energy organelles. The study of this protein family may reveal ubiquitination-mediated mechanisms that coordinate the dynamics of all three energy organelles. Knowledge gained from this line of research may be used to improve the equilibrium of plant energy organelle functions, such as to produce more biomass by maintaining an optimal ratio between photosynthetic and photorespiratory activities.

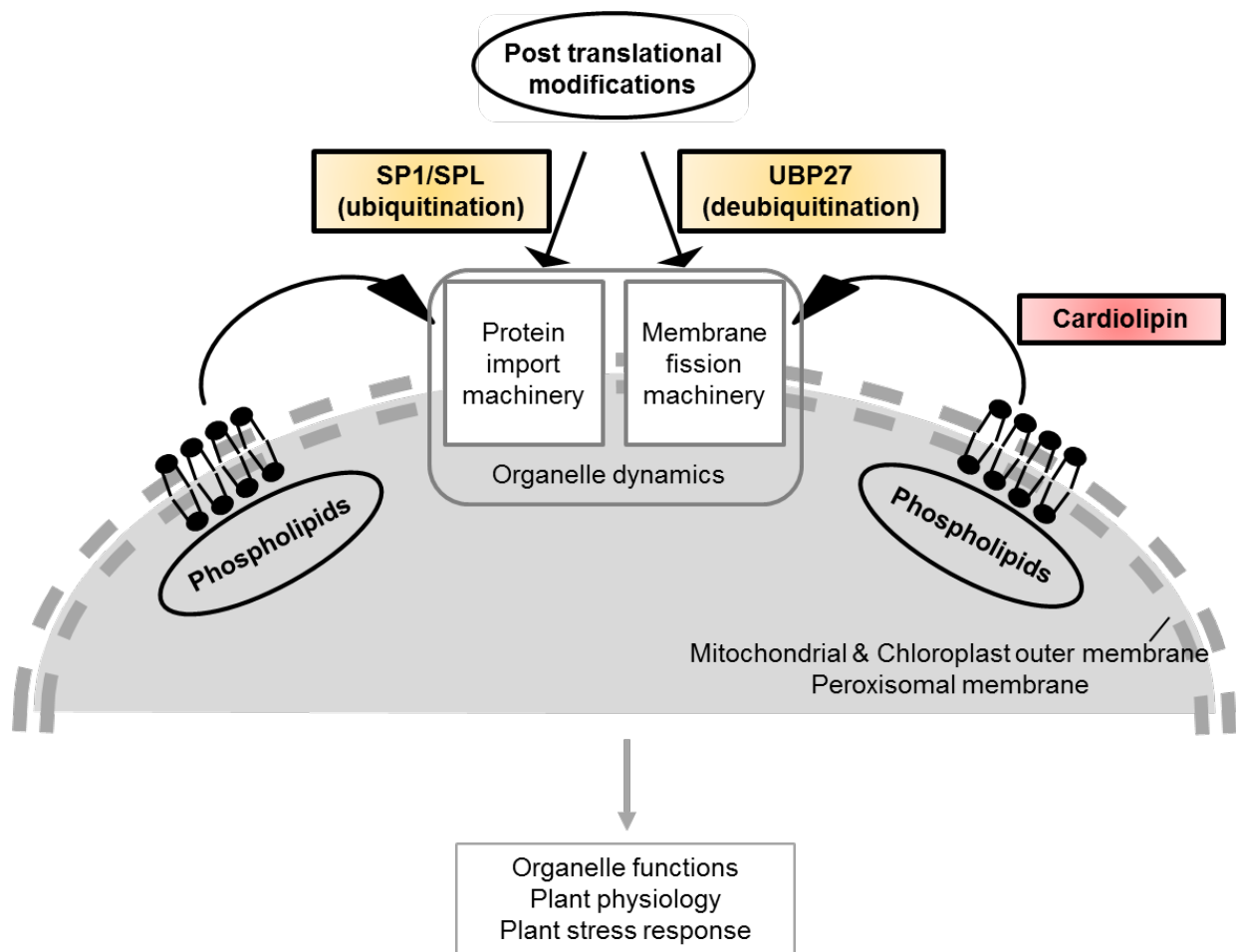


Figure 5.1. A summary of the efforts described in this dissertation to dissect the regulatory mechanisms of plant energy organelle dynamics.

Figure 5.1 (cont'd)

This dissertation research aims at analyzing the regulatory mechanisms of plant energy organelle dynamics. My work focuses on the investigation of membrane fission and protein import processes mainly from two directions: the membrane phospholipids and protein post-translational modifications. The impact of these regulatory mechanisms to organelle functions and general plant physiology, especially plant stress response, is also analyzed. Chapter 2 of this dissertation focuses on cardiolipin – a mitochondrial membrane phospholipid, and revealed that it promotes mitochondrial fission by stabilizing DRP3 higher-order protein complexes. Chapter 3 shows that the mitochondrion-associated deubiquitinase UBP27 contributes to mitochondrial morphogenesis. Chapter 4 characterizes a small family of RING domain-containing proteins – SP1, SPL1 and SPL2. SP1 and SPL1 associate with peroxisomes, mitochondria and chloroplasts. Given that SP1 was previously shown to target the plastid protein import machinery, SP1 and SPL1 possibly modulate function of the mitochondrial and peroxisomal import machineries. SPL2 associates with mitochondria and chloroplasts, resulting in mitochondrial aggregation when its function is disrupted. The substrates of UBP27, SP1, SPL1 and SPL2 in mitochondria and peroxisomes are unknown.

APPENDIX

APPENDIX A

The conserved fission complex on peroxisomes and mitochondria

This section has been published:
Ronghui Pan and Jianping Hu. (2011)
Plant Signaling & Behavior 6: 870-872.
doi:10.4161/psb.6.6.15241.

A.1 Abstract

Peroxisomes are eukaryotic organelles highly versatile and dynamic in content and abundance. Plant peroxisomes mediate various metabolic pathways, a number of which are completed sequentially in peroxisomes and other subcellular organelles, including mitochondria and chloroplasts. To understand how peroxisomal dynamics contribute to changes in plant physiology and adaptation, the multiplication pathways of peroxisomes are being dissected. Research in *Arabidopsis thaliana* has identified several evolutionarily conserved families of proteins in peroxisome division. These include five PEROXIN11 proteins (PEX11a to -e) that induce peroxisome elongation and the fission machinery, which is composed of three dynamin-related proteins (DRP3A, -3B and -5B) and DRP's membrane receptor, FISSION1 (FIS1A and -1B). While the function of PEX11 is restricted to peroxisomes, the fission factors are more promiscuous. DRP3 and FIS1 proteins are shared between peroxisomes and mitochondria, and DRP5B plays a dual role in the division of chloroplasts and peroxisomes. Analysis of the *Arabidopsis* genome suggests that higher plants may also contain functional homologs of the yeast Mdv1/Caf4 proteins, adaptor proteins that link DRPs to FIS1 on the membrane of both peroxisomes and mitochondria. Sharing a conserved fission machine between these metabolically linked subcellular compartments throughout evolution may have some biological significance.

Peroxisomes are single membrane-delimited organelles involved in a variety of metabolic pathways essential to development (Schrader and Fahimi, 2008). Plant peroxisomes participate in processes such as lipid mobilization, photorespiration, detoxification, hormone biosynthesis and metabolism, and plant-pathogen interaction (Nyathi and Baker, 2006; Kaur et al., 2009). A number of these metabolic functions, such as photorespiration, fatty acid metabolism and jasmonic acid biosynthesis, are accomplished through the cooperative efforts of peroxisomes and other subcellular compartments, such as mitochondria and chloroplasts (Kaur et al., 2009; Beevers, 1979; Reumann and Weber, 2006). The function, morphology and abundance of peroxisomes can vary depending on the organism, cell type, developmental stage and prevailing environmental conditions in which the organism resides (Purdue and Lazarow, 2001; Yan et al., 2005). It is now believed that in addition to budding from the endoplasmic reticulum (ER), peroxisomes also multiply from pre-existing peroxisomes via division, going through steps including peroxisome elongation/tubulation, membrane constriction and fission (Yan et al., 2005; Fagarasanu et al., 2007). In the reference plant *Arabidopsis thaliana*, three evolutionarily conserved families of proteins have been identified as key components of the peroxisome division apparatus. Five integral membrane proteins, named PEX11a to -e, are mainly responsible for inducing the elongation and tubulation of peroxisomes in the early stage of peroxisome division (Lingard and Trelease, 2006; Orth et al., 2007; Nito et al., 2007). DRP3A and DRP3B are members of a dynamin-related protein family that powers the fission of membranes and FIS1A and FIS1B are homologous proteins believed to anchor the DRP proteins to the membrane (Arimura et al., 2004b; Arimura and Tsutsumi, 2002; Fujimoto et al., 2009;

Logan et al., 2004; Mano et al., 2004; Scott et al., 2006; Zhang and Hu, 2008b, 2009). Similar to their counterparts in yeasts and mammals, DRP3 and FIS1 are shared by the fission machineries of peroxisomes and mitochondria (Arimura et al., 2004b; Arimura and Tsutsumi, 2002; Fujimoto et al., 2009; Logan et al., 2004; Mano et al., 2004; Scott et al., 2006; Zhang and Hu, 2008b, 2009). We recently reported the unexpected finding that DRP5B, a plant/algal-specific DRP distantly related to the DRP3 proteins and originally discovered for its function in chloroplast division, is also involved in the division of peroxisomes. Using co-immunoprecipitation (co-IP) and bimolecular fluorescence complementation (BiFC) assays, we further demonstrated that DRP5B and the two DRP3 proteins can homo- and hetero-dimerize and each DRP can form a complex with FIS1A and/or FIS1B and most of the *Arabidopsis* PEX11 isoforms (Zhang and Hu, 2010). These results together demonstrate that, despite their distinct evolutionary origins, structures and functions, peroxisomes, mitochondria and chloroplasts use some of the same factors for fission. These data also revealed that, like in yeasts and mammals, the FIS1- DRP complex exists on peroxisomes and mitochondria in plants.

DRP5B, a DRP unique in the plant and photosynthetic algae lineages, seems to be the sole component shared by the division of chloroplasts and peroxisomes (Zhang and Hu, 2010). However, both FIS1 and DRP are found to be required for the division of peroxisomes and mitochondria throughout eukaryotic evolution (Kaur and Hu, 2009; Nagotu et al., 2010), prompting the question: to what extent is the FIS1-DRP complex conserved among diverse species? In the yeast *Saccharomyces cerevisiae*, this fission complex also contains an adaptor encoded by two homologous WD40 proteins, Mdv1

and Caf4, which are partially redundant in function with Mdv1 playing the major role. Mdv1 and Caf4 share an N-terminal extension (NTE) domain with two α -helices, a middle coiled-coil domain (CC) and C-terminal WD40 repeat. Both proteins use the NTE to interact with the tetratricopeptide repeat (TPR) domain-containing N-terminus of Fis1, the CC domain to dimerize and the C-terminal WD40 repeat to interact with and recruit the DRP protein, Dnm1 (Griffin et al., 2005; Tieu et al., 2002). The *Hansenula polymorpha* Mdv1 (Hp Mdv1) also has a dual function in the division of peroxisomes and mitochondria (Nagotu et al., 2008). In addition, a Mdv1/Caf4 homolog, Mda1, was identified from the primitive red algae *Cyanidioschyzon merolae* and found to be involved at least in mitochondrial fission (Nishida et al., 2007). However, higher eukaryotes do not seem to have obvious homologs of Mdv1/Caf4. For example, mammals contain Fis1 and Drp (called DLP1 or Drp1) but no apparent homologs to Mdv1 and Caf4. Instead, a metazoan-specific tail-anchored protein, Mitochondrial Fission Factor (Mff), was recently found to regulate the fission of mitochondria and peroxisomes in a similar manner to Fis1. Mff is essential in recruiting Drp1, at least in mitochondrial division, yet it functions in a Fis1-independent pathway (Gandre-Babbe and Bliiek, 2008; Otera et al., 2010).

To determine whether plants contain structural or functional homologs of Mdv1 and Caf4, we performed blast searches of the *Arabidopsis* genome, which resulted in the retrieval of ~300 WD40 proteins. However, just like the search results from mammals, none of these proteins show significant sequence similarity with Mdv1 and Caf4 beyond the WD40 repeats. To identify proteins with similar domain structures with Mdv1/Caf4, we further analyzed these WD40 proteins, using the online Simple Modular

Architecture Research Tool (<http://smart.embl-heidelberg.de/>). After eliminating proteins apparently inappropriate to be part of this complex, such as kinases and proteins with drastically distinct domain organizations despite of having both WD40 repeats and CC domains, we were able to narrow down to eight proteins. These proteins, which are encoded by At1g04510, At2g32950, At2g33340, At3g18860, At4g05410, At4g21130, At5g50230 and At5g67320, respectively, each contain a central CC domain in addition to the WD40 repeat region and are ranging from 450 to 900 amino acids in length (Fig. A.1A). Subcellular localization studies will need to be performed to determine whether some of these proteins are associated with peroxisomes and mitochondria. If such a WD40 protein is proven to be part of the FIS1-DRP complex in *Arabidopsis*, it will be important to determine whether it simply acts as an adaptor or it also plays other roles, such as to promote and maintain the active structure and conformation of DRP3A/3B at the division site (Fig. A.1B). Consistent with the latter scenario, it was found that Sc Mdv1 accumulates at the division sites after Dnm1 assembles and that the mammalian Fis1 and Drp1 proteins physically interact (Naylor et al., 2006; Yoon et al., 2003). Peroxisomes and mitochondria are functionally linked in a number of metabolic pathways. For example, in plants, they act cooperatively in important processes such as fatty acid metabolism and photorespiration (Kaur et al., 2009). An interesting question to address in the future is whether sharing such a conserved fission machine between peroxisomes and mitochondria throughout evolution has critical biological consequences.

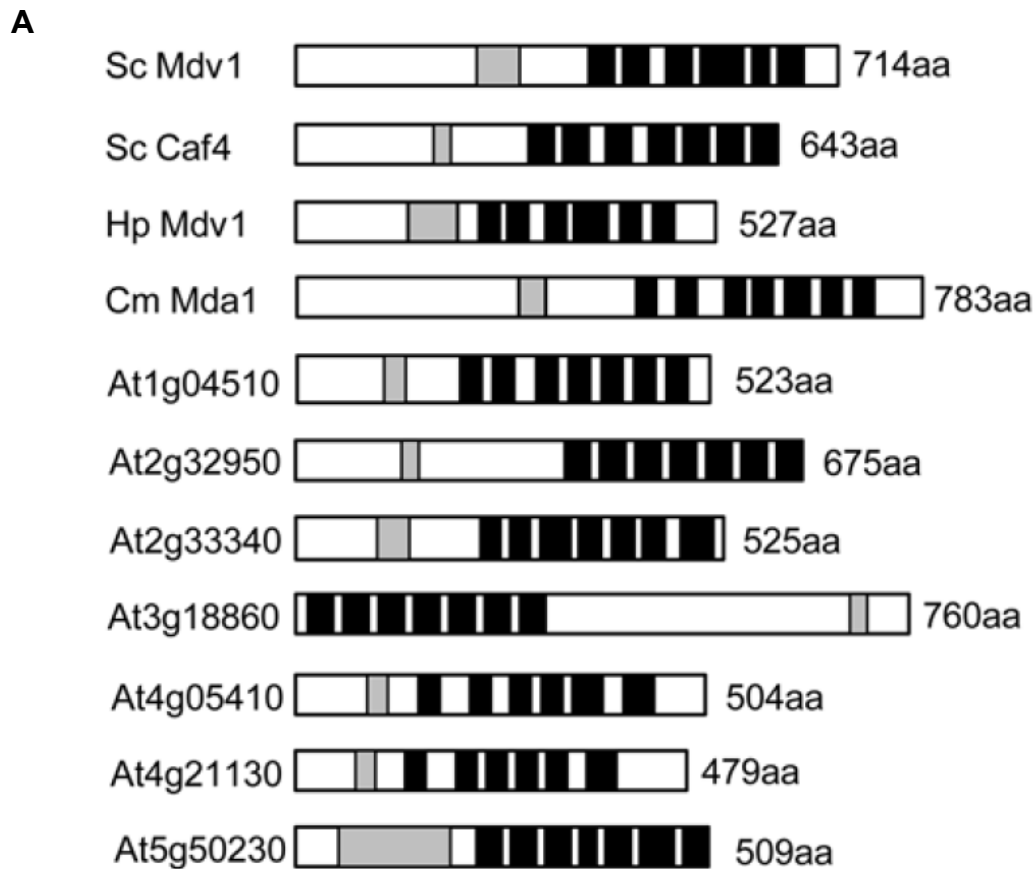
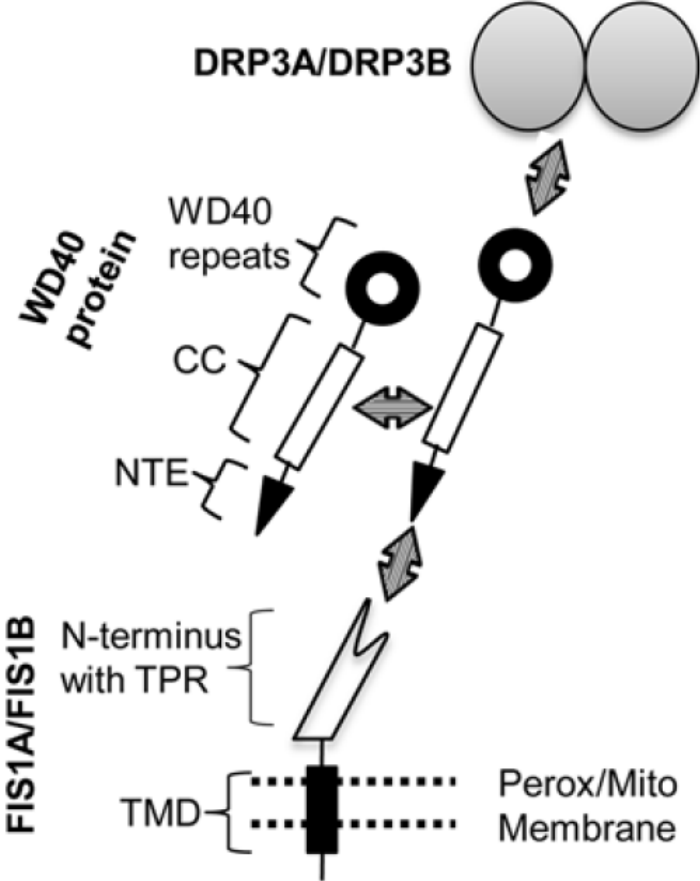


Figure A.1. Domain structure of Mdv1/Caf4 and their homologs or putative homologs. (A) Domain structure of Sc Mdv1 and Sc Caf4 from *S. cerevisiae*, their homologs from *H. polymorpha* and *C. merolae*, and the eight *Arabidopsis* proteins with similar domain organization. Grey boxes indicate the CC domain and black boxes are WD40 repeats. (B) The putative FIS1-WD40-DRP complex in *Arabidopsis*. CC, coiled-coil; NTE, N-terminal extension; TPR, tetratricopeptide repeat; TMD, transmembrane domain.

Figure A.1 (cont'd)

B



REFERENCES

REFERENCES

- Amerik, A.Y. and Hochstrasser, M.** (2004). Mechanism and function of deubiquitinating enzymes. *Biochim. Biophys. Acta* **1695**: 189–207.
- Ammar, M.R., Kassas, N., Chasserot-Golaz, S., Bader, M.F., and Vitale, N.** (2013). Lipids in regulated exocytosis: What are they doing? *Front. Endocrinol. (Lausanne)* **4**: 1–6.
- Arimura, S., Fujimoto, M., Doniwa, Y., Kadoya, N., Nakazono, M., Sakamoto, W., and Tsutsumi, N.** (2008). Arabidopsis ELONGATED MITOCHONDRIA1 is required for localization of DYNAMIN-RELATED PROTEIN3A to mitochondrial fission sites. *Plant Cell* **20**: 1555–1566.
- Arimura, S. and Tsutsumi, N.** (2002). A dynamin-like protein (ADL2b), rather than FtsZ, is involved in Arabidopsis mitochondrial division. *Proc. Natl. Acad. Sci. U. S. A.* **99**: 5727–5731.
- Arimura, S., Yamamoto, J., Aida, G.P., Nakazono, M., and Tsutsumi, N.** (2004a). Frequent fusion and fission of plant mitochondria with unequal nucleoid distribution. *Proc. Natl. Acad. Sci. U. S. A.* **101**: 7805–7808.
- Arimura, S.I., Aida, G.P., Fujimoto, M., Nakazono, M., and Tsutsumi, N.** (2004b). Arabidopsis Dynamin-Like Protein 2a (ADL2a), Like ADL2b, is Involved in Plant Mitochondrial Division. *Plant Cell Physiol.* **45**: 236–242.
- Aung, K. and Hu, J.** (2012). Differential roles of Arabidopsis dynamin-related proteins DRP3A, DRP3B, and DRP5B in organelle division. *J. Integr. Plant Biol.* **54**: 921–931.
- Aung, K. and Hu, J.** (2011). The Arabidopsis tail-anchored protein PEROXISOMAL AND MITOCHONDRIAL DIVISION FACTOR1 is involved in the morphogenesis and proliferation of peroxisomes and mitochondria. *Plant Cell* **23**: 4446–4461.
- Baba, T., Kashiwagi, Y., Arimitsu, N., Kogure, T., Edo, A., Maruyama, T., Nakao, K., Nakanishi, H., Kinoshita, M., Frohman, M.A., Yamamoto, A., and Tani, K.** (2014). Phosphatidic Acid (PA)-Preferring Phospholipase A1 Regulates Mitochondrial Dynamics. *J. Biol. Chem.* **289**: 11497–11511.
- Barsoum, M.J. et al.** (2006). Nitric oxide-induced mitochondrial fission is regulated by dynamin-related GTPases in neurons. *EMBO J.* **25**: 3900–3911.
- Bauwe, H., Hagemann, M., and Fernie, A.R.** (2010). Photorespiration: players, partners and origin. *Trends Plant Sci.* **15**: 330–336.

- Beevers, H.** (1979). Microbodies in Higher Plants. *Annu. Rev. Plant Physiol.* **30**: 159–193.
- Bleazard, W., McCaffery, J.M., King, E.J., Bale, S., Mozdy, a, Tieu, Q., Nunnari, J., and Shaw, J.M.** (1999). The dynamin-related GTPase Dnm1 regulates mitochondrial fission in yeast. *Nat. Cell Biol.* **1**: 298–304.
- Borden, K.L.** (2000). RING domains: master builders of molecular scaffolds? *J. Mol. Biol.* **295**: 1103–1112.
- Bossard, C., Bresson, D., Polishchuk, R.S., and Malhotra, V.** (2007). Dimeric PKD regulates membrane fission to form transport carriers at the TGN. *J. Cell Biol.* **179**: 1123–1131.
- Braschi, E., Zunino, R., and McBride, H.M.** (2009). MAPL is a new mitochondrial SUMO E3 ligase that regulates mitochondrial fission. *EMBO Rep.* **10**: 748–754.
- Braun, H.P., Emmermann, M., Kruff, V., and Schmitz, U.K.** (1992). The general mitochondrial processing peptidase from potato is an integral part of cytochrome c reductase of the respiratory chain. *EMBO J.* **11**: 3219–3227.
- Braun, H.P.H. and Schmitz, U.K.U.** (1999). The protein-import apparatus of plant mitochondria. *Planta* **209**: 267–274.
- Brocard, C. and Hartig, A.** (2006). Peroxisome targeting signal 1: Is it really a simple tripeptide? *Biochim. Biophys. Acta - Mol. Cell Res.* **1763**: 1565–1573.
- Cánovas, F.M., Dumas-Gaudot, E., Recorbet, G., Jorin, J., Mock, H.P., and Rossignol, M.** (2004). Plant proteome analysis. *Proteomics* **4**: 285–298.
- Carrie, C., Giraud, E., Duncan, O., Xu, L., Wang, Y., Huang, S., Clifton, R., Murcha, M., Filipovska, A., Rackham, O., Vrielink, A., and Whelan, J.** (2010a). Conserved and novel functions for *Arabidopsis thaliana* MIA40 in assembly of proteins in mitochondria and peroxisomes. *J. Biol. Chem.* **285**: 36138–36148.
- Carrie, C., Murcha, M.W., Giraud, E., Ng, S., Zhang, M.F., Narsai, R., and Whelan, J.** (2013). How do plants make mitochondria? *Planta* **237**: 429–439.
- Carrie, C., Murcha, M.W., and Whelan, J.** (2010b). An in silico analysis of the mitochondrial protein import apparatus of plants. *BMC Plant Biol.* **10**: 249.
- Cegelski, L. and Schaefer, J.** (2006). NMR determination of photorespiration in intact leaves using in vivo ¹³CO₂ labeling. *J. Magn. Reson.* **178**: 1–10.
- Cereghetti, G.M., Stangherlin, A., Martins de Brito, O., Chang, C.R., Blackstone, C., Bernardi, P., and Scorrano, L.** (2008). Dephosphorylation by calcineurin regulates

translocation of Drp1 to mitochondria. *Proc. Natl. Acad. Sci. U. S. A.* **105**: 15803–15808.

Chacinska, A., Koehler, C.M., Milenkovic, D., Lithgow, T., and Pfanner, N. (2009). Importing Mitochondrial Proteins: Machineries and Mechanisms. *Cell* **138**: 628–644.

Chacinska, A., van der Laan, M., Mehnert, C.S., Guiard, B., Mick, D.U., Hutu, D.P., Truscott, K.N., Wiedemann, N., Meisinger, C., Pfanner, N., and Rehling, P. (2010). Distinct forms of mitochondrial TOM-TIM supercomplexes define signal-dependent states of preprotein sorting. *Mol. Cell. Biol.* **30**: 307–318.

Chacinska, A., Pfannschmidt, S., Wiedemann, N., Kozjak, V., Sanjuán Szklarz, L.K., Schulze-Specking, A., Truscott, K.N., Guiard, B., Meisinger, C., and Pfanner, N. (2004). Essential role of Mia40 in import and assembly of mitochondrial intermembrane space proteins. *EMBO J.* **23**: 3735–3746.

Chan, D.C. (2012). Fusion and fission: interlinked processes critical for mitochondrial health. *Annu. Rev. Genet.* **46**: 265–287.

Chan, E.Y.L. and McQuibban, G.A. (2012). Phosphatidylserine decarboxylase 1 (Psd1) promotes mitochondrial fusion by regulating the biophysical properties of the mitochondrial membrane and alternative topogenesis of mitochondrial genome maintenance protein 1 (Mgm1). *J. Biol. Chem.* **287**: 40131–40139.

Chan, N.C., Salazar, A.M., Pham, A.H., Sweredoski, M.J., Kolawa, N.J., Graham, R.L.J., Hess, S., and Chan, D.C. (2011). Broad activation of the ubiquitin-proteasome system by Parkin is critical for mitophagy. *Hum. Mol. Genet.* **20**: 1726–1737.

Chandler, J.S., McArdle, B., and Callis, J. (1997). AtUBP3 and AtUBP4 are two closely related *Arabidopsis thaliana* ubiquitin-specific proteases present in the nucleus. *Mol. Gen. Genet.* **255**: 302–310.

Chang, C.-R. and Blackstone, C. (2007). Cyclic AMP-dependent protein kinase phosphorylation of Drp1 regulates its GTPase activity and mitochondrial morphology. *J. Biol. Chem.* **282**: 21583–21587.

Chang, C.-R. and Blackstone, C. (2010). Dynamic regulation of mitochondrial fission through modification of the dynamin-related protein Drp1. *Ann. N. Y. Acad. Sci.* **1201**: 34–39.

Chen, H., Detmer, S.A., Ewald, A.J., Griffin, E.E., Fraser, S.E., and Chan, D.C. (2003). Mitofusins Mfn1 and Mfn2 coordinately regulate mitochondrial fusion and are essential for embryonic development. *J. Cell Biol.* **160**: 189–200.

- Chicco, A.J. and Sparagna, G.C.** (2007). Role of cardiolipin alterations in mitochondrial dysfunction and disease. *Am. J. Physiol. Cell Physiol.* **292**: C33–44.
- Cho, D.-H., Nakamura, T., Fang, J., Cieplak, P., Godzik, A., Gu, Z., and Lipton, S.A.** (2009). S-nitrosylation of Drp1 mediates beta-amyloid-related mitochondrial fission and neuronal injury. *Science* **324**: 102–105.
- Choi, S.-Y., Huang, P., Jenkins, G.M., Chan, D.C., Schiller, J., and Frohman, M.A.** (2006). A common lipid links Mfn-mediated mitochondrial fusion and SNARE-regulated exocytosis. *Nat. Cell Biol.* **8**: 1255–1262.
- Chu, C.T. et al.** (2013). Cardiolipin externalization to the outer mitochondrial membrane acts as an elimination signal for mitophagy in neuronal cells. *Nat. Cell Biol.* **15**: 1197–205.
- Clague, M.J., Coulson, J.M., and Urbe, S.** (2012). Cellular functions of the DUBs. *J. Cell Sci.* **125**: 277–286.
- Claros, M.G. and Vincens, P.** (1996). Computational method to predict mitochondrially imported proteins and their targeting sequences. *Eur. J. Biochem.* **241**: 779–786.
- Clough, S.J. and Bent, a F.** (1998). Floral dip: a simplified method for *Agrobacterium*-mediated transformation of *Arabidopsis thaliana*. *Plant J.* **16**: 735–743.
- Collins, J.A., Schandl, C.A., Young, K.K., Vesely, J., and Willingham, M.C.** (1997). Major DNA Fragmentation Is a Late Event in Apoptosis. *J. Histochem. Cytochem.* **45** : 923–934.
- Cribbs, J.T. and Strack, S.** (2007). Reversible phosphorylation of Drp1 by cyclic AMP-dependent protein kinase and calcineurin regulates mitochondrial fission and cell death. *EMBO Rep.* **8**: 939–944.
- Cui, X., Lu, F., Li, Y., Xue, Y., Kang, Y., Zhang, S., Qiu, Q., Cui, X., Zheng, S., Liu, B., Xu, X., and Cao, X.** (2013). Ubiquitin-specific proteases UBP12 and UBP13 act in circadian clock and photoperiodic flowering regulation in *Arabidopsis*. *Plant Physiol.* **162**: 897–906.
- Davis, A.J., Alder, N.N., Jensen, R.E., and Johnson, A.E.** (2007). The Tim9p/10p and Tim8p/13p complexes bind to specific sites on Tim23p during mitochondrial protein import. *Mol. Biol. Cell* **18**: 475–486.
- Desai, M. and Hu, J.** (2008). Light induces peroxisome proliferation in *Arabidopsis* seedlings through the photoreceptor phytochrome A, the transcription factor HY5 HOMOLOG, and the peroxisomal protein PEROXIN11b. *Plant Physiol.* **146**: 1117–1127.

- DeVay, R.M., Dominguez-Ramirez, L., Lackner, L.L., Hoppins, S., Stahlberg, H., and Nunnari, J.** (2009). Coassembly of Mgm1 isoforms requires cardiolipin and mediates mitochondrial inner membrane fusion. *J. Cell Biol.* **186**: 793–803.
- Doan, T., Coleman, J., Marquis, K. a, Meeske, A.J., Burton, B.M., Karatekin, E., and Rudner, D.Z.** (2013). FisB mediates membrane fission during sporulation in *Bacillus subtilis*. *Genes Dev.* **27**: 322–334.
- Doelling, J.H., Yan, N., Kurepa, J., Walker, J., and Vierstra, R.D.** (2001). The ubiquitin-specific protease UBP14 is essential for early embryo development in *Arabidopsis thaliana*. *Plant J.* **27**: 393–405.
- Donaldson, J.G.** (2009). Phospholipase D in endocytosis and endosomal recycling pathways. *Biochim. Biophys. Acta - Mol. Cell Biol. Lipids* **1791**: 845–849.
- Van Doorn, W.G.** (2011). Classes of programmed cell death in plants, compared to those in animals. *J. Exp. Bot.* **62**: 4749–4761.
- Dudek, J., Rehling, P., and van der Laan, M.** (2013). Mitochondrial protein import: common principles and physiological networks. *Biochim. Biophys. Acta* **1833**: 274–285.
- Duncan, O., Murcha, M.W., and Whelan, J.** (2013). Unique components of the plant mitochondrial protein import apparatus. *Biochim. Biophys. Acta* **1833**: 304–313.
- Duncan, O., Taylor, N., and Carrie, C.** (2011). Multiple lines of evidence localize signaling, morphology, and lipid biosynthesis machinery to the mitochondrial outer membrane of *Arabidopsis*. *Plant Physiol.* **157**: 1093–1113.
- Durek, P., Schmidt, R., Heazlewood, J.L., Jones, A., MacLean, D., Nagel, A., Kersten, B., and Schulze, W.X.** (2010). PhosPhAt: the *Arabidopsis thaliana* phosphorylation site database. An update. *Nucleic Acids Res.* **38**: D828–834.
- Earley, K.W., Haag, J.R., Pontes, O., Opper, K., Juehne, T., Song, K., and Pikaard, C.S.** (2006). Gateway-compatible vectors for plant functional genomics and proteomics. *Plant J.* **45**: 616–29.
- Ehrenshaft, M. and Brambl, R.** (1990). Respiration and mitochondrial biogenesis in germinating embryos of maize. *Plant Physiol.* **93**: 295–304.
- Eletr, Z.M. and Wilkinson, K.D.** (2014). Regulation of proteolysis by human deubiquitinating enzymes. *Biochim. Biophys. Acta - Mol. Cell Res.* **1843**: 114–128.
- Emanuelsson, O., Nielsen, H., Brunak, S., and von Heijne, G.** (2000). Predicting subcellular localization of proteins based on their N-terminal amino acid sequence. *J. Mol. Biol.* **300**: 1005–1016.

- Eriksson, A., Sjöling, S., and Glaser, E.** (1996). Characterization of the bifunctional mitochondrial processing peptidase (MPP)/bc1 complex in *Spinacia oleracea*. *J. Bioenerg. Biomembr.* **28**: 285–292.
- Eura, Y., Ishihara, N., Oka, T., and Mihara, K.** (2006). Identification of a novel protein that regulates mitochondrial fusion by modulating mitofusin (Mfn) protein function. *J Cell Sci* **119**: 4913–4925.
- Ewan, R., Pangestuti, R., Thornber, S., Craig, A., Carr, C., O'Donnell, L., Zhang, C., and Sadanandom, A.** (2011). Deubiquitinating enzymes AtUBP12 and AtUBP13 and their tobacco homologue NtUBP12 are negative regulators of plant immunity. *New Phytol.* **191**: 92–106.
- Fagarasanu, A., Fagarasanu, M., and Rachubinski, R.A.** (2007). Maintaining peroxisome populations: a story of division and inheritance. *Annu. Rev. Cell Dev. Biol.* **23**: 321–344.
- Faller, A.** (1978). Energetic swelling and lysis of mitochondria. *Acta Anat* **100**: 573–581.
- Fan, J., Quan, S., Orth, T., Awai, C., Chory, J., and Hu, J.** (2005). The Arabidopsis PEX12 gene is required for peroxisome biogenesis and is essential for development. *Plant Physiol.* **139**: 231–239.
- Fannjiang, Y., Cheng, W.-C., Lee, S.J., Qi, B., Pevsner, J., McCaffery, J.M., Hill, R.B., Basañez, G., and Hardwick, J.M.** (2004). Mitochondrial fission proteins regulate programmed cell death in yeast. *Genes Dev.* **18**: 2785–2797.
- Fernandez-Calvino, L., Faulkner, C., Walshaw, J., Saalbach, G., Bayer, E., Benitez-Alfonso, Y., and Maule, A.** (2011). Arabidopsis plasmodesmal proteome. *PLoS One* **6**: e18880.
- Fetchko, M. and Stagljar, I.** (2004). Application of the split-ubiquitin membrane yeast two-hybrid system to investigate membrane protein interactions. *Methods* **32**: 349–62.
- Figuroa-Romero, C., Iñiguez-Lluhí, J. a, Stadler, J., Chang, C.-R., Arnoult, D., Keller, P.J., Hong, Y., Blackstone, C., and Feldman, E.L.** (2009). SUMOylation of the mitochondrial fission protein Drp1 occurs at multiple nonconsensus sites within the B domain and is linked to its activity cycle. *FASEB J.* **23**: 3917–3927.
- Frank, S., Gaume, B., Bergmann-Leitner, E.S., Leitner, W.W., Robert, E.G., Catez, F., Smith, C.L., and Youle, R.J.** (2001). The Role of Dynamin-Related Protein 1, a Mediator of Mitochondrial Fission, in Apoptosis. *Dev. Cell* **1**: 515–525.
- Freemont, P.S., Hanson, I.M., and Trowsdale, J.** (1991). A novel cysteine-rich sequence motif. *Cell* **64**: 483–484.

- Friedman, J.R., Lackner, L.L., West, M., DiBenedetto, J.R., Nunnari, J., and Voeltz, G.K.** (2011). ER tubules mark sites of mitochondrial division. *Science* **334**: 358–362.
- Friedman, J.R. and Nunnari, J.** (2014). Mitochondrial form and function. *Nature* **505**: 335–343.
- Fröhlich, C., Grabiger, S., Schwefel, D., Faelber, K., Rosenbaum, E., Mears, J., Rocks, O., and Daumke, O.** (2013). Structural insights into oligomerization and mitochondrial remodelling of dynamin 1-like protein. *EMBO J.* **32**: 1280–1292.
- Fujimoto, M., Arimura, S., Mano, S., Kondo, M., Saito, C., Ueda, T., Nakazono, M., Nakano, A., Nishimura, M., and Tsutsumi, N.** (2009). Arabidopsis dynamin-related proteins DRP3A and DRP3B are functionally redundant in mitochondrial fission, but have distinct roles in peroxisomal fission. *Plant J.* **58**: 388–400.
- Gabriel, K., Milenkovic, D., Chacinska, A., Müller, J., Guiard, B., Pfanner, N., and Meisinger, C.** (2007). Novel Mitochondrial Intermembrane Space Proteins as Substrates of the MIA Import Pathway. *J. Mol. Biol.* **365**: 612–620.
- Gadjev, I., Stone, J.M., and Gechev, T.S.** (2008). Programmed cell death in plants: new insights into redox regulation and the role of hydrogen peroxide. *Int. Rev. Cell Mol. Biol.* **270**: 87–144.
- Gandre-Babbe, S. and Blik, A. van der** (2008). The novel tail-anchored membrane protein Mff controls mitochondrial and peroxisomal fission in mammalian cells. *Mol. Biol. Cell* **19**: 2402–2412.
- Gao, H., Kadirjan-Kalbach, D., Froehlich, J.E., and Osteryoung, K.W.** (2003). ARC5, a cytosolic dynamin-like protein from plants, is part of the chloroplast division machinery. *Proc. Natl. Acad. Sci. U. S. A.* **100**: 4328–4333.
- Gebert, N., Ryan, M.T., Pfanner, N., Wiedemann, N., and Stojanovski, D.** (2011). Mitochondrial protein import machineries and lipids: a functional connection. *Biochim. Biophys. Acta* **1808**: 1002–1011.
- Genova, M.L. and Lenaz, G.** (2014). Functional role of mitochondrial respiratory supercomplexes. *Biochim. Biophys. Acta* **1837**: 427–443.
- Glaser, E., Nilsson, S., and Bhushan, S.** (2006). Two novel mitochondrial and chloroplastic targeting-peptide-degrading peptidasomes in *A. thaliana*, AtPreP1 and AtPreP2. In *Biological Chemistry*, pp. 1441–1447.
- Gohil, V.M., Thompson, M.N., and Greenberg, M.L.** (2005). Synthetic lethal interaction of the mitochondrial phosphatidylethanolamine and cardiolipin biosynthetic pathways in *Saccharomyces cerevisiae*. *J. Biol. Chem.* **280**: 35410–35416.

- Gonzalvez, F. and Gottlieb, E.** (2007). Cardiolipin: setting the beat of apoptosis. *Apoptosis* **12**: 877–885.
- Goto, S., Mano, S., Nakamori, C., and Nishimura, M.** (2011). Arabidopsis ABERRANT PEROXISOME MORPHOLOGY9 is a peroxin that recruits the PEX1-PEX6 complex to peroxisomes. *Plant Cell* **23**: 1573–1587.
- Green, B.R.** (2011). Chloroplast genomes of photosynthetic eukaryotes. *Plant J.* **66**: 34–44.
- Griffin, E.E., Graumann, J., and Chan, D.C.** (2005). The WD40 protein Caf4p is a component of the mitochondrial fission machinery and recruits Dnm1p to mitochondria. *J. Cell Biol.* **170**: 237–248.
- Grou, C.P., Carvalho, A.F., Pinto, M.P., Alencastre, I.S., Rodrigues, T.A., Freitas, M.O., Francisco, T., Sá-Miranda, C., and Azevedo, J.E.** (2009). The peroxisomal protein import machinery - A case report of transient ubiquitination with a new flavor. *Cell. Mol. Life Sci.* **66**: 254–262.
- Gu, L., Jones, A.D., and Last, R.L.** (2010). Broad connections in the Arabidopsis seed metabolic network revealed by metabolite profiling of an amino acid catabolism mutant. *Plant J.* **61**: 579–590.
- Guda, C., Guda, P., Fahy, E., and Subramaniam, S.** (2004). MITOPRED: a web server for the prediction of mitochondrial proteins. *Nucleic Acids Res.* **32**: W372–374.
- Guo, C., Hildick, K.L., Luo, J., Dearden, L., Wilkinson, K. a, and Henley, J.M.** (2013). SENP3-mediated deSUMOylation of dynamin-related protein 1 promotes cell death following ischaemia. *EMBO J.* **32**: 1514–1528.
- Guo, T. et al.** (2007). A signal from inside the peroxisome initiates its division by promoting the remodeling of the peroxisomal membrane. *J. Cell Biol.* **177**: 289–303.
- Ha, E.E.-J. and Frohman, M.A.** (2014). Regulation of mitochondrial morphology by lipids. *Biofactors* **40**: 419–424.
- Han, X.-J., Lu, Y.-F., Li, S.-A., Kaitsuka, T., Sato, Y., Tomizawa, K., Nairn, A.C., Takei, K., Matsui, H., and Matsushita, M.** (2008). CaM kinase I alpha-induced phosphorylation of Drp1 regulates mitochondrial morphology. *J. Cell Biol.* **182**: 573–585.
- Harder, Z., Zunino, R., and McBride, H.** (2004). Sumo1 conjugates mitochondrial substrates and participates in mitochondrial fission. *Curr. Biol.* **14**: 340–345.

- Hardtke, C.S., Okamoto, H., Stoop-Myer, C., and Deng, X.W.** (2002). Biochemical evidence for ubiquitin ligase activity of the Arabidopsis COP1 interacting protein 8 (CIP8). *Plant J.* **30**: 385–394.
- Hayashi, M., Nito, K., Toriyama-Kato, K., Kondo, M., Yamaya, T., and Nishimura, M.** (2000). AtPex14p maintains peroxisomal functions by determining protein targeting to three kinds of plant peroxisomes. *EMBO J.* **19**: 5701–5710.
- Heazlewood, J.L., Durek, P., Hummel, J., Selbig, J., Weckwerth, W., Walther, D., and Schulze, W.X.** (2008). PhosPhAt: a database of phosphorylation sites in Arabidopsis thaliana and a plant-specific phosphorylation site predictor. *Nucleic Acids Res.* **36**: D1015–1021.
- Hess, D.T., Matsumoto, A., Kim, S.-O., Marshall, H.E., and Stamler, J.S.** (2005). Protein S-nitrosylation: purview and parameters. *Nat. Rev. Mol. Cell Biol.* **6**: 150–166.
- Höglund, A., Dönnes, P., Blum, T., Adolph, H.-W., and Kohlbacher, O.** (2006). MultiLoc: prediction of protein subcellular localization using N-terminal targeting sequences, sequence motifs and amino acid composition. *Bioinformatics* **22**: 1158–1165.
- Holm, M., Ma, L.G., Qu, L.J., and Deng, X.W.** (2002). Two interacting bZIP proteins are direct targets of COP1-mediated control of light-dependent gene expression in Arabidopsis. *Genes Dev.* **16**: 1247–1259.
- Hong, Z., Bednarek, S.Y., Blumwald, E., Hwang, I., Jurgens, G., Menzel, D., Osteryoung, K.W., Raikhel, N.V., Shinozaki, K., Tsutsumi, N., and Verma, D.P.S.** (2003). A unified nomenclature for Arabidopsis dynamin-related large GTPases based on homology and possible functions. *Plant Mol. Biol.* **53**: 261–265.
- Hoppins, S., Lackner, L., and Nunnari, J.** (2007). The machines that divide and fuse mitochondria. *Annu. Rev. Biochem.* **76**: 751–780.
- Houtkooper, R.H. and Vaz, F.M.** (2008). Cardiolipin, the heart of mitochondrial metabolism. *Cell. Mol. Life Sci.* **65**: 2493–2506.
- Howell, K.A., Millar, A.H., and Whelan, J.** (2006). Ordered assembly of mitochondria during rice germination begins with promitochondrial structures rich in components of the protein import apparatus. *Plant Mol. Biol.* **60**: 201–223.
- Hu, J., Aguirre, M., Peto, C., Alonso, J., Ecker, J., and Chory, J.** (2002). A role for peroxisomes in photomorphogenesis and development of Arabidopsis. *Science* **297**: 405–9.

- Hu, J., Baker, A., Bartel, B., Linka, N., Mullen, R.T., Reumann, S., and Zolman, B.K.** (2012). Plant peroxisomes: biogenesis and function. *Plant Cell* **24**: 2279–2303.
- Hu, J. and Desai, M.** (2008). Light control of peroxisome proliferation during *Arabidopsis* photomorphogenesis. *Plant Signal. Behav.* **3**: 801–803.
- Hua, S. and Sun, Z.** (2001). Support vector machine approach for protein subcellular localization prediction. *Bioinformatics* **17**: 721–728.
- Huang, H. and Frohman, M.A.** (2009). Lipid signaling on the mitochondrial surface. *Biochim. Biophys. Acta* **1791**: 839–844.
- Huang, H., Gao, Q., Peng, X., Choi, S.Y., Sarma, K., Ren, H., Morris, A.J., and Frohman, M.A.** (2011). PiRNA-Associated Germline Nuage Formation and Spermatogenesis Require MitoPLD Profusogenic Mitochondrial-Surface Lipid Signaling. *Dev. Cell* **20**: 376–387.
- Huang, P., Altshuler, Y.M., Hou, J.C., Pessin, J.E., and Frohman, M.A.** (2005). Insulin-stimulated plasma membrane fusion of Glut4 glucose transporter-containing vesicles is regulated by phospholipase D1. *Mol. Biol. Cell* **16**: 2614–2623.
- Ingerman, E., Perkins, E.M., Marino, M., Mears, J. a, McCaffery, J.M., Hinshaw, J.E., and Nunnari, J.** (2005). Dnm1 forms spirals that are structurally tailored to fit mitochondria. *J. Cell Biol.* **170**: 1021–1027.
- Ishihara, N., Fujita, Y., Oka, T., and Mihara, K.** (2006). Regulation of mitochondrial morphology through proteolytic cleavage of OPA1. *EMBO J.* **25**: 2966–2977.
- Ito, J., Batth, T.S., Petzold, C.J., Redding-Johanson, A.M., Mukhopadhyay, A., Verboom, R., Meyer, E.H., Millar, A.H., and Heazlewood, J.L.** (2011). Analysis of the *Arabidopsis* cytosolic proteome highlights subcellular partitioning of central plant metabolism. *J. Proteome Res.* **10**: 1571–1582.
- Iyer, K., Bürkle, L., Auerbach, D., Thaminy, S., Dinkel, M., Engels, K., and Stagljar, I.** (2005). Utilizing the split-ubiquitin membrane yeast two-hybrid system to identify protein-protein interactions of integral membrane proteins. *Sci. STKE* **2005**: pl3.
- Jacoby, R.P., Li, L., Huang, S., Pong Lee, C., Millar, a H., and Taylor, N.L.** (2012). Mitochondrial composition, function and stress response in plants. *J. Integr. Plant Biol.* **54**: 887–906.
- Jagasia, R., Grote, P., Westermann, B., and Conradt, B.** (2005). DRP-1-mediated mitochondrial fragmentation during EGL-1-induced cell death in *C. elegans*. *Nature* **433**: 754–760.

- James, D.I., Parone, P.A., Mattenberger, Y., and Martinou, J.-C.** (2003). hFis1, a novel component of the mammalian mitochondrial fission machinery. *J. Biol. Chem.* **278**: 36373–36379.
- Jänsch, L., Kruff, V., Schmitz, U.K., and Braun, H.P.** (1998). Unique composition of the preprotein translocase of the outer mitochondrial membrane from plants. *J. Biol. Chem.* **273**: 17251–17257.
- Jarvis, P. and López-Juez, E.** (2013). Biogenesis and homeostasis of chloroplasts and other plastids. *Nat. Rev. Mol. Cell Biol.* **14**: 787–802.
- Joshi, A.S., Thompson, M.N., Fei, N., Hüttemann, M., and Greenberg, M.L.** (2012a). Cardiolipin and mitochondrial phosphatidylethanolamine have overlapping functions in mitochondrial fusion in *Saccharomyces cerevisiae*. *J. Biol. Chem.* **287**: 17589–17597.
- Joshi, S., Agrawal, G., and Subramani, S.** (2012b). Phosphorylation-dependent Pex11p and Fis1p interaction regulates peroxisome division. *Mol. Biol. Cell* **23**: 1307–1315.
- Kaewsuya, P., Danielson, N.D., and Ekhterae, D.** (2007). Fluorescent determination of cardiolipin using 10-N-nonyl acridine orange. *Anal. Bioanal. Chem.* **387**: 2775–2782.
- Kagan, V.E. et al.** (2005). Cytochrome c acts as a cardiolipin oxygenase required for release of proapoptotic factors. *Nat. Chem. Biol.* **1**: 223–232.
- Karbowski, M., Neutzner, A., and Youle, R.J.** (2007). The mitochondrial E3 ubiquitin ligase MARCH5 is required for Drp1 dependent mitochondrial division. *J. Cell Biol.* **178**: 71–84.
- Karren, M.A., Coonrod, E.M., Anderson, T.K., and Shaw, J.M.** (2005). The role of Fis1p-Mdv1p interactions in mitochondrial fission complex assembly. *J. Cell Biol.* **171**: 291–301.
- Kashatus, D.F., Lim, K.-H., Brady, D.C., Pershing, N.L.K., Cox, A.D., and Counter, C.M.** (2011). RALA and RALBP1 regulate mitochondrial fission at mitosis. *Nat. Cell Biol.* **13**: 1108–1115.
- Katayama, K., Sakurai, I., and Wada, H.** (2004). Identification of an *Arabidopsis thaliana* gene for cardiolipin synthase located in mitochondria. *FEBS Lett.* **577**: 193–198.
- Katayama, K. and Wada, H.** (2012). T-DNA Insertion in the CLS Gene for Cardiolipin Synthase Affects Development of *Arabidopsis thaliana*. *Cytologia (Tokyo)*. **77**: 123–129.

- Kaur, N. and Hu, J.** (2009). Dynamics of peroxisome abundance: a tale of division and proliferation. *Curr. Opin. Plant Biol.* **12**: 781–788.
- Kaur, N., Reumann, S., and Hu, J.** (2009). Peroxisome Biogenesis and Function. **7**: 1–41.
- Kaur, N., Zhao, Q., Xie, Q., and Hu, J.** (2013). Arabidopsis RING peroxins are E3 ubiquitin ligases that interact with two homologous ubiquitin receptor proteins(F). *J. Integr. Plant Biol.* **55**: 108–120.
- Kawai, F., Shoda, M., and Harashima, R.** (2004). Cardiolipin domains in *Bacillus subtilis* marburg membranes. *J. Bacteriol.* **186**: 1475–1483.
- Keeling, P.J.** (2010). The endosymbiotic origin, diversification and fate of plastids. *Philos. Trans. R. Soc. Lond. B. Biol. Sci.* **365**: 729–748.
- Kerscher, O., Felberbaum, R., and Hochstrasser, M.** (2006). Modification of proteins by ubiquitin and ubiquitin-like proteins. *Annu. Rev. Cell Dev. Biol.* **22**: 159–180.
- Khanam, S.M., Naydenov, N.G., Kadowaki, K., and Nakamura, C.** (2007). Mitochondrial biogenesis as revealed by mitochondrial transcript profiles during germination and early seedling growth in wheat. *Genes Genet. Syst.* **82**: 409–420.
- Kinner, A. and Kölling, R.** (2003). The yeast deubiquitinating enzyme Ubp16 is anchored to the outer mitochondrial membrane. *FEBS Lett.* **549**: 135–140.
- Kittanakom, S., Chuk, M., Wong, V., Snyder, J., Edmonds, D., Lydakis, A., Zhang, Z., Auerbach, D., and Stagljar, I.** (2009). Analysis of membrane protein complexes using the split-ubiquitin membrane yeast two-hybrid (MYTH) system. *Methods Mol. Biol.* **548**: 247–71.
- Kleffmann, T., Russenberger, D., Von Zychlinski, A., Christopher, W., Sjölander, K., Gruissem, W., and Baginsky, S.** (2004). The *Arabidopsis thaliana* chloroplast proteome reveals pathway abundance and novel protein functions. *Curr. Biol.* **14**: 354–362.
- Knoblach, B. and Rachubinski, R.A.** (2010). Phosphorylation-dependent activation of peroxisome proliferator protein PEX11 controls peroxisome abundance. *J. Biol. Chem.* **285**: 6670–6680.
- Kobayashi, S., Tanaka, A., and Fujiki, Y.** (2007). Fis1, DLP1, and Pex11p coordinately regulate peroxisome morphogenesis. *Exp. Cell Res.* **313**: 1675–1686.
- Koch, A., Thiemann, M., Grabenbauer, M., Yoon, Y., McNiven, M.A., and Schrader, M.** (2003). Dynamin-like protein 1 is involved in peroxisomal fission. *J. Biol. Chem.* **278**: 8597–8605.

- Koch, A., Yoon, Y., Bonekamp, N.A., McNiven, M.A., and Schrader, M.** (2005). A role for Fis1 in both mitochondrial and peroxisomal fission in mammalian cells. *Mol. Biol. Cell* **16**: 5077–5086.
- Koehler, C.M., Merchant, S., Oppliger, W., Schmid, K., Jarosch, E., Dolfini, L., Junne, T., Schatz, G., and Tokatlidis, K.** (1998). Tim9p, an essential partner subunit of Tim10p for the import of mitochondrial carrier proteins. *EMBO J.* **17**: 6477–6486.
- Komander, D. and Rape, M.** (2012). The ubiquitin code. *Annu. Rev. Biochem.* **81**: 203–229.
- Kooijman, E.E., Chupin, V., de Kruijff, B., and Burger, K.N.J.** (2003). Modulation of membrane curvature by phosphatidic acid and lysophosphatidic acid. *Traffic* **4**: 162–174.
- Korobova, F., Ramabhadran, V., and Higgs, H.N.** (2013). An actin-dependent step in mitochondrial fission mediated by the ER-associated formin INF2. *Science* **339**: 464–467.
- Kruff, V., Eubel, H., and Jansch, L.** (2001). Proteomic approach to identify novel mitochondrial proteins in Arabidopsis. *Plant Physiol.* **127**: 1694–1710.
- Kurepa, J., Walker, J.M., Smalle, J., Gosink, M.M., Davis, S.J., Durham, T.L., Sung, D.-Y., and Vierstra, R.D.** (2003). The small ubiquitin-like modifier (SUMO) protein modification system in Arabidopsis. Accumulation of SUMO1 and -2 conjugates is increased by stress. *J. Biol. Chem.* **278**: 6862–6872.
- Kuwana, T., Mackey, M.R., Perkins, G., Ellisman, M.H., Latterich, M., Schneider, R., Green, D.R., and Newmeyer, D.D.** (2002). Bid, Bax, and lipids cooperate to form supramolecular openings in the outer mitochondrial membrane. *Cell* **111**: 331–342.
- Kwasniak, M., Pogorzelec, L., Migdal, I., Smakowska, E., and Janska, H.** (2012). Proteolytic system of plant mitochondria. *Physiol. Plant.* **145**: 187–195.
- Labrousse, a M., Zappaterra, M.D., Rube, D. a, and van der Bliek, a M.** (1999). C. elegans dynamin-related protein DRP-1 controls severing of the mitochondrial outer membrane. *Mol. Cell* **4**: 815–826.
- Lane, N. and Martin, W.** (2010). The energetics of genome complexity. *Nature* **467**: 929–934.
- Lanyon-Hogg, T., Warriner, S.L., and Baker, A.** (2010). Getting a camel through the eye of a needle: the import of folded proteins by peroxisomes. *Biol. Cell* **102**: 245–263.

- Law, S.R., Narsai, R., and Whelan, J.** (2014). Mitochondrial biogenesis in plants during seed germination. *Mitochondrion*: in press.
- Legesse-Miller, A., Massol, R.H., and Kirchhausen, T.** (2003). Constriction and Dnm1p recruitment are distinct processes in mitochondrial fission. *Mol. Biol. Cell* **14**: 1953–1963.
- Lenarcic, R., Halbedel, S., Visser, L., Shaw, M., Wu, L.J., Errington, J., Marenduzzo, D., and Hamoen, L.W.** (2009). Localisation of DivIVA by targeting to negatively curved membranes. *EMBO J.* **28**: 2272–2282.
- Lewis, R.N. A. H. and McElhaney, R.N.** (2009). The physicochemical properties of cardiolipin bilayers and cardiolipin-containing lipid membranes. *Biochim. Biophys. Acta* **1788**: 2069–2079.
- Li, F., Chung, T., and Vierstra, R.D.** (2014). AUTOPHAGY-RELATED11 Plays a Critical Role in General Autophagy- and Senescence-Induced Mitophagy in Arabidopsis.
- Li, J.-F., Park, E., von Arnim, A.G., and Nebenführ, A.** (2009). The FAST technique: a simplified Agrobacterium-based transformation method for transient gene expression analysis in seedlings of Arabidopsis and other plant species. *Plant Methods* **5**: 6.
- Li, W., Bengtson, M.H., Ulbrich, A., Matsuda, A., Reddy, V.A., Orth, A., Chanda, S.K., and Batalov, S.** (2008). Genome-Wide and Functional Annotation of Human E3 Ubiquitin Ligases Identifies MULAN, a Mitochondrial E3 that Regulates the Organelle's Dynamics and Signaling. *PLoS One* **3**: e1487.
- Li, X. and Gould, S.J.** (2003). The dynamin-like GTPase DLP1 is essential for peroxisome division and is recruited to peroxisomes in part by PEX11. *J. Biol. Chem.* **278**: 17012–17020.
- Ling, Q., Huang, W., Baldwin, A., and Jarvis, P.** (2012). Chloroplast biogenesis is regulated by direct action of the ubiquitin-proteasome system. *Science* **338**: 655–659.
- Lingard, M. and Trelease, R.** (2006). Five Arabidopsis peroxin 11 homologs individually promote peroxisome elongation, duplication or aggregation. *J. Cell Sci.* **119**: 1961–1972.
- Lingard, M.J. and Bartel, B.** (2009). Arabidopsis LON2 is necessary for peroxisomal function and sustained matrix protein import. *Plant Physiol.* **151**: 1354–1365.
- Lingard, M.J., Gidda, S.K., Bingham, S., Rothstein, S.J., Mullen, R.T., and Trelease, R.N.** (2008). Arabidopsis PEROXIN11c-e, FISSION1b, and DYNAMIN-RELATED

PROTEIN3A cooperate in cell cycle-associated replication of peroxisomes. *Plant Cell* **20**: 1567–1585.

Lingard, M.J., Monroe-Augustus, M., and Bartel, B. (2009). Peroxisome-associated matrix protein degradation in Arabidopsis. *Proc. Natl. Acad. Sci. U. S. A.* **106**: 4561–4566.

Lister, R., Carrie, C., Duncan, O., Ho, L.H.M., Howell, K. a, Murcha, M.W., and Whelan, J. (2007). Functional definition of outer membrane proteins involved in preprotein import into mitochondria. *Plant Cell* **19**: 3739–3759.

Lister, R., Chew, O., and Lee, M. (2004). A transcriptomic and proteomic characterization of the Arabidopsis mitochondrial protein import apparatus and its response to mitochondrial dysfunction. *Plant Physiol.* **134**: 777–789.

Lister, R., Mowday, B., Whelan, J., and Millar, A.H. (2002). Zinc-dependent intermembrane space proteins stimulate import of carrier proteins into plant mitochondria. *Plant J.* **30**: 555–566.

Liu, T., Yu, R., Jin, S.-B., Han, L., Lendahl, U., Zhao, J., and Nistér, M. (2013). The mitochondrial elongation factors MIEF1 and MIEF2 exert partially distinct functions in mitochondrial dynamics. *Exp. Cell Res.* **319**: 2893–2904.

Liu, Y., Wang, F., Zhang, H., He, H., Ma, L., and Deng, X.W. (2008). Functional characterization of the Arabidopsis ubiquitin-specific protease gene family reveals specific role and redundancy of individual members in development. *Plant J.* **55**: 844–856.

Livnat-Levanon, N. and Glickman, M.H. (2011). Ubiquitin-proteasome system and mitochondria - reciprocity. *Biochim. Biophys. Acta* **1809**: 80–87.

Logan, D.C. (2010). The dynamic plant chondriome. *Semin. Cell Dev. Biol.* **21**: 550–557.

Logan, D.C., Millar, A.H., Sweetlove, L.J., Hill, S.A., and Leaver, C.J. (2001). Mitochondrial biogenesis during germination in maize embryos. *Plant Physiol.* **125**: 662–672.

Logan, D.C., Scott, I., and Tobin, A.K. (2004). ADL2a, like ADL2b, is involved in the control of higher plant mitochondrial morphology. *J. Exp. Bot.* **55**: 783–785.

Lord, C.E.N. and Gunawardena, A.H.L.A.N. (2012). Programmed cell death in *C. elegans*, mammals and plants. *Eur. J. Cell Biol.* **91**: 603–613.

Losón, O.C., Song, Z., Chen, H., and Chan, D.C. (2013). Fis1, Mff, MiD49, and MiD51 mediate Drp1 recruitment in mitochondrial fission. *Mol. Biol. Cell* **24**: 659–667.

- Lovering, R., Hanson, I.M., Borden, K.L., Martin, S., O'Reilly, N.J., Evan, G.I., Rahman, D., Pappin, D.J., Trowsdale, J., and Freemont, P.S.** (1993). Identification and preliminary characterization of a protein motif related to the zinc finger. *Proc. Natl. Acad. Sci. U. S. A.* **90**: 2112–2116.
- Luo, M., Luo, M.-Z., Buzas, D., Finnegan, J., Helliwell, C., Dennis, E.S., Peacock, W.J., and Chaudhury, A.** (2008). UBIQUITIN-SPECIFIC PROTEASE 26 is required for seed development and the repression of PHERES1 in Arabidopsis. *Genetics* **180**: 229–236.
- Lutter, M., Fang, M., Luo, X., Nishijima, M., Xie, X., and Wang, X.** (2000). Cardiolipin provides specificity for targeting of tBid to mitochondria. *Nat. Cell Biol.* **2**: 754–761.
- Macasev, D., Newbigin, E., Whelan, J., and Lithgow, T.** (2000). How Do Plant Mitochondria Avoid Importing Chloroplast Proteins? Components of the Import Apparatus Tom20 and Tom22 from Arabidopsis Differ from Their Fungal Counterparts. *Plant Physiol.* **123**: 811–816.
- Magdalan, J., Ostrowska, A., Podhorska-Okołów, M., Piotrowska, A., Izykowska, I., Nowak, M., Dolińska-Krajewska, B., Zabel, M., Szelag, A., and Dziegiel, P.** (2009). Early morphological and functional alterations in canine hepatocytes due to alpha-amanitin, a major toxin of *Amanita phalloides*. *Arch. Toxicol.* **83**: 55–60.
- Malamed, S.** (1965). Structural changes during swelling of isolated rat mitochondria. *Zeitschrift fur Zellforsch.* **15**: 10–15.
- Mannella, C. a, Pfeiffer, D.R., Bradshaw, P.C., Moraru, I.I., Slepchenko, B., Loew, L.M., Hsieh, C.E., Buttle, K., and Marko, M.** (2001). Topology of the mitochondrial inner membrane: dynamics and bioenergetic implications. *IUBMB Life* **52**: 93–100.
- Mano, S., Nakamori, C., Kondo, M., Hayashi, M., and Nishimura, M.** (2004). An Arabidopsis dynamin-related protein, DRP3A, controls both peroxisomal and mitochondrial division. *Plant J.* **38**: 487–498.
- Mano, S., Nakamori, C., Nito, K., Kondo, M., and Nishimura, M.** (2006). The Arabidopsis pex12 and pex13 mutants are defective in both PTS1- and PTS2-dependent protein transport to peroxisomes. *Plant J.* **47**: 604–618.
- Marchi, S., Patergnani, S., and Pinton, P.** (2014). The endoplasmic reticulum-mitochondria connection: one touch, multiple functions. *Biochim. Biophys. Acta* **1837**: 461–469.
- Marsh, D.** (2008). Protein modulation of lipids, and vice-versa, in membranes. *Biochim. Biophys. Acta - Biomembr.* **1778**: 1545–1575.

- Matsuda, N., Suzuki, T., Tanaka, K., and Nakano, A.** (2001). Rma1, a novel type of RING finger protein conserved from Arabidopsis to human, is a membrane-bound ubiquitin ligase. *J. Cell Sci.* **114**: 1949–1957.
- Mayank, P., Grossman, J., Wuest, S., Boisson-Dernier, A., Roschitzki, B., Nanni, P., Nühse, T., and Grossniklaus, U.** (2012). Characterization of the phosphoproteome of mature Arabidopsis pollen. *Plant J.* **72**: 89–101.
- Meeusen, S., DeVay, R., Block, J., Cassidy-Stone, A., Wayson, S., McCaffery, J.M., and Nunnari, J.** (2006). Mitochondrial Inner-Membrane Fusion and Crista Maintenance Requires the Dynamin-Related GTPase Mgm1. *Cell* **127**: 383–395.
- Mileykovskaya, E. and Dowhan, W.** (2000). Visualization of phospholipid domains in *Escherichia coli* by using the cardiolipin-specific fluorescent dye 10-N-nonyl acridine orange. *J. Bacteriol.* **182**: 1172–1175.
- Millar, A.H., Heazlewood, J.L., Kristensen, B.K., Braun, H.P., and Møller, I.M.** (2005). The plant mitochondrial proteome. *Trends Plant Sci.* **10**: 36–43.
- Millar, A.H., Small, I.D., Day, D.A., and Whelan, J.** (2008). Mitochondrial Biogenesis and Function in Arabidopsis. In *The Arabidopsis Book*, pp. 1–36.
- Mishra, P., Carelli, V., Manfredi, G., and Chan, D.C.** (2014). Proteolytic cleavage of Opa1 stimulates mitochondrial inner membrane fusion and couples fusion to oxidative phosphorylation. *Cell Metab.* **19**: 630–641.
- Miyagishima, S., Kuwayama, H., Urushihara, H., and Nakanishi, H.** (2008). Evolutionary linkage between eukaryotic cytokinesis and chloroplast division by dynamin proteins. *Proc. Natl. Acad. Sci. U. S. A.* **105**: 15202–15207.
- Moellering, E.R. and Benning, C.** (2010). Phosphate regulation of lipid biosynthesis in Arabidopsis is independent of the mitochondrial outer membrane DGS1 complex. *Plant Physiol.* **152**: 1951–1959.
- Molnár, G., Bancoş, S., Nagy, F., and Szekeres, M.** (2002). Characterisation of BRH1, a brassinosteroid-responsive RING-H2 gene from Arabidopsis thaliana. *Planta* **215**: 127–133.
- Montessuit, S., Somasekharan, S.P., Terrones, O., Lucken-Ardjomande, S., Herzig, S., Schwarzenbacher, R., Manstein, D.J., Bossy-Wetzel, E., Basañez, G., Meda, P., and Martinou, J.C.** (2010). Membrane remodeling induced by the dynamin-related protein Drp1 stimulates Bax oligomerization. *Cell* **142**: 889–901.
- Moon, B.C., Choi, M.S., Kang, Y.H., Kim, M.C., Cheong, M.S., Park, C.Y., Yoo, J.H., Koo, S.C., Lee, S.M., Lim, C.O., Cho, M.J., and Chung, W.S.** (2005). Arabidopsis

- ubiquitin-specific protease 6 (AtUBP6) interacts with calmodulin. *FEBS Lett.* **579**: 3885–3890.
- Motley, A.M., Ward, G.P., and Hetteema, E.H.** (2008). Dnm1p-dependent peroxisome fission requires Caf4p, Mdv1p and Fis1p. *J. Cell Sci.* **121**: 1633–1640.
- Muliyil, S., Krishnakumar, P., and Narasimha, M.** (2011). Spatial, temporal and molecular hierarchies in the link between death, delamination and dorsal closure. *Development* **138**: 3043–3054.
- Mullen, R.T. and Trelease, R.N.** (2006). The ER-peroxisome connection in plants: Development of the “ER semi-autonomous peroxisome maturation and replication” model for plant peroxisome biogenesis. *Biochim. Biophys. Acta - Mol. Cell Res.* **1763**: 1655–1668.
- Myron, D.R. and Connelly, J.L.** (1971). The morphology of the swelling process in rat liver mitochondria. *J. Cell Biol.* **48**: 291–302.
- Nagotu, S., Krikken, A.M., Otzen, M., Kiel, J. a K.W., Veenhuis, M., and van der Klei, I.J.** (2008). Peroxisome fission in *Hansenula polymorpha* requires Mdv1 and Fis1, two proteins also involved in mitochondrial fission. *Traffic* **9**: 1471–1484.
- Nagotu, S., Veenhuis, M., and Van der Klei, I.J.** (2010). Divide et impera: The dictum of peroxisomes. *Traffic* **11**: 175–184.
- Nakagami, H., Sugiyama, N., Mochida, K., Daudi, A., Yoshida, Y., Toyoda, T., Tomita, M., Ishihama, Y., and Shirasu, K.** (2010). Large-scale comparative phosphoproteomics identifies conserved phosphorylation sites in plants. *Plant Physiol.* **153**: 1161–1174.
- Nakagawa, T. et al.** (2007). Improved Gateway Binary Vectors: High-Performance Vectors for Creation of Fusion Constructs in Transgenic Analysis of Plants. *Biosci. Biotechnol. Biochem.* **71**: 2095–2100.
- Nakamura, K. et al.** (2011). Direct membrane association drives mitochondrial fission by the Parkinson disease-associated protein alpha-synuclein. *J. Biol. Chem.* **286**: 20710–20726.
- Nakamura, N., Kimura, Y., Tokuda, M., Honda, S., and Hirose, S.** (2006). MARCH-V is a novel mitofusin 2- and Drp1-binding protein able to change mitochondrial morphology. *EMBO Rep.* **7**: 1019–1022.
- Nakamura, N. and Shigehisa, H.** (2008). Regulation of Mitochondrial Morphology by USP30 , a Deubiquitinating Enzyme Present in the Mitochondrial Outer Membrane. *Mol. Biol. Cell* **19**: 1903–1911.

- Nakamura, T., Cieplak, P., Cho, D.H., Godzik, A., and Lipton, S.A.** (2010). S-Nitrosylation of Drp1 links excessive mitochondrial fission to neuronal injury in neurodegeneration. *Mitochondrion* **10**: 573–578.
- Narsai, R., Law, S.R., Carrie, C., Xu, L., and Whelan, J.** (2011). In-Depth Temporal Transcriptome Profiling Reveals a Crucial Developmental Switch with Roles for RNA Processing and Organelle Metabolism That Are Essential for Germination in Arabidopsis. *Plant Physiol.* **157**: 1342–1362.
- Naydenov, N.G., Khanam, S.M., Atanassov, A., and Nakamura, C.** (2008). Expression profiles of respiratory components associated with mitochondrial biogenesis during germination and seedling growth under normal and restricted conditions in wheat. *Genes Genet. Syst.* **83**: 31–41.
- Naylor, K., Ingerman, E., Okreglak, V., Marino, M., Hinshaw, J.E., and Nunnari, J.** (2006). Mdv1 interacts with assembled dnm1 to promote mitochondrial division. *J. Biol. Chem.* **281**: 2177–2183.
- Nelson, B.K., Cai, X., and Nebenführ, A.** (2007). A multicolored set of in vivo organelle markers for co-localization studies in Arabidopsis and other plants. *Plant J.* **51**: 1126–1136.
- Neuhaus, H.E. and Emes, M.J.** (2000). Nonphotosynthetic metabolism in plastids. *Annu. Rev. Plant Physiol. Plant Mol. Biol.* **51**: 111–140.
- Neuspiel, M., Schauss, A.C., Braschi, E., Zunino, R., Rippstein, P., Rachubinski, R. a, Andrade-Navarro, M. a, and McBride, H.M.** (2008). Cargo-selected transport from the mitochondria to peroxisomes is mediated by vesicular carriers. *Curr. Biol.* **18**: 102–108.
- Nijman, S.M.B., Luna-Vargas, M.P. a, Velds, A., Brummelkamp, T.R., Dirac, A.M.G., Sixma, T.K., and Bernards, R.** (2005). A genomic and functional inventory of deubiquitinating enzymes. *Cell* **123**: 773–786.
- Nishida, K., Yagisawa, F., Kuroiwa, H., Yoshida, Y., and Kuroiwa, T.** (2007). WD40 protein Mda1 is purified with Dnm1 and forms a dividing ring for mitochondria before Dnm1 in Cyanidioschyzon merolae. *Proc. Natl. Acad. Sci. U. S. A.* **104**: 4736–4741.
- Nito, K., Hayashi, M., and Nishimura, M.** (2002). Direct interaction and determination of binding domains among peroxisomal import factors in Arabidopsis thaliana. *Plant Cell Physiol.* **43**: 355–366.
- Nito, K., Kamigaki, A., Kondo, M., Hayashi, M., and Nishimura, M.** (2007). Functional classification of Arabidopsis peroxisome biogenesis factors proposed from analyses of knockdown mutants. *Plant Cell Physiol.* **48**: 763–774.

- Nowicki, M., Müller, F., and Frentzen, M.** (2005). Cardiolipin synthase of *Arabidopsis thaliana*. *FEBS Lett.* **579**: 2161–2165.
- Nyathi, Y. and Baker, A.** (2006). Plant peroxisomes as a source of signalling molecules. *Biochim. Biophys. Acta - Mol. Cell Res.* **1763**: 1478–1495.
- Opaliński, Ł., Kiel, J. a K.W., Williams, C., Veenhuis, M., and van der Klei, I.J.** (2011). Membrane curvature during peroxisome fission requires Pex11. *EMBO J.* **30**: 5–16.
- Orth, T., Reumann, S., Zhang, X., Fan, J., Wenzel, D., Quan, S., and Hu, J.** (2007). The PEROXIN11 protein family controls peroxisome proliferation in *Arabidopsis*. *Plant Cell* **19**: 333–350.
- Ortiz, A., Killian, J.A., Verkleij, A.J., and Wilschut, J.** (1999). Membrane fusion and the lamellar-to-inverted-hexagonal phase transition in cardiolipin vesicle systems induced by divalent cations. *Biophys. J.* **77**: 2003–2014.
- Osman, C., Voelker, D.R., and Langer, T.** (2011). Making heads or tails of phospholipids in mitochondria. *J. Cell Biol.* **192**: 7–16.
- Otera, H., Wang, C., Cleland, M.M., Setoguchi, K., Yokota, S., Youle, R.J., and Mihara, K.** (2010). Mff is an essential factor for mitochondrial recruitment of Drp1 during mitochondrial fission in mammalian cells. *J. Cell Biol.* **191**: 1141–1158.
- Paepe, R. de, Lemaire, S.D., and Danon, A.** (2014). Cardiolipin at the heart of stress response across kingdoms. *Plant Signal. Behav.* **9**: e29228.
- Palikaras, K. and Tavernarakis, N.** (2014). Mitochondrial homeostasis: The interplay between mitophagy and mitochondrial biogenesis. *Exp. Gerontol.* **56**: 182–188.
- Palmer, C.S., Osellame, L.D., Laine, D., Koutsopoulos, O.S., Frazier, A.E., and Ryan, M.T.** (2011a). MiD49 and MiD51, new components of the mitochondrial fission machinery. *EMBO Rep.* **12**: 565–573.
- Palmer, C.S., Osellame, L.D., Stojanovski, D., and Ryan, M.T.** (2011b). The regulation of mitochondrial morphology: intricate mechanisms and dynamic machinery. *Cell. Signal.* **23**: 1534–1545.
- Pan, R., Jones, A.D., and Hu, J.** (2014a). Cardiolipin-Mediated Mitochondrial Dynamics and Stress Response in *Arabidopsis*. *Plant Cell* **26**: 391–409.
- Pan, R., Kaur, N., and Hu, J.** (2014b). The *Arabidopsis* mitochondrial membrane-bound ubiquitin protease UBP27 contributes to mitochondrial morphogenesis. *Plant J.* **78**: 1047–1059.

- Paradies, G., Paradies, V., De Benedictis, V., Ruggiero, F.M., and Petrosillo, G.** (2013). Functional role of cardiolipin in mitochondrial bioenergetics. *Biochim. Biophys. Acta* **1837**: 408–417.
- Pendle, A.F., Clark, G.P., Boon, R., Lewandowska, D., Lam, Y.W., Andersen, J., Mann, M., Lamond, A.I., Brown, J.W.S., and Shaw, P.J.** (2005). Proteomic analysis of the Arabidopsis nucleolus suggests novel nucleolar functions. *Mol. Biol. Cell* **16**: 260–269.
- Peterhansel, C., Horst, I., Niessen, M., Blume, C., Kebeish, R., Kürkcüoglu, S., and Kreuzaler, F.** (2010). Photorespiration. In *The Arabidopsis book*, p. e0130.
- Petriv, O.I., Tang, L., Titorenko, V.I., and Rachubinski, R.A.** (2004). A new definition for the consensus sequence of the peroxisome targeting signal type 2. *J. Mol. Biol.* **341**: 119–134.
- Pineau, B., Bourge, M., and Marion, J.** (2013). The Importance of Cardiolipin Synthase for Mitochondrial Ultrastructure, Respiratory Function, Plant Development, and Stress Responses in Arabidopsis. *Plant Cell* **25**: 4195–4208.
- Praefcke, G.J.K. and McMahon, H.T.** (2004). The dynamin superfamily: universal membrane tubulation and fission molecules? *Nat. Rev. Mol. Cell Biol.* **5**: 133–147.
- Ptacek, J. et al.** (2005). Global analysis of protein phosphorylation in yeast. *Nature* **438**: 679–684.
- Purdue, P.E. and Lazarow, P.B.** (2001). Peroxisome biogenesis. *Annu. Rev. Cell Dev. Biol.* **17**: 701–752.
- Rapaport, D.** (2003). Finding the right organelle. Targeting signals in mitochondrial outer-membrane proteins. *EMBO Rep.* **4**: 948–952.
- Rapaport, D., Brunner, M., Neupert, W., and Westermann, B.** (1998). Fzo1p is a mitochondrial outer membrane protein essential for the biogenesis of functional mitochondria in *Saccharomyces cerevisiae*. *J. Biol. Chem.* **273**: 20150–20155.
- Rassow, J. and Pfanner, N.** (2000). The protein import machinery of the mitochondrial membranes. *Traffic* **1**: 457–464.
- Ratzel, S., Lingard, M., Woodward, A., and Bartel, B.** (2011). Reducing PEX13 Expression Ameliorates Physiological Defects of Late -Acting Pero
Traffic **12**: 121–134.
- Renner, L. and Weibel, D.** (2011). Cardiolipin microdomains localize to negatively curved regions of *Escherichia coli* membranes. *Proc. Natl. Acad. Sci. U. S. A.* **108**: 6264–6269.

- Renner, L.D. and Weibel, D.B.** (2012). MinD and MinE interact with anionic phospholipids and regulate division plane formation in *Escherichia coli*. *J. Biol. Chem.* **287**: 38835–38844.
- Reumann, S., Quan, S., Aung, K., Yang, P., Manandhar-Shrestha, K., Holbrook, D., Linka, N., Switzenberg, R., Wilkerson, C.G., Weber, A.P.M., Olsen, L.J., and Hu, J.** (2009). In-depth proteome analysis of *Arabidopsis* leaf peroxisomes combined with in vivo subcellular targeting verification indicates novel metabolic and regulatory functions of peroxisomes. *Plant Physiol.* **150**: 125–143.
- Reumann, S. and Weber, A.P.M.** (2006). Plant peroxisomes respire in the light: Some gaps of the photorespiratory C2 cycle have become filled-Others remain. *Biochim. Biophys. Acta - Mol. Cell Res.* **1763**: 1496–1510.
- Reyes-Turcu, F.E., Ventii, K.H., and Wilkinson, K.D.** (2009). Regulation and cellular roles of ubiquitin-specific deubiquitinating enzymes. *Annu. Rev. Biochem.* **78**: 363–397.
- Rikova, K. et al.** (2007). Global Survey of Phosphotyrosine Signaling Identifies Oncogenic Kinases in Lung Cancer. *Cell* **131**: 1190–1203.
- Rimmer, K.A., Foo, J.H., Ng, A., Petrie, E.J., Shilling, P.J., Perry, A.J., Mertens, H.D.T., Lithgow, T., Mulhern, T.D., and Gooley, P.R.** (2011). Recognition of mitochondrial targeting sequences by the import receptors Tom20 and Tom22. *J. Mol. Biol.* **405**: 804–818.
- Rissler, M., Wiedemann, N., Pfannschmidt, S., Gabriel, K., Guiard, B., Pfanner, N., and Chacinska, A.** (2005). The essential mitochondrial protein Erv1 cooperates with Mia40 in biogenesis of intermembrane space proteins. *J. Mol. Biol.* **353**: 485–492.
- Rizzuto, R., Pinton, P., Carrington, W., Fay, F.S., Fogarty, K.E., Lifshitz, L.M., Tuft, R.A., and Pozzan, T.** (1998). Close contacts with the endoplasmic reticulum as determinants of mitochondrial Ca²⁺ responses. *Science* **280**: 1763–1766.
- Ruberti, C., Costa, A., Pedrazzini, E., Lo Schiavo, F., and Zottini, M.** (2014). FISSION1A, an *Arabidopsis* tail-anchored protein, is localized to three subcellular compartments. *Mol. Plant* **7**: 1393–1396.
- Rujiviphat, J., Meglei, G., Rubinstein, J.L., and McQuibban, G.A.** (2009). Phospholipid association is essential for dynamin-related protein Mgm1 to function in mitochondrial membrane fusion. *J. Biol. Chem.* **284**: 28682–28686.
- Sadanandom, A., Bailey, M., Ewan, R., Lee, J., and Nelis, S.** (2012). The ubiquitin-proteasome system: central modifier of plant signalling. *New Phytol.* **196**: 13–28.

- Saracco, S. a, Miller, M.J., Kurepa, J., and Vierstra, R.D.** (2007). Genetic analysis of SUMOylation in Arabidopsis: conjugation of SUMO1 and SUMO2 to nuclear proteins is essential. *Plant Physiol.* **145**: 119–134.
- Schauss, A.C., Bewersdorf, J., and Jakobs, S.** (2006). Fis1p and Caf4p, but not Mdv1p, determine the polar localization of Dnm1p clusters on the mitochondrial surface. *J. Cell Sci.* **119**: 3098–3106.
- Schlame, M. and Haldar, D.** (1993). Cardiolipin is synthesized on the matrix side of the inner membrane in rat liver mitochondria. *J Biol Chem* **268**: 74–79.
- Schlame, M., Ren, M., Xu, Y., Greenberg, M.L., and Haller, I.** (2005). Molecular symmetry in mitochondrial cardiolipins. *Chem. Phys. Lipids* **138**: 38–49.
- Schlüter, A., Fourcade, S., Ripp, R., Mandel, J.L., Poch, O., and Pujol, A.** (2006). The evolutionary origin of peroxisomes: An ER-peroxisome connection. *Mol. Biol. Evol.* **23**: 838–845.
- Schmitz, R.J., Tamada, Y., Doyle, M.R., Zhang, X., and Amasino, R.M.** (2009). Histone H2B deubiquitination is required for transcriptional activation of FLOWERING LOCUS C and for proper control of flowering in Arabidopsis. *Plant Physiol.* **149**: 1196–1204.
- Schrader, M. and Fahimi, H.D.** (2008). The peroxisome: Still a mysterious organelle. *Histochem. Cell Biol.* **129**: 421–440.
- Schrader, M. and Yoon, Y.** (2007). Mitochondria and peroxisomes: Are the “Big Brother” and the “Little Sister” closer than assumed? *BioEssays* **29**: 1105–1114.
- Schuldt, A.** (2011). Membrane dynamics: MIEF1 mingles with mitochondria. *Nat. Rev. Mol. Cell Biol.* **12**: 464.
- Schumann, U., Wanner, G., Veenhuis, M., Schmid, M., and Gietl, C.** (2003). AthPEX10, a nuclear gene essential for peroxisome and storage organelle formation during Arabidopsis embryogenesis. *Proc. Natl. Acad. Sci. U. S. A.* **100**: 9626–9631.
- Schwarzländer, M. and Finkemeier, I.** (2013). Mitochondrial energy and redox signaling in plants. *Antioxid. Redox Signal.* **18**: 2122–2144.
- Scott, I., Tobin, A.K., and Logan, D.C.** (2006). BIGYIN, an orthologue of human and yeast FIS1 genes functions in the control of mitochondrial size and number in Arabidopsis thaliana. *J. Exp. Bot.* **57**: 1275–1280.
- Seguí-Simarro, J.M., Coronado, M.J., and Staehelin, L.A.** (2008). The mitochondrial cycle of Arabidopsis shoot apical meristem and leaf primordium meristematic cells

is defined by a perinuclear tentaculate/cage-like mitochondrion. *Plant Physiol.* **148**: 1380–1393.

- Senapin, S., Chen, X.J., and Clark-Walker, G.D.** (2003). Transcription of TIM9, a new factor required for the petite-positive phenotype of *Saccharomyces cerevisiae*, is defective in *spt7* mutants. *Curr. Genet.* **44**: 202–210.
- Serrano, M. and Guzmán, P.** (2004). Isolation and gene expression analysis of *Arabidopsis thaliana* mutants with constitutive expression of ATL2, an early elicitor-response RING-H2 zinc-finger gene. *Genetics* **167**: 919–929.
- Sesaki, H., Dunn, C.D., Iijima, M., Shepard, K. a, Yaffe, M.P., Machamer, C.E., and Jensen, R.E.** (2006). Ups1p, a conserved intermembrane space protein, regulates mitochondrial shape and alternative topogenesis of Mgm1p. *J. Cell Biol.* **173**: 651–658.
- Sesaki, H., Southard, S.M., Yaffe, M.P., and Jensen, R.E.** (2003). Mgm1p, a dynamin-related GTPase, is essential for fusion of the mitochondrial outer membrane. *Mol. Biol. Cell* **14**: 2342–2356.
- Sharkey, T.** (1988). Estimating the rate of photorespiration in leaves. *Physiol. Plant.* **73**: 146–152.
- Sheahan, M.B., McCurdy, D.W., and Rose, R.J.** (2005). Mitochondria as a connected population: Ensuring continuity of the mitochondrial genome during plant cell dedifferentiation through massive mitochondrial fusion. *Plant J.* **44**: 744–755.
- Shi, L.-X. and Theg, S.M.** (2013). The chloroplast protein import system: from algae to trees. *Biochim. Biophys. Acta* **1833**: 314–331.
- Shim, S.-H., Xia, C., Zhong, G., Babcock, H.P., Vaughan, J.C., Huang, B., Wang, X., Xu, C., Bi, G.-Q., and Zhuang, X.** (2012). Super-resolution fluorescence imaging of organelles in live cells with photoswitchable membrane probes. *Proc. Natl. Acad. Sci.* **109**: 13978–13983.
- Small, I., Peeters, N., Legeai, F., and Lurin, C.** (2004). Predotar: A tool for rapidly screening proteomes for N-terminal targeting sequences. *Proteomics* **4**: 1581–1590.
- Smalle, J. and Vierstra, R.D.** (2004). The ubiquitin 26S proteasome proteolytic pathway. *Annu. Rev. Plant Biol.* **55**: 555–590.
- Smirnova, E., Griparic, L., Shurland, D.L., and van der Bliek, A.M.** (2001). Dynamin-related protein Drp1 is required for mitochondrial division in mammalian cells. *Mol. Biol. Cell* **12**: 2245–2256.

- Song, Z., Chen, H., Fiket, M., Alexander, C., and Chan, D.C.** (2007). OPA1 processing controls mitochondrial fusion and is regulated by mRNA splicing, membrane potential, and Yme1L. *J. Cell Biol.* **178**: 749–755.
- Sorice, M., Manganelli, V., Matarrese, P., Tinari, A., Misasi, R., Malorni, W., and Garofalo, T.** (2009). Cardiolipin-enriched raft-like microdomains are essential activating platforms for apoptotic signals on mitochondria. *FEBS Lett.* **583**: 2447–2450.
- Sparkes, I.A., Brandizzi, F., Slocombe, S.P., El-Shami, M., Hawes, C., and Baker, A.** (2003). An Arabidopsis pex10 null mutant is embryo lethal, implicating peroxisomes in an essential role during plant embryogenesis. *Plant Physiol.* **133**: 1809–1819.
- Stagliano, M.C., DeKeyser, J.G., Omiecinski, C.J., and Jones, D.D.** (2010). Bioassay-directed fractionation for discovery of bioactive neutral lipids guided by relative mass defect filtering and multiplexed collision-induced dissociation. *Rapid Commun. Mass Spectrom.* **24**: 3578–3584.
- Ståhl, A., Moberg, P., Ytterberg, J., Panfilov, O., Von Löwenhielm, H.B., Nilsson, F., and Glaser, E.** (2002). Isolation and identification of a novel mitochondrial metalloprotease (PreP) that degrades targeting presequences in plants. *J. Biol. Chem.* **277**: 41931–41939.
- Stojanovski, D., Koutsopoulos, O.S., Okamoto, K., and Ryan, M.T.** (2004). Levels of human Fis1 at the mitochondrial outer membrane regulate mitochondrial morphology. *J. Cell Sci.* **117**: 1201–1210.
- Stone, S.L., Hauksdóttir, H., Troy, A., Herschleb, J., Kraft, E., and Callis, J.** (2005). Functional analysis of the RING-type ubiquitin ligase family of Arabidopsis. *Plant Physiol.* **137**: 13–30.
- Strittmatter, P., Soll, J., and Bölter, B.** (2010). The chloroplast protein import machinery: a review. *Methods Mol. Biol.* **619**: 307–321.
- Sugiyama, N., Nakagami, H., Mochida, K., Daudi, A., Tomita, M., Shirasu, K., and Ishihama, Y.** (2008). Large-scale phosphorylation mapping reveals the extent of tyrosine phosphorylation in Arabidopsis. *Mol. Syst. Biol.* **4**: 193.
- Sun, M.G., Williams, J., Munoz-Pinedo, C., Perkins, G. a, Brown, J.M., Ellisman, M.H., Green, D.R., and Frey, T.G.** (2007). Correlated three-dimensional light and electron microscopy reveals transformation of mitochondria during apoptosis. *Nat. Cell Biol.* **9**: 1057–1065.
- Tadato, B., Heymann, J.A.W., Song, Z., Hinshaw, J.E., and Chan, D.C.** (2010). OPA1 disease alleles causing dominant optic atrophy have defects in cardiolipin-

- stimulated GTP hydrolysis and membrane tubulation. *Hum. Mol. Genet.* **19**: 2113–2122.
- Taguchi, N., Ishihara, N., Jofuku, A., Oka, T., and Mihara, K.** (2007). Mitotic phosphorylation of dynamin-related GTPase Drp1 participates in mitochondrial fission. *J. Biol. Chem.* **282**: 11521–11529.
- Tamura, Y., Endo, T., Iijima, M., and Sesaki, H.** (2009). Ups1p and Ups2p antagonistically regulate cardiolipin metabolism in mitochondria. *J. Cell Biol.* **185**: 1029–1045.
- Tasseva, G., Bai, H.D., Davidescu, M., Haromy, A., Michelakis, E., and Vance, J.E.** (2013). Phosphatidylethanolamine deficiency in mammalian mitochondria impairs oxidative phosphorylation and alters mitochondrial morphology. *J. Biol. Chem.* **288**: 4158–4173.
- Teixeira, P.F. and Glaser, E.** (2013). Processing peptidases in mitochondria and chloroplasts. *Biochim. Biophys. Acta* **1833**: 360–370.
- TerBush, A.D. and Osteryoung, K.W.** (2012). Distinct functions of chloroplast FtsZ1 and FtsZ2 in Z-ring structure and remodeling. *J. Cell Biol.* **199**: 623–637.
- Thaminy, S., Miller, J., and Stagljar, I.** (2004). The split-ubiquitin membrane-based yeast two-hybrid system. *Methods Mol. Biol.* **261**: 297–312.
- Thoms, S. and Erdmann, R.** (2005). Dynamin-related proteins and Pex11 proteins in peroxisome division and proliferation. *FEBS J.* **272**: 5169–5181.
- Tieu, Q., Okreglak, V., Naylor, K., and Nunnari, J.** (2002). The WD repeat protein, Mdv1p, functions as a molecular adaptor by interacting with Dnm1p and Fis1p during mitochondrial fission. *J. Cell Biol.* **158**: 445–452.
- Tooley, J.E., Khangulov, V., Lees, J.P.B., Schlessman, J.L., Bewley, M.C., Heroux, A., Bosch, J., and Hill, R.B.** (2011). The 1.75 Å resolution structure of fission protein Fis1 from *Saccharomyces cerevisiae* reveals elusive interactions of the autoinhibitory domain. *Acta Crystallogr. Sect. F. Struct. Biol. Cryst. Commun.* **67**: 1310–1315.
- Trounce, I.** (2000). Genetic control of oxidative phosphorylation and experimental models of defects. *Hum. Reprod.* **15 Suppl 2**: 18–27.
- Umezawa, T., Sugiyama, N., Takahashi, F., Anderson, J.C., Ishihama, Y., Peck, S.C., and Shinozaki, K.** (2013). Genetics and phosphoproteomics reveal a protein phosphorylation network in the abscisic acid signaling pathway in *Arabidopsis thaliana*. *Sci. Signal.* **6**: rs8.

- Vicogne, J., Vollenweider, D., Smith, J.R., Huang, P., Frohman, M.A., and Pessin, J.E.** (2006). Asymmetric phospholipid distribution drives in vitro reconstituted SNARE-dependent membrane fusion. *Proc. Natl. Acad. Sci. U. S. A.* **103**: 14761–14766.
- Vierstra, R.D.** (2009). The ubiquitin-26S proteasome system at the nexus of plant biology. *Nat. Rev. Mol. Cell Biol.* **10**: 385–397.
- Vitale, N., Caumont, A.S., Chasserot-Golaz, S., Du, G., Wu, S., Sciorra, V.A., Morris, A.J., Frohman, M.A., and Bader, M.F.** (2001). Phospholipase D1: A key factor for the exocytotic machinery in neuroendocrine cells. *EMBO J.* **20**: 2424–2434.
- Vögler, O., Barceló, J.M., Ribas, C., and Escribá, P. V** (2008). Membrane interactions of G proteins and other related proteins. *Biochim. Biophys. Acta* **1778**: 1640–1652.
- Wagner, K., Mick, D.U., and Rehling, P.** (2009). Protein transport machineries for precursor translocation across the inner mitochondrial membrane. *Biochim. Biophys. Acta - Mol. Cell Res.* **1793**: 52–59.
- Wang, F., Liu, P., Zhang, Q., Zhu, J., Chen, T., Arimura, S.-I., Tsutsumi, N., and Lin, J.** (2012). Phosphorylation and ubiquitination of dynamin-related proteins (AtDRP3A/3B) synergically regulate mitochondrial proliferation during mitosis. *Plant J.* **72**: 43–56.
- Wang, H., Song, P., Du, L., Tian, W., Yue, W., Liu, M., Li, D., Wang, B., Zhu, Y., Cao, C., Zhou, J., and Chen, Q.** (2011). Parkin ubiquitinates Drp1 for proteasome-dependent degradation: implication of dysregulated mitochondrial dynamics in Parkinson disease. *J. Biol. Chem.* **286**: 11649–11658.
- Wang, X., Bian, Y., Cheng, K., Gu, L.-F., Ye, M., Zou, H., Sun, S.S.-M., and He, J.-X.** (2013). A large-scale protein phosphorylation analysis reveals novel phosphorylation motifs and phosphoregulatory networks in Arabidopsis. *J. Proteomics* **78**: 486–498.
- Wasiak, S., Zunino, R., and McBride, H.M.** (2007). Bax/Bak promote sumoylation of DRP1 and its stable association with mitochondria during apoptotic cell death. *J. Cell Biol.* **177**: 439–450.
- Werhahn, W. and Braun, H.P.** (2002). Biochemical dissection of the mitochondrial proteome from Arabidopsis thaliana by three-dimensional gel electrophoresis. *Electrophoresis* **23**: 640–646.
- Westermann, B.** (2008). Molecular machinery of mitochondrial fusion and fission. *J. Biol. Chem.* **283**: 13501–13505.

- Wiedemann, N., Frazier, A.E., and Pfanner, N.** (2004). The protein import machinery of mitochondria. *J. Biol. Chem.* **279**: 14473–14476.
- Wong, E.D., Wagner, J.A., Gorsich, S.W., McCaffery, J.M., Shaw, J.M., and Nunnari, J.** (2000). The dynamin-related GTPase, Mgm1p, is intermembrane space protein required for maintenance of fusion competent mitochondria. *J. Cell Biol.* **151**: 341–352.
- Wong, E.D., Wagner, J.A., Scott, S. V., Okreglak, V., Holewinski, T.J., Cassidy-Stone, A., and Nunnari, J.** (2003). The intramitochondrial dynamin-related GTPase, Mgm1p, is a component of a protein complex that mediates mitochondrial fusion. *J. Cell Biol.* **160**: 303–311.
- Wriessnegger, T., Gübitz, G., Leitner, E., Ingolic, E., Cregg, J., de la Cruz, B.J., and Daum, G.** (2007). Lipid composition of peroxisomes from the yeast *Pichia pastoris* grown on different carbon sources. *Biochim. Biophys. Acta* **1771**: 455–461.
- Xie, Q., Guo, H.-S., Dallman, G., Fang, S., Weissman, A.M., and Chua, N.-H.** (2002). SINAT5 promotes ubiquitin-related degradation of NAC1 to attenuate auxin signals. *Nature* **419**: 167–170.
- Xu, L., Carrie, C., Law, S.R., Murcha, M.W., and Whelan, J.** (2013). Acquisition, conservation, and loss of dual-targeted proteins in land plants. *Plant Physiol.* **161**: 644–662.
- Xu, R. and Li, Q.Q.** (2003). A RING-H2 zinc-finger protein gene RIE1 is essential for seed development in *Arabidopsis*. *Plant Mol. Biol.* **53**: 37–50.
- Xu, Y., Sutachan, J.J., Plesken, H., Kelley, R.I., and Schlame, M.** (2005). Characterization of lymphoblast mitochondria from patients with Barth syndrome. *Lab. Invest.* **85**: 823–830.
- Yamaoka, S. and Leaver, C.J.** (2008). EMB2473/MIRO1, an *Arabidopsis* Miro GTPase, is required for embryogenesis and influences mitochondrial morphology in pollen. *Plant Cell* **20**: 589–601.
- Yamaoka, S., Nakajima, M., Fujimoto, M., and Tsutsumi, N.** (2011). MIRO1 influences the morphology and intracellular distribution of mitochondria during embryonic cell division in *Arabidopsis*. *Plant Cell Rep.* **30**: 239–244.
- Yan, M., Rayapuram, N., and Subramani, S.** (2005). The control of peroxisome number and size during division and proliferation. *Curr. Opin. Cell Biol.* **17**: 376–383.
- Yonashiro, R., Ishido, S., Kyo, S., Fukuda, T., Goto, E., Matsuki, Y., Ohmura-Hoshino, M., Sada, K., Hotta, H., Yamamura, H., Inatome, R., and Yanagi, S.**

- (2006). A novel mitochondrial ubiquitin ligase plays a critical role in mitochondrial dynamics. *EMBO J.* **25**: 3618–3626.
- Yoon, Y. and Krueger, E.** (2003). The mitochondrial protein hFis1 regulates mitochondrial fission in mammalian cells through an interaction with the dynamin-like protein DLP1. *Mol. Cell. Biol.* **23**: 5409–5420.
- Yoon, Y., Krueger, E.W., Oswald, B.J., and McNiven, M.A.** (2003). The mitochondrial protein hFis1 regulates mitochondrial fission in mammalian cells through an interaction with the dynamin-like protein DLP1. *Mol. Cell. Biol.* **23**: 5409–5420.
- Yoshida, Y., Kuroiwa, H., Misumi, O., Yoshida, M., Ohnuma, M., Fujiwara, T., Yagisawa, F., Hirooka, S., Imoto, Y., Matsushita, K., Kawano, S., and Kuroiwa, T.** (2010). Chloroplasts divide by contraction of a bundle of nanofilaments consisting of polyglucan. *Science* **329**: 949–953.
- Zhang, H., Zhou, H., Berke, L., Heck, A.J.R., Mohammed, S., Scheres, B., and Menke, F.L.H.** (2013). Quantitative phosphoproteomics after auxin-stimulated lateral root induction identifies an SNX1 protein phosphorylation site required for growth. *Mol. Cell. Proteomics* **12**: 1158–1169.
- Zhang, X. and Hu, J.** (2010). The Arabidopsis chloroplast division protein DYNAMIN-RELATED PROTEIN5B also mediates peroxisome division. *Plant Cell* **11**: 1–12.
- Zhang, X. and Hu, J.** (2009). Two small protein families, DYNAMIN-RELATED PROTEIN3 and FISSION1, are required for peroxisome fission in Arabidopsis. *Plant J.* **57**: 146–159.
- Zhang, X. and Hu, J.** (2008a). Two small protein families, DYNAMIN-RELATED PROTEIN3 and FISSION1, are required for peroxisome fission in Arabidopsis. *Plant J.* **57**: 146–159.
- Zhang, X.-C. and Hu, J.-P.** (2008b). FISSION1A and FISSION1B proteins mediate the fission of peroxisomes and mitochondria in Arabidopsis. *Mol. Plant* **1**: 1036–1047.
- Zhang, Y. and Chan, D.C.** (2007). Structural basis for recruitment of mitochondrial fission complexes by Fis1. *Proc. Natl. Acad. Sci. U. S. A.* **104**: 18526–18530.
- Zhao, J., Liu, T., Jin, S., Wang, X., Qu, M., Uhlén, P., Tomilin, N., Shupliakov, O., Lendahl, U., and Nistér, M.** (2011). Human MIEF1 recruits Drp1 to mitochondrial outer membranes and promotes mitochondrial fusion rather than fission. *EMBO J.* **30**: 2762–2778.
- Zhao, J., Zhou, H., and Li, X.** (2013). UBIQUITIN-SPECIFIC PROTEASE16 interacts with a HEAVY METAL ASSOCIATED ISOPRENYLATED PLANT PROTEIN27 and modulates cadmium tolerance. *Plant Signal. Behav.* **8**: 25680.

- Zolman, B.K. and Bartel, B.** (2004). An Arabidopsis indole-3-butyric acid-response mutant defective in PEROXIN6, an apparent ATPase implicated in peroxisomal function. *Proc. Natl. Acad. Sci. U. S. A.* **101**: 1786–1791.
- Zolman, B.K., Monroe-augustus, M., Silva, I.D., and Bartel, B.** (2005). Identification and functional characterization of Arabidopsis PEROXIN4 and the interacting protein PEROXIN22. *Plant Cell* **17**: 3422–3435.
- Zunino, R., Braschi, E., Xu, L., and McBride, H.M.** (2009). Translocation of SenP5 from the nucleoli to the mitochondria modulates DRP1-dependent fission during mitosis. *J. Biol. Chem.* **284**: 17783–17795.
- Zunino, R., Schauss, A., Rippstein, P., Andrade-Navarro, M., and McBride, H.M.** (2007). The SUMO protease SENP5 is required to maintain mitochondrial morphology and function. *J. Cell Sci.* **120**: 1178–1188.